UNIVERSITY OF
LIVERPOOL

The Behaviour of Microorganisms in Microfluidic Networks

Thesis submitted in accordance with the requirements of the University of Liverpool for the degree of Doctor of Philosophy

By

Marie Binz

Department of Electrical & Electronics Engineering

July 2012

Keep your dreams alive. Understand to achieve anything requires faith and belief in yourself, vision, hard work, determination, and dedication. Remember all things are possible for those who believe.

Gail Devers

Abstract

This thesis focuses on the characterisation of microorganisms and their responses to poly(dimethylsiloxane) (PDMS) based three-dimensional microfluidic structures. Experiments based on observations of the responses of individual cells to their environment have the potential to make enormous contributions to cell biology and biomedicine. **Chapter 1** presents the thesis aims. In **chapter 2**, an overview of bacteria and filamentous fungi including their physiology and motility mechanisms are presented. The applications of lithography techniques including soft-lithography for studying cells and microorganisms behaviour over flat and profiled surfaces as well as within microfluidic devices are also reviewed. **Chapter 3** described the methodology for the fabrication and manipulation of the PDMS-based networks employed for experimentation and for data analysis.

Chapter 4 investigates the mechanisms that allow fungi to partition the space and negotiate micro-confined networks. *Armillaria mellea* has been introduced in networks of various shapes. *A. mellea* was able to grow through every network exhibiting similar geometry-induced mechanisms. The species growth behaviour was mainly influenced by the geometry of the networks which changed the tip extension velocity and the branching angles. The results obtained suggest that thigmotropism in which hyphal growth occurs is an important parameter in fungal growth dynamics. The hyphae could also find their way toward a network without any wall contact. This suggests that sensing mechanisms does not rely exclusively on thigmotropism but also on the integration of the extra-cellular environment.

In **chapter 5** the swimming behaviour of *Serratia marcescens* and *Pseudomonas stutzeri* in different networks were compared to their behaviour in non-confined environment. Large channels of 100 μm in width had no effect on the bacterial species as the bacteria swam randomly over the surface with gradual changes in their swimming direction and were seen to trace out circular trajectories. Channels of less than 10 μm in width could control bacterial movements in one direction and close to the boundaries. Complex networks of different shape not only revealed similar behaviour for both species but also showed the ability of bacteria to turn corner, to perform 360 ° turn and to follow very intricate paths. The complexity of the network through which the bacteria swam as well as the channels size were identified as the dominating factors in predicting their motility.

In **chapter 6** the behaviour of *S. marcescens* swarming phenotype was investigated after modifying the extra-cellular environment of the networks. Changes in the viscosity of the solution to 3.7 cP for channels that are 15 μm in width showed elongated swarming cells of a size reaching 8 μm to 10 μm in length. 10 μm wide channels were used to observe the swimming-swarming behaviour of *S. marcescens* within a wide range of concentration of Ficoll 400 and caused a decrease in cell velocity in comparison to that measured in LB broth only. The maximum cells size observed was 5.3 μm. **Chapter 7** summarises the thesis main findings and the contributions in the field. Future work is also described.

Acknowledgements

First and foremost I would like to thank my supervisor Professor Dan Nicolau for giving me the opportunity to start a PhD with him and for his advice, help and support. I would like to thank my co-supervisor Professor Clive Edwards for his continued support and patience. In addition I would like to express gratitude to the financial sponsors of this project Leverhulme trust.

Many thanks to my friends (past and present) from my work group and from the department. I would particularly like to thank Marie, Ewa, Elena, Marina, Jenny, Joanna, Harm, Rob, Sherban, Lawrence, Ben, Miguel, Alex and Tobi.

Many thanks to Paul Loughnane who taught me the basics knowledge in microbiology as well as all the students and member of staff from lab H. Thanks to Dr. Rob Poole from mechanical engineering department who kindly teach me how to use the rheometer and thank you to Dr. Brian Faragher from Liverpool School of Tropical Medicine for his advices on statistics.

I would like to thank my great housemates and friend forever Ana, Oyku, Stella, Shashi and Shan. Many thanks to Jules, Kshitija and Jo, for their love and support.

Finally I would like to thank my loving and supportive family- my Mum, Dad, sister, brother and my lovely granny.

Table of Contents

Chapter 1

Introduction

1.1 Why study microorganisms?

Microorganisms colonize inherently microstructured surfaces like soil, wood, leaf litter, plant and animal tissue but little is known about their growth dynamics in such systems. Microorganisms are both beneficial and deleterious for human activities. Bacteria are responsible for some life-threatening diseases like meningitis. They have also positive effects on our health as shown by the colonization of bacteria in our gut. Bacteria produce useful antibiotics; they are employed in biofuel cells and in food production e.g., the manufacture of butter, cheese or yoghurt where they convert lactose to lactic acid. Microorganisms, especially fungi, are essential in the natural cycle of matter as they play a vital role in re-cycling organic compounds. Fungi interact with living and dead organisms as well as with non-living components of the environment that make them a key group in the regulation of ecosystem processes. They are also useful in biotechnology; they serve as bio-factories for the production of antibiotics and enzymes for food processing. Some are a threat to humans and plants causing disease and economic loss in agriculture. Thus, microorganisms occur almost everywhere.

An important area of research is to understand the spatial aspects of population dynamics which is characterized by the microorganisms' movement. Microorganisms that are not under stress will reproduce as fast as possible colonising all type of surfaces as long as nutrients are available. When the environmental conditions change and are against the survival of the species, behaviour changes so that microorganisms induce appropriate adaptive responses for survival. In this work bacteria and filamentous fungi are confined within three-dimensionally microstructured networks that mimic naturally confined spaces and their behaviour is

quantitatively observed. The size, shape and distribution of space in enclosed environments exert an important influence over the dynamics of these organisms. For instance, it is largely unknown how bacteria grow, move, and penetrate pores of very small size. The effects of restricting geometry on bacterial motility have been studied experimentally and theoretically. These approaches trigger questions about how are bacteria able to propagate through constrictions and to what extent does the morphology of the microstructures affect the random motility of bacteria. Filamentous fungi grow in a highly polarized manner forming elongated hyphae. One gram of soil for example may contain up to 200 m of fungal hyphae (Van Der Heijden, Bardgett et al. 2008). For a given geometrical confinement, what are the spaces searching strategies used by fungi to successfully grow and survive? The analysis of the movement of microorganisms at the level of single cell trajectories aims at determining the rules of their behaviour. The knowledge of the factors controlling microorganisms' movement will help to predict the flux of cells through various substrates.

1.2 Why use microfluidics for studying microorganisms?

The visualization of bacteria and fungi in their natural environment is difficult, mainly due to the nontransparency of the media they are living in. This problem can now be overcome through the use of microfluidics technology and poly(dimethylsiloxane) (PDMS). Taking advantage of the well-established fabrication methods of semiconductor technology (Duffy, McDonald et al. 1998, Menz, Mohr et al. 2001), artificial structures in the micrometre range resembling the spatial properties of the habitat of microorganisms can be routinely fabricated. Microfluidics technology can generate easy and reliable three-dimensional microscale structures which are transparent, non-toxic and oxygen-permeable (Whitesides, Otsuni et al. 2001). It is possible to generate structures close to the diameter of microorganisms and control the extra-cellular environment.

Fungal hyphal growth as well as bacterial movement can be readily probed and monitored in real time. Such systems do not need any external pumping or mixing

but work on their own. Microfluidics is a novel and efficient mean to explore the microbial world. The microfluidic networks are ideal to investigate the behaviour of bacteria and filamentous fungi in two main respects:

(i) The networks provide a means of observing bacterial and fungal behaviour in an environment, which is more complex and realistic than a homogeneous agar surface. Natural substrates in which bacteria and filamentous fungi have been found (soil or wood for instance) look like labyrinths made of a variety and randomly distributed obstacles. Thus it is reasonable to suppose that movements in natural substrates are far more complex than on agar, because natural substrates are opaque and difficult to visualize, much of this complexity may have been missed. The PDMS made networks provide a means to re-create some of the complexity of natural environments in a transparent structure where the microorganisms can be directly and easily observed.

(ii) Natural media are heterogeneous and the environment can take different forms which make it difficult to mimic with materials commonly available in microbiological lab, i.e., agar. This can now be addressed through the use of soft lithography associated with PDMS materials that enabled the design of a vast range of structures where the size, the shape and the spatial distribution of the features could be manipulated to match the physical dimensions of bacteria and filamentous fungi (Weibel, DiLuzio et al. 2007).

1.3 Thesis aims

The general aim of the project is to advance the understanding of the behaviour of flagellated bacteria and filamentous fungi in confined spaces through microscopy. There is a great deal of interest in trying to understand and quantify microorganism driven processes at the scale of the natural environment. Studies at the microscale could provide a description of the factors controlling microorganisms' activities,

which could result in improved predictive models for microorganisms' movement in microenvironments.

Fungal mycelium expands through structurally heterogeneous environment, such as building materials, wood and soils. In those circumstances, it is difficult to obtain temporal data on the growth and function of fungal mycelia. In this work, artificial environments were designed to understand how micro-scale structures can influence the growth of fungal mycelia. The aim of this work was therefore to characterize in some detail the dynamic behaviour of *Armillaria mellea*, a soil-borne fungal pathogen of plants, in a designed enclosed environment to mimic complex ecosystems at the micrometre scale (**chapter 4**). Growth parameters such as the branching behaviour and the tip extension velocity were compared in confined and unconfined environments. Accordingly, the research was designed as follows:

(i) Observation of the fungal cells on agar surfaces and on unstructured PDMS (not impeded with microstructures) followed by observation of fungal growth through the microstructure using light microscopy. In the former set of experiments, the branching behaviour and the tip extension velocity were measured. In the latter set of experiments, the species was challenged by microchannels to evaluate its exploratory strategy. The branching behaviour, that is the branching angle and the distance between two branches, and the tip extension velocity were measured.

(ii) Evaluation of the effect of the confinement on the species behaviour by statistical analysis.

Attraction of bacterial cells to boundaries within artificial environment can potentially affect the cell's ability to rotate, maintain an optimal speed or direction which in turn will be beneficial for disrupting aggregation of bacteria as seen for example in biofilm formation or for improving bioremediation of hazardous waste in the environment. Bacterial movement is determined by their motility parameters i.e. run time and turn angle, and will be investigated in this thesis in two bacterial species

– *Serratia marcescens* and *Pseudomonas stutzeri*, two naturally occurring soil bacteria that differ in their arrangement of flagella (one peritrichously flagellated, the other polarly flagellated) - to also distinguish the role of flagellar placement on swimming patterns (**chapter 5**). The aim of the study of bacterial motility was therefore (i) to investigate quantitatively the influence of confinement on the growth of *S. marcescens* and *P. stutzeri* cells in microchannels filled with a nutrient rich medium and (ii) to observe how the micro-confinement modulates the motility, the run and tumble frequency and the boundary accumulation for the two species. Through observation by light microscopy and tracking of the cells in two-dimensions, cell velocity and their growth pattern will be determined.

Serratia marcescens is an example of flagellated bacteria that show a phenotype referred as 'swarming'. Swarming motility occurs when cells are in contact with a surface, the cells measure 5 μm to 30 μm in length and are hyperflagellated. The behaviour of *S. marcescens* was studied within a viscous environment (i) to observe the behaviour of elongated cells at the microscale and (ii) to observe the switch from a swimming phenotype to a swarming phenotype (**chapter 6**).

1.4 Journal publication and conference proceedings

Chapter 4:

Held, M., **Binz, M.**, Edwards, C. and Nicolau, D.V., Nicolau, 'Dynamic behaviour of fungi in microfluidics : a comparative study.', In Imaging, Manipulation, and Analysis of Biomolecules, Cells and Tissues VII, pp. 718213-718219, SPIE, San Jose, CA, USA (2009).

Held, M., **Binz, M.** and Nicolau, D.V., 'Intelligence – A fungal perspective.' in 7th Annual Conference and Postgraduate Day, UKSB, Liverpool (2008).

Chapter 5:

BINZ, M., LEE, A.P., EDWARDS, C. and NICOLAU, D.V., 2010. Motility of bacteria in microfluidic structures. *Microelectronic Engineering,* **87**(5-8), pp. 810-813.

Chapter 2

Literature-Review

2.1 Bacteria

Bacteria are minute organisms unknown until the development of the single-lens microscope in the 17th century by Antoni van Leeuwenhoek (Porter 1976) who obtained a resolving power from his lenses that was greater than the early compound microscope. In 1674, he made the first observations of microbes. He described them as "very little animalcules" in a series of letters to the Royal Society of London between 1674 and 1723.

2.1.1 The bacterial cell

Bacteria along with archaea are the oldest living organisms on the Earth and have evolved nearly 4 billion years ago from a common ancestor. A bacterium is a single, autonomous cell with a prokaryotic organization and dimensions ranging from 0.5 μm to 10 μm. The cell lacks a cell nucleus, cytoskeleton (Gitai 2005), and organelles such as mitochondria and chloroplasts (Berg, Tymoczko et al. 2002). Before the 1950s and the development of the electron microscope, prokaryotic cells were seen as cells of very simple construction and described as a "bag of enzymes". The general structure of a bacterium is presented in Figure 2.1.

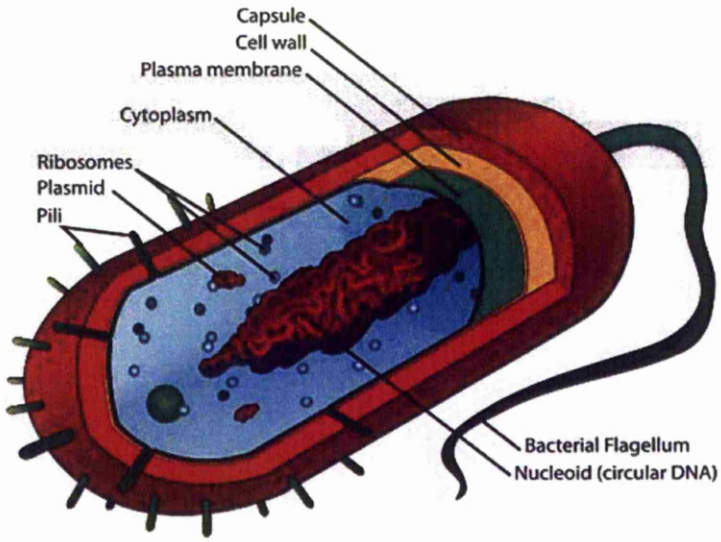

Figure 2.1: Structure of a bacterial cell (© Mariana Ruiz, 2008).

Bacteria have a complex cell wall and a plasma membrane that can form invaginations. The cell wall and the plasma membrane are separated by a periplasmic space. The interior of a bacterial cell contain the cytoplasm, the genetic material as well as ribosomes and inclusion bodies. Many cells are surrounded by a capsule or a slime layer. The motility of bacteria is possible by the use of flagella.

Many bacteria are rod (bacilli) or round (cocci) shaped but also form spirals or helices (Figure 2.2). Cells with rigid spirals are called spirilla and those with flexible spirals are called spirochetes. Besides rod or coccus shape, bacteria can form long multinucleate filaments or hyphae that may branch to produce a mycelium as seen in actinomycetes. Some species have flat cells and are called 'square bacteria'. For a given species, the cells are usually uniform in shape but in some species, the shapes of the cells are variable and lack a characteristic form. The bacteria are called pleiomorphic. Coccal cells can exist as individual cells but also form characteristic association. When cocci divide but remain together in pairs the resultant association is called diplococci (e.g., *Neisseiria)*. When more than two cells adhere together, different pattern are possible. In the genus *Streptococcus* for example cells adhere after multiple divisions in one plane. In *Staphylococcus* the cells divide in different

planes and form irregular grapelike clusters. Some clusters are symmetrical. In the genus *Micrococcus*, the cells divide in two planes and form groups of four cells called tetrads. In the genus *Sarcina*, cells divide in three planes and form cubical packets of eight cells. The other common shape is the bacillus shape that looks like a rod. Bacillus shaped bacteria differ in their length-to-width ratio. Some bacterial cells are so short and wide that they look similar to cocci (coccobacilli). The shape of the rod often varies and may be flat, rounded, cigar-shaped, or bifurcated. Similarly to cocci, bacilli can form pairs or chains (e.g., *Bacillus megaterium* forms long chains).

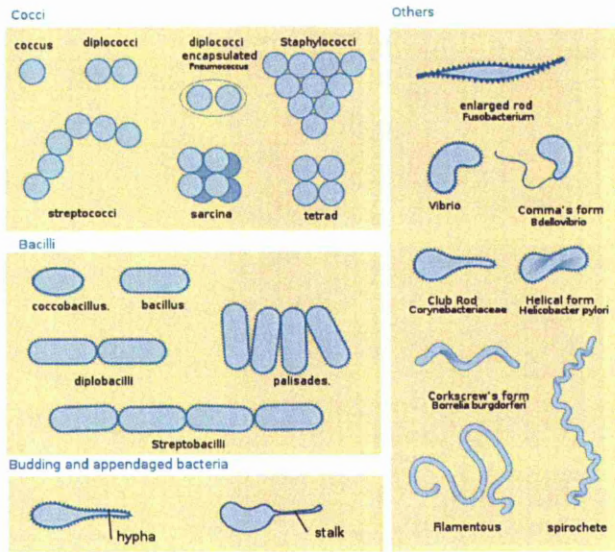

Figure 2.2: The variety of shape of bacteria (© Mariana Ruiz, 2006).

The bacterial cells possess three regions:

Cell envelope

The cell envelope consists of the capsule, cell wall and the plasma cell membrane. According to the composition of the cell walls, bacteria are divided into two further groups Gram-positive and Gram-negative. The differentiation depends on a colorimetric reaction with a crystal violet-iodine dye complex developed by Christian Gram in 1884. Cells with many layers of peptidoglycan can retain the stain and are called Gram-positive. Gram-negative bacteria have only one or two layers of

peptidoglycan and cannot retain the stain. The Gram-positive bacteria's cell wall is thus made from a very thick layer of peptidoglycan (up to 40 layers). This layer which is located beyond the cell membrane confers enormous mechanical strength to the cell wall. Apart from peptydoglycan, the cell wall contains polymer like teichoic and teichuronic acids. The Gram-negative bacteria's cell wall is more complex but contains less peptiglycan layers (only one or two layers) located beyond the periplasm. Gram-negative bacteria are thus mechanically weaker than Gram-positive cells. The periplasm is above the cell membrane and is full of proteins including enzymes. Outside this thin peptidoglycan layer in Gram-negative bacteria is a membrane layer termed the outer membrane that contains lipopolysaccharide that provides the antigenic structure of the surface. Some bacteria have a layer of material localised around the cell wall e.g. a well organized layer that cannot be easily removed is called a capsule. Another type of layer is called the slime layer, which is a zone of diffuse, unorganized material that can be easily removed. Capsules and slime layers are composed of polysaccharides and other materials. Capsules confer to bacteria a protection against phagocytosis or against desiccation.

Appendages

The appendages consist of the flagella and the pili otherwise known as the fimbriae. Some Gram-negative bacteria are covered in fine hair called fimbriae or pili composed of proteins that help the bacteria to adhere to surfaces, substrates and other cells or tissues in nature (Beachey 1981). The flagellum is responsible for the motility of bacteria and may confer pathogenicity. The flagellum is a flexible protein structure about 20 nm in diameter and up to 20 μm in length (Kojima, Blair 2001).

Bacteria that carry a single flagellum are called monotrichous. The ones that possess many flagella at one end of the cell are called lophotrichous. When the bundle of flagella appears at both ends of the cell, the bacterium is amphitrichous and when bacteria are covered with flagella all over the cell body, they are said to be peritrichous (Figure 2.3).

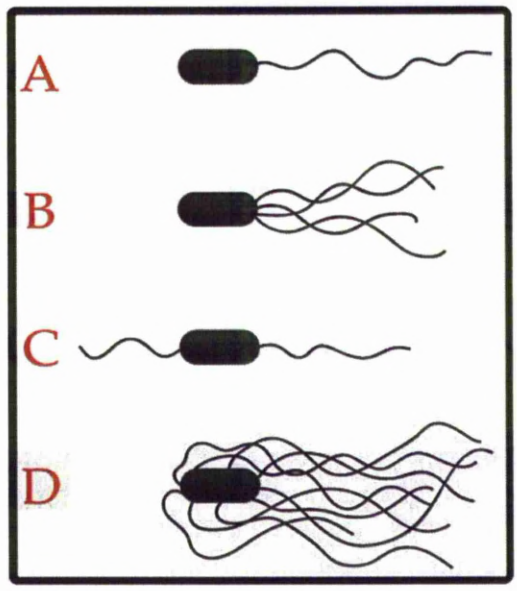

Figure 2.3: The arrangement of flagella. A: monotrichous. B: lophotrichous. C: amphitrichous. D: peritrichous (© Mike Jones, 2006).

Cytoplasmic region

The cytoplasmic region comprises the chromosome (DNA), the ribosomes and other various sorts of inclusions. This region of bacterial cells contains the bacterial chromosome (nucleoid) which is typically one large circular molecule of DNA (Thanbichler, Wang et al. 2005). Sometimes bacterial cells possess smaller extrachromosomal pieces of DNA called plasmids. The total DNA content of a cell is referred as the cell genome. Ribosomes are composed of proteins and RNA. The cytoplasmic region contains also some kind of granules referred to as inclusions.

Bacterial growth

Bacteria grow by asexual binary fission. In the laboratory, they are cultured and maintained either on solid agar or in liquid media. When cells are introduced into growth media, cell division may not begin immediately. This phase is called the lag-phase which is a period of adaptation of the organism to the medium. Once adapted the cells grow and divide; this is the exponential phase which corresponds to rapid growth at constant rate. As they grow the cells use the nutrients available in the medium and produce waste products of metabolism. The consequence is that growth

slows down due either to the lack of nutrients or to the accumulation of waste products. This phase is called the stationary phase. The stationary phase can lead progressively to the death phase when no nutrients are available (Prats, López et al. 2006).

For optimal growth, a bacterium needs nutrients, a source of energy, water, an appropriate temperature, an appropriate pH, presence or absence of oxygen and inorganic ions. The basic requirements for heterotrophic bacterial cells include various carbon sources such as sugars, carbohydrates, amino acids, sterols, alcohols or hydrocarbons. Energy is needed for the chemical reactions that take place within the cell but also for flagellar motility. Phototropic species use light as an energy source whereas chemotrophic species use chemicals available from the environment. During bacterial growth nutrients and waste products enter or leave the cell in solution so bacteria need to live on materials which have available water. For a given type of bacterium, temperature can increase or decrease the velocity rate. *Thermophilic* bacteria have an optimum growth above 45 °C. *Mesophilic* bacteria grow between 15 °C and 45 °C, *psychrophilic* grow below 15 °C and *psychrotropic* bacteria are able to grow at temperature between 0-5 °C but also around 20 °C. Most bacteria grow best at a pH around 7 but some species are able to survive at higher pH (*alkalophiles*) and at lower pH (*acidophiles*). Some bacteria need oxygen (*aerobes*) for their growth other bacteria need the absence of oxygen (*anaerobes*) to grow. All bacteria except *halophiles* bacteria need inorganic ions at low concentration to grow. Ions have various regulatory functions. For example Ca^{2+} ions play a role in chemotaxis and sporulation in *Bacillus subtilis* (Shemarova, Nesterov 2003).

Bacteria also form colonies and can be found in communities, like biofilms (Donlan, Costerton 2002) and fruiting bodies (Shimkets 1999). During biofilm formation, free-swimming or floating bacteria land on and bind to a surface. Cells communicate by signalling molecules, begin to multiply and form a microcolony. The aggregated cells start synthesizing a sugary, slime layer. Living and fully hydrated biofilms are composed of cells (±15 % by volume) and of matrix material (± 85 % by volume). The slime prevents bacteria from drying out, and may also improve nutrient access

and waste elimination. Within planktonic culture solute is carried by the bulk flow of a fluid, inside biofilm diffusion is the predominant transport process within cell aggregates (Stewart 2003). The cells are located in matrix enclosed "towers" and "mushrooms" and within the slimy matrix cells can exist in complex communities. Open water channels are interspersed between the microcolonies that contain the sessile cells (Lawrence, Korber et al. 1991). The biofilm also protects bacteria from antibiotics and toxins. The centre of the microcolony becomes anaerobic and cells may exist in a dormant state. Some cells break free from the biofilm and may then establish at another site.

One of the responses of bacterial cells to changes in the environment is the formation of a heat and desiccation-resistant cell morphology called spores. Spore formation is generally induced by nutrient depletion and spores are less active than vegetative cells. In myxobacteria, like *M. xanthus* for example, spore formation is coupled to the formation of multicellular fruiting bodies (Shimkets, Brun 2000). Fruiting body formation depends on intercellular signalling and coordinated changes in gene expression, as well as on the coordinated motility behaviour of cells.

Prior to the formation of colonies or communities, some bacterial species can communicate with one another. This process is called quorum-sensing. When a population of cells grows, all the cells secrete signal molecules called autoinducers. If the cell density reaches a certain minimum (*quorum*) these molecules will reach a concentration sufficient to activate certain genes within the cells. Different bacteria may produce different autoinducers which regulate different characteristics. In *Vibrio fischeri* for example in a high-density population the *lux* genes are induced and the bacteria produce luminescence. *Vibrio fischeri* colonizes the light organ of the Hawaiian squid *Euprymna scolopes*. The colonization is beneficial for the squid that uses the light to avoid predation. Most Gram-negative quorum sensing is mediated by *N*-acylhomoserine lactone (AHLs) signalling molecules.

2.1.2 Bacterial Motility

Bacteria are found almost everywhere, in the air, soil, water, inside and on different organisms. They respond to changes in their environment like temperature, light intensity, or chemical composition. Most motile bacteria achieve their motility by use of flagella (Macnab, Aizawa 1984). Bacterial flagella were first seen in 1836 by the German naturalist Christian Ehrenberg during work observing Chromatium *okenii*. The five different types of motility are swimming, swarming (with flagella), gliding with pili (twitching), gliding without pili and sliding (Bardy, Ng et al. 2003).

Swimming and swarming (with flagella)

Bacteria like *E. coli* for example swim in liquid media. On average five to eight flagella emerge at the surface of the cell body. Each flagellum is driven by a motor at their base. When all the flagella form a bundle and turn counterclockwise (CCW), the resulting movement is called a run. When the motor turns in the clockwise (CW) direction, the cells tumble and choose a random direction. The switch between CCW and CW modes is due to chemotaxis. In a constant environment a run lasts approximately 1s and a tumble 0.1 s. When a cell runs toward a source of nutrient the tumbling frequency decreases. Alternate swimming and tumbling results in a three-dimensional random walk and cell speeds reach 30 μm/s. Swimming is an individual behaviour whereas swarming involves a group of cells. Swarmer cells like *S. marcescens* exhibit a different phenotype in comparison to swimming cells. Cells are elongated and hyperflagellated (> 50). The movement requires a wet surface and can be demonstrated *in vitro* using a specific concentration of agar (0.7 - 0.8 %). The cells invade a surface in a radial manner. Bacteria can often "switch" between these two types of motility depending on the fluidity of the surrounding environment. Swarming motility has been shown to be widespread among flagellated bacteria and it has been suggested that this behaviour plays an important role in bacterial pathogenesis and biofilm formation (Fraser, Hughes 1999).

Other types of motility (without flagella)

Gliding with pili or twitching make the bacteria move forwards and backwards (Henrichsen 1972). Twitching require retraction of type IV pili as for some forms of gliding. The movement is seen when bacteria are in contact with a solid surface (Bradley 1980).

Gliding is a smooth form of motion and occurs only when cells are in contact with a solid surface. Gliding may occur when nutrient levels are low. The mechanisms driving some forms of gliding are still unknown. As it moves the gliding cell leaves a 'slime trail' (McBride 2001). Matsuyama, Bhasin et al. 1995 studied the spreading behaviour of *S. marcescens* 274 on low-agar medium. They concluded that spreading is a passive translocation dependent on the presence of serrawettin W1 (a nonionic biosurfactant) and independent of the presence of chemotaxis functions. Biosurfactants enable bacteria to spread by loosening the water containment force acting on bacteria at the expanding colony front (Matsuyama, Tanikawa et al. 2011).

The flagellum and the rotary Motor

A flagellum is a filamentous protein structure attached to the cell surface of a motile bacterium (Figure 2.4). Due to the flagellum, a bacterium is able to swim in fluids. The flagellar apparatus consists of three structures composed of different proteins:

(1) *The flagellar filament* is a left-handed helical filament. The flagellar filament is a polymer of the flagellin protein called FliC which terminates in a filament cap called FliD. The filament can be 15 μm long with a diameter of 12-25 nm and is connected to a region called the hook.

(2) *The hook* is a polymer consisting of the FlgE protein and the hook-filament junction proteins FlgK and FlgL.

(3) *The basal body and the motor components.*

The basal body consists of four ring-shaped proteins distributed around a central rod that is anchored in the cell envelope of Gram-negative and Gram-

positive bacteria (DePamphilis and Adler, 1971). The rotary motor of the flagellum consists of a stator (MotA and MotB) and a rod (FlgB, FlgC, FlgF and FlgG). The components of the stator are stationary and embedded in the basal body. The rotor consists of FliG attached to the MS-ring (FliF). The rotor and the stator together generate torque. The flagellar motor rotates due to a proton motive force in which the protons go through the channels, MotA and MotB, provoking a conformational change in the stator which makes the rotor turn. The direction of rotation of the motor is controlled by the C-ring (FliG, FliM, and FliN) (Berg, 2000). Gram-negative marine *Vibrio* spp. have motors that are driven by sodium ions rather than protons (Berg 2002).

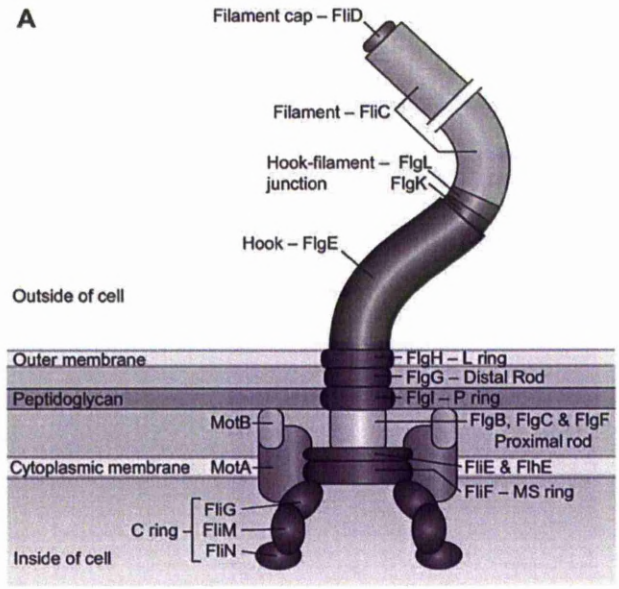

Figure 2.4: The components of bacterial flagella (Copeland, Weibel 2009).

2.1.3 Motility and chemotaxis

Different kinds of taxis have been identified including chemotaxis (movement in response to chemicals), phototaxis (movement in response to light), magnetotaxis (movement in response to a magnetic field), gravitaxis (movement against or with gravity), and thermotaxis (movement in response to temperature).

In 1884 Wilhelm Pfeffer in Tübingen and Theodore Engelman in Utrecht did work on bacterial motility. Theodore Engelman studied the response of swimming bacteria to light, carbon dioxide or oxygen whilst Wilhelm Pfeffer studied the response of bacteria toward a variety of chemicals using a capillary assay. He thought that the bacteria were able to navigate toward the mouth of a capillary tube containing a chemical attractant and used the term "chemotaxis" to describe the phenomenon (Berg 1975). With Julius Adler in the 1960s, the modern era of work on bacterial behaviour started. *Escherichia coli* was the organism of choice because a lot was already known about the biochemistry and increasingly the molecular biology of this organism. Adler published his first paper on the subject, "Chemotaxis in *Escherichia coli*," in 1965 (Adler 1965). The paper included an electron micrograph of *E. coli* with 5 flagella. In 1969 he showed that *E. coli* have chemoreceptors using a capillary assay introduced earlier by Wilhelm Pfeffer (Adler 1969). Since this early pioneering work, it is now known that some pathogenic organisms are motile and others are not. The importance of motility and chemotaxis for pathogenicity is still a matter of active study, although the common belief is that for a given species, motile cells are more virulent then non motile ones. Chemotaxis offers a cell an enormous advantage for long-range migration, which might be expected to play an important role in invasiveness.

2.1.4 The bacteria species used in this thesis

Serratia marcescens

Serratia marcescens is a facultatively anaerobic, motile, rod-shaped Gram-negative bacterium which is peritrichously-flagellated. The cell is typically 0.9 to 2 μm long and 0.5 to 0.8 μm in diameter, and is a member of the family *Enterobacteriaceae*. The bacterium occurs naturally in soil and on plant surfaces and it is able to colonize a wide variety of surfaces in the digestive tracts of rodents, fish, insects and humans (Table 1.1). The bacterium is pathogenic and causes nosocomial infections particularly in immuno-compromised patients (Grimont, Grimont 1992). Additionally the bacterium is responsible for spoilage of various foods. *Serratia marcescens* was identified at the beginning of the 19th century. Serratia in honour of

an Italian physicist named Serafino Serrati and marcescens from the Latin word 'for decaying' because the blood pigment of the colonies found on polenta deteriorated quickly. In liquid media the bacterium typically undergo a "run-and-tumble" random walk (three-dimensional random walk) biased by extracellular signals including chemo-attractants and chemo-repellents (Berg, Brown 1972, Nicolau Jr, Burrage et al. 2008, Wadhams, Armitage 2004). Alternatively *S. marcescens* is able to swarm in a concerted, quorum sensing directed manner when the viscosity of the extra-cellular environment changes. Swarm cells are elongated, multinucleated, aseptate and hyperflagellated and differ in size from the non-swarming variant.

Pseudomonas stutzeri

Pseudomonas stutzeri was first described by Burri and Stutzer at the end of the 19th century (Burri, Stutzer 1895, Van Niel, Allen 1952). *P. stutzeri* is a Gram-negative bacterium that can be found in different ecological niches (soil, rhizosphere or groundwater); it has also been isolated as an opportunistic pathogen from humans. *P. stutzeri* belongs to the class of *Gamma-proteobacteria*. The cells are rod shaped and measure 1 to 3 μm in length and 0.5 μm in width and have a single polar flagellum (Table 2.1). In some strains lateral flagella are also produced. It has been suggested that lateral flagella might be involved in the species' swarming and twitching motility on solid surfaces. The species does not produce fluorescent pigment in contrast to the other members of the fluorescent group of *Pseudomonas* spp. The species is highly chemotactic. Although *P. stutzeri* possesses both flagella and pili, the bacterium has not been described as forming natural biofilms. In monotrichously flagellated bacteria; the rotation of the flagellum in CW and CCW lasts for about the same time and the two modes are alternately repeated. There is a rapid switching (brief stop) then the cells reorient randomly. Cells can reach a speed of ~ 70 μm/s.

	Serratia marcescens	*Pseudomonas stutzeri*
Shape	Rod-shaped	Rod-shaped
Dimensions	0.9 to 2 μm long 0.5 to 0.8 μm in diameter	1 to 3 μm long 0.5 μm in diameter
Arrangement of flagella	peritrichous	monotrichous
Environment	Soil, plant surfaces, Digestive tract (rodents, fish, insects, humans)	Soil, groundwater, rhizosphere

Table 2.1: Comparisons between the two bacterial species.

2.2 Filamentous fungi

Fungi are eukaryotic, heterotrophic organisms with an absorptive mode of nutrition. Most fungi are both unicellular and multinucleate, with rigid chitinous cell walls. They usually exhibit yeast-like or mycelial growth habits. The most intensively studied fungi are the unicellular yeasts *Saccharomyces cerevisiae* and *Candida albicans* and the filamentous fungi *Neurospora crassa* and *Aspergillus nidulans*.

2.2.1 Development of a fungal colony

The basic extension unit of filamentous fungi is the hypha. Fungal hyphae are tube-like structures containing a moving slug of protoplasm and an apical region composed of individual cells (Figure 2.5). Hyphae grow only at their tips. Behind the growing tip, the hypha ages progressively. While the tip is growing, the protoplasm moves continuously from the older regions of the hypha towards the tip. The cytoskeletal components have emerged as the strongest candidates for the driving force for apical growth (Bartnicki-Garcia 2002). The growth of hyphal cells allows the exploration and efficient colonization of new environments. The hyphal growth of filamentous fungi begins by spore germination and spreads uni-directionally from the point of inoculation due to the apical extension and branching events, which lead to a mycelium formation (Bartnicki-Garcia 1973). The beginning of hyphal formation is either spore germination or the hyphae originate from another

hypha during branch formation. "The duplication cycle" is a term introduced by Fiddy, Trinci (1976) to describe the events of growth and division of individual cells within multicellular hyphae. The term makes a distinction from the cell cycle where daughter cells are completely separate (Trinci 1978). The duplication cycle in *Aspergillus nidulans* is well-known (Harris 1997). A uninucleate spore permits the formation of multinucleate hyphal cells because cell division "occurs" through the formation of cross walls termed septa. The hyphae of most fungi have cross walls or septa at regular intervals. One of their main roles seems to be to enable the differentiation of a hypha into a continuous series of compartments. Septum formation is similar to a certain extent with tip growth because for both, a division site must be specified and the biosynthesis of new wall material occurs. Apical tip cells progress through the duplication cycle and maintain their polarized axis of growth whereas sub-apical cells seem to enter a period of mitotic quiescence before establishing a new polarity axis and initiate new branch formation.

The mycelium grows by hyphal extension, and by branching. The branching gives the colony its circular shape. Molin et al. (1992) described the microscopic characteristics of hyphal growth within the mycelium. They showed that the colony extension includes the growth of hyphae in a fixed direction. The fungi exhibit a tropic behaviour, meaning that obstacles in their way can divert their growth direction, but the fact that they show a tendency to maintain their growth direction seems to be independent from external stimuli (Riquelme, Reynaga-Peña et al. 1998). Additionally, Bottone et al. (1998) showed that fungi extend in a unidirectional radial way avoiding back growth.

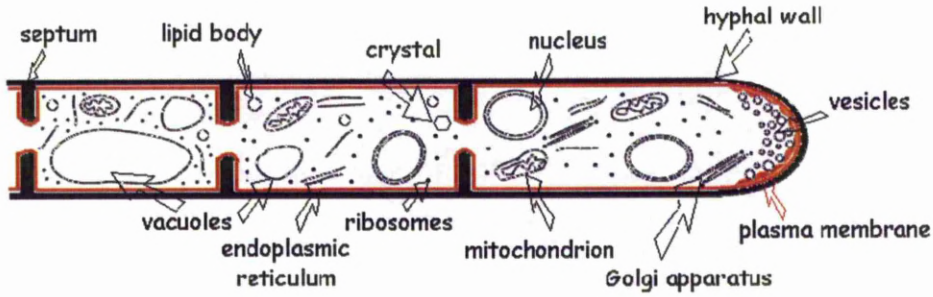

Figure 2.5: Hyphal ultrastructure (© Vicki Tariq, 2011).

2.2.2 Ultrastructural organisation of the hyphal tip

Spitzenkörper – Vesicle Supply Center

Fungal hyphae are cytologically interesting because growth is restricted to the tip. Girbardt examined the hyphal tips of higher fungi (*Oömycetes*, *Zygomycetes*, *Ascomycetes*, *Basidiomycetes*, and *Deuteromycetes*) by light and electron microscopy, and he observed that the differences between growing and non-growing regions are in the internal organization of the cells (Girbardt 1957, Girbardt 1969). An apical body called the "Spitzenkörper" was observed in various fungi. Brunswik in 1924 originally described this ultrastructural organization and concluded that the Spitzenkörper was involved with apical growth of hyphae. Girbardt described the Spitzenkörper and showed that it is present in growing hyphal tips, and forms at spore germination and branch formation sites. He was the first to notice that the Spitzenkörper position correlates with the direction of hyphal elongation. The use of transmission electron microscopy (TEM) made it possible to analyze the ultrastructural organization of hyphal tips. The Spitzenkörper is a complex, multi component structure which contains vesicles of different sizes (Grove and Bracker 1970, Bartnicki-Garcia 1987). Elements such as vesicles of various kind,

microfilaments, microtubules, and ribosomes, are generally present in the Spitzenkörper but not all of them are present in every species or permanently in a single species (Lopez-Franco, Bracker 1996). Additionally the Spitzenkörper composition varies through time. In the 1990s the work from Reynaga Pena et al, 1997 and Lopez-Franco, Bracker 1996 showed that changes in the direction of hyphal growth are anticipated by changes in the position of the Spitzenkörper. There are strong indications that the Spitzenkörper serves as a site that collects vesicles arriving from the subapical region of a hyphae before they fuse with the cell membrane to produce new cell wall surface (Bartnicki-Garcia 1990). More recently, the use of the amphiphilic styryl dye, FM4-64, which stains vesicles within the Spitzenkörper and confocal microscopy, have shown how dynamically vesicles accumulated at the Spitzenkörper (Fischer-Parton, Parton et al. 2000, Dijksterhuis 2003).

According to a mathematical model of fungal morphogenesis (the hyphoid model), the Spitzenkörper acts as a vesicle supply center (VSC), this is a vesicle collection site that emerges from the sub-apical region, and is involved in cell surface expansion (Bartnicki-Garcia, Hergert et al. 1989). The mathematical model is proposed to explain the tubular shape of the fungal growing tip based on secretory vesicles. The model considers that (i) wall-destined vesicles are responsible for wall extension; (ii) the VSC released the vesicles, (iii) the vesicles move from the VSC to the surface in any random direction. The position and movement of the VSC determine the shape of the tip. A stationary VSC releases vesicles that reach the cell surface in about equal numbers in all directions, and the cell grow as a sphere. Any displacement of the VSC from its original central position distorts the spherical shape. A sustained linear displacement of the VSC generates the typical cylindroids shape of fungal hyphae. The model yields the equation:

$$y = x \cot (V. x / N), (I)$$

which defines both the shape and size (diameter) of a hypha by two parameters: N, the amount of wall-destined vesicles released from the VSC per unit time; V, the rate

of linear displacement of the VSC. The ratio N / V defines a parameter in a hypha: the distance (d) between the VSC and the apical wall. Equation (I) becomes:

$$y = x \cot (x / d), \text{ (II)}$$

The value d can be calculated from published micrographs with two measurements: (i) the diameter of the hyphae at any given point and (ii) the distance of this point from the hyphal tip. The d value was used to plot curves as shown in Figure 2.6 which coincides with the originally marked position of the Spitzenkörper (Spk).

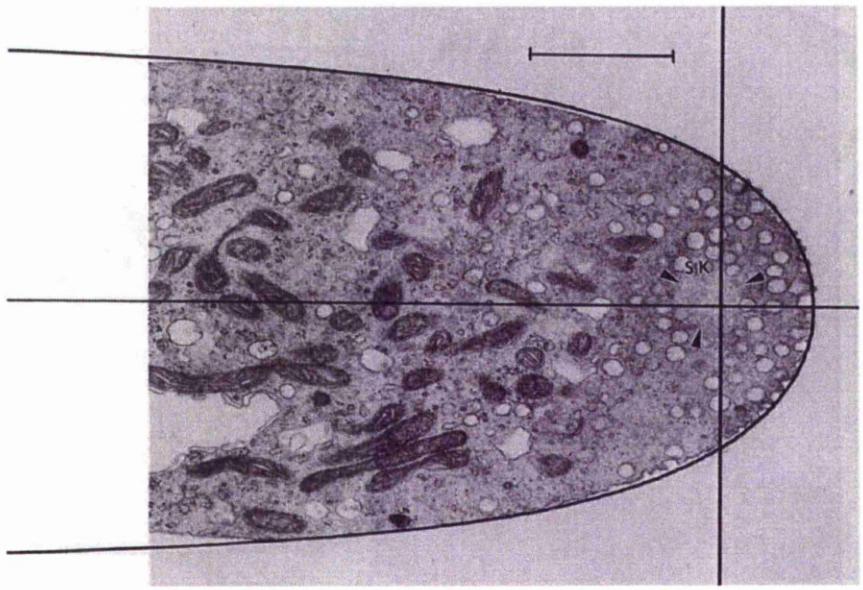

Figure 2.6: Electron microscopic profile of *Armillaria mellea*. There is a close correlation between the VSC (predicted by Equation (I)) and the Spitzenkörper (SK) delineated by the arrows (Bartnicki-Garcia, Hergert et al. 1989). Bar = 1 µm.

Bartnicki-Garcia et al. confirmed that the linear displacement of a VSC gives hyphae a cylindrical shape by testing the hyphoid model on the fungus *Rhizoctonia solani* (Bartnicki-Garcia, Bartnicki et al. 1995). The similarity of profiles between the living hypha and the computer-generated simulation of hyphal morphogenesis supports the

idea that the Spitzenkörper is the structural and functional equivalent of the hypothetical VSC. The work by Reynaga-Pena on apical branching in *Aspergillus niger*, supports the hypothesis that the Spitzenkörper acts as a VSC and coordinates the movement of wall-building vesicles (Reynaga-Peña, Gierz et al. 1997).

Mechanisms of polarized growth are maintained by cytoskeletal function and directed exocytotic events. The importance of the cytoskeleton in hyphal morphogenesis is well established (Bartnicki-Garcia 2002). Microtubules are primarily responsible for long-distance transport of secretory vesicles to the Spitzenkörper while actin microfilaments primarily control the organization of the vesicle within the Spitzenkörper as well as transport to the plasma membrane. Immunolocalization studies and phalloidin staining have shown the presence of actin in the Spitzenkörper and at the hyphal apex (Bourett, Howard 1991, Srinivasan, Vargas et al. 1996, Virag, Griffiths 2004). TEM data suggest that the Spitzenkörper may function as a microfilament-organizing center. The γ-tubulin, which is normally associated with a "microtubule organizing center" (MTOC) was immunolocalized within the Spitzenkörper of *Allomyces macrogynus* (McDaniel, Roberson 2000). For now no γ-tubulin was found in the Spitzenkörper of higher fungi.

2.2.3 Polarized growths and branching

Branching is the initiation of a new centre of polarized growth resulting in cell extension which is a continuous and indefinite process (Riquelme, Fischer et al. 2003). This is why fungi are able to exploit and colonize new substrates. The process includes establishment of polarity then its maintenance. Establishment of polarity means that a spot is chosen for germ tube emergence from a spore and branch emergence from a hypha. Polarity maintenance depends on materials and machinery for making new plasma membrane and cell wall because these are responsible for germ tube emergence, apical extension and septation (Harris, Momany 2004, Harris, Read et al. 2005).

The two distinctive features of filamentous fungi are branching and tip growth (Heath 1995). Filamentous fungi have the ability to extend over long distances because they branch regularly and maintain a fixed growth direction (Riquelme, Reynaga-Peña et al. 1998). The apical cells are generally engaged in nutrient acquisition and sensing of the surrounding environment, whereas sub-apical cells are involved in the formation of new filaments by branching. Fungi exhibit two different branching patterns. When a branch appears at the tip, the branching pattern is called apical or dichotomous branching. This could be triggered by perturbations that slow extension of hyphal tips without interrupting the flow of exocytic vesicles through the cytoplasm. The abnormal accumulation of vesicles leads to the formation of a new tip (Katz, Goldstein et al. 1972, Trinci 1974). In lateral branching, new branches appear behind the growing tip. Work by Riquelme and Bartnicki-Garcia, 2004 distinguished lateral branches from apical branching in *Neurospora crassa*. Lateral branching seems to be associated with the presence of a Spitzenkörper at the branch site, whereas apical branching is linked to the loss of the Spitzenkörper at the hyphal tip. Lateral branching occurs only far from the tip; this is consistent with the fact that the hyphal tip does not allow branch formation and exhibit a phenomenon called apical dominance (Schmid, Harold 1988, Semighini, Harris 2008). The mycelium organization would otherwise be disturbed with uncontrolled branching patterns.

Two models have been presented that could explain how the selection of branching sites occurs - "The septum as a barrier" (Trinci, 1978) and the "spontaneous polarization model" described in *S. cerevisiae* (Wedlich-Soldner, Altschuler et al. 2003, Altschuler, Angenent et al. 2008). In the former model, new branches emerge adjacent to septa which serve as a barrier that provoke an accumulation of exocytic vesicles. In the latter model, lateral branching is characterized by the apparent absence of an association between septation and branching. The branching site could in this case result by the stochastic accumulation of vesicles at a cortical site.

In order to understand the molecular basis needed for tip growth and branch formation, efforts have been based on cytological, ultrastructural and genetic approaches, which include the use of branching mutants. Actin and calcium seem to

play a role in the process (Heath 1995, Grinberg, Heath 1997, Hyde, Heath 1997) as well as tip growth vesicles (Bartnicki-Garcia, Hergert et al. 1989, Trinci 1974, Prosser, Trinci 1979). In *Neurospora crassa* more than 100 loci were found to have an effect on branching and tip growth. Watters, Griffiths 2001, Watters, Humphries et al. 2000, Watters, Virag et al. 2001 studied these mechanisms in *Neurospora crassa* by studying their dependence on temperature and nutrient concentration and also presented a model for lateral branch initiation. The model showed that a branch is initiated when the concentration of vesicles that accumulate at the tip reaches a certain threshold.

2.2.4 Sensing the environment (tropism)

Living organisms sense and respond to the environment. The process is divided into three steps: reception, transduction and response pathways. The external stimuli are converted into molecular signals. Fungi sense their environment; they can sense light, gases, chemicals and surfaces (Bahn, Xue et al. 2007). Research shows the ability of hyphae to change their growth direction (tropism) in response to external stimuli, such as electrical fields or topographical cues. Thigmotropism is a movement in which an organism moves or grows in response to touch or contact stimuli. This behaviour is observed in some plant-pathogen fungi. It has been suggested that stretch activated (SA) ion channels may be involved in the process. For example in *Uromyces*, SA channels seem to be involved in the sensing of substrate topography and induction of appressorium formation (Zhou, Stumpf et al. 1991, Hoch, Staples et al. 1987). A similar study with *C. albicans* showed less response from hyphae to the surface in presence of an SA channel inhibitor (Watts 1998). *Aspergillus niger,* a soil filamentous fungus, did not show thigmotropism under normal conditions. Bowen et al. studied the factors that induced such a response in hyphae through topographical cues and nutrient availability (Bowen, Davidson et al. 2007). The sensitivity of the thigmotropic response appeared to increase under low nutrient conditions and caused a deflection of the hyphal apex to the right or the left. The work showed as well that the extreme hyphal tip became insensitive to any topographical variations in a 60 ° arc. The best studied sensory areas are phototropism and chemical-signalling

processes (Herrera-Estrella, Horwitz 2007). Light provides fungi with information about orientation and spore dispersal.

2.2.5 The filamentous fungus used in this thesis

Armillaria mellea

Armillaria species is a common plant pathogenic Basidiomycete, which causes white rot in both hardwoods and softwoods (Fox, 2000). Many *Armillaria* species are tree pathogens and their biology, genetics and ecology are well known. The genus comprises at least 40 species, which differ in their pathogenicity (Bruhn 1998, Mwenje, Ride 1996). Previous studies focussing on their molecular genetics aimed to investigate secondary metabolites related to the species' virulence (Misiek, Hoffmeister 2008). Such studies are important because *A. mellea* causes economic loss in many countries and is responsible for damage in native or managed forests. It is important to investigate the properties of this species to know how the genus *Armillaria* interacts with its environment.

A particular feature of this species is that it forms rhizomorphs (aggregation of thousands of hyphae). *A. mellea* hyphae infect their host through the bark of the roots and coalesce to form larger and structured assemblages called rhizomorphs that spread and invade other trees. These linear structures are larger and more robust than individual hyphae and have been developed for long distance transport of water and nutrients. Rhizomorphs are 1 to 3 mm in diameter and look like shoestring. Rhizomorphs have been studied extensively and have a high level of connection and form networks. This structure enable the species to exploit efficiently the opportunities provided within its environment (Lamour, Termorshuizen et al. 2007). Rhizomorphs branch monopodially or dichotomously and the growth habit has been related to the species' virulence (Morrison 2004). Work by Solla et al., 2002 looking at penetration behaviour of the roots of *Picea sitchensis* tree by two different *Armillaria* species and *Heterobasidion annosum* has been carried out (Solla, Tomlinson et al. 2002) showing that there are variations in host tree susceptibility toward the different species. *H. annosum* cannot penetrate the bark of the root

without any wounding whereas the *Armillaria* species are able to infect directly the root of the *Picea*. The reasons for these observations are unclear. It is possible that the rhytidome of some gymnosperms prevents or does not stimulate the formation of rhizomorphs (Wahlström, Johansson 1992). Such work will provide a better understanding of host responses to root-invading pathogens, which is useful in the tree cultivation field because the ability to detect and understand resistance in certain type of trees will provide material for incorporation into tree breeding programmes. *Armillaria mellea* is responsible for damage and economic loss due to its characteristics such as virulence as well as its ability to colonize substrates and produce rhizomorphs.

The behaviour of A. mellea as a tree pathogen

Armillaria assembles hyphae into rhizomorphs which slowly aggregate into huge networks. Rhizomorphs sprout the white fan-shaped mats of mycelium which extend the decay up an infected tree's phloem and cambium, separating the wood from the bark, killing the host, and thus encouraging wind-throw. The majority of rhizomorphs are produced during the terminal stages of decay but their amount depends on the species and the habitat. Ions and other substances in solution are absorbed and translocated along these rhizomorphs under turgor pressure. When *A. mellea* rhizomorphs penetrate roots, they process as organized units, growing through the phloem and the cambium. Once the tip of a rhizomorph has reached this point, mycelium produced from the tips of the rhizomorph invades into the wood radially along the plates of the parenchyma ray cells.

Healthy roots can be infected directly if they contact the mycelium on diseased roots. Infection depends on the enzymes and toxins produced by the mycelium breaking down the host tissue to allow invasion and infection. After a rot has been established, providing there is a sufficiently large food base, the mycelium may persist for many years. Infection of a healthy root begins when its bark is acted upon by toxic substances produced by the mycelium. Hyphae also grow down inside the trunk, often spreading between the ray cells, rotting, softening and weakening the heartwood of its host's roots and butt. The species is naturally bioluminescent.

2.3 Application of microtechnology for the control of cells

Microtechnology is the fabrication of materials, structures and systems with micron or submicron-scale features using lithography techniques (Madou 1997). Lithography is the process of producing features on a substrate (silicon or glass) using energy sources like UV light, laser, electron-beam, or X-ray. The development of physical techniques enables the manipulation, isolation, growth and study of single cells and multicellular structures. In this section the application of microtechnology for studying cells and microorganisms control and behaviour over flat and profiled surfaces is discussed.

2.3.1 Spatial control over Cells on flat surfaces

Neuronal and glia cells

Microlithography refers to lithographic patterning methods capable of structuring features in the micrometer range or smaller. Photolithography is one of these methods. For patterning cells, photolithography on hard materials has been widely used. Through this technique, micropatterns are generated using light, photoresist, and mask.

Kleinfeld, Kahler et al. (1988) studied the control and growth of dissociated neurons on a surface with defined regions. They combined silane chemistry and lithographic processing to modify the adhesive properties of the substrate. They succeed in reproducing normal neuronal development on abiotic surfaces.

The use of microlithography which is the most dynamic semiconductor technology and experimental biomedical sciences has lead to the development of biomicrotechnologies. Nicolau, Taguchi et al. (1996) assessed several microlithographic materials and techniques as candidates for patterning artificial arrays of neuronal cells. The neuronal cell's electrical activity makes it an ideal candidate for integration in a bioelectronic device. They showed how the surface photochemistry of the common microlithographic materials can be used to control

the specificity of the neuronal cell attachment on the polymer surfaces. They obtained different surface functionalities like diazo-naphto-quinone (DNQ), carboxylic, imidazole, indene, silylated, and charged groups as well as different hydrophobicities. The neuronal cell attachment was sensitive to chemical functionalization, with favourable influence from charged, imidazole and carboxylic groups. In 1998, they demonstrated how the microlithographic materials and techniques can be upgraded to print patterns of proteins, peptides and silylated surfaces as scaffolds for the selective control of artificial arrays of neuronal and glia cells.

The interaction of neuronal cells with artificial materials in order to control their biomolecular architectures on surfaces has application to several bioengineering fields like biosensing, cell guidance, and molecular electronics.

Mammalian cells

Photolithography has been used for patterning proteins and cells onto surfaces but the technique has some disadvantages for biological applications like biocompatibility. Xia and Whitesides (1999) developed a set of techniques more suitable for biological applications called "soft lithography". Soft lithographic techniques mostly used polydimethylsiloxane (PDMS) because this polymer is biocompatible. These microfabrication techniques typically use variations in charge, hydrophilicity, or chemistry to select the adhesion of cells to a substrate. Thus the combination of surface chemistry and photolithographic techniques enable a better understanding of the influence of the material on the behaviour of the cells. Many studies that involved the patterning of proteins or cells have used self-assembled monolayers (SAMs) of alkanethiols on gold. PDMS is used as a stamp to transfer microscale patterns of chemicals or biomolecules onto the substrate surface. One of the tools of soft lithography is microcontact printing. Microcontact printing has been used to understand the effect of cell shape on cell growth, function, and death to surface modifications. To do so, some regions of the surface are made chemically different to have a selective adhesion of cells to a given substrate.

For example, Singhvi, Kumar et al. (1994) placed cells in adhesive laminin protein-coated islands to have a control over cell growth and protein secretion. The surface was successively exposed to an alkanethiolate that support protein adsorption then to laminin, a protein that belongs to the extracellular matrix (ECM). The system was tested by the plating of rat hepatocytes. The quantification of DNA synthesis in hepatocytes cultured on islands of different size revealed that the synthesis of DNA was highest in cells on unpatterned surfaces. Cells located within the islands revealed that the progressive reduction of the size of the islands resulted in a progressive reduction in growth. The authors showed that it was possible to control the switch between growth and differentiation.

Chen, Mrksich et al. (1998) used microcontact printing techniques to create different islands of patterned substrates with regions that absorb the extracellular matrix and regions that resist extracellular matrix adsorption. They explored how position and shape of bovine and human capillary cells can be modulated by these islands. The spreading of the cells depends on the islands' size and on the distance between different islands. The authors showed as well that cells with a round shape induce cell suicide and cell spreading permit life. They concluded that there is evidence that cell shape itself may act as a signal for cell function.

A direct application of microfabrication and cell culture is the development of cell-based biosensors for the detection and characterization of drugs, toxicants, odorants and other chemicals.

Bacteria

The attachment and patterning of bacterial cells on surfaces offer the possibility of using the cells as a biosensor for sensing and detecting biomolecules. The system is used as well for studying cell-cell interactions and the interactions between the cells and their surrounding environment.

For instance Liang, Smith et al. (2000) used self-assembly of alkyl silane monolayers (SAMs) and optical tweezers to measure the force of adhesion between

uropathogenic *Escherichia coli* cells expressing type I pili and a mannose-presenting SAM. The combination of SAMs and optical tweezer enable the characterisation of microbial adhesion in terms of specific molecular interactions. Bacterial adhesion through biofilm formation occurs on medical devices which lead to patient infections. Katsikogianni, Missirlis (2010) investigated the effect of the surface chemistry and the solution ionic strength under different shear rates on the adhesion and growth of two *S. epidermidis* strains. Adhesion was found to be dependent on the monolayer's terminal functionality. The increase in ionic strength enhanced adhesion to various substrates.

2.3.2 Spatial control over Cells on profiled surfaces

Fungi and bacteria

Fungal pathogens can penetrate plants either through an intact host surface or through natural openings such as stomata. Germ tubes of rust fungi produce appressoria which are terminal swellings when they are in contact with plant stomata. Appressorium induction leads to the formation of infection structures. Microfabrication enables the fabrication of surfaces with different topography that will help investigate the role of the host topographical signals in the induction of appressoria.

Read, Kellock et al. (1997) used a silicon wafer to create microtopographies in polystyrene. They investigated more precisely the influence of ridge spacing and height on the induction of infection by *P. graminis tritici* and *P. hordei*. Closely spaced ridges induced germ tubes differentiation. In a similar way Hoch, Staples et al. (1987) showed that the bean rust fungus *Uromyces appendiculatus* is able to sense minute difference in leaf surface topography in order to infect the host plant.

Held et al. (2009) used artificial microstructures to test the dynamic responses of *Neurospora crassa*, a filamentous fungus and *Escherichia coli* a Gram-negative bacterium. The structures were made from PDMS and consist of 5 x 5 arrays of microstructures (cylindrical and micropyramids) varying in size and density. The

fungi invaded the nutrient poor areas and did not avoid the microstructures. They observed that the cylindrical structures could confine and guide hyphal growth whereas micropyramids induced a slightly different behaviour. The hyphae attached to the edges and corners of the pyramidal bases and were seen to grow up to the apex so that *N. crassa* sensed its environment. The authors concluded that this particular behaviour was induced by the geometry, distance, and density of the features. The micropyramids also modified *E. coli* swimming behaviour. *E. coli* fixed to the pyramids through its flagellum thus changing the traditional run and tumble motion into a circular motion. This observation could lead to a means of studying the rotary motors of motile bacteria away from a surface without any interference from surface attractions.

Mammalian cells

Mammalian cells respond to topographic substrates which are known as contact guidance. In the native environment, contact guidance is essential in the processes of cell migration, proliferation, differentiation, and apoptosis and is profoundly influenced by the extracellular matrix (ECM). The ECM is composed of several glycosaminoglycans. Micro and nanofabrication make it possible to fabricate substrates similar to the native environment of the cells and enable the study of the cell's response.

Cells types are sensitive to the topographic substrate and respond in different ways depending on the feature size, the geometry (Flemming, Murphy et al. 1999) or the substrate stiffness (Discher, Janmey et al. 2005). The most notable effect of topography is the impact on cell geometry. The geometry of the topography as well as the size of the features affects the morphology, attachment, adhesion, proliferation, cytoskeleton organization and migration of the cells.

Cells respond to nano-grating geometries (narrow groove of different shapes) by aligning and elongating in the direction of the grating axis. This has been observed in various cell types such as for example human fibroblasts, human endothelial cells, human embryonic stem cells or bovine smooth muscle cells (Choi, Hagvall et al.

2007, Bettinger, Zhang et al. 2008, Gerecht, Bettinger et al. 2007, Yim, Reano et al. 2005). Some studies have observed the alignment of cells both parallel and orthogonal to the nanogratings axis (Teixeira, McKie et al. 2006). Some cells do not respond at all to nanogratings (Meyle, Gültig et al. 1995).

Cells respond in a different manner to nanogratings, nanopost and nanopit features for example it has been showed that in general nanogratings enhanced the adhesion of cells (Teixeira, Abrams et al. 2003, Karuri, Liliensiek et al. 2004) while nanoposts and nanopits reduce the initial cell attachment of for example rat fibroblasts (Curtis, Casey et al. 2001) and human osteoblasts (Biggs, Richards et al. 2007).

Nanogratings make the cell proliferation rates decrease as shown for human endothelial cells (Bettinger, Zhang et al. 2008). There are no real rules concerning nanoposts or nanopits and their effect on cell proliferation. Cell migration is affected by nanogratings. For example endothelial cells (Bettinger, Zhang et al. 2008), epithelial cells (Dalton, Walboomers et al. 2001, Rajnicek, Foubister et al. 2007), osteoblast cells (Lenhert, Meier et al. 2005), and C6 glioma cells (Wang, Ohlin et al. 2008) moved toward the features with higher velocities.

Engineering substrates has the potential to induce cell phenotype but also cell genotype. Nanotopography is known to alter the gene expression profile of various cell types. For instance human fibroblasts express a higher level of fibronectin mRNA due to contact with titanium nanogratings geometries (Chou, Firth et al. 1995). Contact with nanopits resulted in down-regulation of many fibroblasts genes including those associated with apoptotic initiation, DNA repair, and transcription regulation (Dalby, Gadegaard et al. 2008).

2.4 Microfluidics

Microfluidics deals with the behaviour, precise control and manipulation of fluids that are geometrically constrained to a small (sub-millimetre) scale. Microfluidics systems have application in chemical, biological and medical fields.

2.4.1 Behaviour of fluids at the microscale

Microfluidics offers advantages given by miniaturization that include smaller working volumes, shorter reaction times and the possibility of performing parallel experiments. At this particular scale, different physical phenomena become dominant over those experienced in everyday life (Lee, Hung et al. 2005). The viscous forces dominate over the inertial forces so the fluid transport systems move to the regime of viscous dominated flow, turbulence is non-existent, surface tension becomes a powerful force, and diffusion becomes the basic method for mixing. All these fundamental changes in hydrodynamics occur when the Reynolds number (Re) is very small ($Re << 1$). The Reynolds number can be calculated by:

$$Re = \rho \upsilon Dh / \mu,$$

where ρ is the fluid density, υ is the characteristic velocity of the fluid, μ is the fluid viscosity, and Dh is the hydraulic diameter. At $Re << 1$, diffusion can be calculated by:

$$D = d^2 / 2t$$

d is the distance a particle moves in a time t, and D is the diffusion coefficient of the particle. Because distance varies with the square power, diffusion becomes very important on the microscale. At sizes above a few hundred microns, diffusion is very slow and can be ignored. The time to mix by diffusion is:

$$t = l^2 / D,$$

where l is the largest size of the container.

The surface tension forces at the microscale are important and are the result of the cohesion between liquid molecules at the liquid/gas interface. The surface tension (γ) is the magnitude F of the force per unit length L over which the force acts:

$$\gamma = F / L$$

The pressure (ΔP) contained within a spherical drop of liquid is:

$$\Delta P = 2\gamma / R,$$

where R is the radius of the spherical drop. If the surface is hydrophobic, then ΔP is the pressure one needs to overcome the surface tension to fill the microchannels. By treating a surface to be hydrophilic, water will penetrate without any applied pressure.

2.4.2 Fabrications of microfluidic devices

The current techniques that have been used for fabricating microfluidic devices include micromachining, soft lithography, embossing, *in situ* construction, injection molding, and laser ablation. For biological applications, the more suitable technique is soft lithography which was developed by Whitesides, Otsuni et al. (2001).

Soft lithography is a set of non-photolithographic techniques for microfabrication, based on printing and molding using elastomeric stamps with the patterns of interest. The central component most widely used in soft lithography is poly(dimethylsiloxane) (PDMS). Polymers are the materials of choice for microfluidic devices because of their properties of low cost, flexibility and light propagation. The polymer is poured onto a hard master and then peeled off the master to create channels, valves and, chambers. When the PDMS stamp is sealed against a piece of glass or PDMS for example it creates a three-dimensional network of channels that can be filled with any liquid medium.

Fabrication of the master by rapid prototyping

To build a microfluidic chip by soft lithography (Duffy, McDonald et al. 1998, McDonald, Duffy et al. 2000), involves drawing the desired design with a CAD tool

(computer-aided design). The photomask is created and placed over a substrate (silicon wafer or glass) that is precoated with a thin layer of photoresist (see below). When exposed to UV light, the photoresist will harden only in areas patterned on the mask, and the rest will wash away with a developer, leaving a master pattern for polymer (Figure 2.7-A).

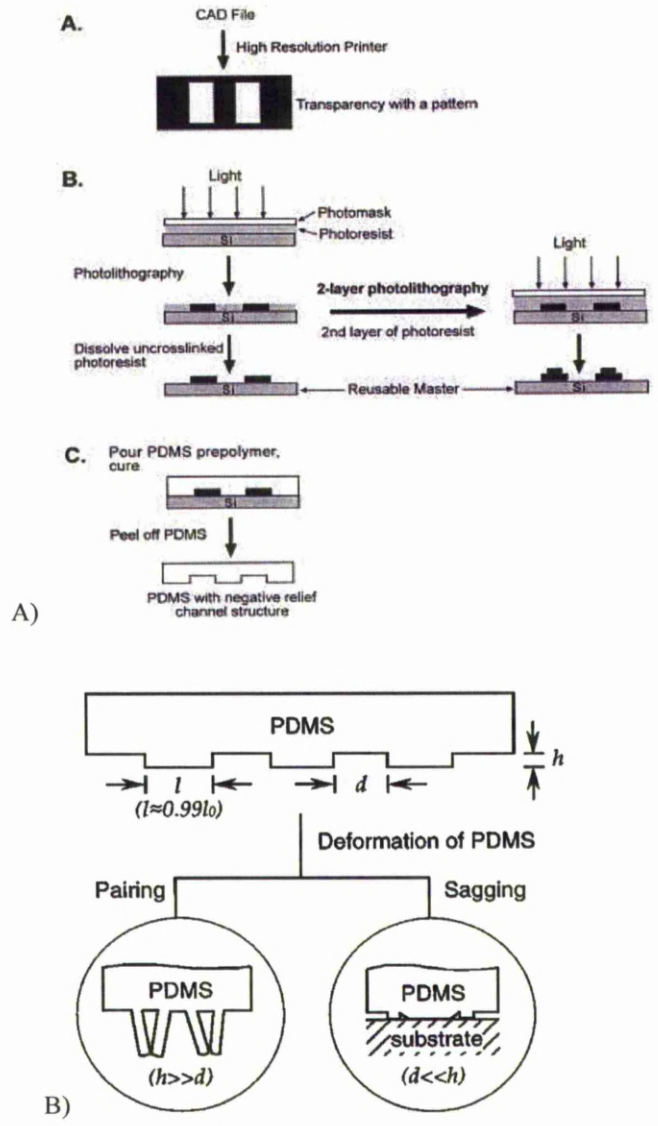

Figure 2.7: A): Fabrication of the master and the PDMS stamp. A: Steps for rapid prototyping, B: fabrication of a master, C: replica molding of microfluidic systems (Stroock, Whitesides 2002). B): The representative ranges of values for the dimensions h, d, and l are 0.2 – 20, 0.5 – 200, and 0.5 – 200 μm, respectively (Xia, Whitesides 1998).

Fabrication of silicon mold by DRIE (Deep Reactive Ion Etching)

In order to produce a piece of polymer with features in it, a mold that contains the inverse pattern of the final product is required. For mold application, various materials have been employed. Among these materials, silicon has been highly characterised. Currently there are two methods to construct silicon molds. The first method is wet anisotropic etching and the second method is deep reactive ion etching (DRIE). DRIE through the so-called Bosch process is a powerful tool to realize deep etching with vertical sidewalls (Laermer, Urban 2003).

Cast Moulding: fabrication of PDMS stamps

The elastomeric stamp or mold is prepared by cast molding (Whitesides, Ostuni et al. 2001). By cast moulding a master can produce about 50 PDMS stamps. It becomes very easy to replicate micro or nanoscale features accurately over a large area as well as reducing the damage to the master. By this procedure it is possible to obtain multiple copies of three-dimensional features from one master. The PDMS slab can be further used for replicating the structure in another material (replica moulding); it can be used directly as microchambers or patterning cells on a surface. Replica moulding is a technique for duplicating the shape, size and pattern of features from an elastomeric master (usually PDMS) in one single step.

2.4.3 Physical and Chemical properties of PDMS

PDMS is a silicone-type elastomer that consists of repeating $-OSi(CH_3)_2-$ units; the CH_3 groups make the surface hydrophobic (Stroock, Whitesides 2002). Industrial synthesis can begin from dimethylchlorosilane and water by the following net reaction: $n[Si(CH_3)_2Cl_2] + n[H_2O]$. The surface can be made hydrophilic by exposure to air plasma for a couple of minutes to oxidize the surface to silanol (Si-OH) (Makamba, Kim et al. 2003). The surface remains hydrophilic in contact with water otherwise, rearrangements occur approximately within 30 minutes when in contact with air. Prior to the addition of any liquid the PDMS must be rendered hydrophilic by exposure to UV light. For instance oxidized PDMS sealed against oxidized glass form irreversible Si-O-Si bonds between the layers.

PDMS is cheap, easy to produce and manipulate. PDMS is not only seen as a structural material but possesses useful properties for biological studies like the use of small volumes of reagents, solvents or cells at a low cost, short reaction times and the possibility to carry out multiple operations at the same time (Kuncová-Kallio, Kallio 2006). The fabrication of PDMS is easy and it is not time-consuming. It can be cast against a mold with fidelity down to 0.1 μm and it has interesting physical and chemical properties (Xia, Whitesides 1998);

1. The surface of PDMS has a low interfacial free energy and a good chemical stability. The patterned molecules do adhere reversibly and do not react chemically with the surface.
2. The PDMS is not hydroscopic thus it does not swell with humidity.
3. The PDMS is gas permeable.
4. The elastomer has a good thermal stability up to 186 °C. At high temperatures, PDMS acts like a viscous liquid, similar to honey. However at low temperatures it acts like an elastic solid, similar to rubber. In other words, if you leave some PDMS on a surface overnight, it will flow to cover the surface and mold to any surface imperfections.
5. The elastomer is optically transparent down to ~300 nm.
6. The PDMS elastomer is isotropic and homogeneous and can be deformed in controllable manner. The PDMS stamp can be reused over several months.
7. The interfacial properties of PDMS can be changed either by changing the prepolymers or by treating the surface with plasma.
8. Another very interesting property is that PDMS is inert and nontoxic. Such properties make PDMS suitable material for work with living cells.

The limitations of using PDMS are;

1. The PDMS shrinks by ~1 % upon curing. The cured PDMS can swell in some nonpolar organic solvents like toluene and hexane.

2. The elasticity and thermal expansion of PDMS make it difficult to get high accuracy in registration across a large area and may limit the use of soft lithography in multilayer fabrication and/or nanofabrication.
3. When the aspect ratio (h/l) (Figure 1.7-B) is too high or too low, the elastomeric character of PDMS will cause the microstructures in PDMS to deform or distort and generate defects in pattern.
4. The oxidized PDMS is unstable in air and returns to the hydrophobic state after ~30 min.

Various PDMS fluids ranging from low to high viscosity are used in a wide range of industrial applications, such as manufacturing textiles, paper, and leather goods (Noll 1968). PDMS fluids also serve as antifoams, softeners, or water repellents. In consumer applications, PDMS fluids can be found in personal-, household- and automotive care products (Noll 1968). They are used as softeners in skin care products, conditioners in hair care, additives in polish formulations, water proofers and as a component of other surface treatments. Some PDMS materials are also sold as end products such as transformer dielectric fluids and heat transfer liquids.

2.4.4 Applications of microfluidic devices

Soft lithography is a technique for fabricating channels and patterns which are appropriate for the manipulation of living cells at the micron/submicron scale (Whitesides, Ostuni et al. 2001). Here the emphasis is made on the application of microfluidics and PDMS in the study of cell behaviour.

Stem cells

Stem cells are special cells that can differentiate into different cell types (Ramalho-Santos, Willenbring 2007). The growth, death, differentiation and migration of stem cells are dependent on environmental cues. Once a stem cell has received physico-chemical signals to differentiate, a number of gene and protein expression occurs. In conventional cell culture, the environment is not controllable and does not mimic the *in vivo* one. The ability to control the microenvironment is fundamental for

identifying factors involved in cell proliferation and differentiation. 3D microfluidic devices can provide a stable and predictable microenvironment for the cells.

In the area of cell differentiation, the effect of physical and chemical factors on stem cells has been recently investigated using microfluidic systems. For example Metallo et al. (2008) applied physiological levels of shear stress to hESC-derived endothelial cells and showed that the physical stimuli can induce changes in cell morphology and gene expression. The shear forces the cells to elongate and align in the direction of the flow by modulating gene expression (Metallo, Vodyanik et al. 2008). By using a microfluidic device that is able to control the extracellular environment of cells in chambers Ellison et al. (2009) showed the existence of unknown survival factors in mouse embryonic stem cells (Ellison, Munden et al. 2009).

Neurons

In neurological research, the ability to culture neurons on microchips is becoming an important diagnostic tool. One limitation is that neural cells do not survive at low concentration which makes the isolation and observation of individual cells difficult. The high permeability of PDMS to molecular exchange makes this polymer a valuable tool in work involving neural cells. Griscom, Degenaar et al. (2002) grew neurons in arrays of micro chambers, connected through microfluidics channels made of glass and PDMS. This method allowed the patterning of physically isolated neurons and the growth of axons in preferential directions due to confinement. The thickness of the PDMS still allows chemical interaction between the cells so they are able to survive. The thickness of the PDMS isolated the cells electrically. Neurons are cells that need extracellular signals at different phases of their development. Another use of microfluidics is to study the response of neurons to different signals. Gomez, Schmidt et al. (2007) used microfabrication and PDMS to create cross-shaped wells. They aimed to simultaneously analyze the responses of neurons to physical and chemical cues.

C. elegans

Microfluidics devices were found to be a valuable tool to study *Caenorhabditis elegans,* a nematode worm with a nervous system of only 302 neurons. *C. elegans* is a model organism for neurobiology studies. The advantage of using such a simple organism is that the role of each cell in the neural pathway can be determined. The substrate commonly used in *C. elegans* research is a planar agarose surface, which is different from the natural environment where the worm is found. Natural environments include soil, compost, leaf and fruit litter, and several invertebrate hosts. The advantages brought by microfluidics devices to *C. elegans* studies are that they can mimic properties of the natural environment that in turn make possible behavioural studies. The forms and the trajectories in the devices can also be controlled and the extra-cellular environment such as temperature or various stimuli can be manipulated. The polymer PDMS is also compatible with high magnification microscope objectives observations.

Lockery, Lawton et al. (2008) presented two micron-scale devices. An artificial soil device mimicking soil particules and a sinuous microfluidic channel with a variety of amplitudes and wavelengths. The worm was shown crawling with ease through both devices. Qin, Wheeler (2006) observed the exploration capability of a group of worms in mazes with and without the presence of food as well as the effects of dopamine on exploration. Dopamine is a neurotransmitter involved in motion and learning. In a second set of experiments they investigated the correlation between the food search and learning process in individual worms. Park, Hwang et al. (2008) studied *C. elegans* locomotion in microstructures made from agar and the role of mechanosensation in the movement through the proposed media.

Fungi: exploration of microfluidics networks

Microfabricated surfaces have been used to understand signal perception effects by fungi. The use of surfaces that induce signals perceived by fungal cells makes available the study of fungal growth orientation and fungal penetration (Hoch, Staples et al. 1987). In this work microstructured networks were used to observe the behaviour of fungal cells in confined environments. In nature, filamentous fungi

colonise microscale media such as decaying wood, soil, leaf litters, plant and animal tissues, which are a "natural" maze. Confinement has effects on fungal cells and the resulting behaviour is a consequence of how fungi sense and develop strategies within confined natural environments. In their natural habitat, filamentous fungi's activity affects the local environment around their hyphae at the micrometer scale. The fact that their environment is highly heterogeneous makes the study of fungal growth difficult. Fungal growth behaviour is still not fully understood and has been extensively studied mainly on planar agar substrates, where cells exhibit a different behaviour compared to that occurring in natural environments. Filamentous fungi have to explore irregular surfaces or grow through porous media and have to adapt to different external conditions like temperature, light, humidity.

A number of researchers have investigated the behaviour of microorganisms in complex PDMS networks, for example (Hanson et al. 2006) and (Held et al. 2010) described the growth and colonization of microfabricated structures by several fungal species. They showed how the fungal species responded to the topography by changing their branching behaviour. Studying bacterial behaviour within complex geometries as well as their accumulation near boundaries is of great interest from a simulation point of view.

Previous work has been published on fungal growth in mazes. Nakagaki (2001) observed the maze solving capabilities of the amoeba-like true slime mould *Physarum polycephalum* which is a unicellular organism and is able to solve complex mazes relatively easily (Nakagaki 2001, Nakagaki, Yamada et al. 2001, Nakagaki, Yamada et al. 2000). Hanson observed the maze solving capabilities of *Pycnoporus cinnabarinus* in artificial structures (Hanson, Nicolau Jr et al. 2006, Filipponi, Hanson et al. 2005a). This work highlighted interesting observations. The fungus was able to find the entry of the maze and resolve it easily. This is extraordinary because when seeking food, starving hyphae have a random search whereas in this study the fungus converged toward the maze entrance and grew inside the microchannels. The branching rate was much higher and near-exclusively triggered by tip to wall collisions of the parent hypha with obstacles. The species

seems to possess a "directional memory" in the confined environment; the hypha turn by collision with an obstacle but in the exact direction that they had when they branched from the parents filaments. The growth of the species has been simulated.

Bacteria

Microfluidics associated to PDMS has many characteristics that make it useful for the study of bacterial motility, chemotaxis and quorum sensing. The channels can be created to mimic the natural environment of bacterial cells and the extra-cellular environment can be varied. DiLuzio, Turner et al. (2005) studied the motility of *E. coli* in channels in which the porosity of the channel surfaces changed. Bacteria prefer hydrogel surfaces and swim preferentially at the right hand-side because of the clockwise rotation of the cell body. Hulme, DiLuzio et al. (2008) developed a system to sort motile strains of bacteria based on cell length. The authors showed that ratcheting microchannels can control the direction of movement of swimming cells that swam in different directions.

Microfluidics is also useful for chemotaxis assays. It is possible to create gradients that are stable. Mao, Cremer et al. (2003) studied the concentration gradients of chemorepellants and chemoattractants at the nM level. They discovered that L-leucine is a bacterial chemoattractant at low concentrations and a repellent at high concentrations.

Bacterial cells communicate by secreting soluble molecules in the surrounding environment. When the density of bacterial cells reaches a certain level; these molecules alter the expression of bacterial genes. This behaviour is called quorum sensing and is involved in bioluminescence, swarming motility, pathogenicity and biofilm formation. Park, Wolanin et al. (2003) studied the growth of *E. coli* and *Vibrio harveyi* in PDMS microfluidic devices. Cells of *E. coli* accumulated in enclosed areas like dead-ends. The authors concluded that chemotaxis between cells is able to produce the density of cells required for quorum sensing.

Chapter 3

Materials and Methods

3.1 Preparation of the test microstructures

3.1.1 Descriptions of the silicon master and the different microstructures

A silicon mold was prepared by standard photolithography techniques and deep reactive ion etching (DRIE) using the standard Bosch recipe (Hanson, Nicolau Jr et al. 2006). The silicon master contained six different patterned areas. Each area was 1mm x 1mm and consisted of 25 small 100 μm x 100 μm microfluidic structures (Figure 3.1). The small microfluidics structures are intercalated with 100 μm x 100 μm spaces called 'plaza'-like spaces. The channels in the microstructures were 2 μm to 15 μm wide, allowing microbial growth and spread on the surface (fungal filaments are up to 10 μm wide whereas bacterial cells measure 0.5 to 0.8 μm in diameter). All the mazes were fabricated using polydimethylsiloxane (PDMS; Sylgard 184, Dow-Corning) and produced by replica molding of PDMS from the silicon master.

The mazes represent original structures with different designs and some of them have different features (square, round features or dead ends). All of them have different levels of complexity. The different structures have a channel depth of 10 μm (Figure 3.2).

Diamond (Figure 3.2, A): The *Diamond* structure consisted of a structure made of 16 small squares for which there are many paths to the exit. The exit is situated opposite the entrance.

Round-about (Figure 3.2, B): Within the *Round-about* structure, the cells have to follow sequentially two rounded structures and there are two possibilities for entry into the first round-about. The structure showed the ability of the species to follow rounded features and to perform turns of up to 135 °. There are two round-about features placed in opposite directions. The round-about maze was the only one that required circular paths.

Cellular (Figure 3.2, C): The *Cellular* structure consisted of a main path in the middle and a lateral path with different angles of ± 30 °, 45 °, 60 ° and 90 ° respectively. Many paths lead to the exit and the structure tested the cells' ability to turn at different angles. This is different from the other mazes, where features are right-angled.

Small Maze (Figure 3.2, D): The *Small maze* comprised some right-angled features but also some small roundabout ones as well as some features with a rounded tip/extremity. The channels were very narrow ~ 5 μm. In this maze different paths lead to the exit.

Stripe (Figure 3.2, E): The *Stripe* structure consisted of parallel channels decreasing in width from 10μm to 2 μm. The impact of the variation in width of the channels can be observed in parallel.

Big maze (Figure 3.2, F): The *Big maze* structure has a much larger edge length (1 mm) than the previous structures and the channels are 15 μm wide. This maze is more complicate than the other structures and contains numerous dead ends and corners where the cells can be trapped.

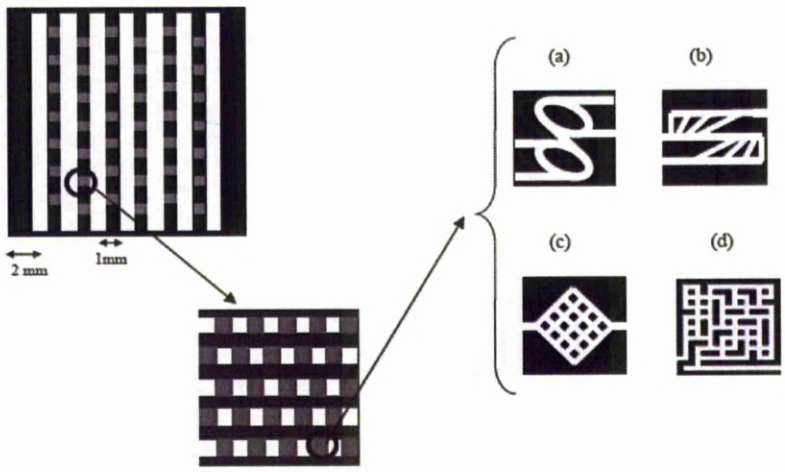

A)

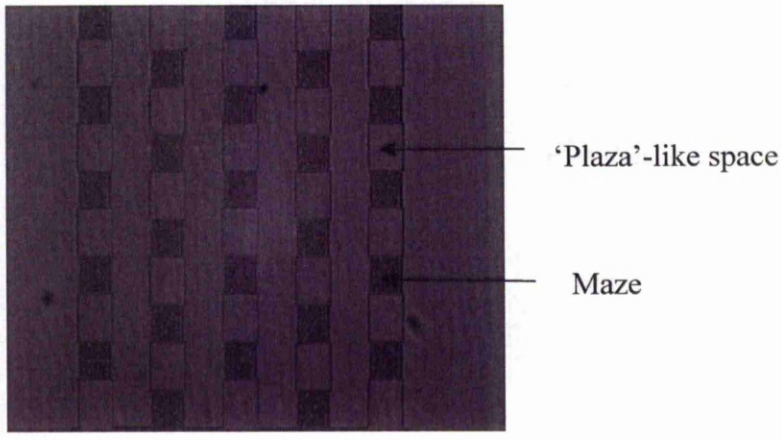

B)

Figure 3.1: A): The silicon master and the small microfluidics structures (Filipponi, Hanson et al. 2005b). B): The PDMS stamp.

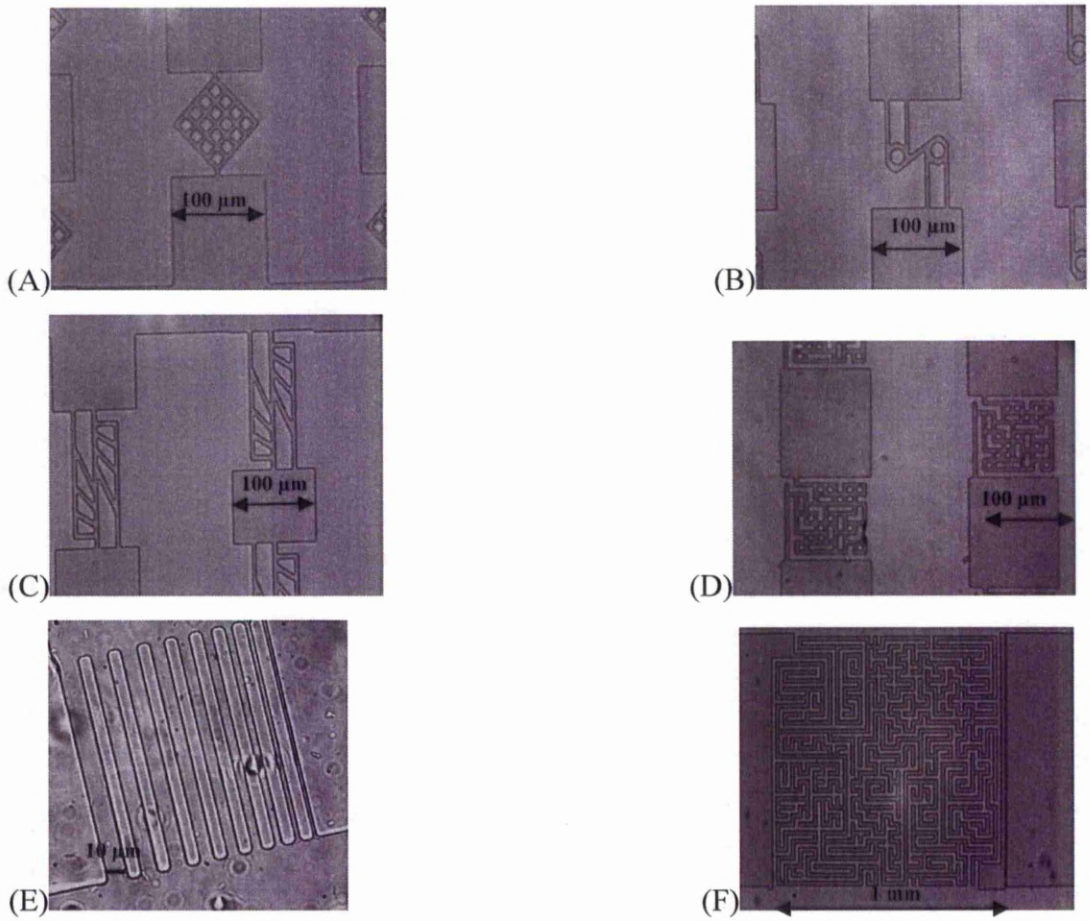

Figure 3.2: The test structures comprise the (A) *Diamond*-like structures, (B) *Round-about* structures, (C) *Cellular* structures, (D) *Small maze* structure, (E) *Stripe* structures and (F) *Big maze* structures.

3.1.2 Preparation of the PDMS mold

Sylgard 184, a Dow Corning Corporation product, is a silicone elastomer kit. The kit contains two chemicals: Base (part A) and Curing Agent (part B), that are mixed in 10:1 mass ratio. Both chemicals are transparent and viscous in nature. The solution was stirred vigorously for 2 minutes with a stir rod. The mixing produced air bubbles that had to be removed by degassing the PDMS under a vacuum for approximately 30 minutes. The PDMS was poured over the master that was placed inside a petri dish within 15 minutes of de-gassing. The mixture was then cured for at least 8 h at 65 °C to complete cross linking and therefore non-toxicity to the cells. Curing for too

long caused the PDMS to become harder and prone to cracking whereas curing for less than the recommended time caused the PDMS to be sticky and floppy. The PDMS was finally peeled off the silicon master and was ready to use.

The silicon masters have a silicon hydroxide layer so the surface is hydrophilic which can be unfavourable for the release of cured PDMS. To prevent the PDMS sticking to the master, the surface of the master was treated with HMDS (1,1,1,3,3,3 – Hexamethyldisilazane). The addition of HMDS on top of the silicon resulted in a hydrophobisation of the surface, and therefore making it easier to peel off (Zen, Neher et al. 2005). The silicon master was heated at approximately 120 °C for 15 to 20 minutes in order to remove the thin water layer from the surface. A few drops of HMDS were dropped into the petri dish. HMDS evaporated and an HMDS atmosphere established in the dish. The heating was switched off and the system cooled down slowly. HMDS precipated as a thin layer on the silicon master surfaces in the petri dish. After cooling down, the master was ready for application of the PDMS.

3.1.3 Cleaning of the silicon master

The cleaning procedure for the silicon masters started with the detachment from the glass petri dish. The sticky tape was soaked with the solvent toluene for several hours. The master could be removed easily. The toluene swells PDMS residues but does not remove them. The masters were rinsed with water and subsequently dried on a hot plate at medium temperature. Hot sulphuric acid (98 %) with a temperature of 80 °C cracked the polymer chains in PDMS and after a few minutes of immersing the masters every residue was removed. The cleaned masters were rinsed gently with deionised water, ethanol and again deionised water. The masters were then dried and kept in a clean glass petri dish.

3.2 Bacterial growth conditions

The *Serratia marcescens and Pseudomonas stutzeri* cultures used for this work were obtained from the School of Biological Sciences, University of Liverpool culture collection.

3.2.1 Obtaining bacterial colonies on agar plates

The nutrient medium used to grow *S. marcescens* and *P. stutzeri* was Luria-Bertani (LB) liquid broth. The nutrient agar medium was obtained by mixing 1 % of LB broth (Becton Dickinson) and 1.5 % of Agar Agar (Merck) with distilled water. Difco LB medium consisted of 0.5 % yeast extract, 1 % tryptone, and 1 % NaCl prepared in deionized H_2O and adjusted to pH 7.2. The solution was sterilised by autoclaving for 15 minutes at 150 °C and after cooling poured into Petri-dishes. Once the agar was set and dry, the plates were ready for use. By streaking an agar plate with a drop of a liquid culture medium, individual bacterial cells could be separated over the surface of the agar and then grown as individual colonies. The Petri dishes with the culture were inverted and placed in the incubator at 30 °C.

3.2.2 Conditions to obtain motile bacteria

3.2.2.1 Motility in Luria-Bertani medium

Cells of *Serratia marcescens* and *Pseudomonas stutzeri* were grown in Luria-Bertani (LB) liquid broth in a round polypropylene tube containing 5 ml of medium with aeration at 30 °C.

In all the experiments described in this thesis, cells were used in their mid-exponential phase of growth which corresponded to an OD_{600} (Optical Density at a wavelength of 600 nm) of 0.6 for *S. marcescens* and 0.5 for *P. stutzeri*. To determine the growth of *S. marcescens* and *P. stutzeri*, cells were grown in Luria-Bertani (LB) liquid broth overnight. The next day cells were re-suspended in fresh LB medium

and diluted to OD_{600} = 0.1. The OD_{600} was then measured every 15 minutes. All absorbance measurements were made with a Beckman model ultraviolet-visible spectrophotometer. The medium became more and more turbid as the bacteria increased in number by division so that less light was transmitted through the tube. The measurement of OD (also called absorbance) is an indirect measurement of cell biomass (alive and dead cells) and is calculated as follow:

$$A = \log_{10} I_0/I$$

A: Absorbance

I_0: Intensity of the light passing through the reference

I: Intensity of the light passing through the sample

3.2.2.2 Motility in viscous medium

Serratia marcescens cells display a swarming phenotype when the cells grow within a viscous environment. In the laboratory the concentration of agar that is required to initiate a swarming phenotype in *S. marcescens* is between 0.7 % and 0.8 %. Conditions that would simulate a restraining environment were created by adding agents such as Ficoll, a polysaccharide polymer that can be used to mimic the viscosity of 0.45 – 0.8 % agar within microstructures. Ficoll 400 (molecular weight [MW] 400,000; Sigma-Aldrich) a polysaccharide polymer was added to LB broth. The viscosity of the final media (1 to 10 cP) used in the experiments was determined by using a TA Instruments Rheolyst AR 1000N controlled-stress rheometer.

3.2.3 Quantification of bacterial colonies, growth rate and generation time

To quantify viable cells a plate count was done. A sample of bacteria was diluted several times in PBS (phosphate buffer) from 10^{-1} to 10^{-8} and 0.1 ml samples of appropriate dilutions spread on to an agar plate. Each viable cell will divide and form a colony on the agar that can be seen with the naked eye. The number of colonies

corresponded to the number of cells present in the sample which were expressed as colony forming units per ml (cfu/ml).

The growth rate was measured as follow:

$$\text{Growth rate (k)} = (\log_{10} X_t - \log_{10} X_0) / (0.301 * (T_t - T_0)),$$

where T_t and T_0 represents the time interval and X_t and X_0, the corresponding absorbance.

The generation time was calculated as follow:

$$\text{Generation time } (T_{gen}) = 1 / k$$

3.2.4 Flagella stain

The protocol used was from West, Burdash et al. (1977) and consisted of the preparation of two solutions. Solution 1, the mordant, was made by mixing 25 ml of a saturated aqueous solution of aluminium potassium sulphate, 50 ml of a 10 % (v/v) tannic acid solution, and 5 % (w/v) ferric chloride solution. Solution 2, the stain, was made of 100 ml of a 5 % (w/v) silver nitrate solution. To 90 ml of silver nitrate, 2 to 4 ml of concentrated ammonium hydroxide were added until the brown precipitate formed disappeared. More silver nitrate was added (2 ml to 20 ml) until a faint cloudiness persisted.

The bacterium grown on LB agar and incubated at 30 °C was smeared on to microscope slides that had been cleaned with ethanol. The smears were air dried and then covered first with solution 1 for 4 min, rinsed gently with distilled water and then covered with solution 2. Heat was applied until steam formed, and the stain remained for 4 min after which the slides were gently rinsed with distilled water and air dried and viewed under the microscope.

3.3 Fungal culture

3.3.1 Fungal strain and culture medium

The *Armillaria mellea* culture used for this work was obtained from the School of Biological Sciences, University of Liverpool culture collection and was maintained on Potato Dextrose Agar (PDA) at 4 °C. *Armillaria mellea* growth medium consisted of 2.4 % potato dextrose broth (PDA - SIGMA) and 1.5 % Agar-Agar (MERCK). Similarly to bacteria, the solution was sterilised by autoclaving for 15 minutes at 150 °C and poured into Petri-dishes. Once the agar had set and dried, the plates are ready to use.

3.3.2 Fungal growth

Armillaria mellea was subcultured onto fresh PDA plates and incubated at 30 °C. The colony needed three to four days to grow on agar plates.

3.4 Experimental assemblies

Just before use, the PDMS structure was treated under UV for approximately one hour to render it hydrophilic and to enable the PDMS to seal the base material, which is a plastic-made petri dish, a piece of PDMS or glass.

For bacterial growth observations, the experimental procedure is illustrated in Figure 3.3 A. *Serratia marcescens* was grown to mid-exponential phase in Luria-Bertani medium. A droplet of cells was loaded directly into the complex geometries made from PDMS through open edges. Prior to inoculation, the structures were filled either with Luria-Bertani (LB) liquid broth or by LB broth containing 3 % to 15 % (v/v) of Ficoll 400 (viscosity at 25 °C of 2 to 10 cP) by placing the samples in a vacuum chamber. To avoid the adhesion of cells to the glass, the addition of a surface-active agent such as bovine serum albumin (BSA) to the broth was necessary.

For fungal growth observations, the experimental procedure is illustrated in Figure 3.3 B. The final experimental assembly consisted of the PDMS structure and 2 pieces of agar placed near the lateral openings; one agar block was inoculated with fungal hyphae. The petri dish or the piece of PDMS formed the floor of the structure whereas the ox-PDMS formed the sidewalls and the ceiling. The colony needed three to four days to reach the open space area of the PDMS after inoculation at room temperature (20 °C to 25 °C). The microstructures were filled with deionised water (dH_2O). The assembly was deposited inside a parafilm-sealed polystyrene petri dish to prevent evaporation of the water and to allow gas exchange.

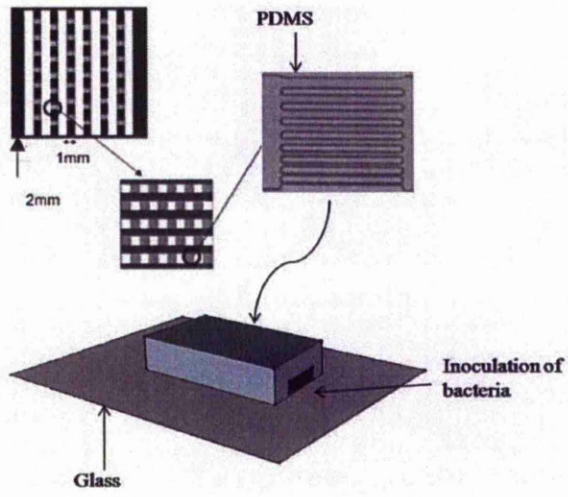

A)

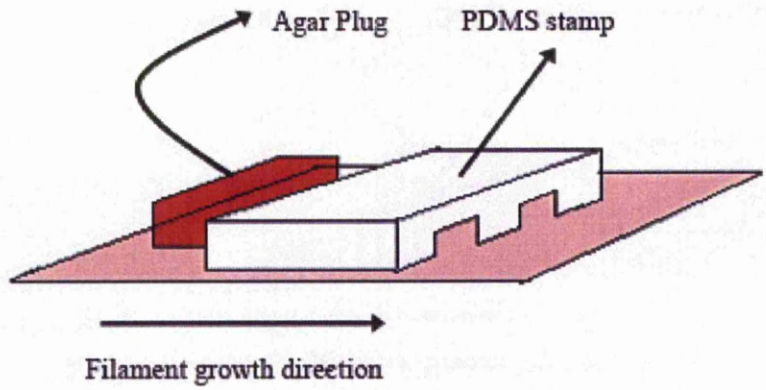

B)

Figure 3.3: A): Experimental assembly for bacterial growth observations. The base was an oxidized glass microscope slide and the sidewalls and ceiling were the oxidized PDMS. 10 to 20 µl of a culture of cells were loaded directly into the PDMS structures through open edges. B): Experimental assembly for fungal growth observations. Representation of the PDMS stamp sealed against a plastic petri dish with a piece of agar (Hanson, Filipponi et al. 2005).

3.5 Data gathering and analysis

3.5.1 Optical systems

To image the population of swimming bacterial cells, the microscope slide containing the PDMS structure was placed on the stage of a Zeiss upright microscope equipped with an Andor iXon EMCCD camera that collected images at 32 frames per second. A Leica DM LB2 upright microscope was also used. The images sequences were taken using the 60x magnifications lens. The microscope was equipped with a Spot camera (Diagnostic Instruments, Inc., USA) that collected images at 5 frames per second.

Hyphal growth was observed with an inverted trinocular microscope (Motic AE21 or Brunel SPI-98) equipped with 25x and 40x magnifications phase contrast objectives and a USB digital camera (Motic 2300 with 3 Megapixel resolutions). Pictures were collected every 2 minutes.

3.5.2 Image processing and data representation

For both work concerning fungal growth and bacterial motility, the tracking of the cells in each frame and the calculation of the cells velocity were performed using RETRAC 2.10.0.5 (http://mc11.mcri.ac.uk/Retrac/index.html) and ImageJ and the plugin MtrackJ. The tracking software enabled information on individual hyphae and on individual bacterial cell to be gathered from a recorded video resulting in individual cell paths. In order to produce videos, pictures were imported into Image-Pro Plus 6.1. For the measurement of the length between 2 branches and hyphal branching angles pictures were imported into "Motic Images Plus 2.0" (Motic China Group Co., Ltd.). For the measurement of the bacterium deflection angle, the calculations were performed as follow:

The calculation of the distance between 2 coordinates (X, Y) is given by the Pythagoras theorem (Figure 3.4-A):

$$(AB)^2 = (Y_2-Y_1)^2 + (X_2-X_1)^2$$
$$(AB) = \sqrt{((Y_2-Y_1)^2 + (X_2-X_1)^2)}$$

The calculation of the deflection angle is given by the cosine theorem (Figure 3.4-B):

$$b^2 = a^2 + c^2 - 2\,ac\,\cos(\beta)$$
$$\beta = \cos^{-1}((a^2 + c^2 - b^2) / 2ac)$$
$$\delta = 180 - \beta = \text{deflection angle}$$

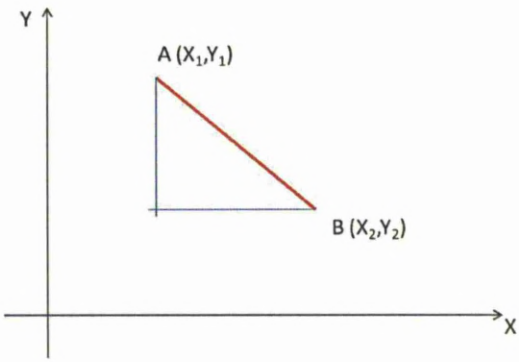

A)

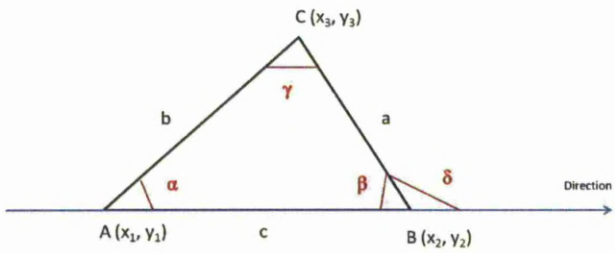

B)

Figure 3.4: A) Representation of the distance between two points (A, B) with the coordinates. B) Representation of the deflection angle or angle δ. The deflection angle is the angle between a straight direction and the direction after a tumble.

To calculate the linear acceleration of an object, the following equation was applied:

$$a = \Delta v / \Delta t,$$

where Δv represents the change in velocity and Δt represents the change in time.

Finally, the frequency distributions were represented using OriginPro8.5.

3.5.3 Statistical analyses

To assess the effect of confinement on fungal growth, statistical analyses were carried out on both groups of data measured on unstructured PDMS and in the confined areas. Changes in branching distances, branching angles and tip extension velocities were analysed as follow. Statistical analyses concerning bacterial motility were carried out by comparing the motility parameters within the 'plaza'-like space to the one measured within the different networks.

Data were tested for normality by evaluation of the 'normal probability plot' in Minitab 15 (Shapiro-Wilk). The 'normal probability plot' is a graphical technique for normality testing: assessing whether or not a data set is approximately normally distributed which is a pre-requisite for applying a Student' *t*-test. The data were tested for equal variances by using *F* procedures. Data sets with obvious deviations from linearity and positively (right) skewed were log transformed to satisfy normality assumption. Normally distributed data (either raw or after log transformation) were compared by using Student' *t*-test procedures with pooled or unpooled variances, as appropriate, based on *F*-tests for equal variances. Not normally distributed data sets where compared by using a Mann-Whitney *U* test.

Throughout the thesis the statistical results were reported by indicating the T-values, P-values (either the exact value or an approximation) and DF, which represent the degree of freedom or P-values only. Significant results were obtained with P-value < 0.05.

Chapter 4

The exploration of complex geometries by the filamentous fungus *Armillaria mellea*

4.1 Introduction

The aim of this chapter is to quantify the growth behaviour of *Armillaria mellea* and to compare it on flat agar surfaces to that in various geometrical confined environments filled with nutrient deficient medium. It is important to obtain an understanding of the growth and function of fungal mycelia in heterogeneous environment in order to develop pathogen control.

Armillaria mellea is a basidiomycete fungus that is well known as an important pathogen of trees, often having lethal consequences. The species is found throughout the world and takes advantage of stresses that affect trees (Guillaumin, Mohammed et al. 1993). It has developed an efficient strategy to invade the bark of major roots. However, *A. mellea* is both a parasite and a saprophyte. The latter lifestyle enables the fungus to reside in soil for many years until the opportunity to invade a healthy tree arises (Rosso, Hansen 1998). *A. mellea* has a unique system for spreading from tree to tree which is called a rhizomorph system. A rhizomorph is an aggregation of hyphae organized into a root-like structure (Lamour, Termorshuizen et al. 2007).

It is difficult to observe growth of fungi in their natural habitat, largely due to the opaque nature of the media. PDMS-based microfluidics enables the fabrication of micro-channels with a variety of forms and shapes that match the physical dimensions of the fungus. Furthermore, it is possible to observe the growth of hyphae directly in these enclosed environments. For instance, pores with diameters in the low micrometre range, filled with a nutrient medium, resemble the body of plant cells within the cell walls; complex and/or periodic channel networks mimic the

apoplast in between the primary cell walls of plants whereas thin membranes mimic a resistance that needs to be overcome by appressoria (Bechinger et al. 1999; Apoga et al. 2004). Fungal exploration and exploitation of complex natural environments requires optimal survival and growth strategies at the colony, hyphal, and intra hyphal level, with hyphal space-searching strategies playing a central role. A new methodology for the characterisation and analysis of hyphal space-searching strategies has been used, which uses purposefully designed three-dimensional microfluidics structures mimicking some of the characteristics of natural environments of the fungi.

Preliminary work on the basidiomycete *Pycnoporus cinnabarinus* (Hanson, Nicolau Jr et al. 2006) and the ascomycete *Neurospora crassa* (Held, Edwards et al. 2009, 2011, Held, Binz et al. 2009) using the same set of microfabricated networks used for this study have highlighted a number of interesting observations that will be discussed in this chapter. The fundamental questions are: what are the space searching strategies used by fungi to successfully colonize various microconfined environments? How do they 'decide' on a course of action? The study of the growth dynamics of *A. mellea* and a comparison with that of *N. crassa* or *P. cinnabarinus* will help to understand if the observable behaviour is generic to all fungi or is species specific.

4.2 Results

A. mellea was first grown on an agar surface where baseline measurements concerning the growth of the species were made. Second, the species was loaded on to a piece of PDMS called unstructured PDMS where it grew to provide a second set of measurements of growth parameters. Finally measurements were made when the species entered different fabricated three dimensional microenvironments to provide information on hyphal growth in different types of microfluidic networks. At each step, the growth pattern was analysed statistically.

4.2.1 *A. mellea* growth behaviour on agar surfaces

In order to investigate the growth characteristics of *A. mellea* on an agar surface, the species was cultured on potato dextrose agar (PDA) and placed on an inverted microscope with video recording capability. The parameters of interest for this section were (i) the branching angles i.e. the angles between the branches emanating laterally from a parent hypha and the parent hypha itself, referred to as lateral angles, and the angles between two apical branches referred to as apical angles, (ii) the branching distance, i.e. the distance between two subsequent branches, and (iii) the apical growth rates, which was the growth velocity of a single hypha at the edge of a colony (Figure 4.1). 60 different hyphae were tracked on different agar plates.

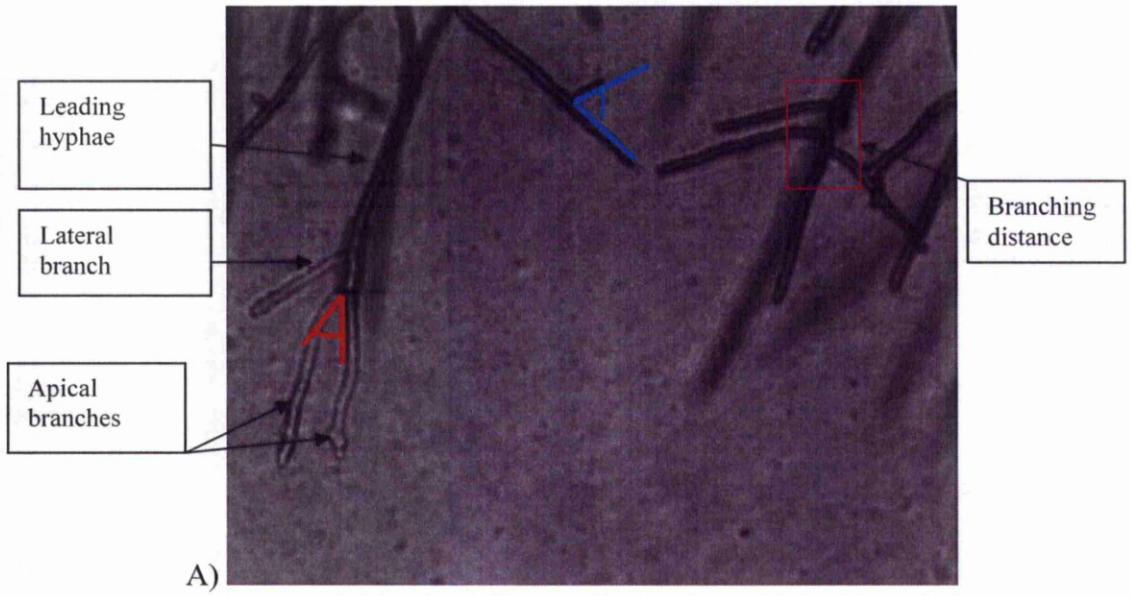

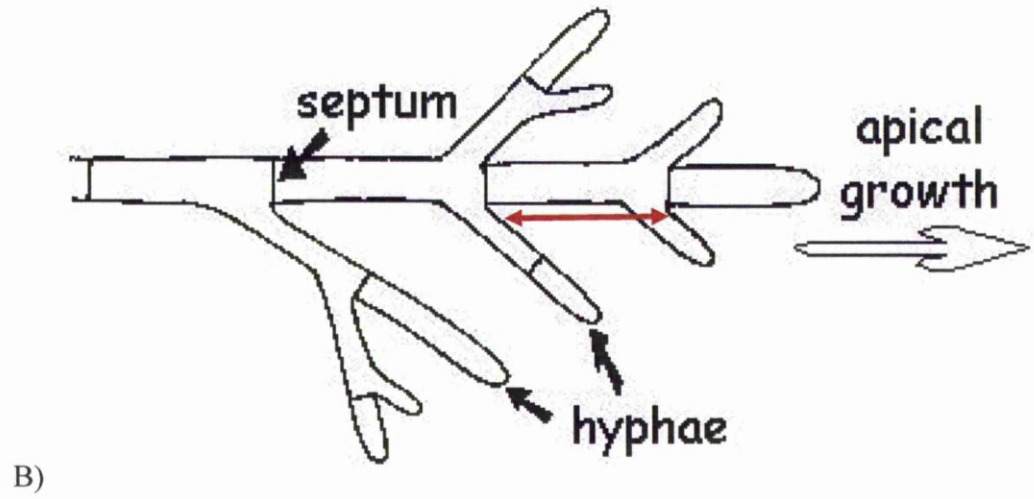

Figure 4.1: A): *Armillaria mellea* growing on a potato dextrose agar plate. The growing parameters are indicated by black arrows. The lateral branching angle was the angle between a lateral branch and the parent hyphae (blue lines). The apical angle was the angle between two apical branches (red lines). The apical growth rates were calculated from the overall change in length of each filament. The branching distance was the distance between two consecutive lateral branches (red box in Figure A) and red arrow in the cartoon (© Vicki Tariq, 2011) in Figure B). The Figure A) was taken at the growing edge of the mycelium (25x magnification).

Table 4.1 summaries the measured growth parameters and Figure 4.2 represents the distributions of the different growth parameters observed on agar. *A. mellea* branched periodically. Typically, two types of branch formations were observed during the growth of *A. mellea* on agar. Apical branching was characterized by the formation of an equal pair of new tips at the hyphal apex. The distribution of the apical angles is irregular with two peaks at around 40 ° and 85 °. The mean apical angle was 56.3 ± 19.0 °. The second type of branching was lateral branching. Lateral branches begin to emerge behind the growing tip, rendering the newly formed branch clearly distinguishable from the parent hyphae. The majority of the lateral branches emerge at angles ranging from 30 ° to 90 °. The mean lateral branching angle was 55.9 ± 20.6 °. Apical branches occurred less frequently than lateral branches. On the nutrient-rich surface of agar substrates, hyphal growth was dense and individual hyphae were often difficult to distinguish. It appears that the distribution of the branching distances is positively skewed with a mean of 40.3 ± 28.6 μm. The hyphae of *A. mellea* maintained fixed growth directions with the polarization axes determined at the respective branching points. The tip extension velocity data were symmetric and normally distributed. The mean tip extension velocity was 0.017 ± 0.006 μm/s. The diameter of individual hyphae ranged between 3 μm and 5 μm.

	Branching angle (°)		Branching distance (μm)	Tip extension velocity (μm/s)
	Apical	Lateral		
Average	56.3	55.9	40.3	0.017
Maximum value	88.8	97.9	117.2	0.039
Minimum value	33.1	17.5	5	0.002
Standard deviation	19.0	20.6	28.6	0.006
Median	48.1	56.5	28.9	0.017
Number of values	13	75	42	2156

Table 4.1: Descriptive statistics of the growth parameters of *A. mellea* growing on agar substrates.

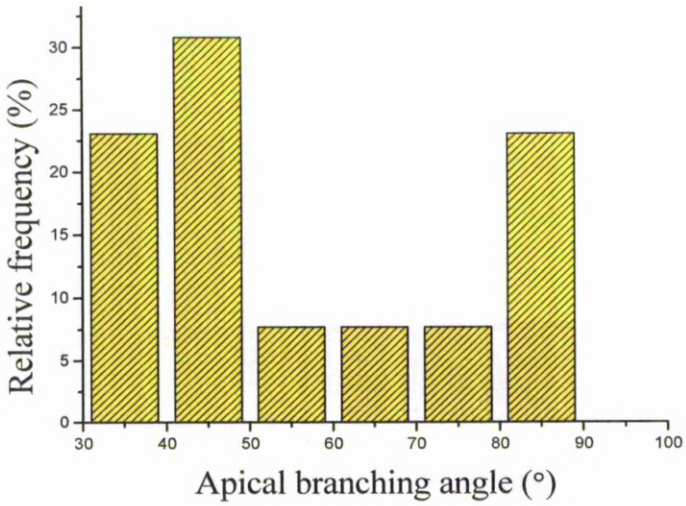
Relative frequency (%)
0
5
10
15
20
25
30
30
40
50
60
70
80
90
100
Apical branching angle (°)

A)

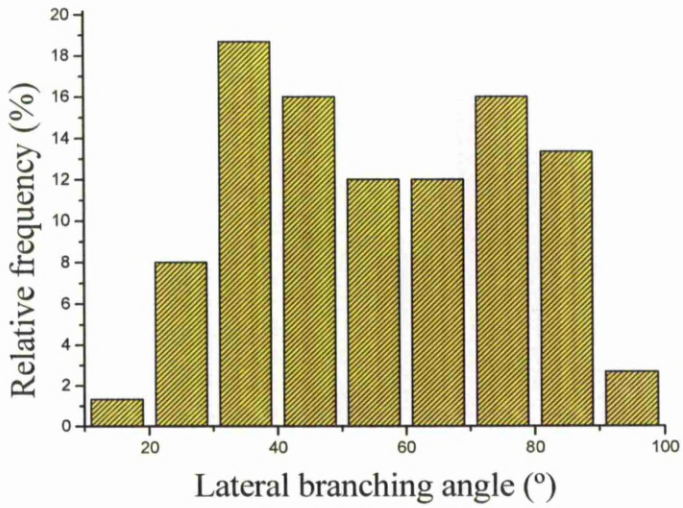
Relative frequency (%)
0
2
4
6
8
10
12
14
16
18
20
20
40
60
80
100
Lateral branching angle (°)

B)

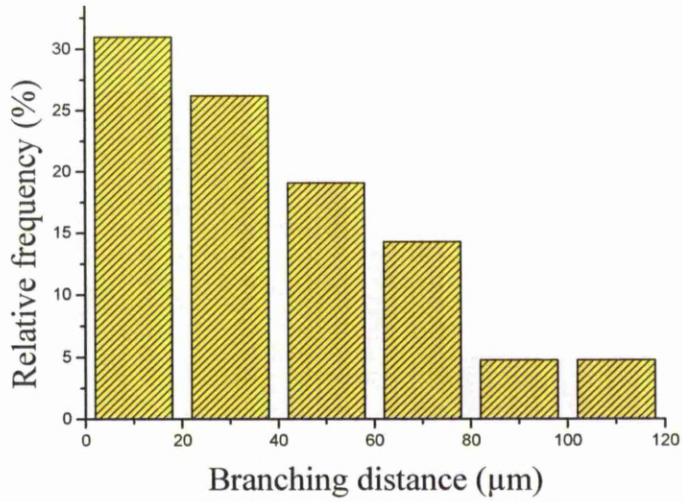

C)

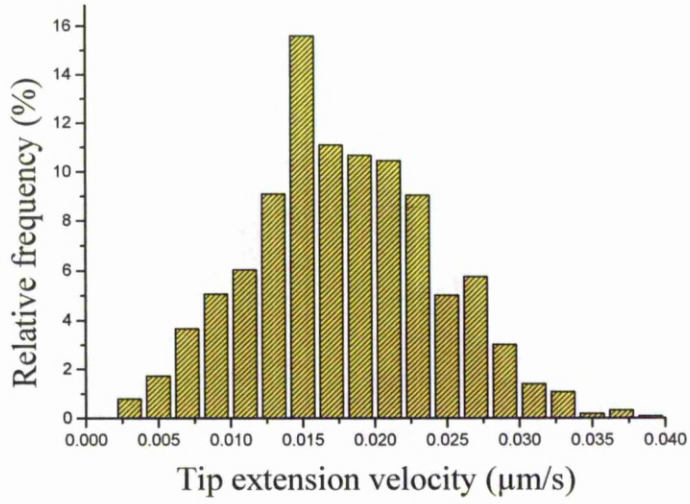

D)

Figure 4.2: Distributions of A) apical branching angles; B) lateral branching angles with fitted binomal distribution; C) branching distances; D) tip extension velocities with fitted normal distribution measured for hyphae of *A. mellea* growing on PDA.

4.2.2 *A. mellea* growth behaviour on unstructured PDMS

In order to investigate the exploratory behaviour of *A. mellea* on unstructured PDMS and within a given set of mazes, a piece of hydrophilic PDMS was sealed to a microscope slide and placed in a Petri dish. Sterile distilled water was used to fill the microstructures in order to suppress directional clues. A piece of agar containing the growing mycelium was placed near the lateral entry (see chapter 3 section 3.4). The Petri dish was then placed on an inverted microscope with video recording capability for further analysis as mentioned previously. The parameters studied in this section were the branching angles, the distance between two branches and the hyphal growth rate.

The growth patterns on unstructured PDMS were measured just before the filaments entered the microstructured areas so the surface was flat and obstacle free. As on agar surfaces lateral and dichotomous branching angles were seen during the growth of *A. mellea* on unstructured PDMS (Figure 4.3). 149 different hyphae were tracked in this environment.

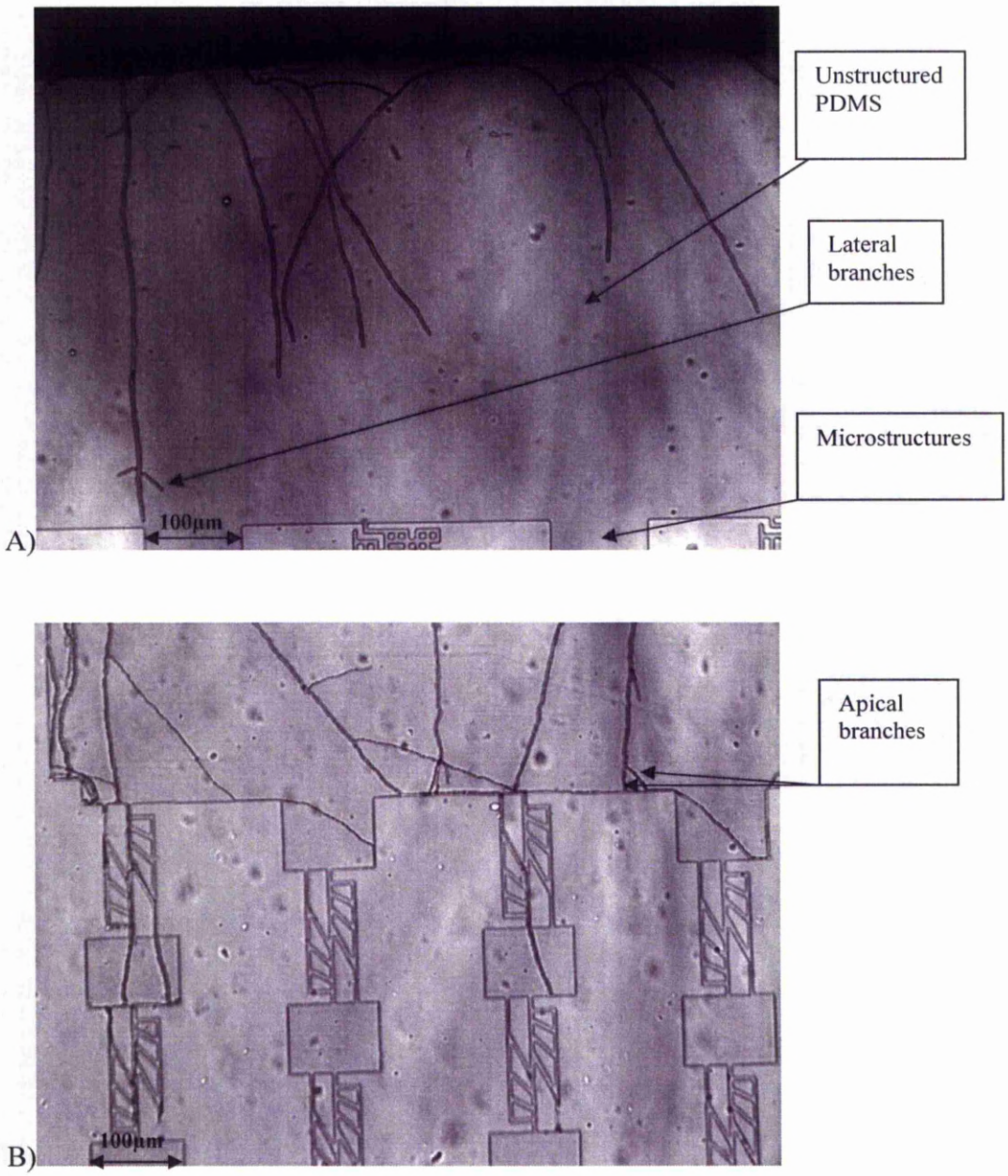

Figure 4.3: (A and B): Effects of unstructured PDMS on growth of *A. mellea* - the two pictures show the area located just before the networks (here the *Small mazes* (A) and the *Cellular* (B) networks) where data concerning growth parameters were collected (25x magnification).

The hyphae branched significantly less while growing along the PDMS surface giving rise to a network of filaments less dense than on agar substrates. Table 4.2 summaries the measured growth parameters and Figure 4.4 shows the distributions of the different growth parameters on unstructured PDMS. The distribution of the apical branching data is negatively skewed with most of the measurement clustered around 90 °. The lateral branching data were normally distributed (P-value = 0.096). The mean apical branching angle and the mean lateral branching angle on this nutrient-free surface were 60.0 ± 26.9 ° and 60.3 ± 19.0 ° respectively. In general, the newly branched hyphae did not maintain their initial growth direction and after a couple of micrometers redirected their growth closer to the leading hyphae. The distribution of the branching distance shows a single peak around 10 μm. The mean branching distance was 31.8 ± 28.7 μm. A right-skewed distribution was found for the tip extension velocity data. The mean tip extension velocity was 0.010 ± 0.006 μm/s.

	Branching angle (°)		Branching distance (μm)	Tip extension velocity (μm/s)
	Apical	Lateral		
Average	60.0	60.3	31.8	0.010
Maximum value	98.4	99.7	101.6	0.024
Minimum value	10.1	23.5	3	0.001
Standard deviation	26.9	19.0	28.7	0.006
Median	62.0	53.4	17.3	0.009
Number of values	12	72	38	3573

Table 4.2: Descriptive statistics of the growth parameters of *A. mellea* growing on unstructured PDMS.

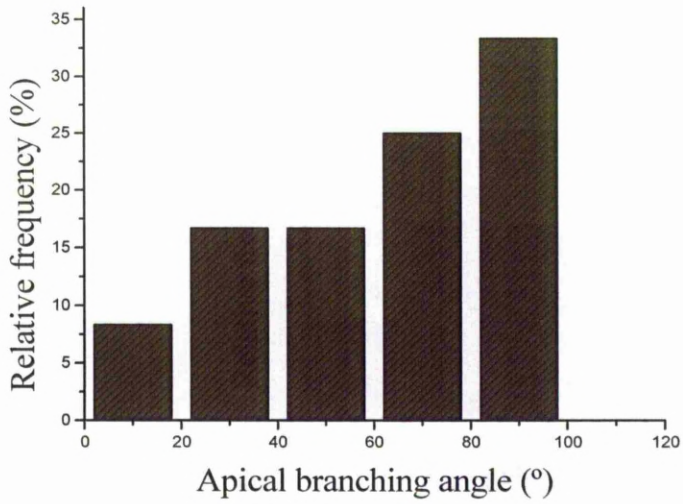
Relative frequency (%)
0
5
10
15
20
25
30
35
0
20
40
60
80
100
120
Apical branching angle (°)

A)

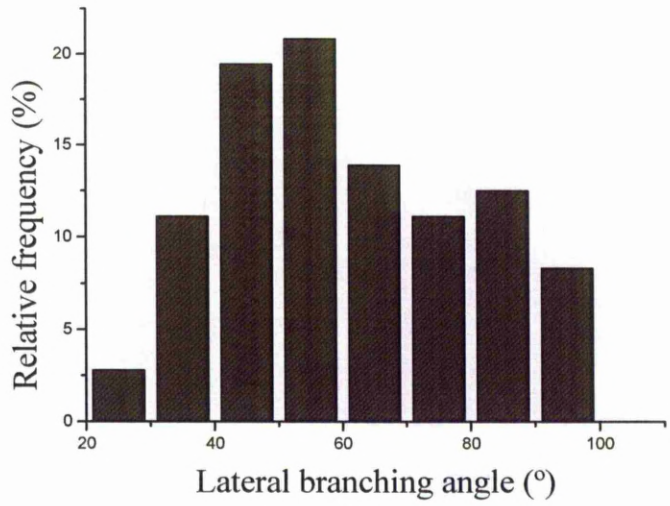
Relative frequency (%)
0
5
10
15
20
20
40
60
80
100
Lateral branching angle (°)

B)

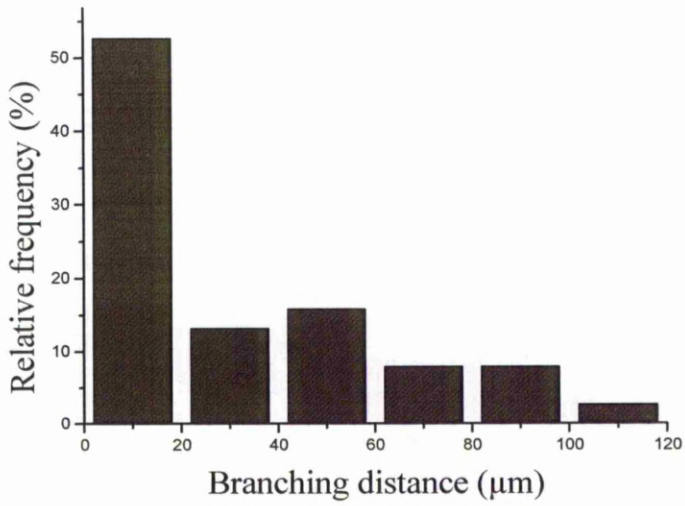

C)

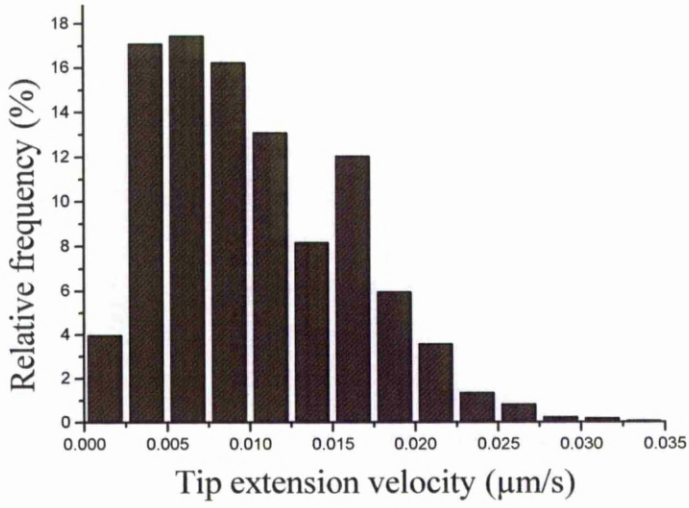

D)

Figure 4.4: Distributions of A) apical branching angles; B) lateral branching angles with fitted normal distribution; C) branching distances; D) tip extension velocities with fitted normal distribution measured for hyphae of *A. mellea* growing on unstructured PDMS.

The effects of unstructured PDMS on the fungus behaviour were evaluated statistically (P-value < 0.05). Student t-test was chosen for normally distributed data. Non-normally distributed data were compared using a Mann-Whitney test. The

statistical analysis shows that this environment had no significant effects on the apical branching angles (P-value = 0.64, Mann-Whitney test) and the lateral branching angles (T-value = -1.34, P-value = 0.18, DF = 145, two-tailed pooled Student's *t*-test) in comparison to the agar surface. The PDMS environment had a significant effect on the filament extension rates (T-value = 45.67, P-value < 0.01, DF = 3992, two-tailed unpooled Student's *t*-test) and the branching distances (P-value < 0.01, Mann-Whitney test).

4.2.3 Characteristics of growth in the microfluidics network

In the microfluidics structures, the fungus grew within an environment made from PDMS. PDMS is both optically transparent and gas permeable so the fungus remained visible and viable. The fungus was enclosed in three-dimensional structures filled with dH_2O. Tip extension velocity, hyphal branching and the distance between two successive branches were measured when the hyphae entered the patterned areas until the exit, as defined for each network. Additionally the measurable growth parameters included the ratio between the number of hyphae exiting the network *versus* the total number of hyphae that entered the network initially and the ratio between the numbers of networks without branching *versus* the numbers of networks with branching for each network.

The aim was to understand the exploratory behaviour of the species and to determine the extent to which this artificial habitat affected the growth of *A. mellea*. To do so, the effects of confinement on *A. mellea*'s growth behaviour were evaluated statistically. The data concerning "confinement" were the data from all tested microstructured networks (*Small maze*, *Diamond*, *Round-about* and *Cellular*) whereas the data concerning "non-confinement" were the ones measured on unstructured PDMS. An appropriate statistical test was performed focusing on the different parameters: the tip extension velocity, the branching angle and the branching distance. The results in this section are presented for a variety of networks.

4.2.3.1 *Small maze* network

The *Small maze* contains a large density of features of different shapes, which provokes frequent collisions between the obstacles and the hyphal tips. The channel widths were approximately 5 µm and similar to the hyphal diameter (Figure 3.6). A total of 49 different hyphae out of 27 networks were observed within the *Small maze* networks.

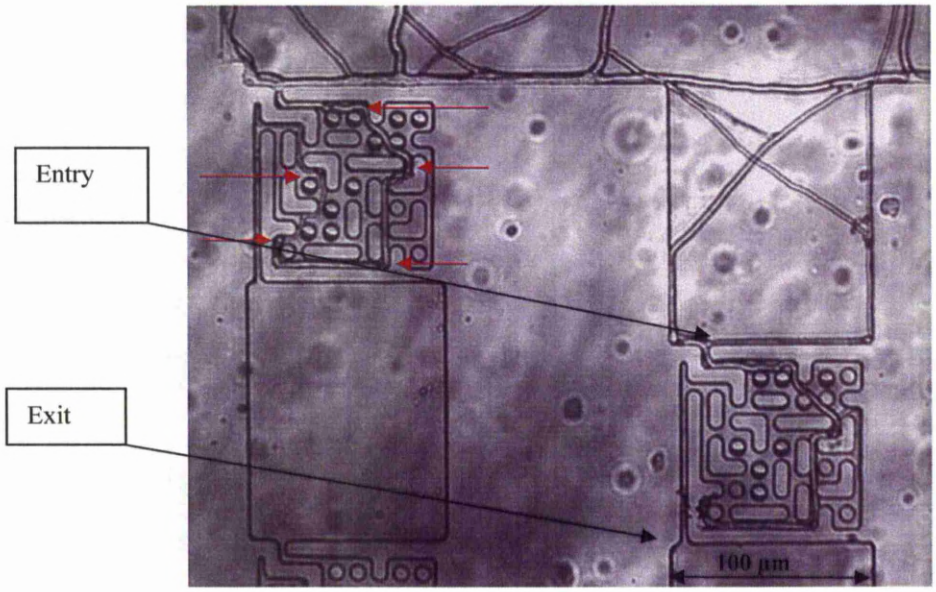

Figure 4.6: Hyphae growing within the *Small maze* networks, (40x magnification). The red arrows, in the left upper network, indicate the flexibility of the hyphae within the networks. Instead of stopping its apical extension, the hyphae continued to extend apically, causing hyphal bending.

A. mellea navigated the *Small maze* network successfully, i.e., one or more hyphae were able to reach the entry of a network, grow inside and exit the network as delimited in Figure 4.6. Within the network, the hyphae were passively directed in the direction of the exit through apical extension after contact with the confining walls. Within the *Small maze* network, the hyphae could navigate along different paths in order to reach the exit. However, the species resolved the mazes always in a similar way and using similar paths as illustrated in Figure 4.6, suggesting a growth algorithm. The confinement suppressed the 'spontaneous' branching events in this

maze and branching events were rare. In case a hypha hits an obstacle it splits into two hyphae that emanate from the collision point trying to grow around the obstacle. The species branched only after "tip-to-wall" collisions. Table 4.3 summaries the growing parameters and Figure 4.7 presents the corresponding histograms. The distribution of the branching angles showed a single peak centered on 95 °. The mean branching angle was 90.7 ± 18.4 °. The branching angles were about 30 ° to 40 ° larger than observed in open spaces (the mean branching angle on unstructured PDMS was about 60 °). The features influenced the branching angle, rendering it close to orthogonal. After the parent hypha hit the wall and initiated a branching event the second branch appeared either within the next two minutes or after a significant delay of ~20 minutes. The ratio of the number of branches that appeared shortly after the collision *versus* after a significant delay was 0.40 (2:5). The ratio of number of networks without branching events *versus* number of networks with branching events was 2.86 (20:7). The branching distance distribution was positively skewed. The mean branching distance was 52.2 ± 57.1 µm. The distribution determined for the tip extension velocity is uniform and fitted a normal distribution. The mean tip extension velocity was 0.009 ± 0.005 µm/s. This rate was the result of discontinued growth through the maze due to corner collisions.

	Branching angle (°)	Branching distance (µm)	Tip extension velocity (µm/s)
Average	90.7	52.2	0.009
Maximum value	126	204.6	0.029
Minimum value	62.9	6.2	0.001
Standard deviation	18.4	57.1	0.005
Median	91.0	35.0	0.009
Number of values	11	10	1563

Table 4.3: Descriptive statistics of the growth parameters of *A. mellea* growing within the *Small maze* network.

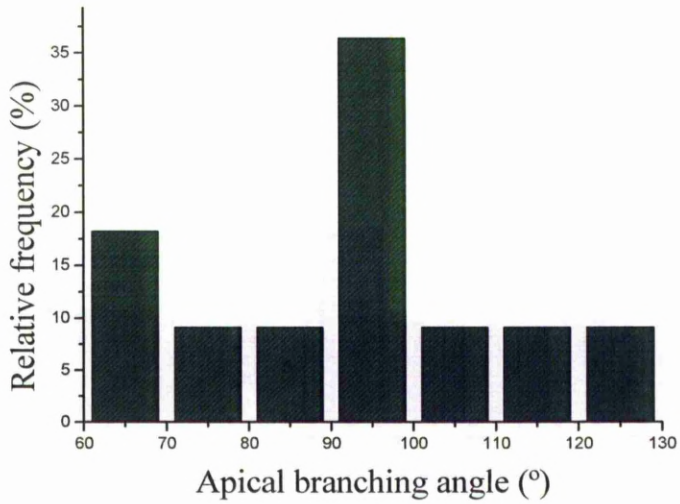
Relative frequency (%)
0
5
10
15
20
25
30
35
60
70
80
90
100
110
120
130
Apical branching angle (°)

A)

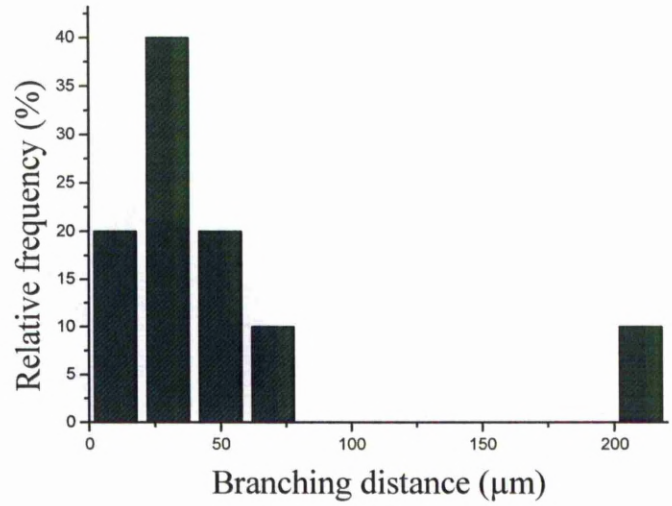
Relative frequency (%)
0
5
10
15
20
25
30
35
40
0
50
100
150
200
Branching distance (μm)

B)

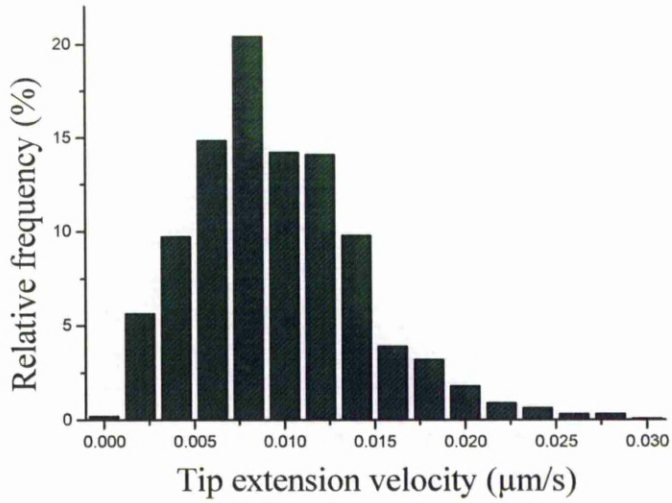

C)

Figure 4.7: Distributions of A) branching angles with fitted normal distribution; B) branching distances; C) tip extension velocities with fitted normal distribution measured for hyphae of *A. mellea* growing within the *Small maze* network.

After entering the maze, the hypha followed the design of the channel until it hit an obstacle, which resulted in a change of growth direction. The species navigated the maze most commonly with a single hypha and the overall success rate which is the ratio of the number of hyphae exiting the *Small maze* network *versus* the total number of hyphae that entered the *Small maze* network initially was 0.27 (13:49). The right-angled features present in the network and highlighted by the red arrows in Figure 3.6 caused the hyphae to slow down. The hyphae showed a corner-flexibility. Instead of stopping the filament's growth, the corners provoked the filament to bend and to restart growth. The time to restart its growth ranged from t = 12 min to t = 1h00.

The tip extension velocity was significantly changed by the confinement (T-value = 4.01, P-value < 0.01, DF = 3505, two-tailed unpooled Student's *t*-test) as the branching angles (P-value < 0.01, Mann-Whitney test). The branching distances were unchanged by the confinement (P-value = 0.18, Mann-Whitney test).

4.2.3.2 *Diamond* network

The *Diamond* network contains a high density of features with similar shape, which, similarly to the *Small maze,* provokes frequent collisions between the features and the hyphal tip (Figure 3.8). A total of 70 different hyphae out of 53 networks were observed within the *Diamond* network.

Hyphae that entered the network hit the edge of a small square, which deflected their initial growing direction. *A. mellea's* hyphae followed this structure in a flexible manner. The shape of the small squares influenced the magnitude of the branching angle. The contact with the corner of a small square often induce a branching event leading to an exploration of the maze through multiple hyphae (Figure 3.8-A). The ratio of number of networks without branching events *versus* number of networks with branching events was 1.52 (32:21).The hyphae could also grow through the structure without branching as shown in Figure 3.8-B. Hyphae could move between the squares located in the middle by alternately changing their growth direction to the right and left resulting in a *zigzag* growth pattern (Figure 3.8-C, green circles). Therefore, the hyphae were only temporarily diverted by the geometry as they usually maintained a fixed growth direction.

A)

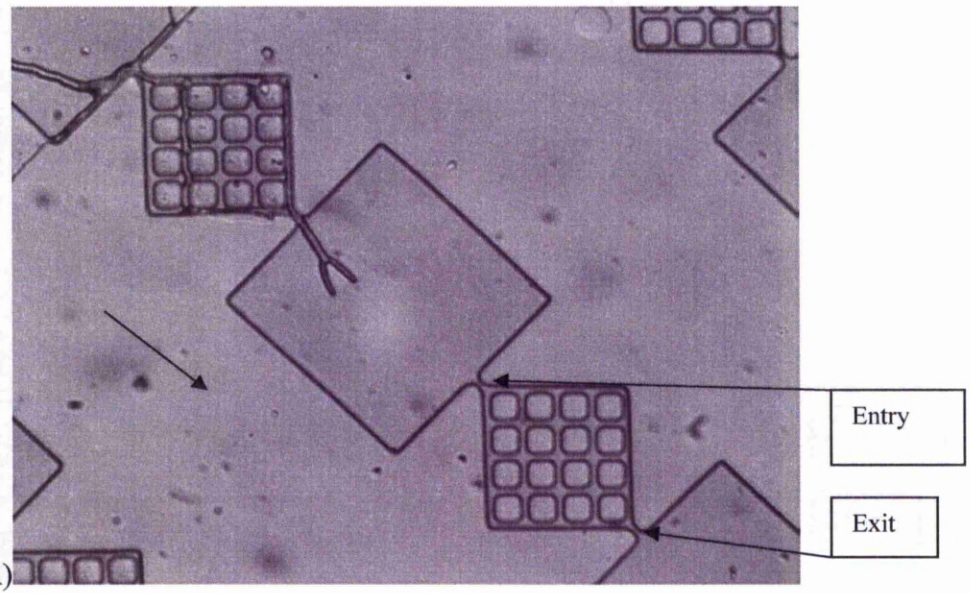

B)

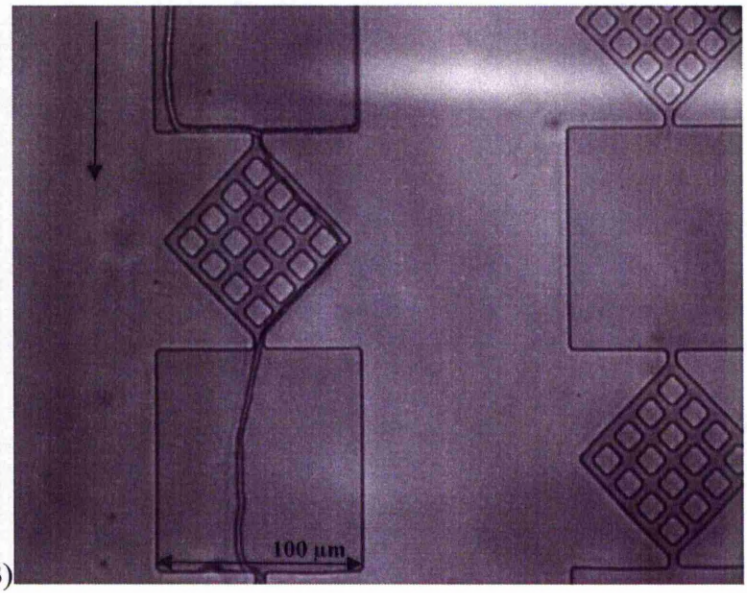

C)

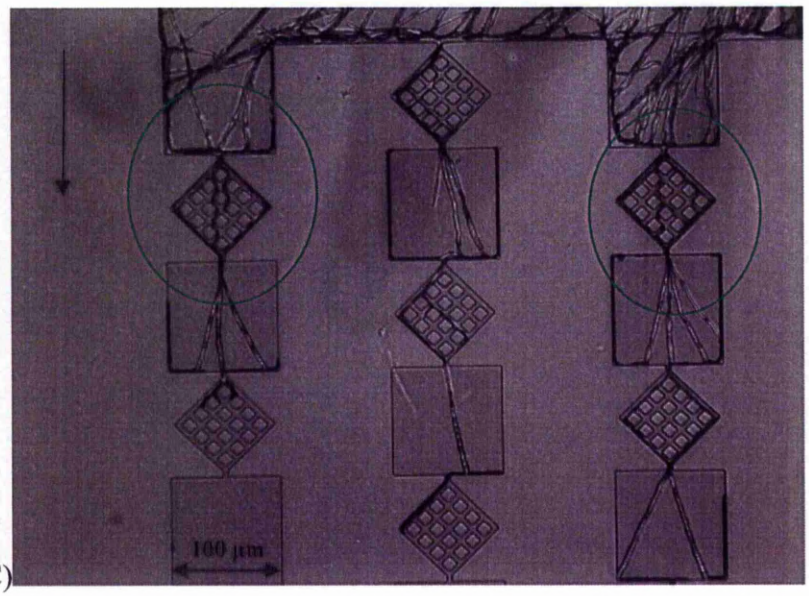

Figure 4.8: (A, B and C): Hyphae growing in *Diamond* structures. The set of pictures shows the *Armillaria mella* branching patterns in the *Diamond* structure. In picture A), the hypha branched after "tip-to-wall" collision at an angle around 90 ° and exhibited an apical branching angle in the space between the two mazes, (40x magnification). In B), the hypha grew without branching, (40x magnification) and in picture, C), two hyphae *zigzagged* between the pillars (green circles), (25x magnification). The black arrows indicate the hyphal growth direction.

Table 4.4 summaries the growth parameters and Figure 4.9 presents the corresponding histograms. The distribution of the branching angles is symmetrical with a single peak centered on 95 °. The mean branching angle was 102.6 ± 27.2 ° with an irregular distribution. The mean branching distance was 25 ± 12.2 µm. Similar to the *Small maze* network, the distribution of the tip extension velocities was symmetric and fitted a normal distribution. The mean tip extension velocity was 0.008 ± 0.003 µm/s. The overall success rate which is the ratio of the number of hyphae exiting the *Diamond* network *versus* the total number of hyphae that entered the *Diamond* network initially was 1.06 (74:70).

	Branching angle (°)	Branching distance (µm)	Tip extension velocity (µm/s)
Average	94.5	25.0	0.008
Maximum value	113.1	44	0.015
Minimum value	67.8	12.2	0.001
Standard deviation	9.3	12.2	0.003
Median	93.7	22.8	0.009
Number of values	19	16	181

Table 4.4: Descriptive statistics of growth parameters of *A. mellea* growing within the *Diamond* network.

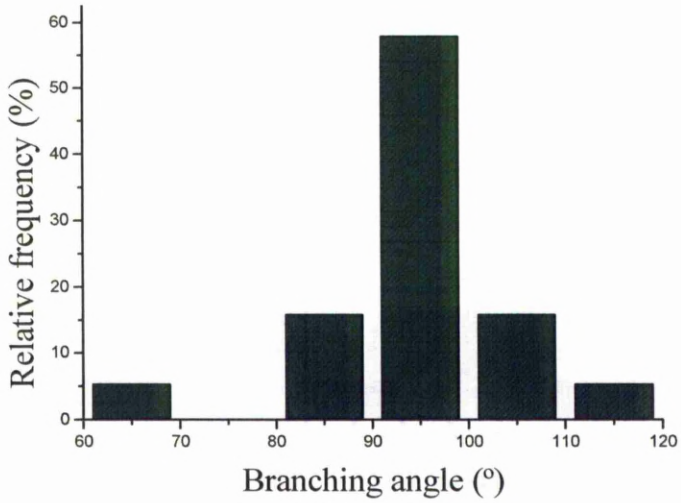

A)

B)

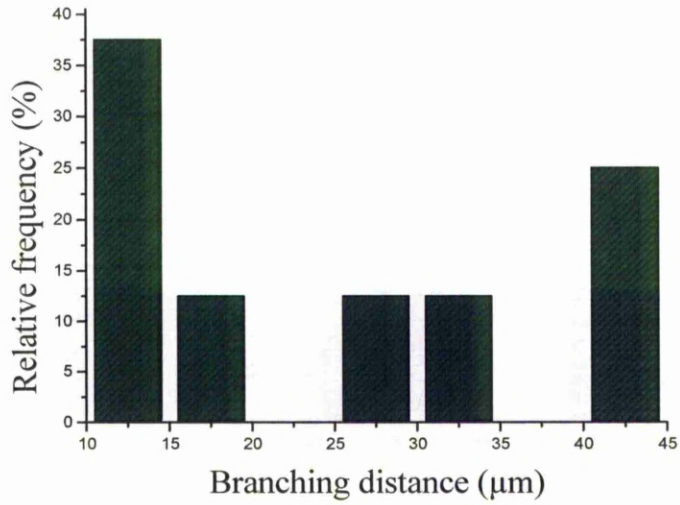

C)

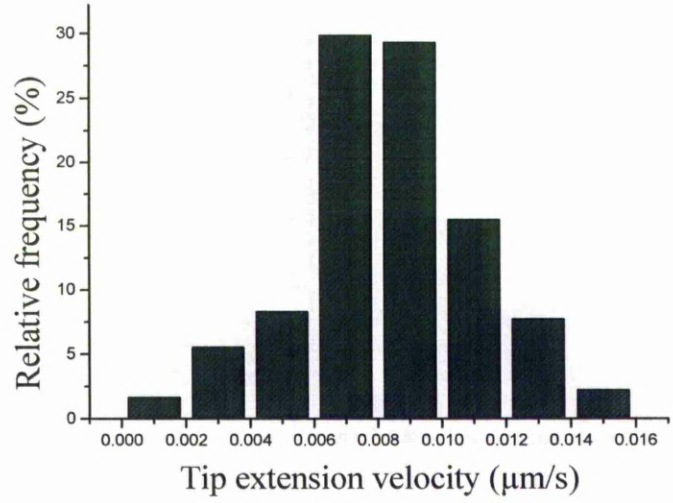

Figure 4.9: Distributions of A) branching angles with fitted normal distribution; B) branching distances; C) tip extension velocities with fitted normal distribution measured for hyphae of *A. mellea* growing within the *Diamond* network.

The tip extension velocity was significantly changed by the confinement (T-value = 7.55, P-value < 0.01, DF = 267, two-tailed unpooled Student's *t*-test) as the branching angles (P-value < 0.01, Mann-Whitney test). The branching distances were unchanged by the confinement (P-value = 1, Mann-Whitney test).

4.2.3.3 *Round-about* network

The *Round-about* network was a unique one because it tested the ability of the hyphae to grow via a complete 360 ° turns or a semi-complete turns (less than 180 °). The two round-about features are placed one after the other in an opposite direction and there are two possibilities to enter this structure. A total of 45 different hyphae out of 43 networks were observed within the *Round-about* structure.

Generally, *A. mellea* grew easily within the *Round-about* network. The filaments appeared to be guided within the network by the circular features. The direction taken by the hyphae at the exit of the first round-about was determined after "tip-to-wall" contact with the second round-about as illustrated in Figure 3.10-A (red arrows) by deflecting the hyphae to the right or to the left side of the feature. The overall success rate which is the ratio of the number of hyphae exiting the *Round-about* network *versus* the total number of hyphae that entered the *Round-about* network initially was 0.89 (40:45). From the two pictures, it can be seen that the two hyphae were flexible and bent close to approximately 90 ° in contact with the features. Branching events were rare as the hyphae were predominantly following the structures and performed turns at 135 °. Usually a branching event appeared at the second round-about. The ratio of number of networks without branching events *versus* number of networks with branching events was 6.17 (37:6). During the experiments, branching events took place only once per network so no branching distances could be measured. Figure 4.10-B shows that the initial path chosen by the fungus was important since the right entry did not lead to the exit but led the filament to grow back out of the network.

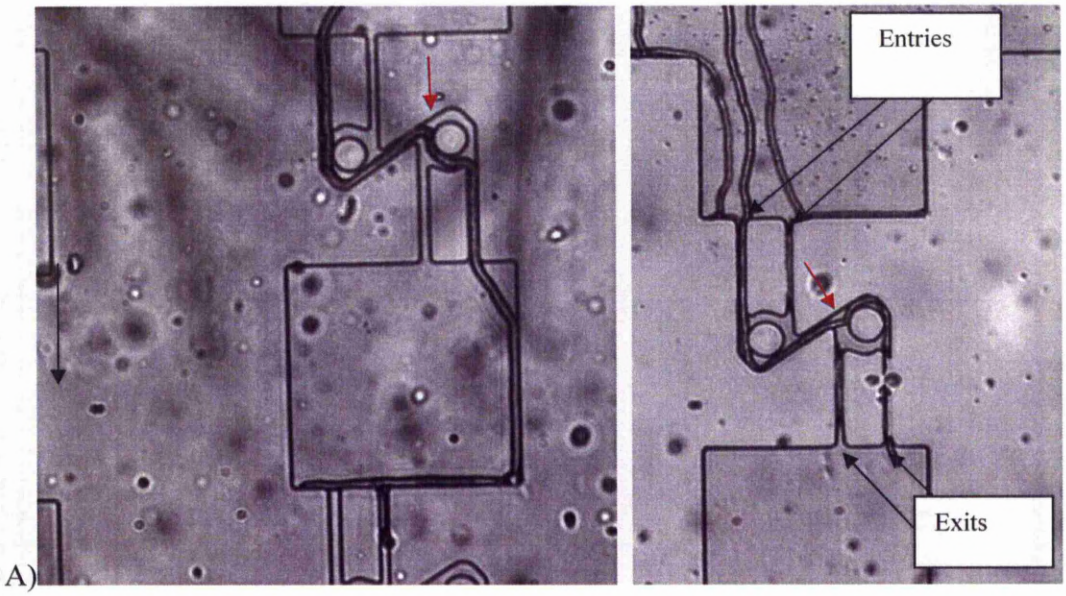

A)

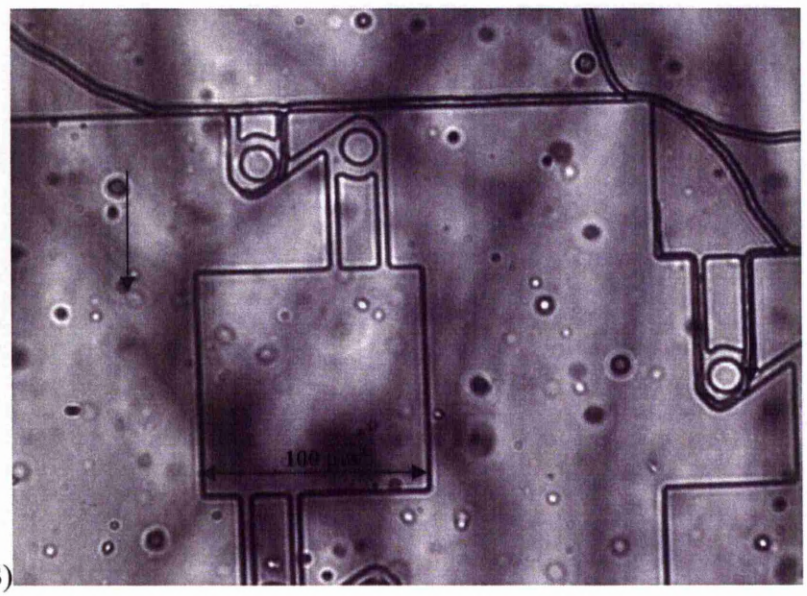

B)

Figure 4.10: Hyphae growing in a *Round-about* structure, the black arrows indicate the hyphal growth direction. As seen in Figure A), the hypha initially passively follows the design of the first round-about and hits the second one, which causes a 'decision' on the further growth direction (red arrows). Figure B) shows two hyphae within two different round-about directed to grow back out of the structures rather than towards the second round-about by their choice of entering the maze via the right entry instead of the left one. The black arrows indicate the fungus growth direction. (40x magnification).

Table 4.5 summaries the growth parameters and Figure 4.11 presents the histogram of the tip extension velocity. The mean branching angle was 119.3 ± 10.3 ° (there is no histogram representation because the sample contains only 6 data points). The distribution of the tip extension velocities is bimodal with two peaks at 0.008 and 0.015 µm/s (Figure 4.11). The mean tip extension velocity in this structure was 0.011 ± 0.005 µm/s.

	Branching angle (°)	Branching distance (µm)	Tip extension velocity (µm/s)
Average	119.3	/	0.011
Maximum value	129.8	/	0.024
Minimum value	102.1	/	0.001
Standard deviation	10.3	/	0.005
Median	119.5	/	0.011
Number of values	6	/	287

Table 4.5: Descriptive statistics of the growth parameters of *A. mellea* growing within the *Round-about* network.

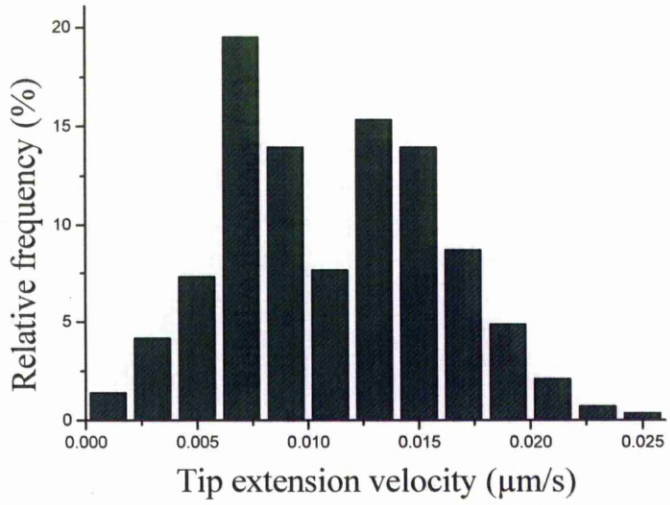

Figure 4.11: Distributions of tip extension velocities with fitted binomal distribution measured for hyphae of *A. mellea* growing within the *Round-about* network.

The tip extension velocity was significantly changed by the confinement (P-value < 0.01, Mann-Whitney test) as the branching angles (T-value = -7.47, P-value < 0.01, DF = 76, two-tailed pooled Student's *t*-test).

4.2.3.4 *Cellular* network

This *Cellular* network consisted of a main path in the middle and four lateral paths with different angles of ± 30 °, 45 °, 60 °, and 90 ° respectively. A total of 73 different hyphae out of 48 networks were observed within the *Cellular* structure.

A. mellea was able to grow through the *Cellular* network either with or without branching events. In the later case, the growth direction was either straight (Figure 4.12-A) or using lateral paths to find the exit (Figure 4.12-B, red circle). The ratio of number of networks without branching events *versus* number of networks with branching events was 3.80 (38:10).

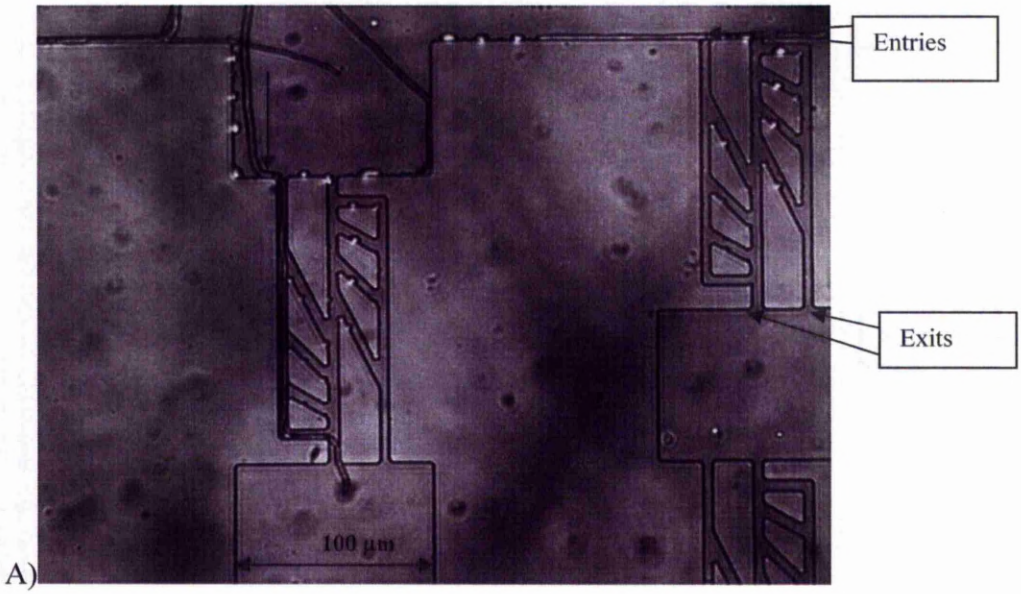

A)

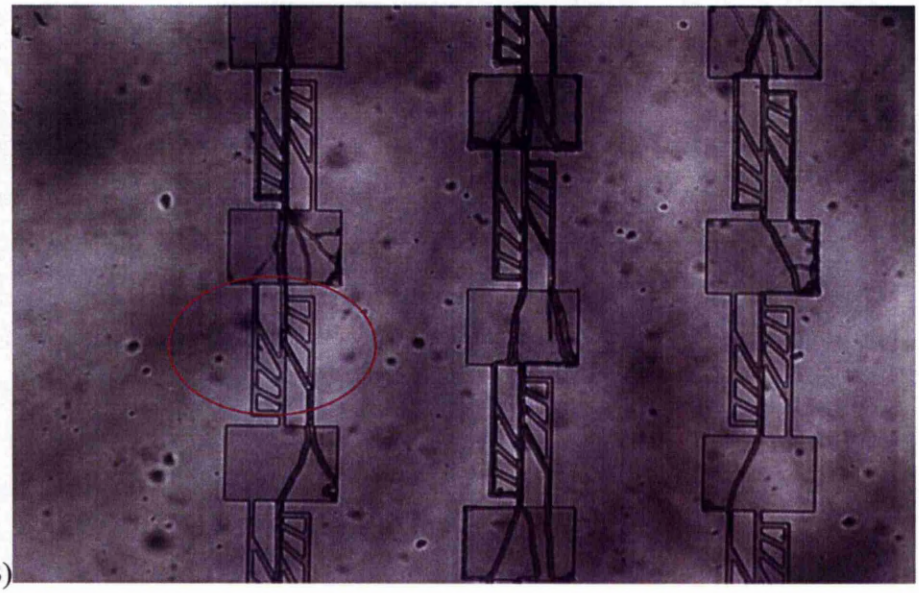

B)

Figure 4.12: Picture A), shows a hypha growing in a *Cellular* structure using a straight path (40x magnification). Picture B), shows a hypha choosing a lateral path (red circle) (25x magnification). The black arrows indicate the hyphal growing direction.

Table 4.6 summaries the species' growth parameters and Figure 4.13 presents the corresponding histograms. The branching angle distribution seems to be uniform and ranges from 12 ° to 96 °. The mean branching angle measured in this structure was 45.5 ± 25.6 ° indicating a preference for the third channel. The distribution of the branching distances exhibits a single peak at 15 μm. The mean branching distance was 21.6 ± 14.9 μm. The tip extension velocity distribution is bimodal with two peaks at 0.005 and 0.015 μm/s with a mean of 0.013 ± 0.006 μm/s (Figure 4.13). The overall success rate which is the ratio of the number of hyphae exiting the *Cellular* network *versus* the total number of hyphae that entered the *Cellular* network initially was 1.03 (75:73).

	Branching Angle (°)	Branching distance (μm)	Tip extension velocity (μm/s)
Average	45.5	21.6	0.013
Maximum value	96.6	50	0.029
Minimum value	12.1	6	0.001
Standard deviation	25.6	14.9	0.006
Median	47.3	15.5	0.14
Number of values	16	11	209

Table 4.6: Descriptive statistics of the growth parameters of *A. mellea* growing within the *Cellular* network.

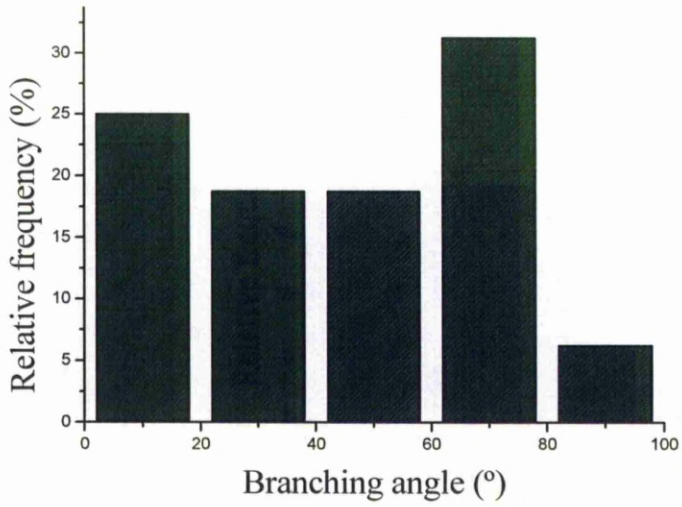
Relative frequency (%)
0
5
10
15
20
25
30
0
20
40
60
80
100
Branching angle (°)

A)

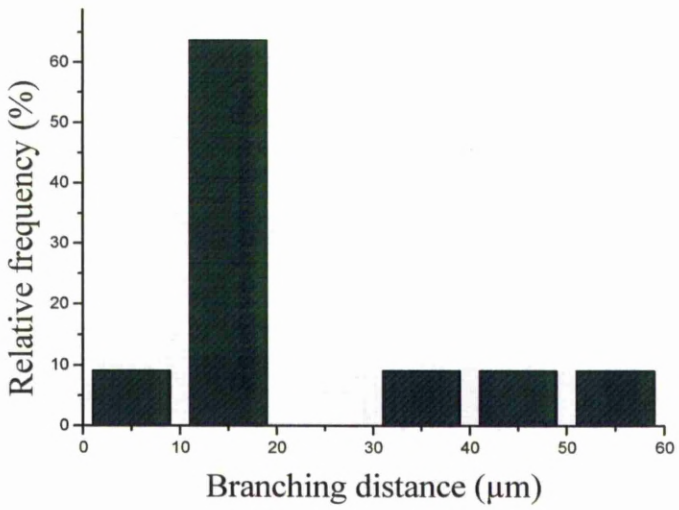
Relative frequency (%)
0
10
20
30
40
50
60
0
10
20
30
40
50
60
Branching distance (μm)

B)

C)

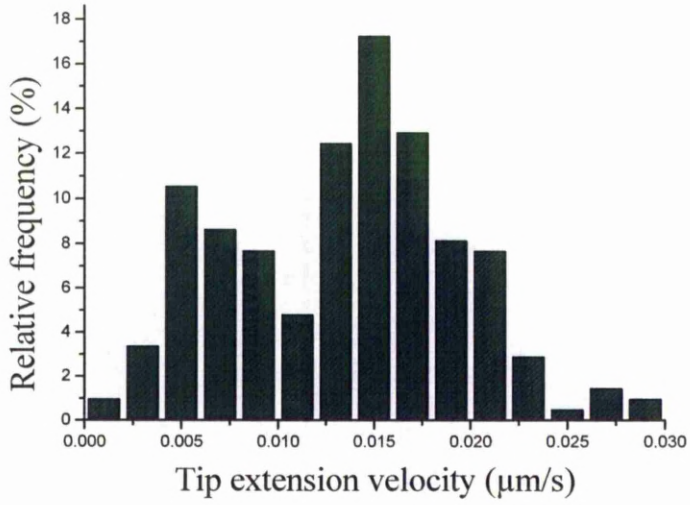

Figure 4.13: Distributions of A) branching angles; B) branching distances; C) tip extension velocities with fitted binomal distribution measured for hyphae of *A. mellea* growing within the *Cellular* network.

The tip extension velocity was significantly changed by the confinement and grew faster than on unstructured PDMS (T-value = -8.68, P-value < 0.01, DF = 3780, two-tailed pooled Student's *t*-test). The branching angles (P-value = 0.05, Mann-Whitney test) and the branching distances were unchanged by the confinement (P-value = 0.60, Mann-Whitney test).

Table 4.7 summaries the growth parameters of *A. mellea* on agar, on unstructured PDMS and within every network. Under low nutrient conditions, the mycelium of *A. mellea* was sparsely branched, whereas on nutrient-rich agar the branching pattern was dense. The number of branches decreased as the fungal colony grew further from the nutrient source into the microchannels which could be the consequences of the limited nutrients in the microchannels. The colony expanded randomly in every direction on open agar but in the confined areas, filaments exhibited a more controlled behaviour. The test shows that the confinement had an effect on the species' growth pattern. Confinement within the *Small maze*, the *Diamond* and the *Round-about* structures increased the branching angle whereas in the *Cellular*

structure the mean branching angle was reduced. An increased number of "tip-to-wall" collisions in the *Diamond* and the *Cellular* structures caused increased branching as compared to the *Small maze* structure. Due to the particular shape of the *Round-about* structure, it did not provoke regular branching. Branching distances were unchanged by the confinement. The hyphal growth directions were directed by the geometry of the mazes. *A. mellea* branches were induced by wall contact only and at the point of collision. The angles were about 30 ° to 40 ° larger than when measured in the open space and were about 90 ° within the networks due to the influence of the features. The response to a corner collision appeared to follow a certain hyphal algorithm because the process always took place as follows: the hypha hit the corner of a feature within a network, discontinued growth; the tip bulged and eventually resumed growth into the unobstructed direction out of the corner. In the 'plaza'-like space, branching occurred rarely. The tip extension velocity was significantly changed on the unstructured PDMS compared to on agar and also significantly changed within the networks than on unstructured PDMS. Structures like the *Diamond* and the *Small maze* networks, slowed down the hyphal growth rate more than the *Cellular* and *Round-about* networks (from 0.008 μm/s to 0.010 μm/s respectively). It seems to be the case that structures with a high density of internal features had a higher impact on fungal growth. The fungus was observed to navigate a given maze, like the *Small maze* network, using similar paths. In general, the species slid along the wall without attaching to it and was able to find the exit.

	Branching angle (°)	Branching distance (µm)	Tip extension velocity (µm/s)
Agar	**Apical: 56.3** ± 19.0 **Lateral: 55.9** ± 20.6	**40.3** ± 28.6	**0.017** ± 0.006
Unstructured PDMS	**Apical: 60.0** ± 26.9 **Lateral: 60.3** ± 19.0	**31.8** ± 28.7	**0.010** ± 0.006
Small maze	**90.7** ± 18.4	**52.2** ± 57.1	**0.009** ± 0.001
Diamond	**94.5** ± 9.3	**25.0** ± 12.2	**0.008** ± 0.003
Round-about	**119.3** ± 10.3	/	**0.011** ± 0.005
Cellular	**45.5** ± 25.6	**21.6** ± 14.9	**0.013** ± 0.006

Table 4.7: Summary of the descriptive statistics of the growth parameters of *A. mellea* growing on agar, unstructured PDMS and within all tested networks. The values represent the mean (± standard deviation).

4.2.4 *A. mellea* general behaviour mediated by the structures or structures-independent behaviour

The fungus exhibited a specific behaviour influenced by the geometry of the maze but some general observations can be highlighted.

4.2.4.1 Behaviour when hitting a wall

Between two mazes and inside the networks, the hyphae regularly hit the walls and the features within the mazes. These collisions triggered two different responses;

either a deflection to the right or to the left or the hyphal tip split into two daughter hyphae.

Wall contact resulting in a deflection without branching

Hyphal wall collisions with an 'impact angle' smaller than 30 ° triggered no branching response but the hyphae followed the wall geometry. At an 'impact angle' between 30 ° and 70 ° the responses were in 10 % to 15 % of all cases no branching event and in ~ 1% of all cases a branching event (Figure 4.14 and Figure 4.15, red circles). Figure 4.16, summaries the behaviour of individual hyphae when they hit a wall. The mean angle was 52.3 °, standard deviation of 23.9 ° (233 values). This adaptation to the geometry is possibly due to the flexibility of the hyphal tip. This flexibility enables hyphae to penetrate into narrow channels and to 'choose' a growth direction to the left or to the right after a wall collision. The hyphae chose mostly the direction leading to the entry of a maze (Figure 4.15) and therefore to a continuation of growth through the microchannels away from the colony centre. Therefore, the species did not redirect its growth to avoid confinement.

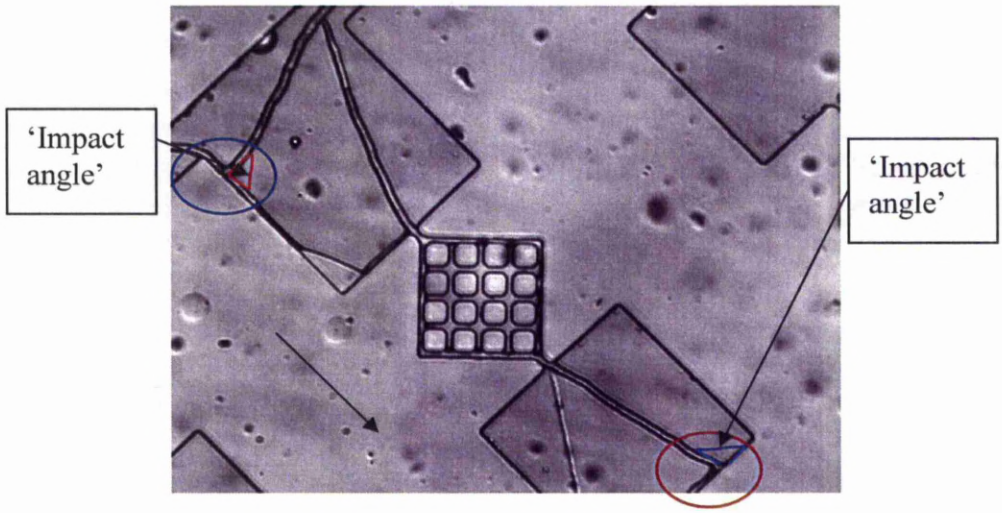

Figure 4.14: Whether the hyphal tip splits or not depends on the angle of collision with the wall. The hyphae either split (blue circle) otherwise the hyphae curve (red circle). The black arrow indicates the hyphal growth direction, (40x magnification).

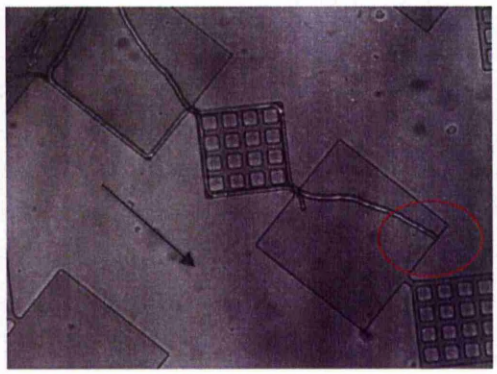

t = 0 minute

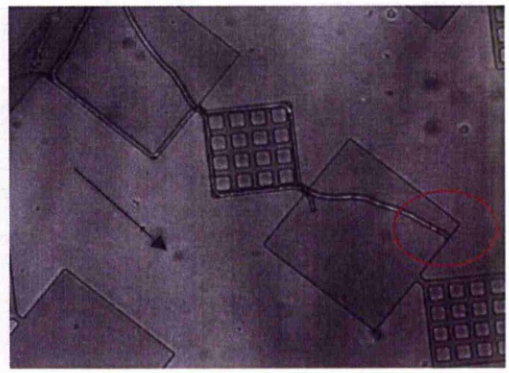

t = 4 minutes

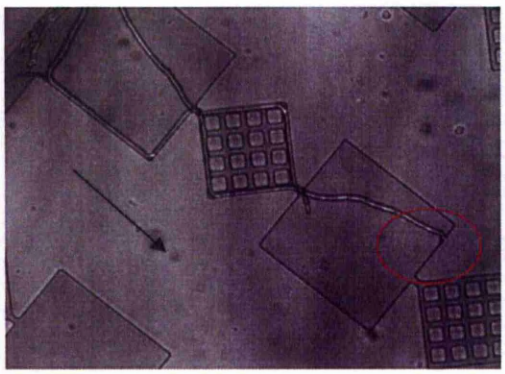

t = 8 minutes

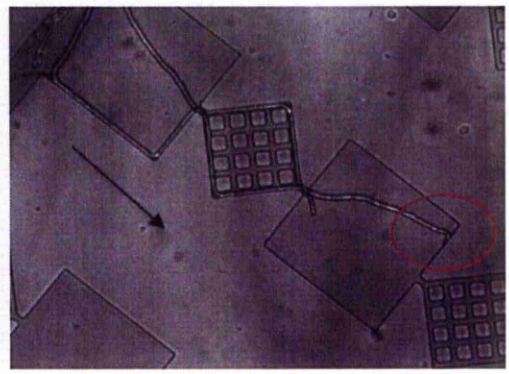

t = 12 minutes

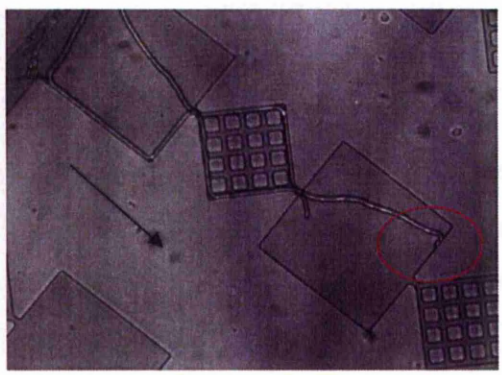

t = 16 minutes

Figure 4.15: Hyphal ability to curve against a wall (the pictures have been taken every 4 minutes at 40x magnification): t = 0 min, the hypha encounters a wall, at t = 4 min, the hypha grows toward the wall and starts a reorientation at t = 8 min. The hypha bends and continues apical extension at t = 12 min and t = 16 min. The black arrow indicates the hyphal growth direction.

Contact with the wall triggers branching

At 'impact angles' of more than 70 °, in about 10 % out of all cases, the response observed was tip splitting into two hyphae that grew in opposite directions away from the collision point, as shown in Figure 4.14 (blue circle) and in Figure 4.16. The mean angle was 95.0 °, standard deviation of 25.3 ° (38 values). The data indicated that the level of tip-splitting response increased according to the angle at which the hyphae collided with the wall.

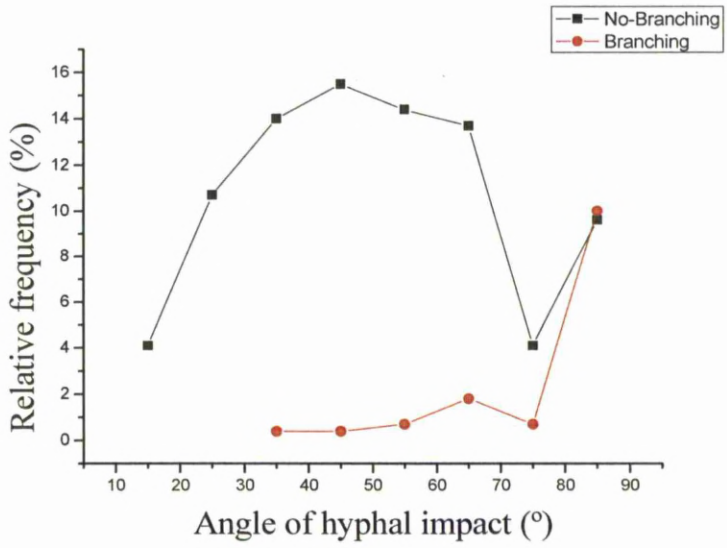

Figure 4.16: Variation of the thigmotropic responses of *A. mellea* according to the angle of impact with a wall.

4.2.4.2 Hyphal searching for entrances and exits from the network

Hyphae approached the entry of a maze either by growing in a direction that aims towards the entry (Figure 4.17, red circle) or following a response to wall collision (Figure 4.17, blue circle). The ratio between the numbers of hyphae that navigated to the entry without any contact with a wall *versus* the number of hyphae that navigated to the entry after contact with a wall was 0.19 (8:42). The fungus was observed to actively target the entrance, which was not more than a 10 μm wide opening in a 100 μm wide wall. Table 3.8 summaries *A. mellea'* success rate within the different

networks. For the *Small maze* and the *Round-about* networks the success rates were 0.27 and 0.89 respectively. The rare initiation of branches as well as the complexity of the networks was responsible of the rate smaller than one. On the contrary, an increased number of hyphae formed by branching and exiting the structure were responsible for the rate larger than one for the *Diamond* and the *Cellular* networks (1.06 for the *Diamond* and 1.03 for the *Cellular* networks).

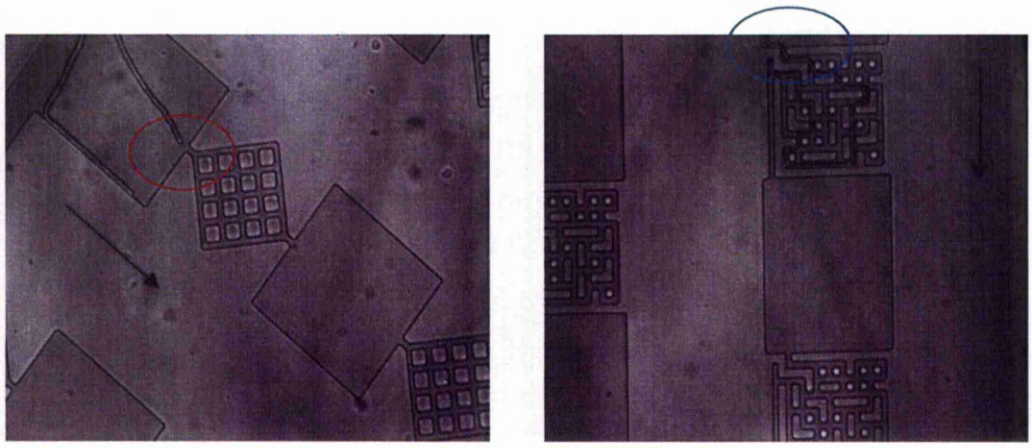

Figure 4.17: Shows the different behaviours observed before entering a maze, i.e. active growth toward the entry (red circle) and entry into the maze after a contact with a wall (blue circle). The black arrow indicates the hyphal growth direction. (40x magnification).

	Small maze	*Diamond*	*Round-about*	*Cellular*
Success rate (exit versus entrance rate)	0.27 (13:49)	1.06 (74:70)	0.89 (40:45)	1.03 (75:73)

Table 4.8: Success rate of *A. mellea* within all the microfluidics networks. The success rate represents the ratio of the number of hyphae exiting the structures versus the total number of hyphae that entered the structure initially. The numbers of hyphae are the one enclose within the brackets. For the *Diamond* and the *Cellular* network the values are larger than one because of the branching of hyphae inside the structure, which enabled several hyphae to find the exit from the same structure. For the *Small maze* and the *Round-about* the values are smaller than one because of rare branching events and less hyphae reaching the exit.

4.2.4.3 Corner flexibility

The response to collisions with corners usually followed a distinct order: the hypha hit a corner then discontinued its growth, the tip bulged and the hypha eventually continued growth away from the corner. The filament response was either to successfully turn the corner or to stop growth. In the *Small maze* network, for example, *A. mellea* turned corners in 70 % of cases (n = 19) but did not turn and stopped in the remaining 30% of cases (n = 8).

Table 4.9 summaries the general observations of the behaviour of *A. mellea*. Even without nutrient cues, *Armillaria mellea* found the entry of the networks with ease. The microstructures containing a high density of features causing frequent wall collisions resulted in slower growth and apex perturbation, which in turn induced either tip splitting or a reorientation when the filament managed to adapt to the geometry. The networks provoked branching by physical obstruction.

Apical growth rate	Decreased within all the networks
Branching rates	Vast decrease within the networks, branching occurred occasionally
Branching angles	Increased, close to orthogonal
Wall collision	Loose attachment to the wall and initiation of branches after "tip-to-wall" collision
Corner response	In the *Small maze* network, hyphae turn corners in 70% (19) of cases and do not turn and stop growth in the remaining 30% (8)
Hyphal flexibility	The apex is flexible resulting in a successful growth through the channels and adaptation to the geometry

Table 4.9: Summary of the behaviour of *A. mellea* in microfluidic networks. The brackets enclose the numbers of data points.

4.3 Discussion

4.3.1 Introduction

In this study, three parameters were examined, the tip extension velocity, the branching angles and the distances between two successful branches. Statistical analysis showed a strong influence of confinement on the species' tip extension velocity and branching angles regardless of the mazes used. Confinement affected the growth pattern of *A. mellea* in terms of decreasing hyphal extension rates and increasing hyphal branching angles.

The natural environments of filamentous fungi are complex and diverse (Evans, Hedger 2001). The laboratory substrate commonly used in research, a planar agar surface, fails to reflect the complexity of filamentous fungi's natural environments (Fricker, Lee et al. 2008; Kasuga, Glass 2008; Gougouli, Koutsoumanis 2010). *A. mellea* is a woody plant pathogen that causes wood decay in an enclosed environment that has a variety of physical and chemical conditions (Plomion, Leprovost et al. 2001). The mycelia networks allow fungi to colonize new environments and have a natural ability to grow in microscale channels. Although the natural environment of fungi might be more complex than the tested microstructures, their application to the fungus revealed a specific search behaviour of *A. mellea* that could in turn reveal deeper insight into fungal growth in general.

4.3.2 *A. mellea* branching patterns and exploratory behaviour

As the filaments grew from a nutrient-rich to a nutrient-free area and from an open to a confined area, which comprised a variety of obstacles, the growth parameters changed. Agar plates traditionally encourage mycelial proliferation so the growth pattern that *A. mellea* exhibited on a potato dextrose agar plate represented its optimum. *A. mellea* exhibited apical branching whereas the predominant branching pattern exhibited by filamentous fungi is lateral branching (Harris 2008). The branching pattern enabled the mycelium to fully explore its environment and exploit

nutrient sources efficiently. The data measured within the microconfined networks show that hyphal extension rates were affected negatively (except for the *Cellular* network) by confinement and by the collisions with the internal features. The interaction with the geometry of the networks suppressed branching, which appeared be triggered externally by "tip-to-wall" collisions resulting in increased branching angles. Hyphae that grew on unstructured PDMS showed a reduced branching pattern in comparison to agar surfaces suggesting that growth and branching were not only limited by the obstacles but also by availability of nutrients. Hyphal extension is generally promoted by the transport of nutrients within and between hyphae (Shepherd, Orlovich et al. 1993, Hyde, Ashford 1997) which allow hyphae to extend for relatively long distances through nutrient-poor areas. Although the growth dynamics of *A. mellea* was disrupted due to the surface changes, hyphae continued extension away from the colony centre. This high degree of adaptability to heterogeneous environments is a key feature of *A. mellea* as a plant pathogen.

Confinement within the microstructures completely suppressed the 'normal' branching pattern of *A. mellea* observed on agar. Multiple branching in microstructures generally has many advantages. The fungus is more likely to find the exit more quickly because each hypha will explore a different path. Additionally, the multiple branching modes enhance the survival of the fungus because the fungus will maximize its efficiency to use the nutritional resource available. *Armillaria mellea* devoted less biomass for the exploration of the structures and solved the networks frequently with a single hypha (with a simple response). A single hypha exploring the maze has a lower probability to find the exit quickly but requires fewer resources. It seems that *A. mellea* prefers the 'saving energy option'. The branching rate appeared to be low because of the nutrient deficient environment.

On unstructured PDMS, *Armillaria's* newly formed filaments exhibited a definite behaviour whereby the hyphae gradually redirected their growth to smaller angles; this could be in accordance with the fact that in natural environments the hyphae aggregate at some point to form rhizomorphs. A rhizomorph is an aggregation of thousands of hyphae organized into a root-like structure that offers significant

advantages to the fungus because this structure is much less fragile than single hyphae.

Model of Wood decay

Wood is a porous medium with a complex hierarchical structure (Figure 3.17). At the macroscopic scale wood consists of growth rings. On the mesoscopic scale, the growth rings are formed by cells that vary in their geometry and dimensions according to their function. Softwood is made of two types of cells: tracheids and rays which are positioned radially in order to transport nutrients across the growth rings. At the microscopic scale, the lumens of the cells (i.e. the voids within the cells) are interconnected through pits. At the submicroscopic level the cell wall is composed of layers of macromolecules, such as cellulose, lignin and hemicelluloses, which are the main nutrient sources of wood-decay fungi, besides water and oxygen.

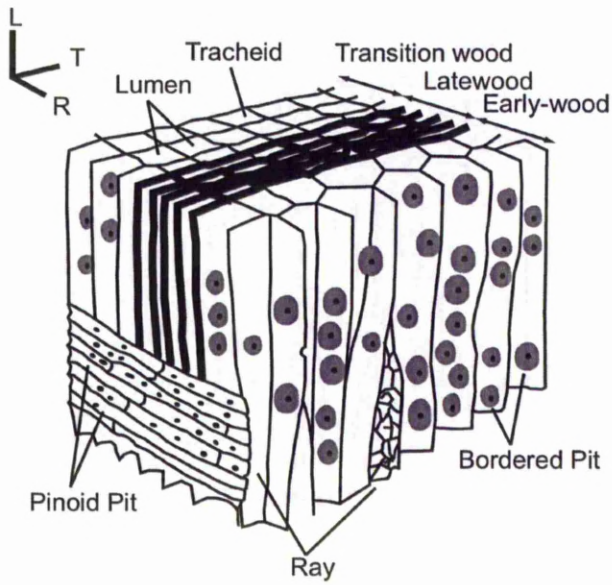

Figure 3.17: Schematic organization of the trunk of a tree layer by layer in the longitudinal (L), radial (R) and tangential (T) directions (Fuhr, Schubert et al. 2011).

Physical quantification of the microscopic decay patterns of fungi is difficult, because of the opacity of wood and the heterogeneity of its structure. Many authors have tried to deal with the decay pattern of *P. vitreus* (Schwarze, Landmesser 2000; Lehringer, Hillebrand et al. 2010) or have performed quantification on macroscopic wood properties (Schwarze, Landmesser et al. 2006; Schwarze, Spycher et al. 2008). One powerful method to achieve a physical quantification of the microscopic decay pattern of a fungus is through mathematical modeling. Wood does canalize hyphal growth because of the directed distribution of the pits and cell walls, which restricts the availability of nutrients. In the longitudinal direction the tracheids determine the direction of the mycelium and the rays canalize the hyphae in the radial direction. The pits are the main pathway for the fungus to move from tracheid to tracheid. According to the model developed by Fuhr, Schubert et al. (2011) who observed the colonization of a white-rot fungus, *Physisporinus vitreus*, the hypha first enters a tracheid and then grows from pit to pit. During growth along the tracheid apical branching occurs. When the end of the tracheid is reached the spread of the mycelium in the longitudinal direction stops and lateral branching occurs. After some time, the hypha is able to reach a new tracheid through an open pit and the colonization process starts again. Mechanical force and chemical secretions from the hyphae promote the progression through the tissues. The substrate is colonized step by step with alternating phases of restricted and unrestricted growth according to the nutrient availability. With increasing fungal infection, the wood becomes more porous.

It is possible to develop hyphal growth models with the help of simulations that are not just limited to the centimeter scale rather to the microscopic scale as shown by the model presented by Fuhr, Schubert et al. (2011). Quantifiable parameters included the degradation rate but the model gave no information about the branching behaviour such as the exact branching angles and the inter-branching distance. PDMS substrates differ both physically and chemically from natural habitats colonized by fungi but more quantitative information about how complex systems like fungus-wood interact are directly measurable.

4.3.3 *A. mellea* adaptation and sensory behaviour within the network

The results showed that *A. mellea* successfully and dynamically navigated different type of mazes, i.e., one or more hyphae reached the exit and was able to explore them. Once the hyphae find the entry they were also very efficient to find the exit of every network tested. Filamentous fungi naturally explore environments via apical cells that capture nutrients and are engaged in the sensing of the local environment (Harris 2008). The mazes tested were very different from each other and the species seemed to adapt rapidly to new environments. In order for a single hypha to explore the maze, it must be very flexible enabling a variety of turns including u-turns in channels as narrow as 5 μm. The *Small maze* was always explored in a similar fashion suggesting that a robust set of growth algorithms determines the growth dynamics. An interesting aspect revealed during this study was that the hyphae did not require any nutrient-related clues to explore and resolve the networks. Previous studies by Nakagaki et al. (2000) have demonstrated the capability of a slime mold to connect two nutrient sources via the shortest path through a maze-like structure.

It is unclear which mechanisms fungi use to navigate the mazes. Growth is generally directed either by tactic or tropic mechanisms. Tropism is defined as a directional growth response of an organism to an external stimulus. Thigmotropism, a movement in which an organism moves or grows in response to touch or contact stimuli, was identified to play an important role in both plant and human fungal pathogens (Hoch, Staples et al. 1987, Brand, Gow 2009). Previous work by Bowen, Davidson et al. 2007 with *Aspergillus niger* has demonstrated a variation in the levels of thigmotropic sensitivity based on the angle at which the hyphae impact the channel walls. The thigmotropic responses were investigated using microfabricated surface topographical cues. The work showed that the thigmotropic response (hyphal deflections away from ridges) decreased as the impact angle increased in nutrient-depleted conditions. The non-thigmotropic response was hyphae crossing over ridges without deflection. Bowen suggested that touch-sensing may not operate efficiently at the extreme apex of the apical dome. In contrast to *A. niger*, *A. mellea's* filaments split into two new filaments after a mechanical contact with an obstacle at an impact

angle of approximately 90 °. Similarly to *A. niger*, at a smaller angle of interaction to a wall, *A. mellea's* filaments were observed to choose "left versus right" and to adhere to the wall. In *A. niger*'s case, the nutrient deficient environment appeared to cause decreased thigmotropic sensitivity of hyphal impact with obstacles > 70 °. The stress caused by the environment may have disrupted the supply of cell wall- and membrane-building blocks to the tip, causing the hyphal apex to remain undeveloped and unable to respond to thigmotropic signals. The microfluidic system used in this thesis provided a tight confinement in the three spatial dimensions. Obstacles made the hyphae bulge because the hyphae cannot overcome the wall. Katz, Goldstein et al. (1972) and Trinci (1974) suggested that tip splitting occurs in response to abnormal accumulation of exocytic vesicles at the hyphal tip. The supply of vesicles exceeds their capacity to be incorporated into the existing tip leading to the formation of a new tip and thereby disrupting apical dominance. For *A. mellea* the tip splits into two hyphae when a hypha hits an obstacle at angle > 70 °. The two hyphae emanate from the collision point trying to grow around the obstacle. The hypha first hit the wall, the apex bulged. The hypha then resumed its growth followed by the appearance of a second hypha. This is possible due to the high flexibility of the apex. During this process the Spitzenkörper must split into two and the cytoskeleton must rearrange to deliver vesicles to both sites.

As an opportunistic wood pathogen, environmental sensing is important for *Armillaria mellea*. The filaments of the fungus were observed to converge towards the entries of a maze. This observation suggests that the species' space searching methods also include non-thigmotropic sensing. According to Hanson, Filipponi et al. (2005) the environmental cues for this response may be the changes in self-generated gradients (metabolic products, ions, gradients of oxygen, and so forth). Filamentous fungi are likely to possess sensory receptors that could be involved in this mechanism. Filamentous fungi have conserved signal-transduction pathways that allow them to sense changes in their environment. They are able to sense light, gases or chemicals (Bahn, Xue et al. 2007). For *A. mellea*, tropism is a bending response that orientates a hypha towards a particular direction.

4.3.4 Comparison with *Neurospora crassa* and *Picnoporus cinnabarinus*

The set of experiments presented in this work have also been conducted with two other fungal species: *Neurospora crassa* (Held, Edwards et al. 2009, 2011, Held, Binz et al. 2009) and *Picnoporus cinnabarinus* (Hanson, Nicolau Jr et al. 2006). The growth parameters, i.e. branching angles, branching distances and tip extension velocities of these species changed due to confinement and their general behaviour was different in comparison to the one exhibited by *Armillaria mellea*. Nevertheless, there were some similarities between two or even all three species. *Armillaria mellea* and *Picnoporus cinnabarinus* are both plant pathogens and belong to the phylum Basidiomycota. Thus they may share more common points with each other than with *Neurospora crassa*. *N. crassa* belongs to the phylum Ascomycota and its natural environment is dead plant matter after fires.

Similarities for all the species included the fact that the branching angle increased within the structures. The hyphal tip splits subsequent to wall collisions was also observed for *N. crassa*. The tip extension velocity growth rates were unchanged by confinement for *P. cinnabarinus* but changed in comparison to agar. The tip extension velocity was reduced by the confinement for *N. crassa* and *A. mellea*. Hyphal branching was significantly amplified by confinement through interaction with the microstructured geometry within the *Small maze* for *P. cinnabarinus*. Hyphal branching generally increased for *N. crassa* but was suppressed by narrow and periodic structures as observed for *A. mellea*. The convergence of hyphae toward the entry of mazes has only been observed for *P. cinnabarinus* and *A. mellea*. A major finding and difference for *A. mellea* compared to the two other species was directional memory. Directional memory is defined as: after the hyphae turned because of the geometry, they maintained the exact direction that they had previously from parent filament branching (Hanson, Nicolau Jr et al. 2006). *A. mellea* did not show any directional memory, expressed by several observations. Firstly, the growth directions of individual hyphae followed the geometry of the networks, i.e. the hyphae were passively guided by the maze walls. Secondly, in the *Small maze*, the hyphae navigated the maze always in a similar fashion despite the differing initial

growth directions of the hyphae prior to entering the maze. If the fungus possessed directional memory, individual hyphae should explore different areas of the maze but they do not. Thirdly, on unstructured PDMS, after branching, the newly formed hyphae redirected their growth to a smaller angle and extended parallel to the parent hyphae. All the species were able to turn corners in 63 % of all cases for *N. crassa* and 21 % of all cases for *P. cinnabarinus*. The hyphal apex of *N. crassa* is flexible resulting in close wall attachment and therefore adaptation to the geometry. However, the mature parts of the hyphae are rather stiff. The apex and the hyphae of *P. cinnabarinus* are quite stiff. The apex of *A. mellea* hyphae is flexible, resulting in a successful growth through the channels and adaptation to the geometry. Within the networks, there were a large number of collisions with the features. The tips of *N. crassa* hyphae split into two new branches if the collision angle is 90.0 ± 35.0 °. *A. mellea* hyphae were 'loosely' attached to the wall and tip splitting were initiated more frequently (~ 10 % of all cases) when the collision angle was between 70 ° and 90 °. Inside the mazes, the species was often observed to grow against the walls, therefore exhibiting a behaviour observed during tree colonization (invasion strategies include direct penetration into cells). *P. cinnabarinus* hyphae were observed to 'nose' along the wall.

The data showed that different fungal species respond in different ways to confinement. These behaviours suggest distinct adaptations to their respective ecological niches. It suggests also that the branching mechanisms might be different for each species. For example within the *Small maze* networks, the number of branches increased for *N. crassa* and *P. cinnabarinus*. Therefore, it is concluded that both species employ branching as a strategy for colonizing the maximum surface available. In contrast, *A. mellea* predominantly navigates the networks with only one hypha. The findings from this study combined with the results from *N. crassa* and *P. cinnabarinus* suggest that filamentous fungi generally respond actively to the different networks, hence making thigmotropism an important parameter of fungal growth.

4.4 Conclusions

From the work presented in this chapter interesting responses which are distinct structure-independent and structure-dependent has been shown. *A. mellea* found the entry of the different network easily because the hyphae grew toward the channel which was not expected from a random search. Once the hyphae found the entry, they were also very efficient to find the exit of every network. Although *A. mellea* could grow through every network, the design significantly changes the behaviour. In terms of (i) velocity which decrease in comparison to the growth rate measured on agar and unstructured PDMS, (ii) branching behaviour which only occurred after "tip-to-wall" collision at an angle superior to 70 ° and (iii) branching angle which was identical to the obstacles' shapes (~90 °) and therefore larger than within an obstacles free environment. The apex of *A. mellea* was very flexible and could adapt easily to the geometry of the features which indicate that these characteristics could be biologically beneficial in its natural environment. In conclusion hyphal growth can be directed within complex microstructures. Different species were already tested within the same set of networks which lead to the conclusion that different species showed different behaviour so some responses are species-specific but also similarities which mean that some responses are generic to all fungi (Hanson, Nicolau Jr et al. 2006, Held, Edwards et al. 2011).

Further investigation with fluorescence and confocal microscopy techniques will enable the understanding of fungal growth via the observation of intra-cellular events. Many other questions can be investigated concerning fungal branching process. Species-specific responses open the avenue for the design of surfaces that are species selective and for studies that can reveal new search algorithms. Simulations can for instance be done to show which species are the more efficient to solve a given set of mazes.

Chapter 5

Motility of *Serratia marcescens* and *Pseudomonas stutzeri* in complex geometries

5.1 Introduction

This chapter aims to quantify the movement of bacterial cells through various geometrical environments. The model organisms used here are *Serratia marcescens* and *Pseudomonas stutzeri*. The two species differ in their arrangement of their flagella around the body and consequently their motility behaviour differs. *S. marcescens* is peritrichously flagellated which means that the cell body is surrounded by two or more flagella. *P. stutzeri* possess a single polar flagellum. In culture with high nutrient concentration the swimming behaviour of peritrichously flagellated bacteria is called a "random walk" which is a uniform movement (Berg, Brown 1972). Monotrichously flagellated bacterium swim essentially back and forward and are unable to tumble. The clockwise rotation of a bundle of peritrichous flagella corresponds to a brief stop of a monotrichous flagellum between counterclockwise and clockwise rotation. Thus the clockwise flagellar rotation in monotrichously flagellated bacteria plays a different role from that of peritrichously flagellated bacteria (Magariyama, Ichiba et al. 2005).

Both species are naturally occurring soil bacteria. Soil is an environment presenting complex surfaces that are inherently microstructured and heterogeneous. This study will give insights about the behaviour of these two bacterial species at the microscale.

The swimming motion of bacteria, particularly in non-confined environments has been widely studied (Adler, Dahl 1967; Berg, Brown 1972; Ford et al. 1991; Philips, Quinn et al. 1994) but considerably less is known about motion in confined environments. The past studies involving bacteria in confinement have been done essentially with *E. coli* which is peritrichously flagellated. Work concerning monotrichously flagellated bacteria is not as detailed, especially concerning confinement. Does the geometry affect the species differently? Do the different arrangements of the flagella confer any advantages?

Using data available, it will be possible to predict the movement of bacterial cells through various substrates and to measure the factors controlling bacterial movement in these environments. This may help to understand how bacteria move in soil matrices, penetrate water filtering systems or form biofilms.

5.2 Results

The effects of a wide range of restricted geometries of different shape and complexity were examined on the swimming behaviour of *S. marcescens* and *P. stutzeri*. Single cell motility was determined by different parameters: cell velocity, cell acceleration, and the deflection angle, which is the angle between a straight direction and the direction after a tumble as shown in Figure 5.1-A. Another parameter quantified was the influence of boundaries on bacterial cells by identifying the smallest distance between a bacterium and the nearest wall (Figure 5.1-B). The x and y coordinates of the trajectories of the bacteria were generated by manual tracking with Retrac or ImageJ. From the coordinates the acceleration and the deflection angle were calculated (See Materials and Methods, section 3.5.2). The velocity data were given by the software.

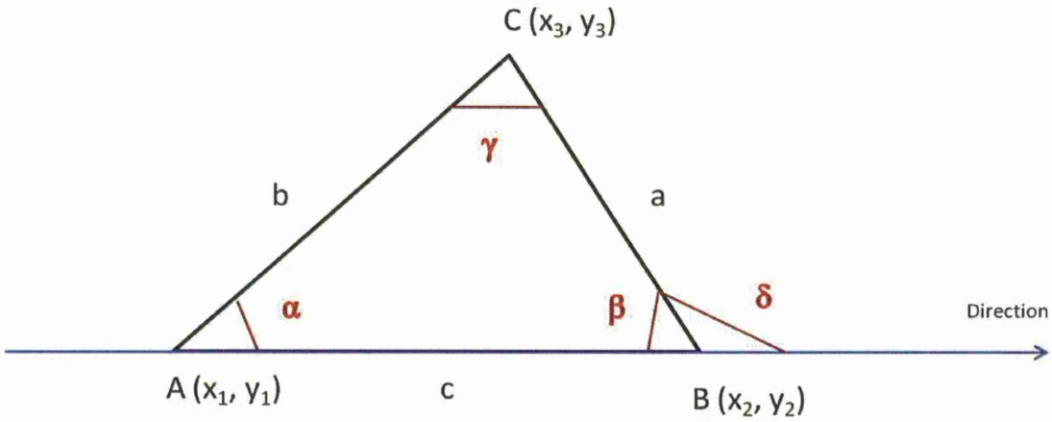

A)

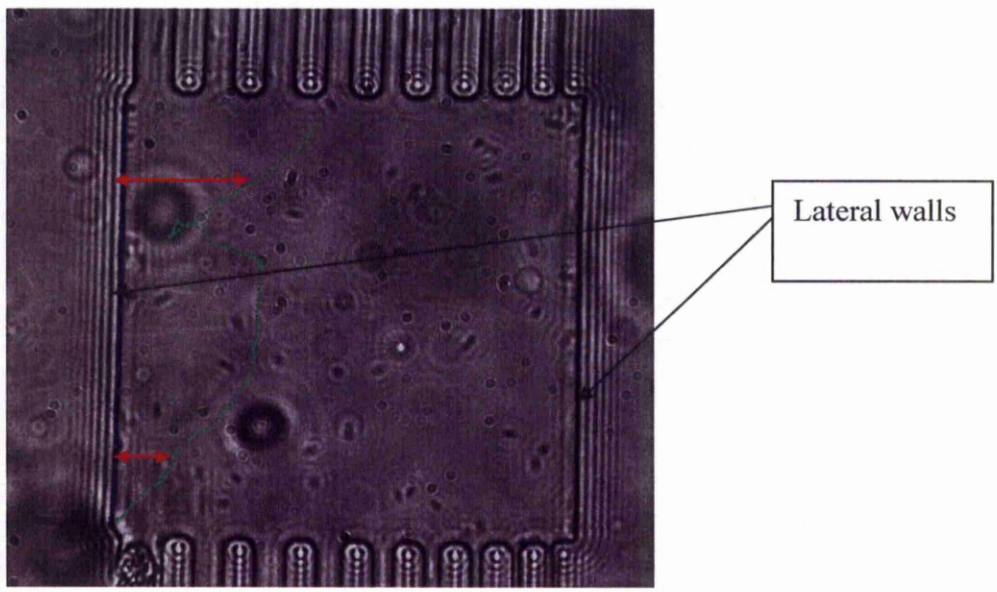

B)

Figure 5.1: A): Definition of the deflection angle. The positions A, B and C represent the coordinates of a bacterial cell swimming through a medium. From A to B, the cell is doing a run then tumbles and changes its swimming direction toward C. The deflection angle (δ) represents the angle between a straight direction and the direction after a tumble as indicated in the figure. B): As the bacteria swam over the surface (green plot) the minimum distance between the cell movement and the lateral wall (red arrows) was measured. This was done for each green dot which is the bacterial movement tracked and divided frame by frame. The 'plaza'-like space is 100 μm wide so the minimum distance between a bacterium and the nearest wall would be 0 μm and the maximum 50 μm.

5.2.1. Flagella staining, growth curve and colonies counting

Figure 5.2 A - B shows the flagella staining of *S. marcescens* and a drawing of a monotrichously flagellated bacterium similar to *P. stutzeri*. The cellular body of *S. marcescens* as well as the flagella are highly discernible. The cell possesses multiple flagella (4 to 5) that are here bundled up at one polar end. The flagella look very straight and the cell is representative of the swimming state.

A)

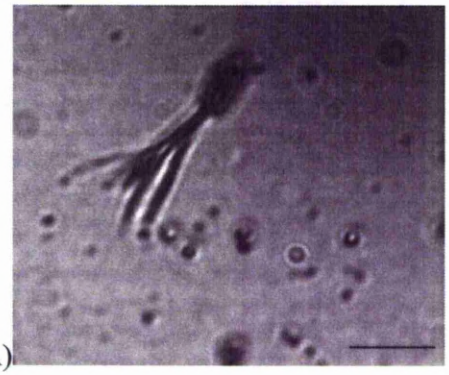

B)

Figure 5.2: A) *S. marcescens* flagella stained by silver nitrate (100x oil immersion objective). Bar = 5 µm. B) Schematic representation of a polarly-flagellated bacterium (not to scale).

For all the experiments, the bacterial cells were loaded into the microfluidics structures when they had reached the mid-exponential phase of growth (OD_{600} between 0.6 and 0.8 for *S. marcescens* and OD_{600} of 0.5 for *P. stutzeri*). Figure 4.3 represents *S. marcescens* and *P. stutzeri* growth curves. Mid-exponential phase represents the stage of maximum growth during which the cells are supposed to be very motile. The cell density of *S. marcescens* in LB growth medium at mid-

exponential phase was determined to be ~5.10^8 CFU/ml (colony-forming unit). The time needed for the population to double during the exponential phase was 33 minutes. The time needed for the population of *P. stutzeri* to double was 61.2 minutes and the cell density at OD_{600} of 0.5 was determined to be ~10^8 CFU/ml. Under the same condition of temperature, pH, oxygen and nutrients the two species have variations in generation time.

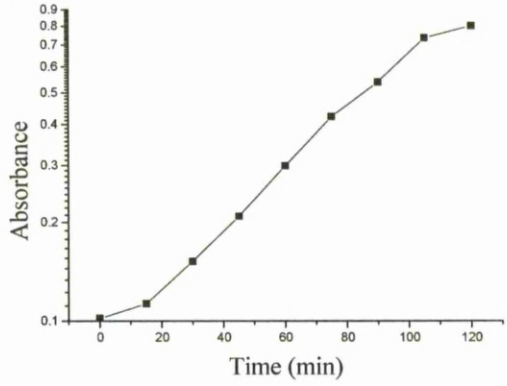

A)

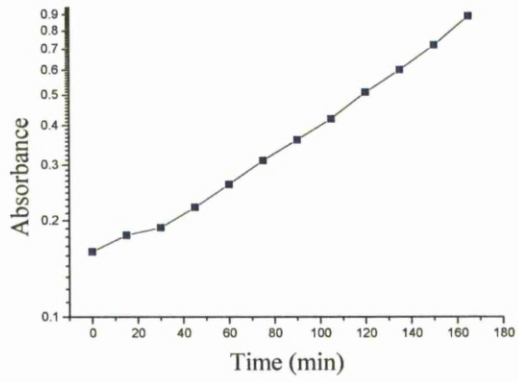

B)

Figure 5.3: *Serratia marcescens* (A) and *Pseudomonas stutzeri* (B) growth curve in LB medium where we can distinguish different phases of growth. The lag-phase (0-20 minutes), which is a period of slow growth and the bacteria are adapting in the growth medium. The exponential phase (20 to 100 minutes for *S. marcescens* and 20 to 180 for *P. stutzeri*) is a phase of exponential growth. The population is doubling every replication cycle. The stationary phase (after 120 minutes for *S. marcescens*) occurs when the nutrients become limiting.

5.2.2 Bacterial swimming behaviour within the different networks

5.2.2.1 'Plaza'-like area

The 'plaza'-like square measures 100 μm by 100 μm and is 10 μm deep. The lateral walls as well as the ceiling are made from PDMS and the floor is made from glass. Two of the lateral walls are directly connected to the geometries. The 'plaza'-like space is filled with LB growth medium, the environment is therefore homogeneous. 50 bacteria for each species were tracked within the 'plaza'-like area. For this section as well as for the following one, the bacteria were observed at the mid-plane. The field of view was 140 μm by 160 μm using a 60x objective lens.

S. marcescens in this large square showed some of the movement observed in unbound liquid media (Berg, 2004). The track of one cell appeared as a series of approximately straight segments, during which the cell moves forward, separated by turns of random angle. The swimming cells swam randomly over the surface. Changes in direction are "gradual" (~20 °) or "abrupt" (~90 °) (Figure 5.4-A). A deflection angle distribution was measured in the 'plaza'-like space. The mean deflection angle was 30.8 ± 34.0 ° and the distribution was exponential with a bias toward smaller turn angles (Figure 4.5). Smaller angles represent fewer changes in direction. *S. marcescens* cells were observed to trace out a clockwise circle (when viewed from above) (Figure 5.4-B).

The tracking of free-swimming cells of *P. stutzeri* showed a similar set of plot of trajectories already observed with *S. marcescens*. The resulting motile behaviour consisted of forward and backward movements. Figure 5.4-C shows a typical back-forward movement. The switching between forward and backward modes is rapid and corresponds to a brief stop (Homma et al. 1996). The traditional forward-backward movement did not repeat itself; the bacterium showed unidirectional swimming over long distances (Figure 5.4-E). Similarly to *S. marcescens*, *P. stutzeri* cells displayed clockwise circular movement (Figure 5.4-D). A deflection angle

distribution was measured (Figure 5.5). The mean turn-angle was 18.4 ± 15.6 °; the distribution was exponentially distributed with a bias toward smaller angles (main peak at 0-10 °) which correspond to a bacterium continuing in a direction close to its original direction.

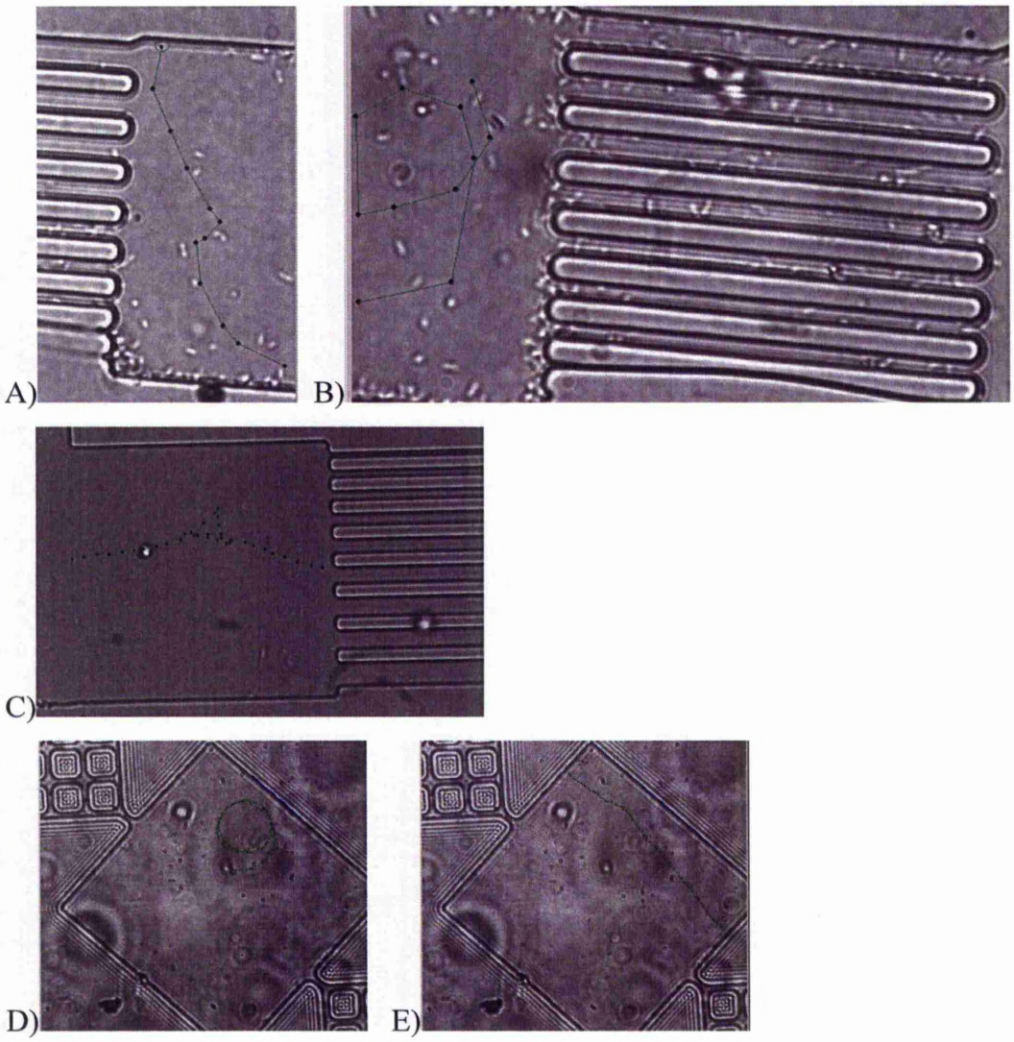

Figure 5.4: *S. marcescens* (A and B) and *P. stutzeri* (C, D and E) set of trajectories within the 'plaza'-like space. The 'plaza'-like space represents the free space between the networks (here the *Stripe* and *Diamond* networks). The plots were generated by manual tracking with Retrac. It can be seen that the free-swimming bacteria are either swimming in relatively straight lines A) and E) or trace out circular trajectories B) and D). The Figure 4.4 C) shows *P. stutzeri* swimming forward and backward.

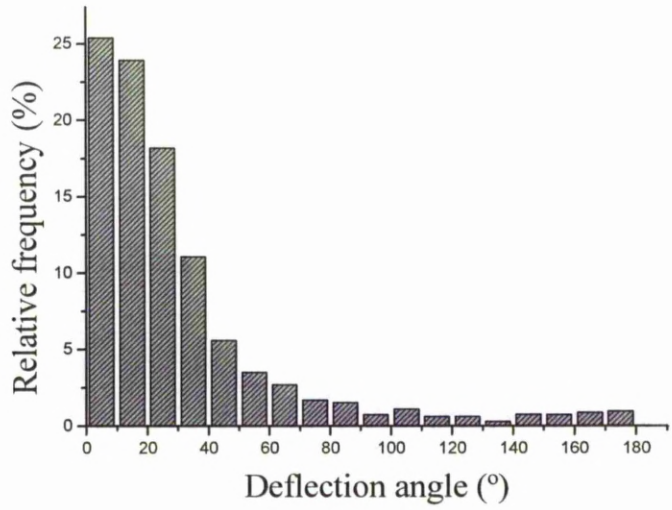

A)

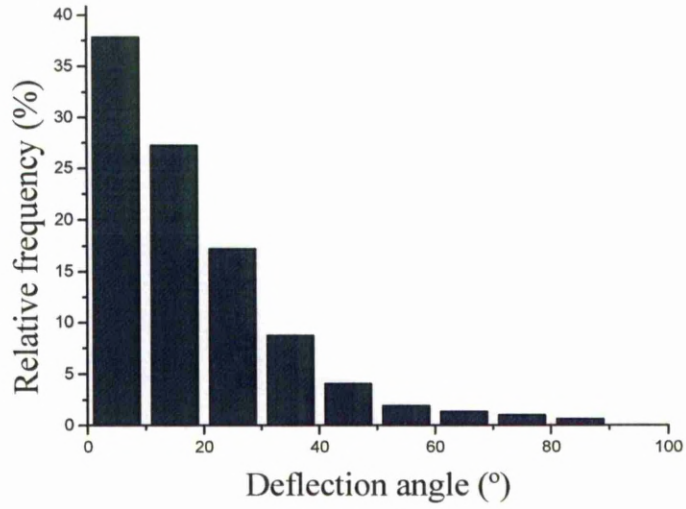

B)

Figure 5.5: *S. marcescens* (A) and *P. stutzeri* (B) deflection angle distribution within the 'plaza'-like space. The distributions are similar and exponential with a bias toward smaller angles.

The mean velocity of *S. marcescens* single cells was 19.7 ± 9.6 μm/s (Figure 5.6-A). The distribution seemed to be uniform and normal. The peaks of acceleration of *S. marcescens* ranged from 0 to 150 $\mu m/s^2$. The distribution was normal (Figure 5.7-A).

The mean velocity measured in the 'plaza'-like space for *P. stutzeri* reached 27.0 ± 11.3 µm/s (Figure 5.6-B). The main peaks of linear acceleration were between 0 and 50 µm/s^2 (Figure 5.7-B). Both distributions were normal. *P. stutzeri* swam faster than *S. marcescens*.

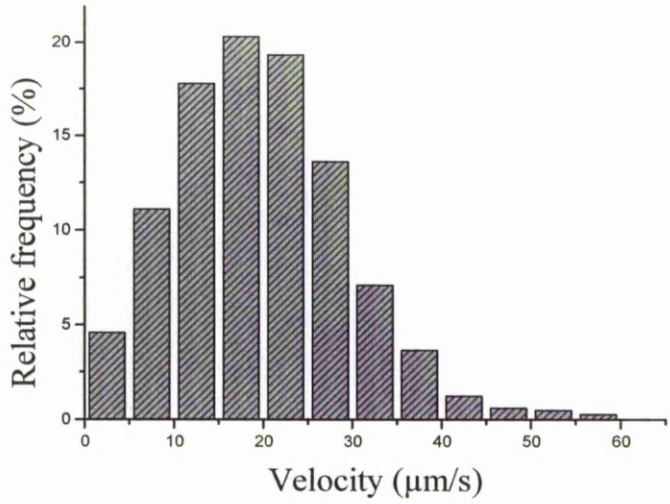

A)

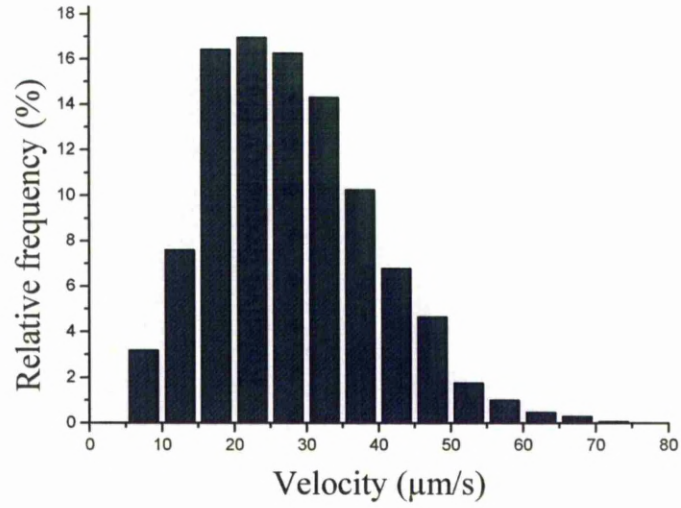

B)

Figure 5.6: *S. marcescens* and *P. stutzeri* velocity distribution within the 'plaza'-like space with fitted normal distribution. The velocity of each bacterial cell was directly calculated by Retrac.

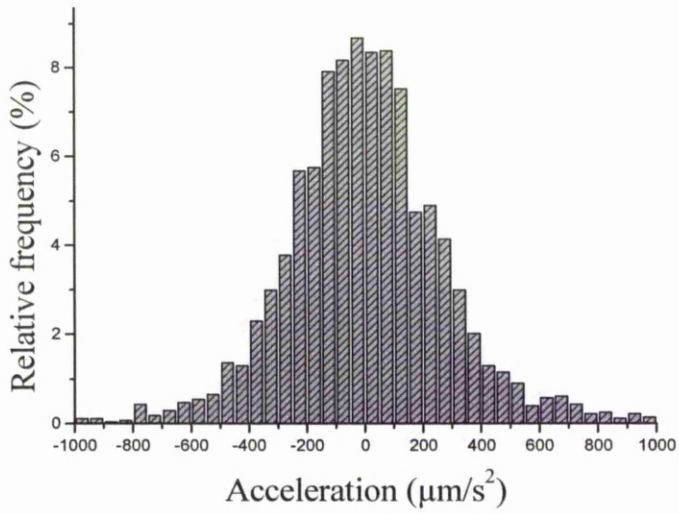

A)

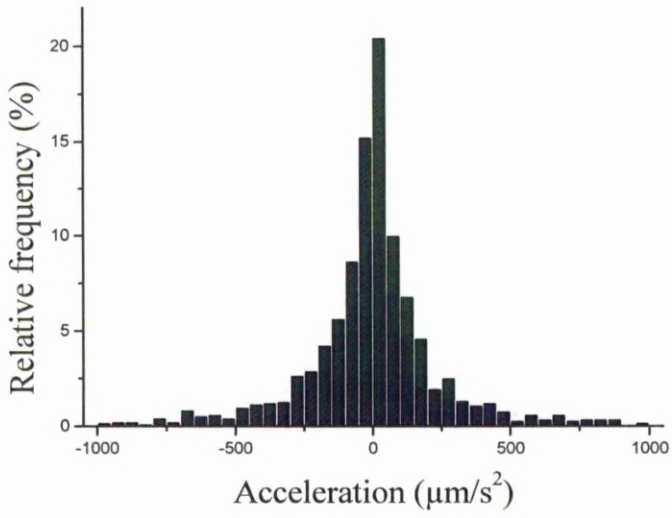

B)

Figure 5.7: *S. marcescens* and *P. stutzeri* acceleration distribution within the 'plaza'-like space with fitted normal distribution. The acceleration data were calculated from the velocity data calculated by Retrac.

Within the 'plaza'-like space, the bacterial movement is restricted to two-dimensions, which result in only two possibilities; straight motion or turn in the reverse direction after a tumble. According to our videos, the cell population swam

either toward the micro-channels or toward the lateral walls. To quantify whether the bacterium had a particular affinity for the wall, we measured for each path the smallest distance between a cell and the lateral wall in order to determine their preferred position. According to Figure 5.8-A, *S. marcescens* cells were present everywhere with a preference for positions at 10-15 μm and 25-30 μm from the lateral wall (main peak at 12.5 μm). It seemed that the cells' velocities were not affected at all by the boundaries. Figure 5.9-A shows a constant velocity whatever the cells' position. *P. stutzeri* cells showed a tendency to swim toward the edges of the 'plaza'-like space as well as towards the microstructures. According to Figure 5.8-B, the bacteria are present everywhere but there is a preferred position at 5-20 μm from the lateral wall (main peak at 12.5 μm). Figure 5.9-B shows no really effect of the boundaries on the cells' velocities.

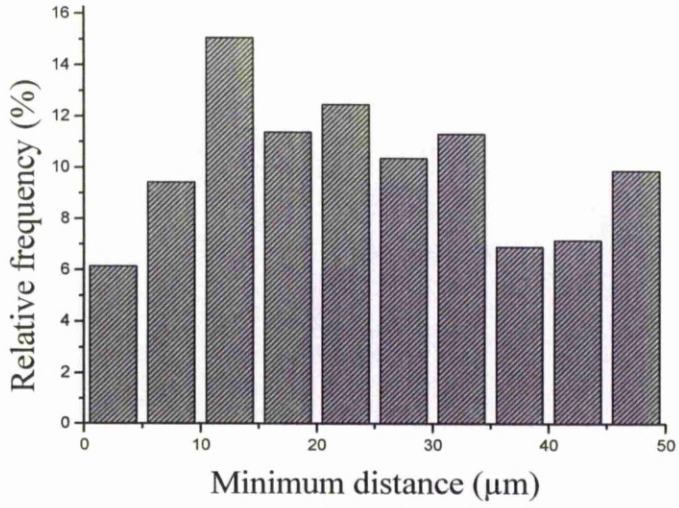

A)

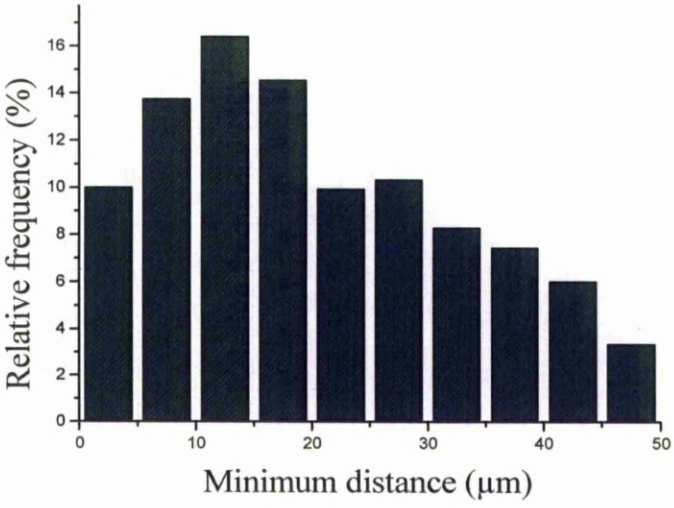

B)

Figure 5.8: Distribution of the minimum distance of *S. marcescens* (A) and *P. stutzeri* (B) cells from the lateral wall with fitted normal distribution. As the bacteria swam on the surface of the 'plaza'-like space the distance between a cell and the lateral wall was systematically recorded in order to determine the preferred position of the cells.

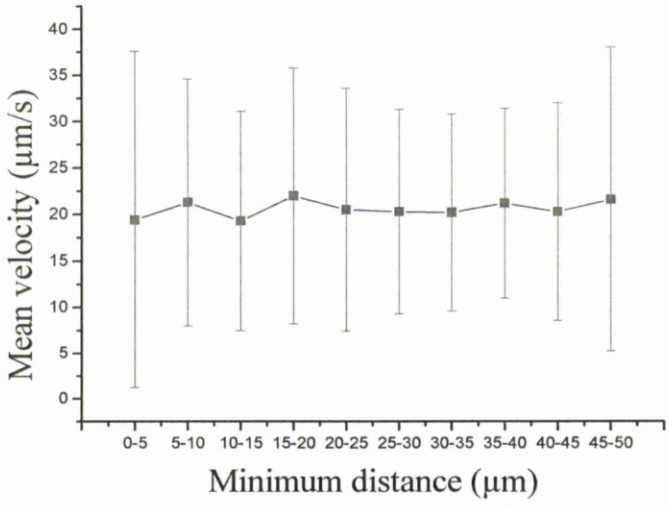

A)

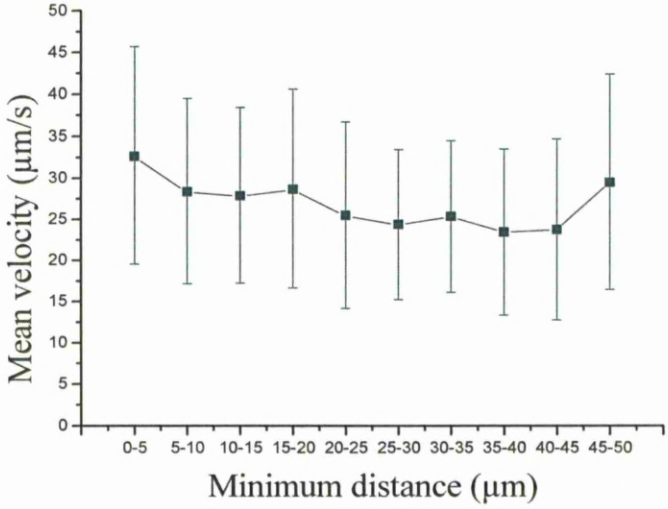

B)

Figure 5.9: Correlation between the cells' velocity and the minimum distance to the lateral wall for *S. marcescens* (A) and *P. stutzeri* (B). The velocity was constant indicating that there was no influence from the lateral walls. The bars represent the standard deviation.

Table 5.1 presents a summary of the motility data for both species in the 'plaza'-like space. *S. marcescens* and *P. stutzeri* shared some common behaviour such as circular trajectories or straight paths. The observed circular trajectories are not perfect circles with a fixed radius. Instead deviations from a circular trajectory can be observed with a varying radius. *P. stutzeri* smaller deflection angles indicate that the dominant patterns of the species were straight paths with small deviation from the original trajectory. *S. marcescens* was able to change its swimming direction more often than *P. stutzeri*. *P. stutzeri* swam faster than *S. marcescens* over the surface. None of the species seemed to experience any effect from the lateral boundaries in term of swimming speed and both species were able to move all over the surface. The motile behaviour of *P. stutzeri* to that of *S. marcescens* appeared to be quite different.

	Mean velocity (μm/s)		Acceleration range ($\mu m/s^2$)		Mean deflection angle (°)	
Species	*Sm*	*Ps*	*Sm*	*Ps*	*Sm*	*Ps*
'Plaza'-like space	19.7 (± 9.6) (2858)	27.6 (± 11.3) (1707)	0-150 (2858)	0-50 (1661)	30.8 (± 34.0) (2778)	18.4 (± 15.6) (1647)

Table 5.1: Summary of the motility data of *S. marcescens* (*Sm*) and *P. stutzeri* (*Ps*) measured in the 'plaza'-like space. Data represent the mean (± standard deviation) except for the data concerning the acceleration where only the range is indicated. The brackets enclose the numbers of data points for every parameter.

Both populations of cells were now observed in different networks. As described in chapter 3 section 3.1.1, all networks showed different levels of complexity and different designs. Natural habitats are usually porous and tortuous. Complex mazes were used under the assumption that an enclosed environment would provide a means to systematically perturb the cell population. The geometries allow monitoring of how the population of bacteria adapt to live in confined environments and allow monitoring the population of cells in one experiment.

5.2.2.2 *Stripe* network

The effects of different channel widths (2 to 10 μm) on motility of *S. marcescens* and *P. stutzeri* were investigated. The motility parameters measured were the velocity, acceleration and deflection angles as well as the species' positions within the channels.

80 cells of *S. marcescens* were tracked within the *Stripe* structures. Bacterial cells reaching the edge of a channel underwent a directional motion following closely the PDMS wall with small deviation in the swimming trajectory from a straight path within the networks (Figure 5.10). Crossings from one wall to the opposite wall were also observed. The cells could easily swim through every channel regardless of size and swam very close to the lateral wall. As the width of the channels decreased, the bacteria maintained nearly constant straight motion. The mean deflection angle was also measured in the *Stripe* network (Figure 5.11). The mean deflection angle of 20.5 ± 17.8 ° was smaller in the 10 μm channel compared with those observed in the 'plaza'-like space. This can be explained by the size of the channels; the freedom of movement was much greater in the 'plaza'-like space than in the *Stripe* network.

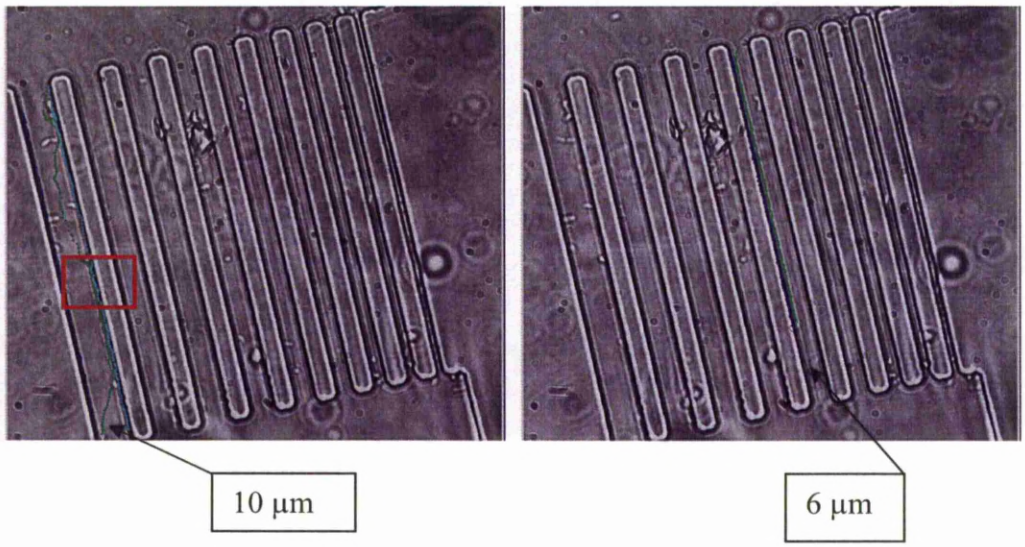

Figure 5.10: Set of plots of *S. marcescens* swimming within the 10 µm and 6 µm channels of the *Stripe* network. The plots were generated by manual tracking with Retrac and show examples of trajectories of a single bacterium. Within the 6 µm wide channel the bacterium swim forward and close to the channel wall. Within the 10 µm wide channel the forward swimming is interrupted by a tumble (red box) which makes the cell temporarily move away from the wall.

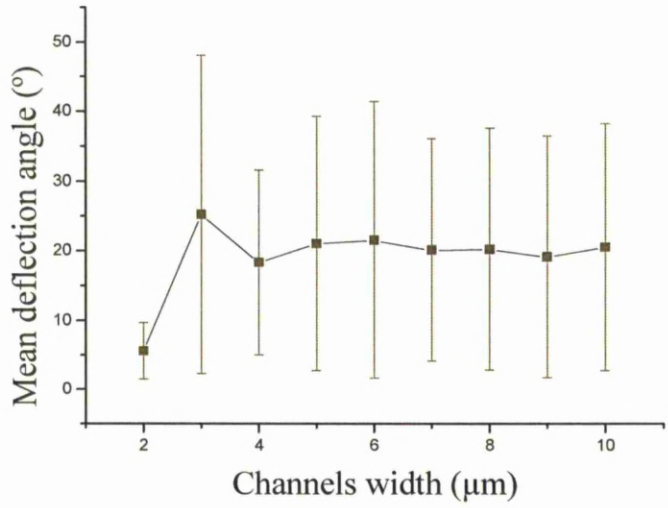

Figure 5.11: Mean deflection angle of *S. marcescens* measured for each channel (2 µm to 10 µm) of the *Stripe* network. The deflection angles are constant with the exception of the 2 µm channel. The bars represent the standard deviation.

The mean velocity was 29.8 ± 10.2 μm/s in the 10 μm channel and decreased slightly (exception was the 5 μm channel) to reach 24.6 ± 7.2 μm/s in the 2 μm channel (Figure 5.12). The bacteria swam faster within the *Stripe* micro-channels than in the 'plaza'-like 100 μm channels. The peak of acceleration was between 0 and 50 $\mu m/s^2$ (Figure 5.13). Within the 'plaza'-like space the acceleration values were more widespread than in the *Stripe* network showing that the *Stripe* network induces a more constant motility rate. The minimum distance between a bacterial cell and the lateral wall was also measured to check any hydrodynamic force effects. The exponential distribution indicates a cell's strong affinity for a wall. The peak of maximum density of bacteria was always localized within 1 μm from the lateral wall (Figure 5.14).

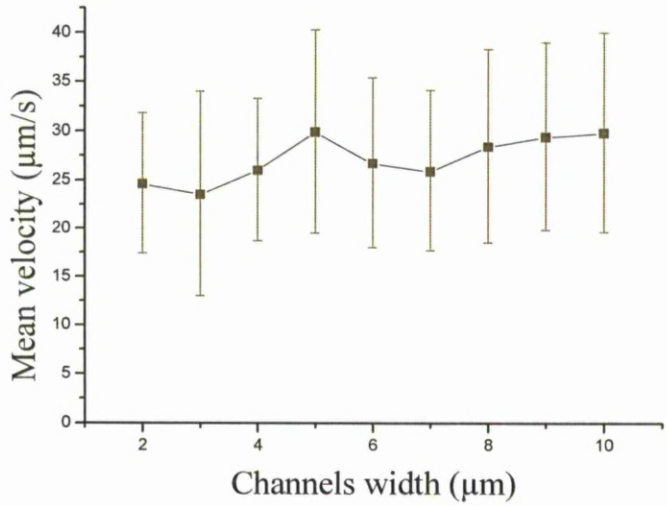

Figure 5.12: Mean velocity of *S. marcescens* measured for each channel (2 μm to 10 μm) of the *Stripe* network. The velocity decreased slightly from the 10 μm channel to the 2 μm channel. The bars represent the standard deviation.

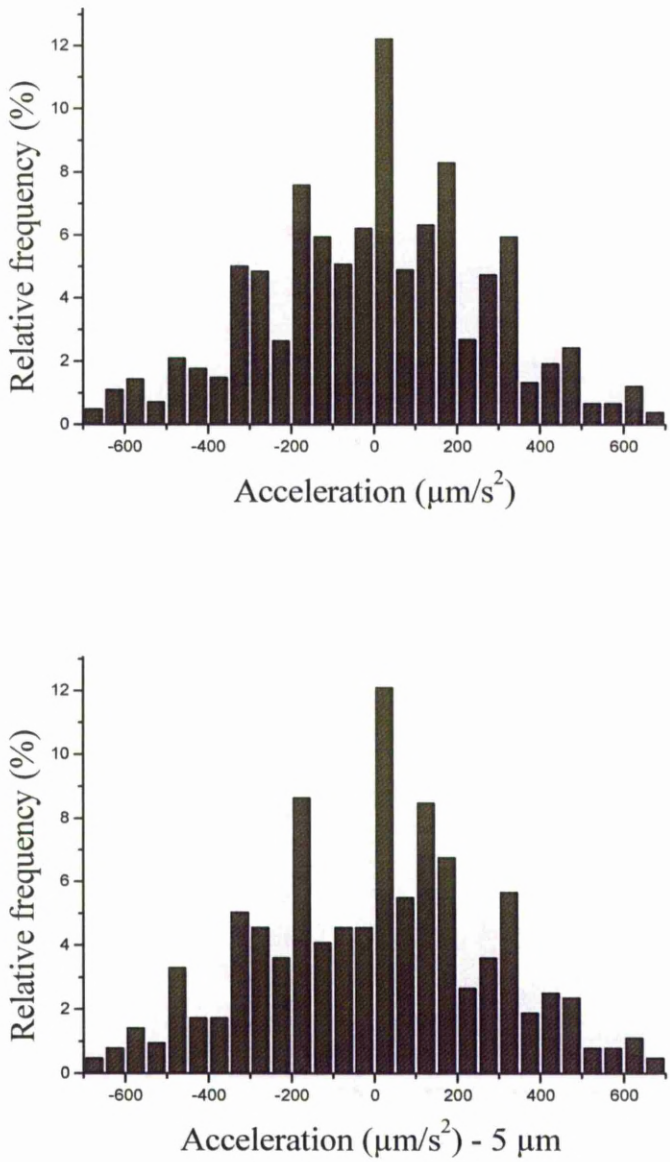

Figure 5.13: Distribution of acceleration of *S. marcescens* in the 10 μm and 5 μm channels with fitted normal distribution. Similar distributions were measured in the 9-, 8-, 7-, 6-, 4-, 3-, and 2 μm channels (See appendix I). A peak of acceleration was seen at 50 $\mu m/s^2$.

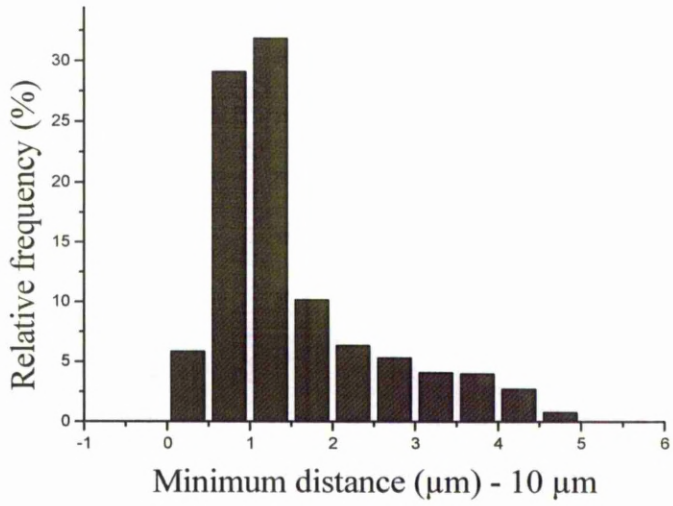

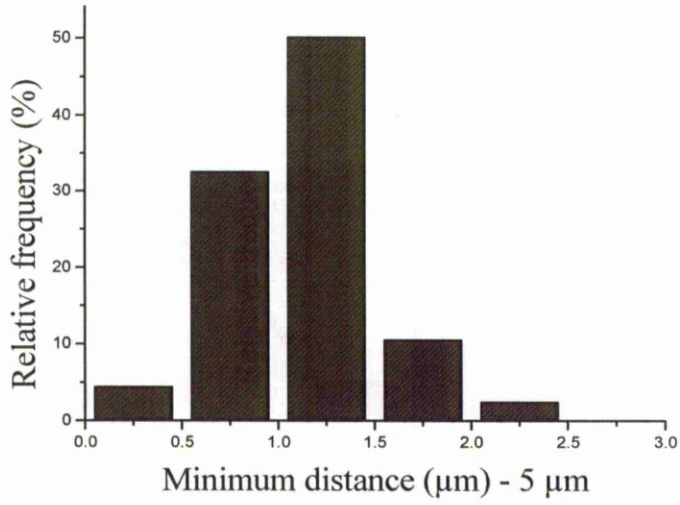

Figure 5.14: Distribution of the minimum distance between *S. marcescens* cells and the channel wall within the 10 μm and the 5 μm wide channels with fitted normal distribution. Similar distributions were measured in the 9-, 8-, 7-, 6-, 4-, 3-, and 2 μm channels (See appendix I). Most of the cells are distributed within 1μm from the channel wall.

P. stutzeri tracking within the *Stripe* network revealed that the cells were moving constantly forward following closely the channels walls (Figure 5.15-A). In some channels, the motion appeared wavy and the bacterium alternated between the two walls (Figure 5.15-B). Back-forward movements were seen within the channels. A deflection angle distribution was measured in every channel. The mean deflection angle was found to be quite constant for the channels between 10 µm to 5 µm (19-20 °) then the angle decreased to reach 6.8 ° in the 3 µm channel (Figure 5.16).

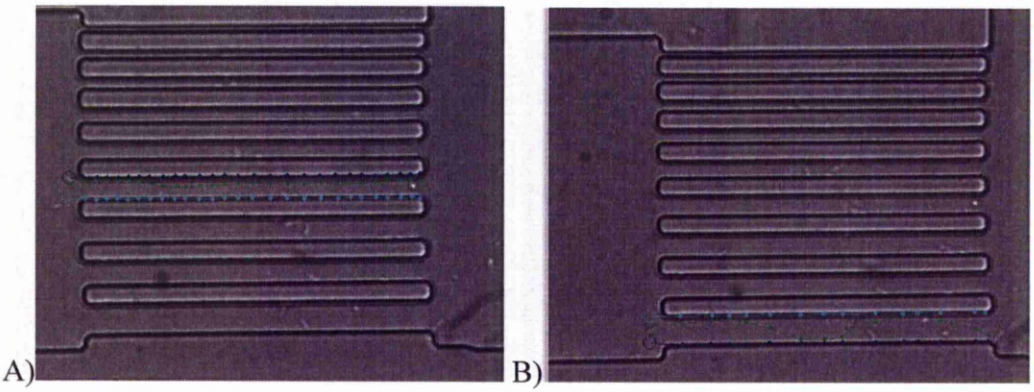

Figure 5.15: Example of *P. stutzeri* trajectories within the *Stripe* network. The set of plots was generated by manual tracking with Retrac. *P. stutzeri* cells both moved forward and close to the wall (A) or exhibited a wavy motion (B).

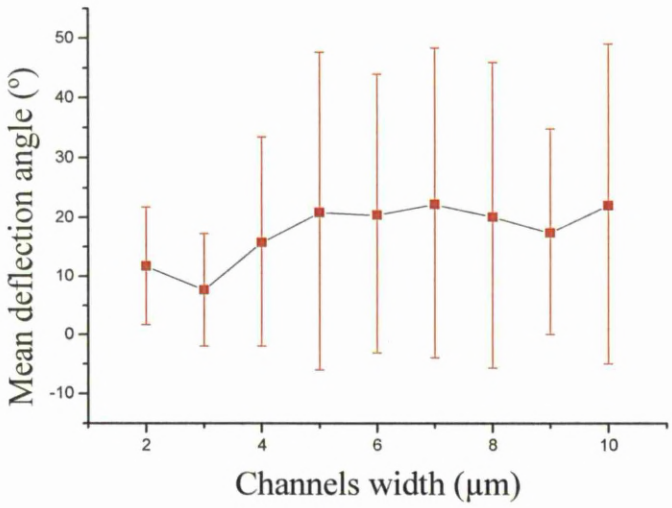

Figure 5.16: Mean deflection angle of *P. stutzeri* measured for each channel (2 μm to 10 μm) of the *Stripe* network. The deflection angles are constant until the 5 μm channel then decreased. The bars represent the standard deviation.

The mean velocity was 27.9 ± 13.4 μm/s in the 10 μm channel. The velocities of the cells were the same in comparison to the 'plaza'-like space. The mean velocity was affected by the channel width in narrower channels only. In the 2 μm channel the mean velocity was 12.7 ± 7.1 μm/s (Figure 5.17). The main acceleration peak was between 0 to 50 $\mu m/s^2$ (Figure 5. 18).

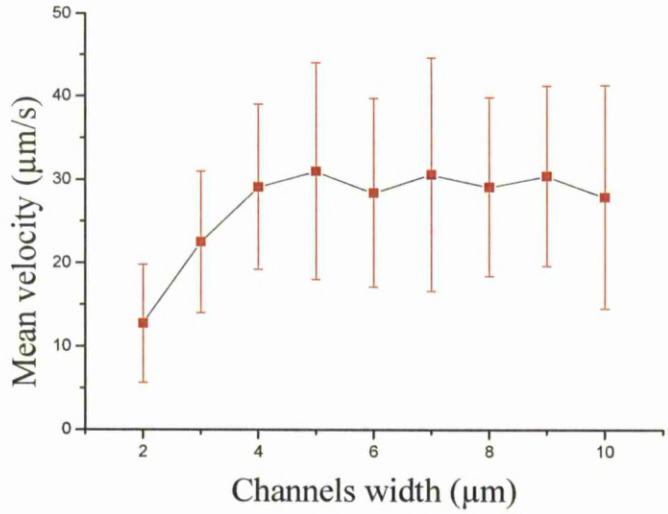

Figure 5.17: Mean velocity of *P. stutzeri* measured for each channel (2 µm to 10 µm) of the *Stripe* network. The velocity is constant and similar to the 'plaza'-like space until the 4 µm channel then decreased. The bars represent the standard deviation.

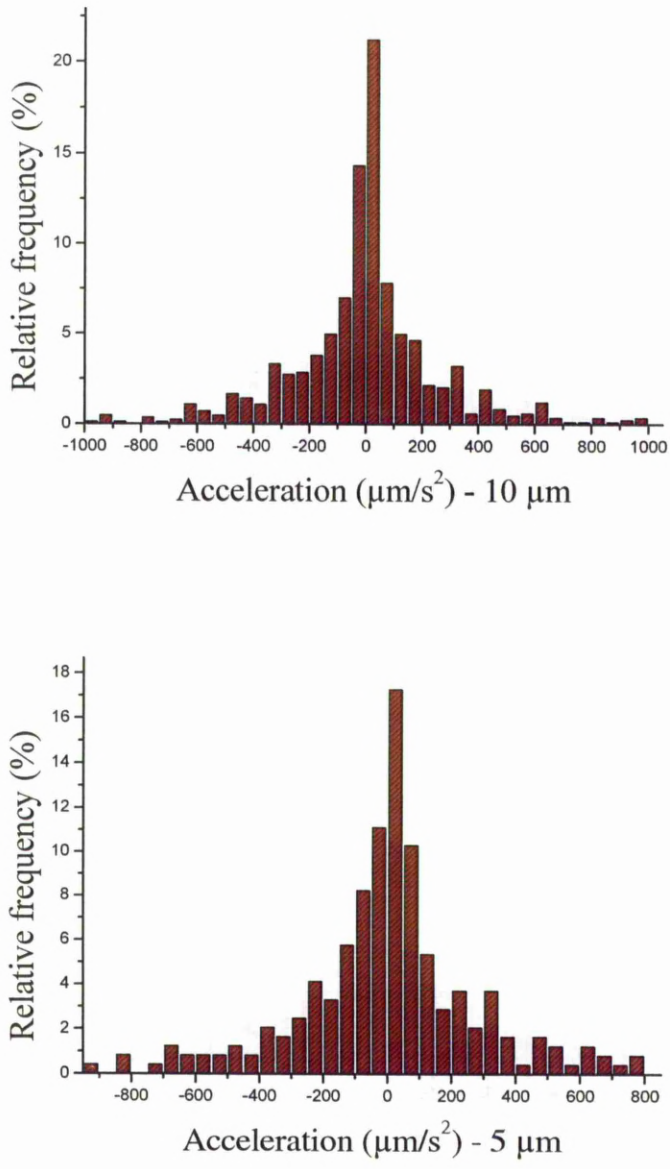

Figure 5.18: Distribution of acceleration of *P. stutzeri* in the 10 μm and 5 μm channels with fitted normal distribution. Similar distributions were measured in the 9-, 8-, 7-, 6-, 4-, 3-, and 2 μm channels (See appendix I). The main peak of acceleration is at 50 $\mu m/s^2$.

Similarly to *S. marcescens* the cells' distribution close to each channel walls, which is the minimum distance (Figure 5.19) was measured. The density distribution in the 10 μm channel showed the maximum density of cells within 1 μm from the wall. The distribution in the 5 μm channel showed no preference for a particular distance.

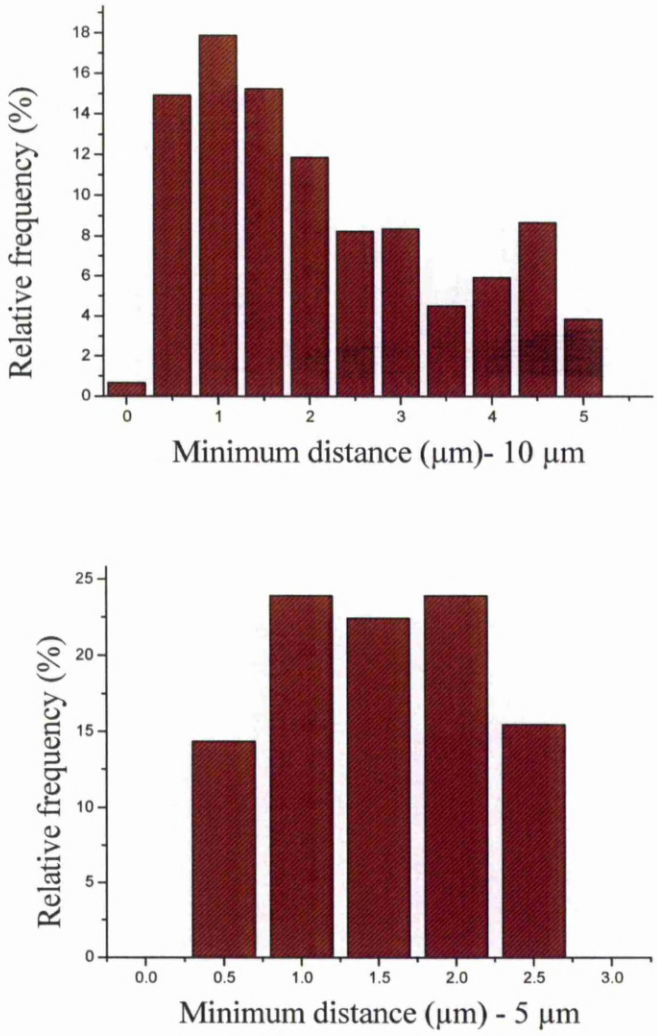

Figure 5.19: Distribution of the minimum distance between *P. stutzeri* cells and the channel wall within the 10 μm and the 5 μm wide channels with fitted normal distribution. Similar distributions were measured in the 9-, 8-, 7-, 6-, 4-, 3-, and 2 μm channels (See appendix I). Within the 10 μm channel the cells show an affinity for the channel wall but not within the 5 μm channel.

Table 5.2 summarises the motility data for *S. marcescens* and *P. stutzeri* within the 'plaza'-like space and within the *Stripe* networks. The species' behaviour appeared to be different in the micro-channels. The *S. marcescens* swimming pattern is a run and tumble in one direction. *P. stutzeri* showed similar but also different swimming patterns: forward movement with much longer runs and also wavy motions. Additionally *P. stutzeri* did not seem to swim very close to the wall of the micro-channels. The species did not experience the 'wall effect' as much as *S. marcescens* did.

	Mean velocity (μm/s)		Acceleration range (μm/s^2)		Mean deflection angle (°)	
Species	*Sm*	*Ps*	*Sm*	*Ps*	*Sm*	*Ps*
'Plaza'-like space	19.7 (± 9.6) (2858)	27.9 (± 11.3) (1717)	0-150 (2858)	0-50 (1661)	30.8 (± 34.0) (2778)	18.4 (± 15.6) (1647)
2μm	24.6 (± 7.2) (537)	12.7 (± 7.1) (99)	0-50 (508)	0-50 (92)	5.6 (± 4.1) (412)	11.7 (± 10.0) (92)
3μm	23.5 (± 10.5) (723)	22.5 (± 8.5) (182)	0-50 (723)	0-50 (165)	25.2 (± 22.9) (710)	7.6 (± 9.6) (161)
4μm	25.93 (± 7.3) (611)	29.1 (± 9.9) (338)	0-50 (611)	0-50 (318)	18.3 (± 13.3) (603)	15.7 (± 17.7) (318)
5μm	30.0 (± 10.4) (660)	31.0 (± 13.0) (260)	0-50 (660)	0-50 (249)	21.0 (± 18.3) (644)	20.8 (± 26.8) (250)
6μm	26.7 (± 8.7) (1220)	28.4 (± 11.3) (542)	0-50 (1222)	0-50 (518)	21.5 (± 19.9) (1205)	20.4 (± 23.5) (518)
7μm	25.9 (± 8.2) (563)	30.6 (± 14.0) (898)	0-50 (563)	0-50 (874)	20.1 (± 16.0) (552)	22.2 (± 26.1) (866)
8μm	28.4 (± 9.9) (1484)	29.1 (± 10.7) (675)	0-50 (1484)	0-50 (654)	20.2 (± 17.4) (1450)	20.1 (± 25.8) (653)
9μm	29.4 (± 9.6) (906)	30.4 (± 10.8) (571)	0-50 (906)	0-50 (555)	19.1 (± 17.4) (882)	17.4 (± 16.2) (538)
10μm	29.8 (± 10.2) (1899)	27.9 (± 13.4) (870)	0-50 (1899)	0-50 (849)	20.5 (± 17.8) (1860)	22.0 (± 27.0) (841)

Table 5.2 Motility data of *S. marcescens* (*Sm*) and *P. stutzeri* (*Ps*) measured in the 'plaza'-like space and within all the channels (2 μm to 10 μm) of the *Stripe* network. Data represent the mean (± standard deviation) except for the data concerning the acceleration where only the range is indicated. The brackets enclose the numbers of data points for every parameter.

The effects of the Stripe network on bacterial behaviour were evaluated statistically (P-value < 0.05). Statistics were performed focusing on the following parameters: the velocity, the acceleration and the deflection angle (Table 5.3).

Each channel width of the *Stripe* network influenced the velocity parameter of *S. marcescens* (two-tailed unpooled Student's *t*-test except for the 8 μm wide and 9 μm wide channels where a two-tailed pooled Student's *t*-test was used). The deflection angle parameter was also influenced by the *Stripe* network (two-tailed unpooled Student's *t*-test of log-transformed values). The micro-channels did affect the acceleration parameter, except for the 9 μm wide channel (two-tailed unpooled Student's *t*-test).

The confinement had an effect on the velocity parameter for *P. stutzeri* except within the 4 μm, 6 μm and 10 μm wide channels (two-tailed unpooled Student's *t*-test except for the 6 μm wide, 8 μm wide and 9 μm wide channels where a two-tailed pooled Student's *t*-test was used). The effect of the confinement on the deflection angle parameter was statistically significant for the 2 μm wide, 3 μm wide and 5 μm wide channels (two-tailed unpooled Student's *t*-test of log-transformed values, except for the 9 μm wide channel where a two-tailed pooled Student's *t*-test of log-transformed values was used). The confinement had no effect on the acceleration parameter (two-tailed unpooled Student's *t*-test).

		Serratia marcescens			*Pseudomonas stutzeri*		
Channel width		Velocity	Acc.	Deflection angle	Velocity	Acc.	Deflection angle
2µm	T-value	-13.69	-3.45	37.43	19.97	0.03	4.30
	P-value	< 0.01	< 0.01	< 0.01	< 0.01	0.97	< 0.01
	DF	934	3359	768	129	779	87
3µm	T-value	-8.92	-2.04	12.67	7.85	-0.57	12.72
	P-value	< 0.01	0.04	< 0.01	< 0.01	0.57	< 0.01
	DF	1048	2281	978	256	817	183
4µm	T-value	-18.06	-2.18	7.88	-2.01	-0.01	3.90
	P-value	< 0.01	0.03	< 0.01	0.05	0.99	< 0.01
	DF	1111	1692	1081	524	419	381
5µm	T-value	-22.94	-5.93	5.79	-3.61	-0.16	0.53
	P-value	< 0.01	< 0.01	< 0.01	< 0.01	0.87	0.60
	DF	931	2899	1108	322	296	288
6µm	T-value	-22.82	-2.34	6.54	-0.89	0.34	0.01
	P-value	< 0.01	0.02	< 0.01	0.37	0.73	0.99
	DF	2516	3438	2625	2238	769	770
7µm	T-value	-15.82	-2.42	6.03	-5.01	-0.43	-1.22
	P-value	< 0.01	0.02	< 0.01	< 0.01	0.67	0.22
	DF	892	1293	891	1527	1420	1501
8µm	T-value	-28.01	-2.31	9.23	-2.38	0.31	1.12
	P-value	< 0.01	0.02	< 0.01	0.02	0.76	0.26
	DF	4340	4082	3275	2370	1089	909
9µm	T-value	-26.45	-1.81	8.63	-4.56	-0.46	1.31
	P-value	< 0.01	0.07	< 0.01	< 0.01	0.65	0.19
	DF	3762	2290	1845	2264	851	1960
10µm	T-value	-34.31	-2.39	9.10	-0.03	-0.01	-0.14
	P-value	< 0.01	0.02	< 0.01	0.98	0.99	0.89
	DF	3892	4706	4349	1506	1559	1317

Table 5.3: Results given by Minitab 15 when testing the effect of the *Stripe* network on the motility behaviour of *S. marcescens* and *P. Stutzeri* in comparison to the motility behaviour measured within the 'plaza'-like space. The results of the different Student's *t*-test were reported by the T-value, P-value and DF (Degree of Freedom). The tab shows that the *Stripe* network significantly changed the behaviour of *S. marcescens* for the three parameters. The *Stripe* significantly changed the behaviour of *P. stutzeri* only in term of velocity and deflection angle and for some channels width only.

The confinement had a limited impact on the motility parameters of *P. stutzeri* in comparison to the 'plaza'-like area except for channels size smaller than 4 μm. For *S. marcescens*, the motility parameters as well as the behaviour of the species were different within the *Stripe* network in comparison to the 'plaza'-like area. The interaction of the flagella with the channels changed the behaviour of the bacteria.

5.2.2.3 *Comb* network

The *Comb* structure consists of meandering channels with different widths (5-10-15 μm). This network could therefore be used to evaluate how complex patterns impacted on the swimming motility of *S. marcescens* and *P. stutzeri*. The species was challenged with very intricate paths of different width.

S. marcescens bacterial cells confined within the *Comb* structures followed closely the shape of the structures over limited distances when swimming within a 5 μm wide channel. In this very narrow channel, the cells seemed to be incapable of continuously executing a linear trajectory and instead swam in a *zigzag* manner (Figure 5.20-A_c). The mean velocity was 14.6 ± 9.2 μm/s (n = 415 and refers to the numbers of data points). Within the 5 μm channels, the cells of *P. stutzeri* were able to follow the intricacies of the microstructure and followed closely the wall boundaries over long distances (Figure 5.20-F). The cells attached to the wall quite frequently. Cells of *P. stutzeri* swam at a similar speed to *S. marcescens*, the mean velocity was 13.0 ± 7.5 μm/s (n = 353).

Within the 10 μm channel, the behaviour of *S. marcescens* was similar to the one observed in the 15 μm channel. The cells had difficulty following the frequent turns in this structure (Figure 5.20-A_b). As the channel width increased, the cells kept a directional trajectory and alternated from the right to the left side of the channels over long distances as observed previously in the straight channels (Figure 5.20-A_a). The fluctuations in distance of the bacterium to the channel wall subsequently led to variation of the swimming speed and swimming trajectory. The bacterial

trajectories may be altered because of collisions with the walls, thus impacting on the rate at which the cells spread through the microfluidics structures. The motility speed decreased as the channels width decreased from 25.7 ± 15.1 μm/s within the 15 μm (n = 721) channel to 16.4 ± 9.9 μm/s within the 10 μm channel (n = 224) to 14.6 ± 9.2 μm/s within the 5 μm channel (Figure 5.21-A). Within the 10 μm channel, *P. stutzeri* cells could either follow the intricacies over a limited distance (Figure 5.20-E) or the cells were trapped and swam in every direction (Figure 5.20-D). The mean velocity was 17.1 ± 10.0 μm/s (n = 329). Within the 15 μm channels, the cells of *P. stutzeri* alternated their movement from one wall to the opposite wall following the boundaries (Figure 5.20-C). A different behaviour was also observed when cells swam forward over limited distances but then swam in the reverse direction. This was dependent on the complexity of the obstacles in the way. The path taken by the cells seemed to be chosen randomly and the cells went off in many directions (Figure 5.20-B). The mean velocity was 20.9 ± 11.8 μm/s (n = 478). Figure 5.21-B summarises the mean velocity of the cells per channel width.

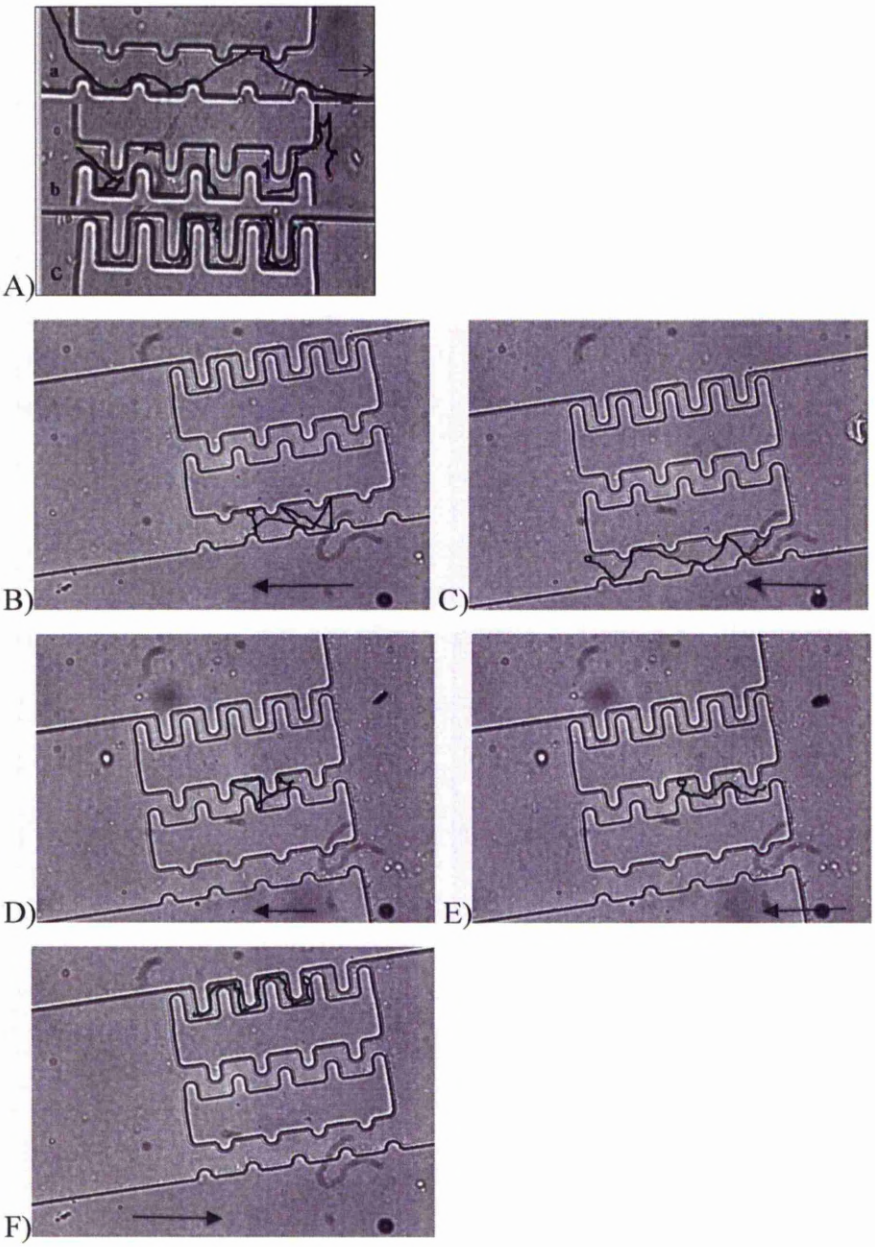

Figure 5.20: A) Represents the set of trajectories formed by *Serratia marcescens* swimming in the *Comb* network in three different channel widths. The plots were generated by manual tracking with Retrac. Image **a** is a 15 µm wide channel, image **b** is a 10 µm wide channel and image **c** is a 5 µm wide channel. The cells showed different motion in the three different channels: from a directional motion in the widest channel to a more random motion within the 10 µm and 5 µm wide channels. Pictures B), C), D), E), and F) represents the trajectories formed by *Pseudomonas stutzeri* swimming in the *Comb* network in three different channel widths. Images B and C are a 15 µm wide channel, image D and E are a 10 µm wide channel and image F is a 5 µm wide channel. The black arrows indicate the swimming direction.

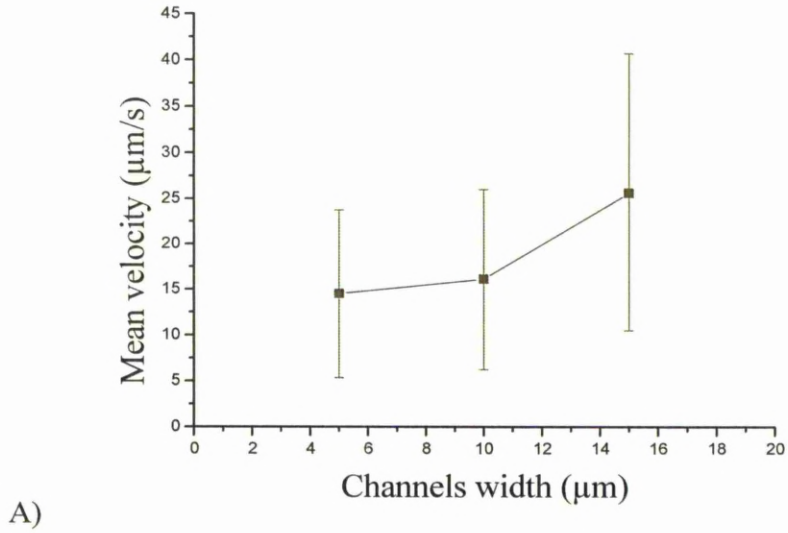

A)

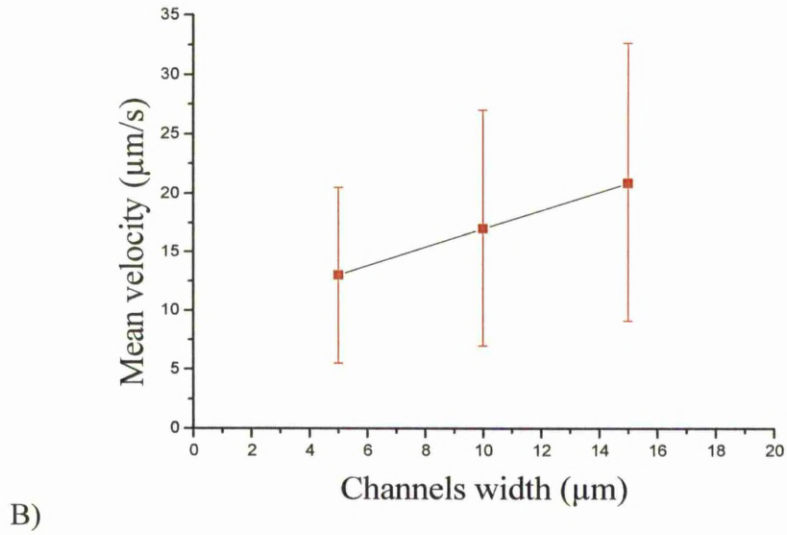

B)

Figure 5.21: Variation of bacterial velocity within the *Comb* network according to the channels width (5, 10 and 15 µm) for *S. marcescens* (A) and *P. stutzeri* (B). Bars represent the standard deviation.

The 5 µm and 10 µm channels negatively affected the motility of *P. stutzeri* cells. The additional complexity of the network makes motion more difficult. For *P. stutzeri* the mean cell velocity in the *Comb* structure was below the mean cell velocity in the 'plaza'-like space. For *S. marcescens* only the mean velocity in the 5 µm and 10 µm channels were below the mean velocity in the 'plaza'-like space. The

Comb structure prevents the cells spreading further on the surface and constrained the swimming cells within small areas.

The effect of the *Comb* network on the two species velocity was evaluated statistically (P-value < 0.05). The *Comb* network had an impact on the swimming behaviour of both species (Tab 4.4) (*S. marcescens*: two-tailed pooled Student's *t*-test except for the 15 μm wide channel where a two-tailed unpooled Student's *t*-test was used; *P. stutzeri*: two-tailed unpooled Student's *t*-test except for the 15 μm wide channel where a two-tailed pooled Student's *t*-test was used).

		Serratia marcescens	*Pseudomonas stutzeri*
Channels width		Velocity	Velocity
5μm	T-value P-value DF	10.28 < 0.01 3271	30.59 < 0.01 726
10μm	T-value P-value DF	5.04 < 0.01 3080	17.57 < 0.01 502
15μm	T-value P-value DF	-10.31 < 0.01 872	11.75 < 0.01 2173

Tab 5.4: Results given by Minitab 15 when testing the effect of the *Comb* network on the motility behaviour of *S. marcescens* and *P. Stutzeri* in comparison to the motility behaviour measured within the 'plaza'-like space. The results of the different Student's *t*-test were reported by the T-value, P-value and DF (Degree of Freedom). The tab shows that the *Comb* network significantly changed the behaviour of *S. marcescens* and *P. stutzeri* for the velocity parameter.

5.2.2.4 *Diamond* network

The *Diamond* network consists of a structure made of 16 small squares. Those structures tested the ability of the bacterial cells to swim through non-linear paths. The channel width is constant and about 5 µm in width.

The mean velocity of *S. marcescens* recorded in the *Diamond* structure was 19.8 ± 8.2 µm/s (n = 870). The bacterial cells were attracted by wall boundaries and followed closely the PDMS wall. Longer runs (Figure 5.22-A) punctuated by tumbles in which cells randomly reoriented producing new swimming directions were observed. The cells did not only choose straight paths but moved within the channels and explored them. Some places within the network enabled the cell to fully tumble and for the cells to reorient randomly and move in the opposite direction (Figure 5.22-B).

The mean velocity of *P. stutzeri* recorded in the *Diamond* structure was 19.7 ± 9.8 µm/s (n = 369). Within the *Diamond* network, the cells followed the network walls closely (Figure 5.22-D). The cells were able to move everywhere and were able to reorient themselves efficiently by swimming backward. Once the cells entered the network they had difficulty to exit it and seemed to be trapped. The cells were able to swim through the squares (Figure 5.27-C).

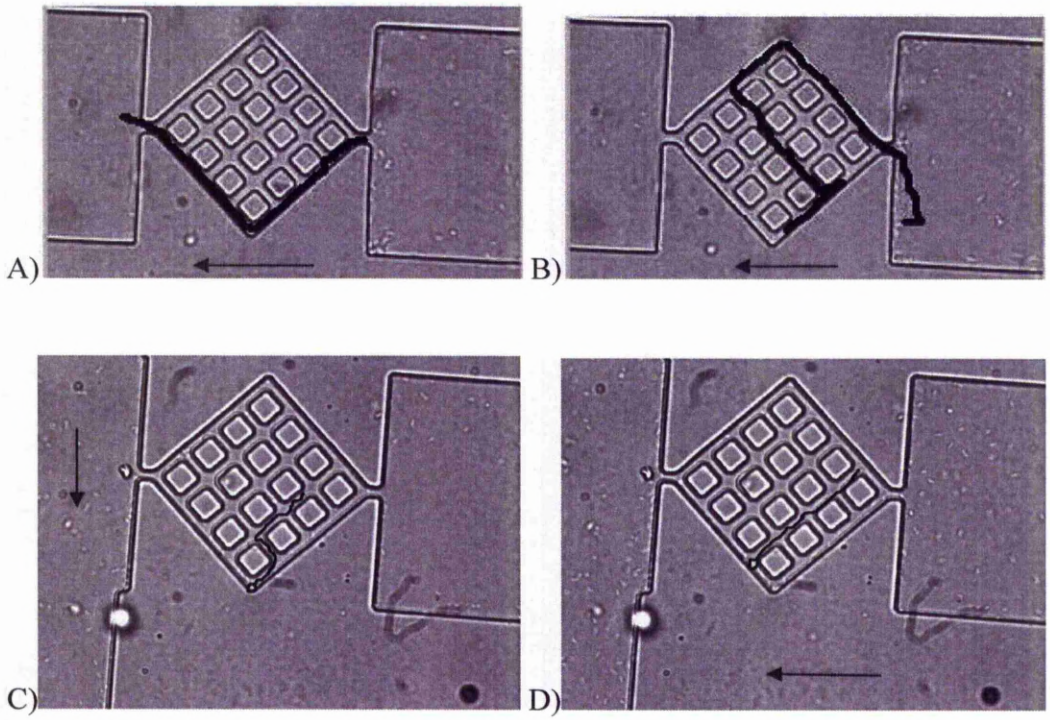

Figure 5.22: Examples of trajectories formed by *S. marcescens* (A and B) and *P. stutzeri* (C and D) in the *Diamond* network. The trajectories are quite diverse. Either the cells chose straight path or swam through the pillars. The black arrows indicate the swimming direction.

The velocity of *S. marcescens* was not significantly changed by the confinement (T-value = -0.18, P-value = 0.85, DF = 3726, two-tailed pooled Student's *t*-test) but was significantly changed for *P. stutzeri* (T-value = 13.56, P-value < 0.01, DF = 500, two-tailed unpooled Student's *t*-test of log-transformed values).

5.2.2.5 *Cellular* network

The *Cellular* structure consists of a main path in the middle and a lateral path with different angles of ± 30 ± 45 ± 60 and ± 90 ° respectively. The mean velocity of *S. marcescens* recorded in the *Cellular* structure was 18.0 ± 8.4 µm/s (n = 1874) and the mean for *P. stutzeri* was 18.3 ± 9.7 µm/s (n = 713). Within the *Cellular* structure, both species did not follow only straight paths (Figure 5.23-A and B) but explored the network through lateral paths also and were able to swim around a whole square

(Figure 5.23-C, D, E, F and G). Figure 5.23-G shows an example of forward-backward swimming by *P. stutzeri* within the channel.

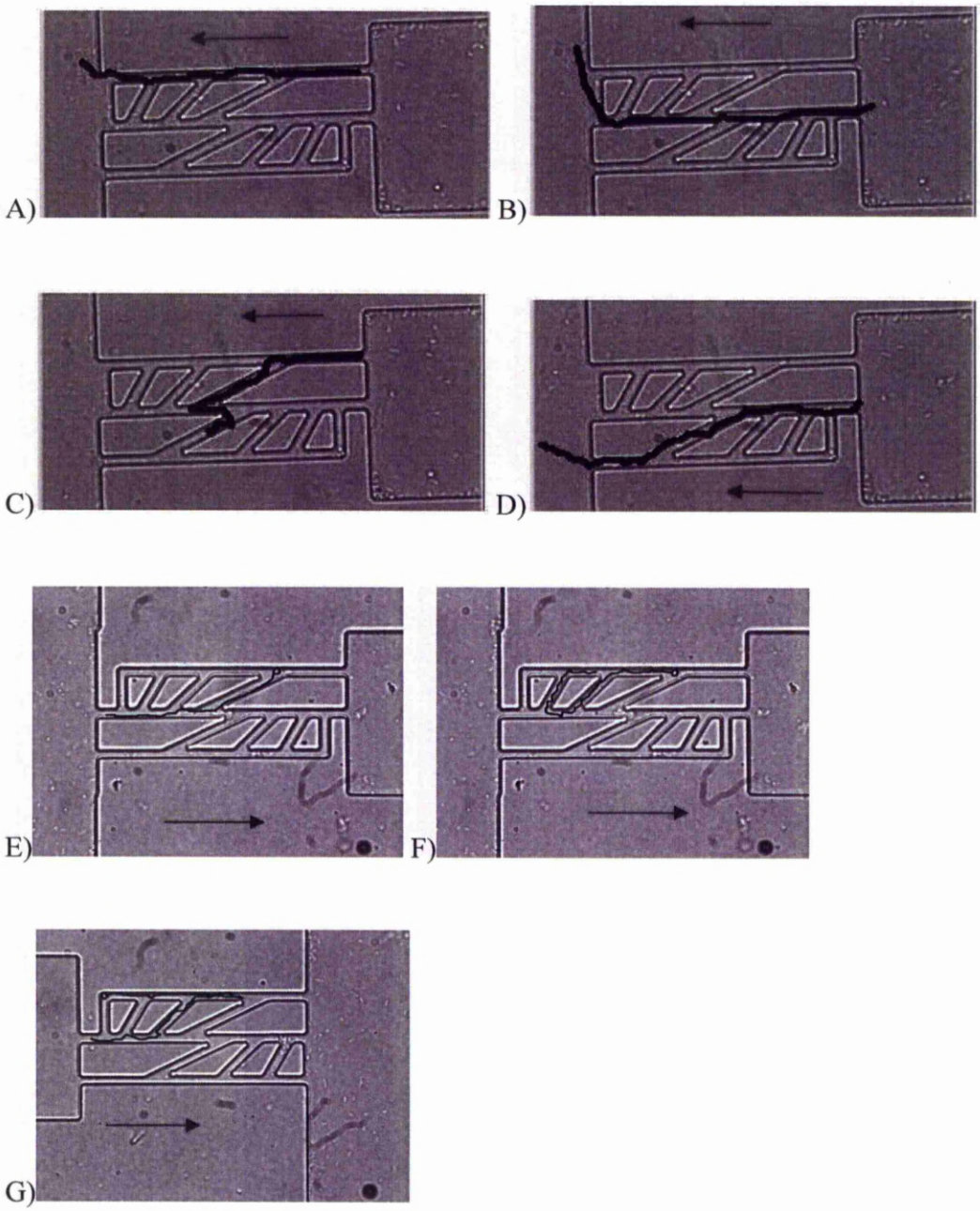

Figure 5.23: Examples of trajectories formed by *S. marcescens* (A, B, C and D) and *P. stutzeri* (E, F and G) in the *Cellular* network. The species could swim through the different lateral path as well as through the main straight paths. The black arrows indicate the swimming direction.

The velocity of *S. marcescens* was significantly changed by the confinement (T-value = 6.38, P-value < 0.01, DF = 4364, two-tailed unpooled Student's *t*-test). As for *P. stutzeri* (T-value = 20.19, P-value < 0.01, DF = 1110, two-tailed unpooled Student's *t*-test).

5.2.2.6 *Round-about* network

In the *Round-about* structure, the cells have to follow sequentially two rounded structures and there are two possibilities to enter the maze. The mean velocity of *S. marcescens* recorded in the *Round-about* structure was 20.3 ± 8.7 μm/s (n = 934). Similarly to the *Diamond* network, within the *Round-about* network the cells tumble and randomly reoriented themselves producing new swimming directions as illustrate in Figure 5.24-B, 5.26-A.

The mean velocity *P. stutzeri* recorded in the *Round-about* structure was 20.0 ± 9.7 μm/s (n = 588). The cells were able to turn around the round-about features either half-turn (Figure 5.24-C) or complete turn (Figure 5.24-E). Figure 5.24-D, shows that a cell is not always able to find the exit but change its direction.

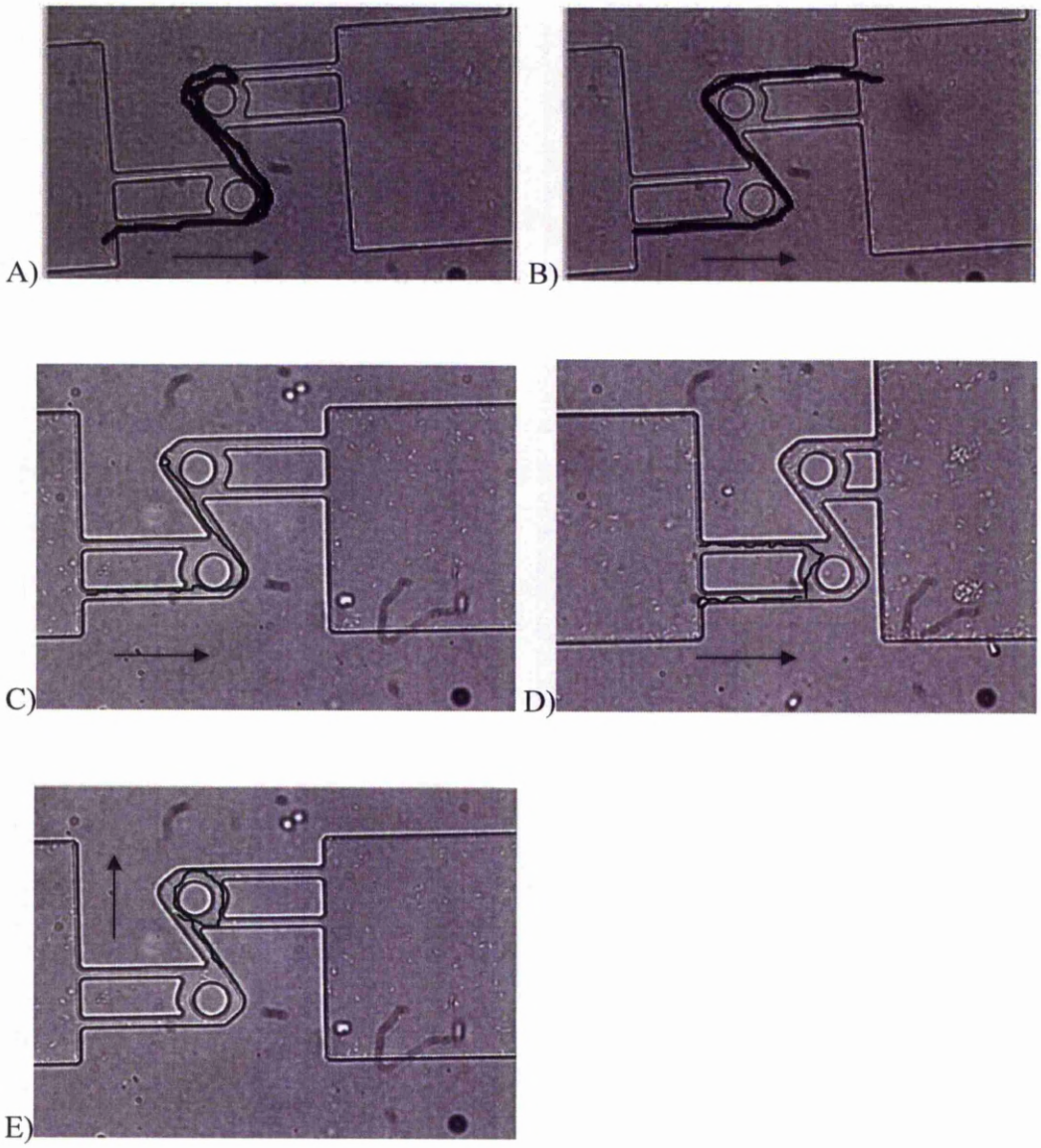

Figure 5.24: Examples of trajectories formed by *S. marcescens* (A and B) and *P. stutzeri* (C, D and E) within the *Round-about* network. The species could swim through the round-about features or make turn at 360 °. The black arrows indicate the swimming direction.

The velocity of *S. marcescens* was not significantly changed by the confinement (T-value = -1.78, P-value = 0.08, DF = 1727, two-tailed unpooled Student's *t*-test) but was significantly changed for *P. stutzeri* (T-value = 15.54, P-value < 0.01, DF = 911, two-tailed unpooled Student's *t*-test of log-transformed values).

Table 5.5 shows a summary of the two species' behaviour within all the microfluidics networks in comparison to the 'plaza'-like space. *S. marcescens* and *P. stutzeri* cells were challenged by different micro-confined places and were able to swim within the micro-channels. While the *Stripe* network could direct the motion of the cells, the *Comb* structures demonstrated the difficulty for cells to swim through intricate paths. In general, the cells showed different motion in the three different channels: from a directional motion in the widest channel to a more random motion within the 10 μm and 5μm wide channels. The channel width had an effect on the velocity of the cells. Because of the intricacies of the microstructures, the collisions with the matrix were very high thus the direction could change. The trajectories observed and the velocities measured within the *Round-about, Diamond* and the *Cellular* networks were similar for both species. The matrix had an impact on the rate at which the species spread through the networks in comparison to the 'plaza'-like space. That was especially the case for *P. stutzeri*, the Student's *t*-test was statistically significant for the three networks; only the *Cellular* network was statistically significant for *S. marcescens*. Except for the *Comb* network, it was always possible to follow *S. marcescens* cells from an entry to an exit of a network. *P. stutzeri* cells were often followed over limited distances because the cells attached to a wall and stopped swimming.

	S. marcescens	*P. stutzeri*
'Plaza'-like space	19.7 ± 9.6 µm/s Straight path Circular trajectories No attraction to the lateral wall	27.9 ± 11.3 µm/s Straight path Circular trajectories No attraction to the lateral wall
Stripe (2 to 10 µm)	From 24.6 ± 7.2 µm/s to 29.8 ± 10.2 µm/s Swim close to the channels wall Small deviation from a straight path Enhanced motility as the channels width increased	From 12.7 ± 7.1 µm/s to 27.9 ± 13.4 µm/s Swim close to the channels wall deviation from a straight path Wavy pattern
Comb	*5 µm* 14.6 ± 9.2 µm/s follow the intricacies over limited distance *10 µm* 16.4 ± 9.9 µm/s follow the intricacies over limited distance *15 µm* 25.8 ± 15.1 µm/s directional movement and switching from right to left	*5 µm* 13.0 ± 7.5 µm/s follow the intricacies either over limited or long distance *10 µm* 17.1 ± 10.0 µm/s follow the intricacies either over limited or long distance *15 µm* 20.9 ± 11.8 µm/s directional movement and alternance from right to left or forward-backward motion
Diamond	19.8 ± 8.2 µm/s Long run Exploration of different path Reorientation possible after a tumble	19.7 ± 9.8 µm/s Long run Exploration of different path
Cellular	18.0 ± 8.4 µm/s Follow straight and lateral path	18.3 ± 9.7 µm/s Follow straight and lateral path Reorientation possible
Round-about	20.3 ± 8.7 µm/s Cells follow the rounded features (180 °) Reorientation possible after a tumble	20.0 ± 9.7 µm/s Cells follow the rounded features (180 ° or 360 °)

Table 5.5: Summary of the behaviour as well as the mean velocity (± standard deviation) showed by *S. marcescens* and *P. stutzeri* in the 'plaza'-like space and within the different networks.

5.3 Discussion

5.3.1 Introduction

The motility parameters of *S. marcescens* and *P. stutzeri* observed in restricting geometries varied with respect to the micro-channels size and complexity demonstrating that the species can swim through pores only slightly larger than their own body. Statistical analysis showed similar but also different influences of confinement on both species' behaviour regardless of the network used.

5.3.2 Relevance of microfabrication for bacterial motility study

Free-living bacteria colonize a vast range of biotic and abiotic surfaces where they have to face different environmental conditions. The environment is constantly changing and bacteria respond to it by modifying their speed and direction. These surfaces are inherently microstructured complex and heterogeneous. For example soil, could be compared to a labyrinth made of a variety of obstacles. Soil consists of grains (mineral grains, rock fragments) with water and air in the voids between grains. The soil's particles have different size, shape and composition. The soil community includes ranks of invertebrate animals that alter the physical structure of the soil as they tunnel and feed, aerating the soil and forming channels for infiltration of water (Craig 1978). *S. marcescens* and *P. stutzeri* colonize among other environment, the soil in which they interact with minerals, fluids and other organisms. The size, shape and distribution of this space exert a major influence over the dynamics of these soil organisms. It has been estimated that one gram of soil may contain 10^{10}-10^{11} bacteria (Van der Heijden, Bardgett et al. 2008). Bacteria are restricted to the extent by which they can move by their body sizes. Although bacteria can move through pores as large as their diameter, most bacteria and bacterial colonies are found in pores three times their diameter (Ranjard, Richaume 2001).

Agar is the most common medium used in laboratories to study bacterial swimming, however, in natural environments, bacterial behaviour deviates significantly from that on a flat agar surface. Agar fails to reproduce the complexity of the bacterial natural environment and as a result does not reveal their adaptability. Although monitoring bacterial movement, behaviour and growth in the natural environment would be the ideal situation this is inherently difficult due to the non-transparent nature of the media they inhabit. This problem can now be addressed through microfluidics technology, namely soft lithography. This is used for the construction of microfluidic networks whereby patterns on a master are replicated with an elastomeric material, usually poly(dimethylsiloxsane) (PDMS), which is a biocompatible and transparent polymer. This technique enables the design of a vast range of topographies where the size, the shape and the spatial distribution of the features can be manipulated to match the physical dimensions of most microorganisms (Quake, Scherer 2000; Weibel, DiLuzio et al. 2007; Whitesides, Ostuni et al. 2001). Confinement restricts bacterial movement in two-dimensions (x and y direction), which results in only two possibilities; straight motion or a turn in the reverse direction. Due to the confinement bacteria remain in focus for longer time and over a determined length. Microstructures can be used to control the microenvironment of the cells which opens the possibility of using similar PDMS artificial networks to study bacterial motility. These networks provide a means for re-creating at least some of the complexity of the natural environment in a way that can be directly observed and quantified. This makes it possible to study how single bacteria behave near surfaces and through fluid in order to understand how bacteria may initiate biofilms, permeate porous media or infiltrate groundwater systems.

5.3.3 The effect of the confinement on the bacterial motility

5.3.3.1 Effect of the boundaries within the 'plaza'-like space

In the large channel i.e. the 'plaza'-like space, *P. stutzeri* and *S. marcescens* were able to swim freely everywhere. The tracking in two dimensions of *S. marcescens* and *P. stutzeri* showed straight path with few changes in direction. The few

directional changes occurred because of chemotaxis toward amino-acids in homogeneous solution (Berg, Brown 1972). Bacteria detect gradients in nutrients and move to regions of higher concentration (Berg 2004). The gradient-detecting mechanism in bacteria involves dozens of proteins whose reactions require up to 200 ms; this mechanism allows the bacteria to react to the sensed gradients (Segall, Manson et al. 1982). The flagellar motors of peritrichous and monotrichous bacteria turn either in the counterclockwise or in the clockwise direction which enable the cell to vary its swimming direction (Figure 5.25). At the scale in which bacteria live, Brownian motion occurs. This is showed by the random drifting of particles. After observation of the species behaviour, it is clear that the species were not affected by it.

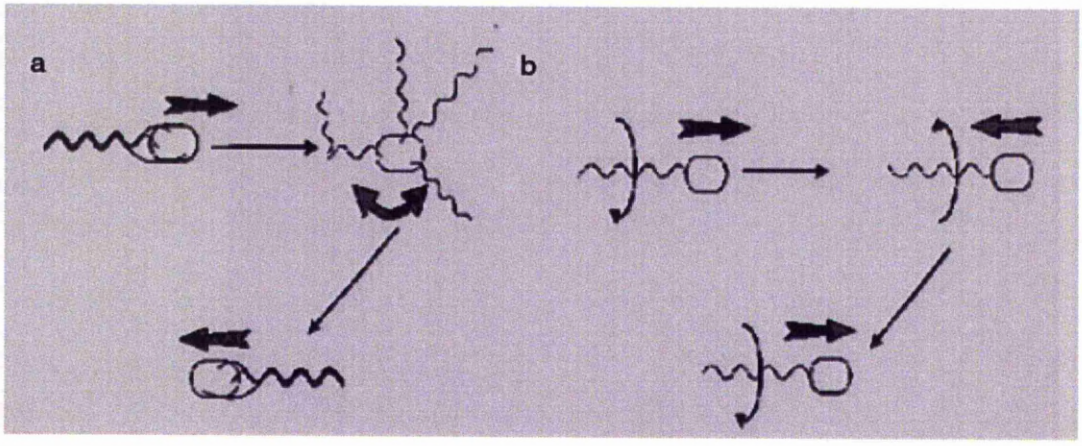

Figure 5.25: Run and tumble movement of peritrichously-flagellated bacteria like *S. marcescens* (a) and forward motion of monotrichously-flagellated bacteria like *P. stutzeri* (b) (Armitage 2006).

The 'plaza'-like space is 100 μm wide and 10 μm deep. Some studies indicated that cells are affected by the surface only when they swim within 10 μm of the surface as the hydrodynamic interactions decrease slowly with distance (Berg, Turner 1990; Frymier, Ford 1997; Biondi, Quinn et al. 1998). The literature usually indicates a velocity of ~ 30 μm/s for *S. marcescens* and a velocity of ~ 40 μm/s for *P. stutzeri* which is faster than the mean velocity recorded in the 'plaza'-like area. So here the cells were affected by two rigid boundaries. According to the results presented in

Figure 5.6, *S. marcescens* showed a non-negligible percentage of cells (~33%) swimming very slowly (< 15 μm/s). The cells could be attached to the surface or were nonmotile. Frymier, Ford et al. (1995) hypothesized that short-range forces (van der Waals, electrostatic and steric interactions) between the swimmer and the boundary may have trapped the cells near surfaces. Short range forces are responsible for cells' adherence to the surface. In contrast, long-range hydrodynamic interactions are sufficient to make the cells swim for longer time along the surface but at a fixed distance from the surface which explain the straight path.

Finally, the bacterial cells were observed to display circular trajectories. This behaviour has been already observed with peritrichously flagellated bacteria like *E. coli* (Frymier, Ford et al. 1995; Vigeant, Ford 1997) and monotrichously flagellated bacteria like *Vibrio alginolyticus* (Kudo, Imai et al. 2005; Magariyana, Ichiba et al. 2005). *E. coli* cells near solid surfaces do not have straight runs but were observed to trace out clockwise circles. This movement has been described when cells are very close to a surface because they experience more drag force per unit area than away from a surface. Close to a solid surface, a rotating cell body and the flagellar filament each experience a net lateral drag force but in opposite directions because the cell body and the flagellar filament rotate in opposite directions. Hydrodynamic interference between the rotating flagellum and the boundary generates lateral force to the swimming direction which causes the circular trajectory (Nakai, Kikuda et al. 2009). Li, Tam et al. 2008, showed that Brownian motion effect is amplified near a surface (the observations were made within 300 nm from the surface). As a consequence, Brownian motion will (i) alter the orientation of cell body and thus the bacterial swimming direction and (ii) change the distance between the cell and the surface therefore varying the surface-cell hydrodynamic interaction. Hydrodynamic interaction decreases as the distance between the cell and the surface increases and a larger distance provoke a larger radius of curvature, and vice versa (Lauga, DiLuzio et al. 2006). The result is variations in the circle radius as observed for both species. Additionally, DiLuzio, Turner et al. 2005 showed for *E. coli*, that the direction of curvature of the trajectory of the cell indicates whether the cells are swimming closer to the top surface or to the bottom surface. At the bottom surface, the cell trajectories

appear clockwise and at the top surface the cell trajectories appear anticlockwise. Both directions of the trajectories for both species were observed.

5.3.3.2 Effect of the boundaries within the *Stripe* network

S. marcescens and *P. stutzeri* changed the way in which they swim due to the changes in their physical environment. The confinement (the presence of boundaries) perturbed their motion. The physical constraints that bacteria have to master at the small scales are very different from those that we encounter. Inertia is negligible and viscous drag is paramount. Therefore microorganisms have evolved propulsion strategies (Berg 2004). Hydrodynamic drag, constraints to movement of flagella, and adhesion forces are three possible physical constraints which limit the movement of bacterial in various restricted environment. Within the *Stripe* network, the larger channel was 10 μm large and the narrowest 2 μm. On the contrary to the 'plaza'-like space the cells were affected by four rigid boundaries.

(i) Hydrodynamic drag may slow down bacterial swimming. The hydrodynamic effects provide a stabilizing influence of the trajectories of motile bacteria, keeping them near the surface despite constant disturbances from Brownian effects. *S. marcescens*' velocity was enhanced in the 10 μm channel in comparison to the 'plaza'-like space but decreased slowly as the channel width decreased. In narrower channels (2 μm and 3 μm wide channels) the bacteria swam very close to four parallel surfaces which probably produced more constraints on bacterial movement in comparison to wider channels thus affecting the bacterial velocity. The velocity of *P. stutzeri* decreased only from the 5 μm channel but was the same within the 10 μm channel and the 'plaza'-like space. Narrow channels constrained *P. stutzeri* movement.

(ii) Adhesive and friction forces acting between the cell and the channel walls. The bacterium swim very close to the walls so the bacterium is in contact with the wall of the channel and experience adhesive and frictions

forces. These forces are in the range from 1 pN to 10 nN so they are superior to the force generated by the flagellar motors which is approx. 0.5 pN (Yao, Jericho et al. 2002; Chattopadhyay, Moldovan et al. 2006). Work by Vigeant, Ford et al. (2002) shows that *E. coli* can swim in a very close proximity (~40 nm) to a planar surface. It has been established that bacteria regularly swim in close proximity to surfaces and prefer some types of surfaces. These properties can be used to guide bacterial movement in microfluidic structures. Within the microfluidic networks the bacterium swam close to two planar surfaces and two lateral walls. When the diameter of the bacterium becomes comparable to the width of the channel the bacterium is in close contact with the two lateral walls and the surface which add more constraints on the bacterial cell.

(iii) Within the microchannels, bacteria swam very close to the walls. For *S. marcescens*, the deflection angle distribution showed a bias toward very small angle which indicated quasi straight motion. *S. marcescens* motion is a "run and tumble". The tumbling motion was executed with difficulty since flagella are unable to extend fully, which probably explains the observed linear motion. When cells eventually tumbled, they temporarily moved away from the micro-channel wall. Flagellar filaments of bacteria are long (10-20 μm). The bundle of flagella has a diameter of approx. 0.5 μm. The flagella of the cells measured between 6 μm to 10 μm in length. Rotational Brownian motion is another factor which could explain why the cells detached from the wall because it directly alters the orientation of the cell body and thus the swimming direction. The bacterial cells then re-associated with a channel wall randomly. *P. stutzeri* deflection angle showed as well a bias toward smaller angles which decreased even more from the 5 μm channel width due to the tighter confinement. The forward swimming is caused by counterclockwise flagellar rotation and backward swimming by clockwise rotation (Homma, Oota et al. 1996). The switching between forward and backward motion corresponds to a brief stop and the frequency is modulated by chemotaxis. Forward motion was largely encouraged by confinement.

Brownian motion perturbs the cell trajectory (McCarter 2001). Kogure, Ikemoto et al. (1998) have observed that there is a positive correlation between the probability of attachment to a glass surface and the swimming speed of *V. alginolyticus*. Faster cells may stay longer near the surface because the attractive forces are probably stronger (Magariyana, Ichiba et al. 2005). If cells are "slow" a "run and tumble" or a run-back might be possible.

The results for the *Stripe* network showed that the two species have different velocity in the confined space. Swimming speed is dependent on motor torque, cell shape, and the shape, length, number, and location (polar or peritrichous) of the filaments. Those parameters vary among bacterial species.

5.3.3.3 Effect of the boundaries within the tortuous network

Structures like the *Comb*, the *Diamond*, the *Cellular* and the *Round-about* represent complex networks where the bacteria have to cope with not only the channel width but also with multiple choice direction, corner and dead end. Within those particular networks, the cells could navigate through several paths and follow closely the walls boundaries. When possible the cells tumble, reorient themselves and produce new swimming directions. The bacterial trajectories were altered because of the collisions with the matrix. As the tortuosity (or the complexity) of the structures increase as seen for example with the *Comb* network there is an increase also in bacterium-obstacle collisions. The speed at which *P. stutzeri* is able to swim through the complex networks appeared to be very similar to that of *S. marcescens*. The statistical test also suggested that the complexity of all the networks had an impact on the cell motility of *P. stutzeri* in comparison to the 'plaza'-like space but less on *S. marcescens*. The bacteria speed may be altered because of collisions with the matrix thus impacting on the rate at which the population invade the networks. Duffy, Ford (1997) compared the turn angle and the run time distribution of *P. putida* and *E. coli* and evaluated through simulation their motility in relation with obstacles in porous media with an average of 39 μm in diameter. They concluded that the bimodal turn angle distribution of *P. putida* (main peaks at 30 ° and 160 °)

reduced collisions with obstacles in porous media in comparison to the unimodal distribution of *E. coli* (main peak at 45 °). Turn angle around 30 ° means straight path but turn angle around 160 ° means reverse direction. So the ability to turn frequently in the reverse direction is an advantage in porous media in comparison to longer run. *P. putida* showed a better strategy to evolve within porous media. *P. stutzeri* is able to turn in the reverse direction in an unbound medium but within the networks the cells swam closer to the lateral wall with little possibilities to change their swimming direction. The confinement decreased the probabilities of direction-switching so both species showed a unimodal turn angle distribution and as a result both species showed a similar strategy. It seems that the width of the channels (5 μm, 10 μm or 15 μm) and the complexity of the networks influenced the motility behaviour of the bacteria. The behaviour of *S. marcescens* and *P. stutzeri* was then not random but guided by the confinement.

5.4 Conclusions

The micro-channels could direct bacterial growth which leads to statistical significant observations. Within an unbound medium peritrichously-flagellated bacteria like *S. marcescens* "run and tumble" and re-orientate themselves along new direction while monotrichously-flagellated bacteria like *P. stutzeri* swim back and forth. The following changes were observed within the microfluidics devices: (i) larger channel (100 μm in width) like the 'plaza'-like space led to continuous forward and circular motion for both species, (ii) bacteria were present all over the surface so there was no significant effect from the boundaries in term of velocity and cell attachment. The swimming behaviour of both species was affected by the width and the design of the networks. The *Stripe* network enhanced the swimming speed of *S. marcescens* more than within the 'plaza'-like space and very close to the lateral wall. As the width of the channels decreased, the speed also decreased and *P. stutzeri* swam equally fast within most of the micro-channels, exhibiting wavy motion and moving very close to the boundaries. On the other hand, very narrow channels, close to the dimension of the species (3 μm and 2 μm) made the species slow down. A decrease in cell speed in narrow channels was attributed to hydrodynamic interaction

(Ramia, Tullock et al. 1993). In more complex meandering networks (*Comb*), similarities in the behaviour of both species were seen. *S. marcescens* and *P. stutzeri* showed the ability to follow the intricate pattern of the network over limited distances. Networks with angles (*Diamond* and *Cellular* networks) showed that both species were able to use straight path but also used lateral paths, i.e. their ability to navigate corners. Finally, circular paths (*Round-about* network) showed the species ability to perform 360 ° turn. Bacteria showed flexibility in their natural environment and directional persistence due to the strong affinity for boundaries and limited opportunities to move backward. The full range of bacterial responses to physical stimuli has been characterised through the networks. It appears that the complexity of the porous system through which the bacterium swims is the dominating factor in predicting its motility. The PDMS-based microfluidics systems therefore offer a critical advantage over agar surfaces, with respect to a more realistic resemblance of the natural environment of bacteria.

Future work will focus on the development of new networks that specify the decision making processes for bacteria can be developed. These networks could have more 'cross-junction' combined with round-about that determines their directionality. Another idea could be the comparison of bacteria with different patterns of flagellation different from the one used in this thesis. Other species that have internalised filaments can also be studied i.e. spirochetes.

Chapter 6

The motility of *Serratia marcescens* cells in viscous confined environment

6.1 Introduction

Serratia marcescens is a peritrichously flagellated bacterium that swims in liquid media. The transfer of the cells in liquids to a sticky surface is accompanied by phenotypic changes and the cells start to swarm. The cells that differentiate into the swarming phenotype through contact to surfaces are elongated, multinucleated, and the density of flagella on their surface increases 3-50 fold per unit area of cell surface (Copeland, Weibel 2009) (Figure 6.1). Like swimming, swarming motility relies on flagellar action. The populations of swarming cells migrate collectively across a surface and in contact with other cells as "multicellular rafts" at an approximate rate of 2-10 μm/s consuming nutrients in the underlying medium (Harshey 2003). The phenotype is reversible, swarming cells are able to differentiate back into the swimming phenotype when the surrounding medium is liquid. In this chapter, experiments were performed (i) to initiate the switch between swimming and swarming cells and (ii) to monitor the behaviour of a population of swimming and swarming cells within a porous and viscous environment. Such conditions would simulate a restraining environment similar to viscous surfaces and were created by adding agents such as Ficoll to the bacteria growth medium (Alberti, Harshey 1990). Ficoll is a highly branched polymer of sucrose and epichlorhydin capable of modifying the viscosity of solutions. Cells swimming through a solution containing 5 % to 10 % of Ficoll 400 reportedly differentiate into the swarming phenotype and are 5 μm to 30 μm long (Alberti, Harshey 1990).

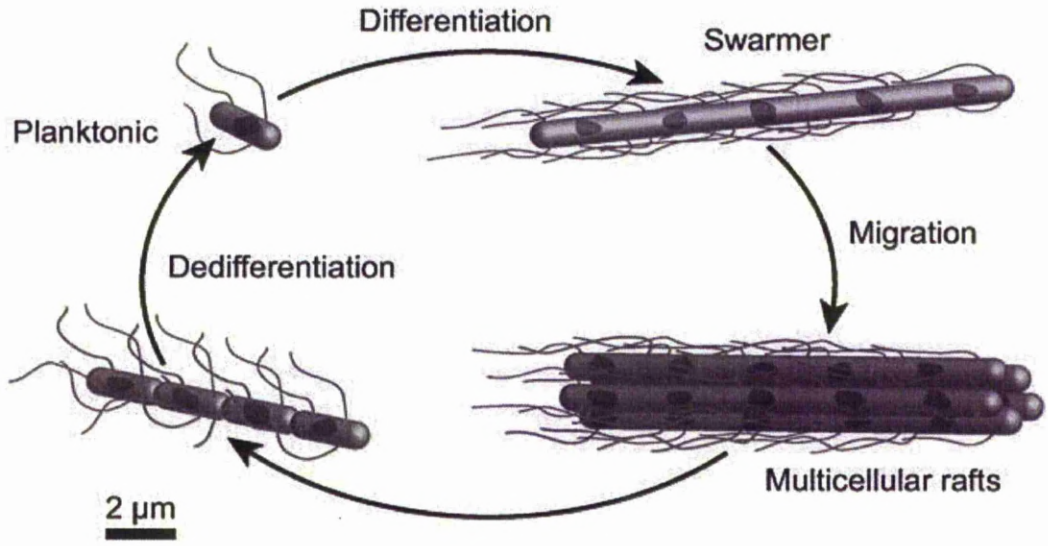

Figure 6.1: "Life cycle" of motile bacterial cells showing the differentiation from a swimming phenotype to a swarming phenotype. Swarming cells are elongated, multinucleated and move cooperatively over the surface as "multicellular rafts". Swarming cells are able to differentiate back into the swimming phenotype (Copeland, Weibel 2009).

The study of swimming and swarming behaviour of *S. marcescens* cells in viscous environment is relevant because *S. marcescens* colonize a variety of surfaces in soil and water. The species is also an opportunistic pathogen which is able to colonize the digestive tracts of rodents, plants, insects, fish, and humans. Most of those surfaces are viscous-elastic environments rather than liquid (Grimont, Grimont 1978). *S. marcescens* is able to form biofilms where the cells live in viscous conditions formed by various polymer solutions. According to Labbate, Queck et al. 2004 and Rice, Koh et al. 2005, swarming cells are also found in the biofilm life cycle.

How bacteria can swim through mucus gels remains poorly understood and is the subject of much research (Copeland, Weibel 2009). Microfluidics systems are very useful for the isolation and the observation of bacterial motility because it can give a direct indication of bacterial behaviour in realistic hydrodynamic conditions.

6.2 Results

6.2.1 Agar plates

S. marcescens cells display both a swimming and a swarming phenotype. The optimal concentration of agar to initiate a swarming phenotype is between 0.5 to 0.8 % agar (Eberl, Winson et al. 1996; Alberti, Harshey 1990). A drop of *S. marcescens* saturated culture were added to the centre of 0.7 % LB agar plates to study outward swarming behaviour from a central point. The plates were incubated at 30 °C. Swarming began within 8 - 16 hours. The inoculation site turn pink-red shortly after the swarming motion develops. The swarming motion itself progresses across the plate in waves that appear as concentric rings (Figure 6.2) with the most active bacteria at the edge of the swarm (Eberl, Molin et al. 1999). Figure 6.3 shows the morphology of a swimming and a swarming cell.

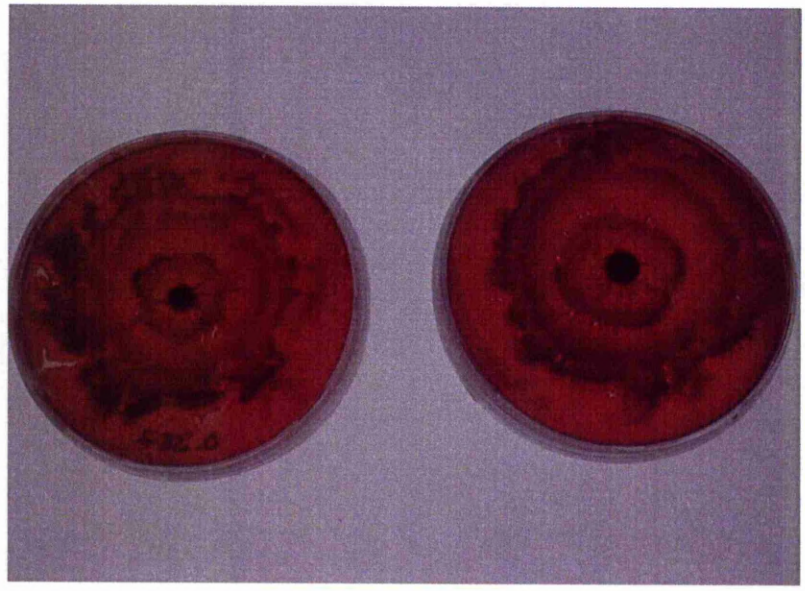

Figure 6.2: Swarming motility of *Serratia marcescens* on 0.7 % agar. The solution of cells which was diluted 10 times was added in the middle of an agar plate and incubated at 30 °C. Swarming starts after 8 to 16 hours and appear as concentric rings coloured in red.

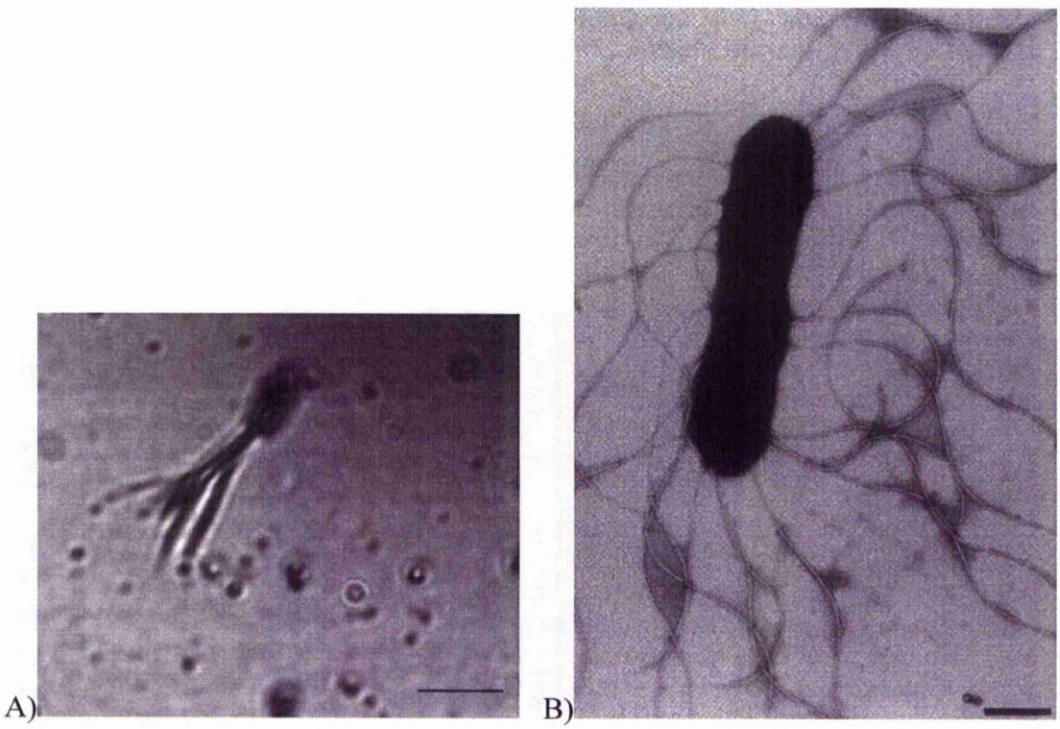

Figure 6.3: A) Morphology of *S. marcescens* swimming phenotype (Silver nitrate flagella stain). Bar = 5 µm. B) Morphology of *S. marcescens* in low concentration agar (electron micrograph, Alberti, Harshey 1990) (Bar represents 1 µm).

6.2.2 Effect of Ficoll 400 on the swimming phenotype of *S. marcescens*

Alberti, Harshey (1990) demonstrated that it was possible to initiate the *S. marcescens* swarming phenotype by using conditions that imposed a physical constraint on bacterial cells like viscous media. They found that Ficoll 400 was very efficient in initiating swarming motility. The viscosity of the final media used in the experiments described here was determined by using a TA Instruments Rheolyst AR 1000N controlled-stress rheometer. Figure 6.4 presents the viscosity of Ficoll 400 in centipoise (cP) at 25 °C for the solutions of LB broth containing 0 % Ficoll 400 (w/v), 3 % Ficoll 400, 6 % Ficoll 400, 7 % Ficoll 400, 9 % Ficoll 400, 12 % Ficoll 400, 15 % Ficoll 400 and 20 % Ficoll 400. The viscosity of the solutions ranged from 1.1 cP for a solution containing 0 % Ficoll 400 to 16 cP for a solution containing 20 % Ficoll 400.

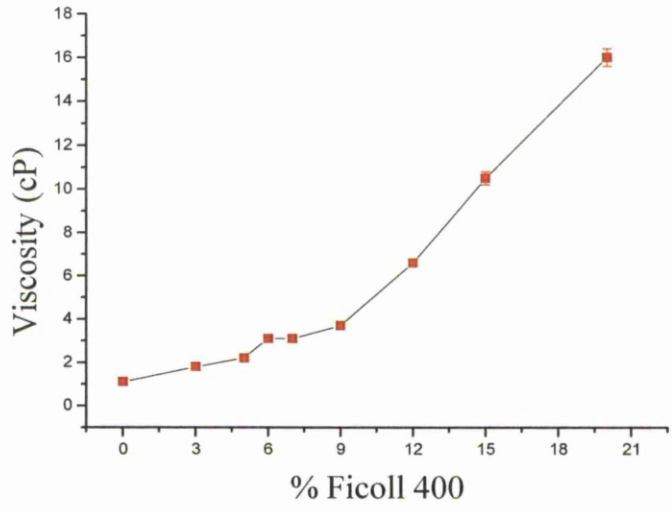

Figure 6.4: Viscosity in centipoise measured at 25 °C of LB broth with increasing percentage of Ficoll 400 (from 0 % to 20 %).

Cells of *S. marcescens* were grown in LB medium and were added to the *Big maze* structure (Figure 6.5-A) which was filled with LB medium and containing 7 % to 9 % Ficoll 400. The *Big maze* structure is made with 15 µm wide channels and contains numerous dead ends and corners where the cells can be trapped. Wide channels are more suitable to observe swarming cells because of the space available.

Our experiments showed that it was possible to induce and observe single elongated cells (> 5 µm long) among rod-shaped swimming cells (2-3 µm long) in microfluidics networks (Figure 6.5-B, blue circles and Figure 6.5-C, orange boxes).

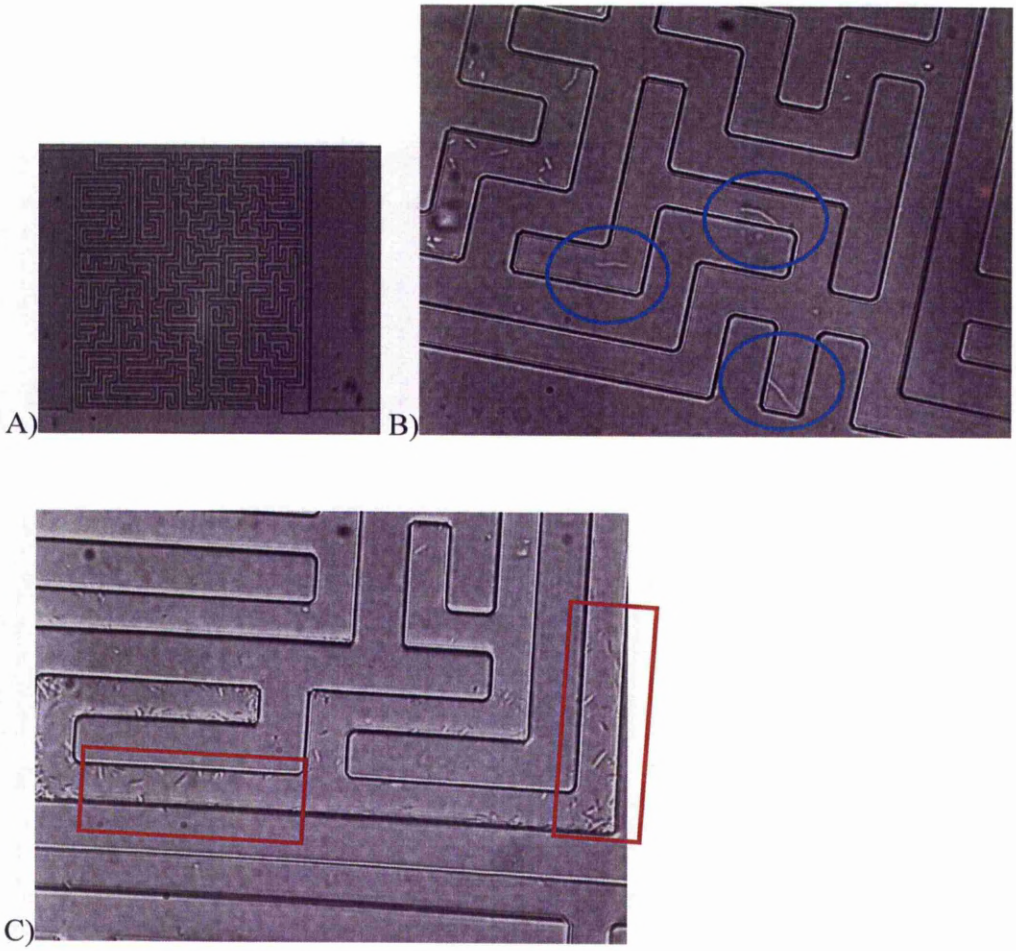

Figure 6.5: A) The *Big maze* network is 1 mm long and 1 mm large with 15 µm wide channels. Figure B) shows, within the blue circles, elongated cells of *S. marcescens* within the *Big maze* network filled with LB and 9 % Ficoll 400. The orange squares in Figure C) show a population of cells that contain short and elongated cells. The network was filled with LB broth and containing 7 % Ficoll 400.

Within the large channels, the cells were either swimming forward and close to the boundaries or swam in the middle of the channels for some time before moving close to the boundaries (Figure 6.6-A). In LB broth only (Figure 6.6-B), cells swam constantly close to a wall with few switching to the opposite wall.

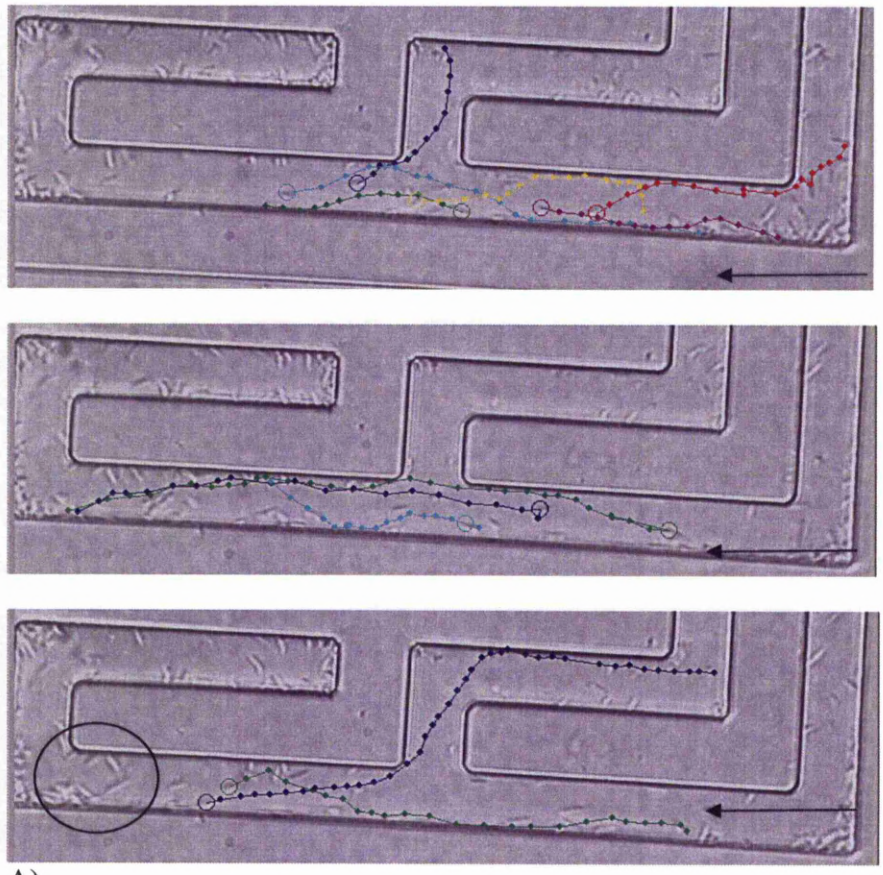

A)

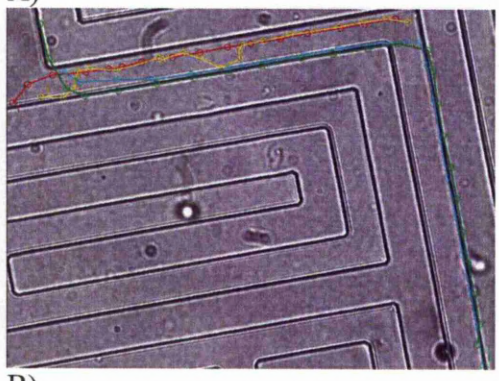

B)

Figure 6.6: A) Set of trajectories generated by ImageJ of *S. marcescens* in the *Big maze* structure filled with LB and 7 % of Ficoll 400. The population of cells exhibited directional motion and smooth curvature. The black circle shows individual swarming cells (~10 μm long). B) Set of trajectories generated by ImageJ of *S. marcescens* in the *Big maze* structure filled with LB broth only. The cells were swimming close to a wall and were seen to switch between the two sides of the channels. The black arrows indicate the direction of movement in the mazes.

S. marcescens cells that swam within the *Big maze* network as shown in Figure 6.6 were measured using ImageJ software. The mean cells size found was 5.6 ± 1.3 μm in length (n = 102). Cells observed in LB broth had a mean cells size of 2.9 ± 0.6 μm in length (n = 99) (Figure 6.7-A). According to Alberti, Harshey (1990), cells swimming in broth typically measured about 2.7 μm and swarming cells taken from the edge of an active swarming colony measured about 6.3 μm. Figure 6.7-B represents the distribution of sizes of the cells swimming within LB broth containing 7 % of Ficoll 400 (3.1 cP). More than half of the sample measured more than 5.5 μm with a very small percentage (~4 %) more than 8 μm in length. About 40 % of the cells, measured between 3 μm and 5 μm. The mean velocity recorded for the swarming cells (length > 5 μm) was 22.2 ± 5.8 μm/s (n = 825). The distribution is normal (Figure 6.8-B). Cells that swim in LB broth only had a mean velocity of 18.5 ± 5.7 μm/s (n = 664) (Figure 6.8-A).

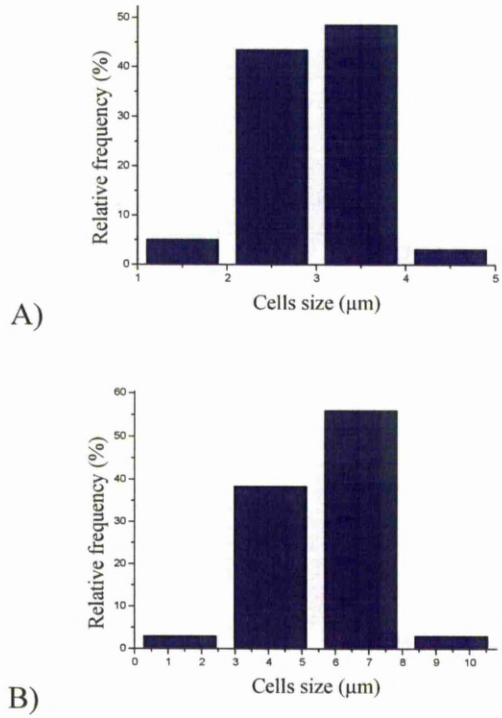

Figure 6.7: Cells length of *S. marcescens* grown in A) LB broth and loaded within the *Big maze* filled with LB broth and grown in B) LB broth and loaded within the *Big maze* filled with LB broth and containing 7 % Ficoll 400 (3.1 cP).

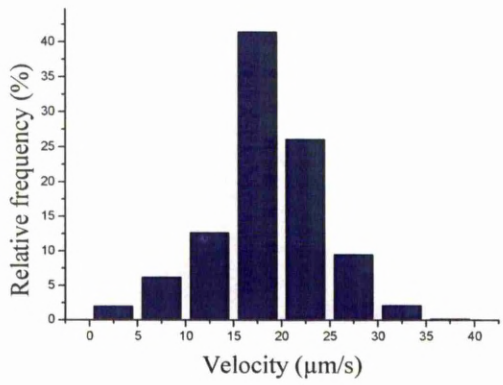

A)

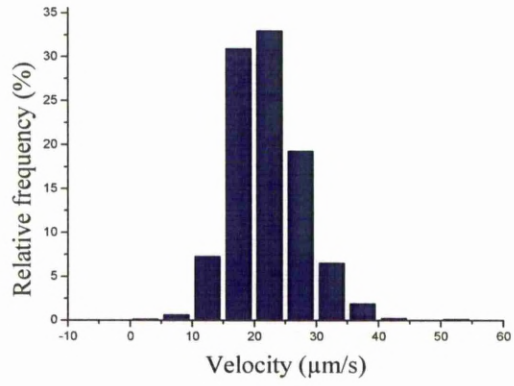

B)

Figure 6.8: Distribution of *S. marcescens* velocity (with fitted normal distribution) within the *Big maze* network filled with A) LB broth and B) LB broth containing 7 % Ficoll 400 (3.1 cP).

Swarming is a collective behaviour of a population done via quorum sensing of cells (Steager, Kim et al. 2007). The tendency of cells to swim away from each other or in close relationship as observed on a swarm plate has been checked. In general cells swam away from each other. Figure 6.9 showed that during a short period of time some cells came in close relation with each other probably forced to interact because of the narrow space.

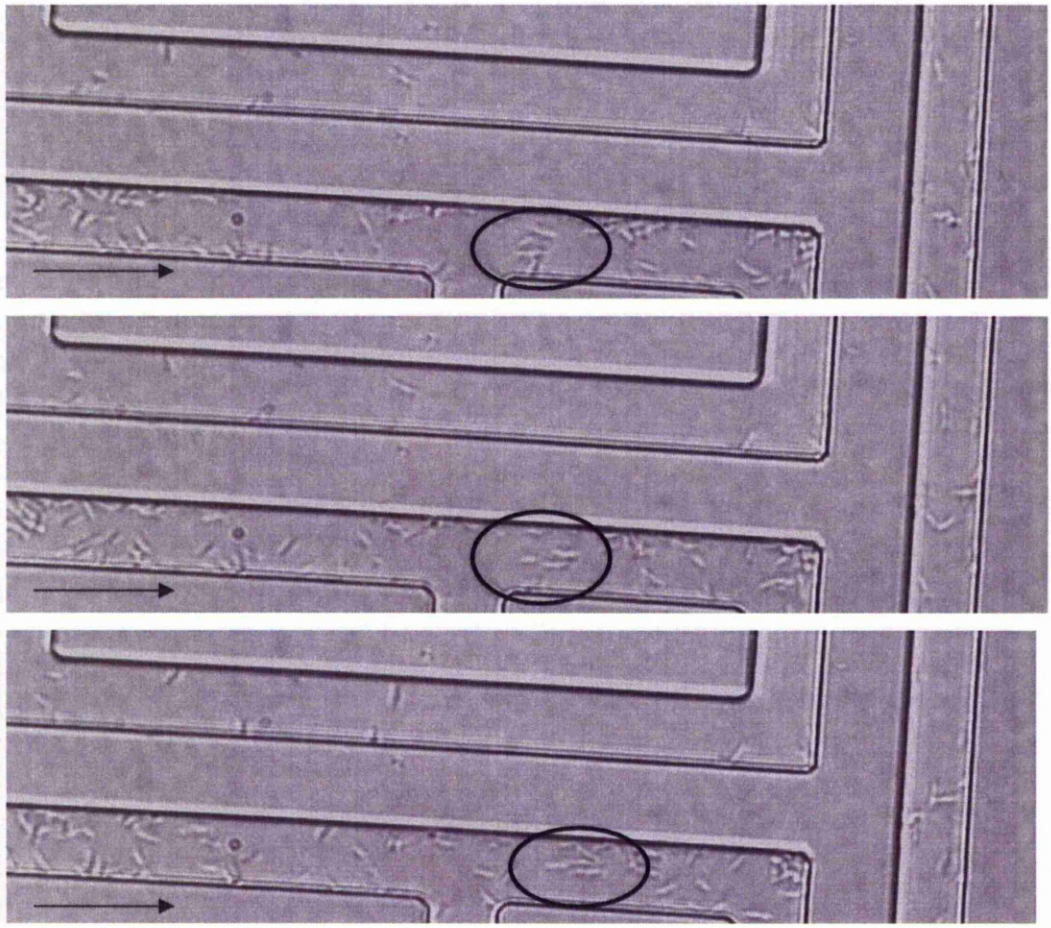

Figure 6.9: Set of pictures showing the close interactions of some of the swarming cells with each other (black circle). The population of cells swam within the *Big maze* network filled with LB broth and containing 7 % Ficoll 400. The black arrows indicate the direction of movement in the mazes.

The velocity of *S. marcescens* was significantly changed by the viscous media (T-value = -12.48, P-value < 0.01, DF = 1489, two-tailed pooled Student's *t*-test). The cells size was also significantly changed by the viscous media (T-value = -15.83, P-value < 0.01, DF = 172, two-tailed unpooled Student's *t*-test of log-transformed values).

The experiments showed that it was possible to initiate and isolate swarming cells within the microfluidics networks through the use of Ficoll 400. The majority of the cell population measured more than 5 μm in length. A small proportion measured

more than 8 μm in length. Within the *Big maze* network the cells swam in one direction away or close to the lateral wall. Some of the swarming cells could swim in close interaction with each other probably forced to interact because of the narrow space but also due to hydrodynamic interactions between two swimming bacteria (Ishikawa, Sekiya et al. 2007).

6.2.3 Effect of Ficoll 400 on the motility behaviour of *S. marcescens*

For this section the *Stripe* network was used. As presented in Chapter 5, the *Stripe* network consists of straight channels with different widths (from 2 μm to 10 μm). The *Stripe* network in general and the 10 μm wide channel in particular (Figure 6.10) were used to observe the dynamics of swimming and swarming cells and to measure the cell velocity along straight channels of definite length. The second parameter that was determined was the cell's size. Bacterial cells were grown in LB broth or in LB broth containing different concentration of Ficoll 400 and then loaded into the network. When grown in LB broth only, the cells exhibited the swimming phenotype only. When grown in LB broth and Ficoll 400 it would be expected that there would be a mixed population of swimming and swarming cells. The network was either filled with LB broth only or with LB and different concentrations of Ficoll 400. The experiments were designed to observe (i) the effect of viscosity on the swimming cells when the cells were grown in LB broth but loaded in the network filled with LB and different concentration of Ficoll 400 (section 6.2.3.1), (ii) the behaviour of swimming and swarming cells when cells were both grown and loaded in the network filled with LB broth and different concentration of Ficoll 400 (section 6.2.3.2) (in this section, the concentration of Ficoll 400 in the broth and the *Stripe* network are the same), (iii) the effect of LB broth on the population of swimming and swarming cells when the cells were grown in LB broth and different concentration of Ficoll 400 and loaded into the network filled with LB broth only (section 6.2.3.3).

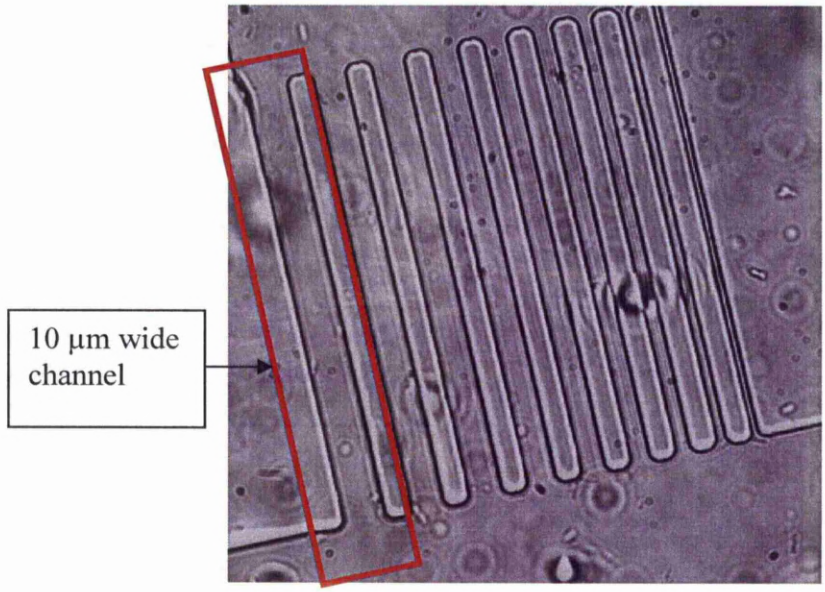

Figure 6.10: *Stripe* network. The red box marks the boundary of the 10 μm wide channel.

The growth of *S. marcescens* in LB broth and LB broth containing 7 % Ficoll 400 is shown in Figure 6.11. The concentration of 7 % Ficoll 400 was selected because the work by Alberti, Harshey (1990) showed that the best swarm cell production was obtained with 5 % to 10 % Ficoll 400. The experiments presented in section 6.2.2 of this chapter confirmed also the choice of 7 % Ficoll 400. A lag phase was observed for both conditions but cells stayed for longer time in the lag phase state in the Ficoll environment (30 minutes) in comparison to the LB broth (15 minutes). Exponential growth occurred from 30 to 135 minutes in the Ficoll medium and from 15 to 105 minutes in LB broth. In LB broth, the bacterial population appeared to reach the stationary phase earlier, after 90 minutes of exponential growth while the species in the viscous solution reached the stationary phase after 105 minutes of exponential growth. The time needed for the population to double during the exponential phase was 33 minutes in LB broth. In LB broth containing 7 % Ficoll 400 the doubling time was 38.5 minutes. The growth curves of *S. marcescens* grown in LB medium and LB medium containing 7 % Ficoll 400 showed that viscosity did not have any significantly negative effect on growth other than a slightly longer lag phase and a minor reduction in growth rate.

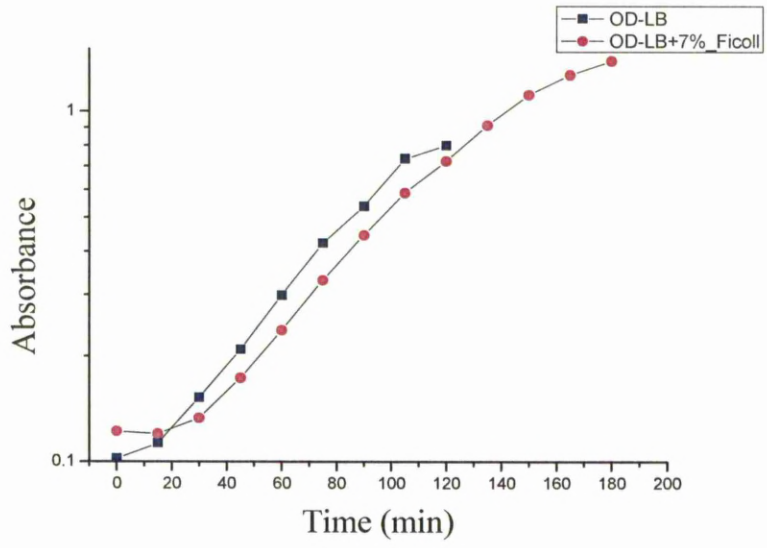

Figure 6.11: *Serratia marcescens* growth in LB medium (blue squares) and in LB broth containing 7 % Ficoll 400 (pink circles) where we can distinguish different phases of growth. The lag-phase (0-15 minutes for the LB environment and 0-30 minutes for the LB and Ficoll environment) is a period of slow growth when the bacteria are adapting to the growth medium. The exponential phase (15 to 105 minutes for the LB environment and 30 to 135 for the LB and Ficoll environment) is a phase of unrestricted growth under these conditions. The stationary phase (after 105 minutes for the LB broth environment and after 135 minutes for the LB and Ficoll environment) occurs when the nutrients become limiting.

6.2.3.1 Effect of viscosity on the swimming behaviour of *S. marcescens*

Cells of *S. marcescens* were incubated in LB medium until the cells reached the late exponential phase. 20 µl to 30 µl of *S. marcescens* cell culture were added to the *Stripe* network which was filled with different concentration (3 %, 7 %, 9 %, 12 % and 15 %) of Ficoll 400 in order to modulate the viscosity of the medium from 1.1 to 10.5 cP.

S. marcescens swam at a speed of 29.8 ± 10.2 µm/s in the buffer without Ficoll 400 (viscosity = 1.1 cP). Ficoll 400 made the cells swim at a rate below the mean velocity measured in LB medium. The cells swimming speed decreased gradually to reach

18.6 ± 6.0 µm/s at a viscosity of 10.5 cP (Figure 6.12). The measurement of the cells size (Figure 6.13) showed that as the viscosity of the medium increased, the size of the cells increased to reach 4.6 ± 1.0 µm for a viscosity of 3.7 cP then the cells size was constant. The swimming velocity was inversely proportional to the viscosity of the medium. The change in cells size was proportional to the viscosity and altered the swimming velocity which decreased as the cells size increased.

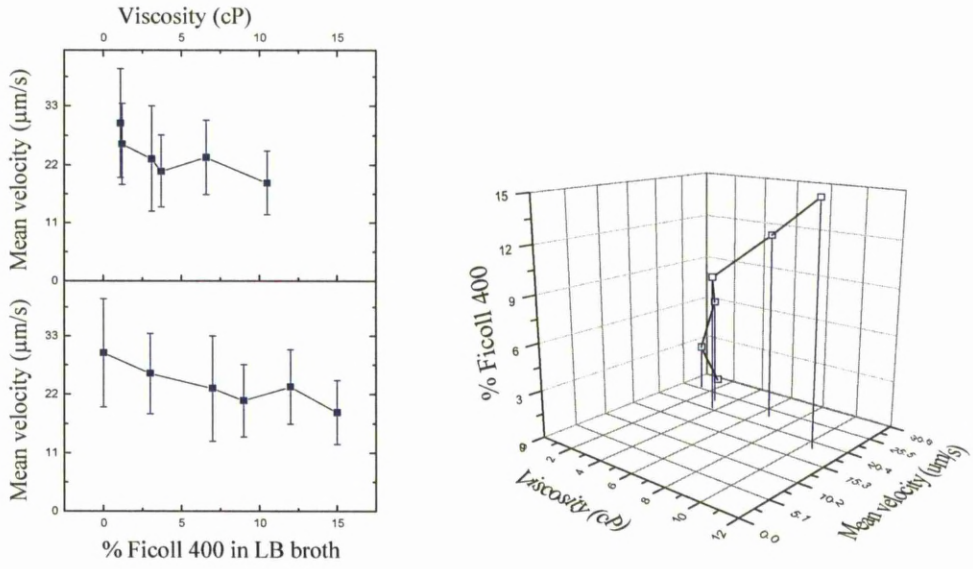

Figure 6.12: Shows the swimming speed profile of cells incubated in LB medium against the percentage of Ficoll 400 in LB broth and against the viscosity of the medium. Each curve was represented individually. The 3D curve represents velocity in µm/s versus viscosity in cP and viscosity in cP versus % Ficoll 400. Cells were loaded into the *Stripe* network filled with LB broth and 3 % to 15 % of Ficoll 400. Bars represent the standard deviation.

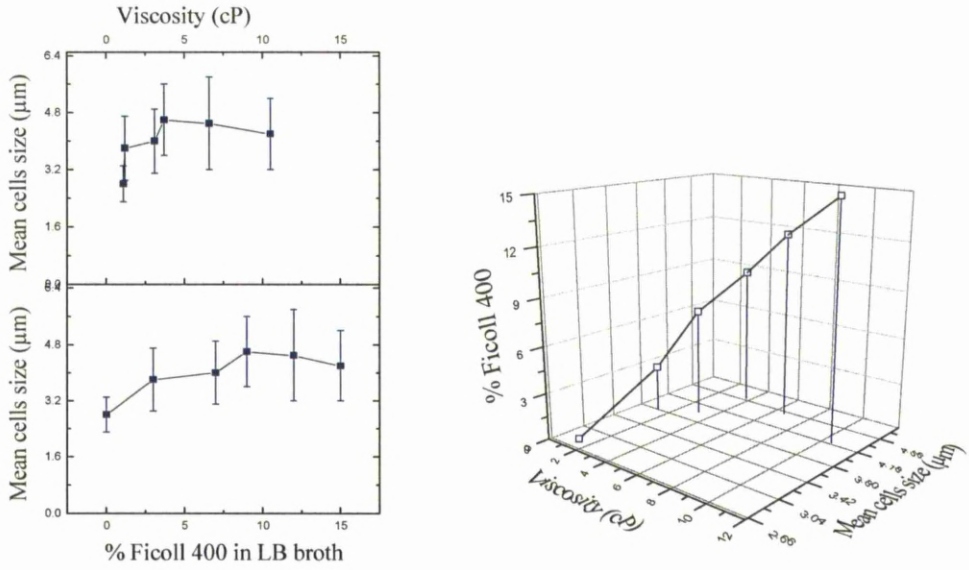

Figure 6.13: Mean cells size measured when cells where incubated in LB medium and loaded into the *Stripe* network filled with LB broth and 3 % to 15 % Ficoll 400. The mean cells size was represented against the percentage of Ficoll 400 in LB broth and against the viscosity of the medium. The curves were represented individually. The 3D curve represents cells size in µm versus viscosity in cP and viscosity in cP versus % Ficoll 400. Bars represent the standard deviation.

Two-tailed Student's *t*-tests were performed to check the impact of Ficoll 400 on the swimming speed and the cells size of *S. marcescens* cells. The results are represented in Table 6.1. The velocity was significantly changed by the confinement (two-tailed unpooled Student's *t*-test, except for 7 % and 9 % Ficoll 400 where a pooled Student's *t*-test was used). The viscous environment affected the swimming speed negatively. The cells size was also affected by the experimental conditions as shown by the Student's *t*-test (two-tailed unpooled Student's *t*-test except for 15 % Ficoll 400 where values were log-transformed).

Control-LB	3%	7%	9%	12%	15%
Velocity: 29.8 ± 10.2 (n = 1899)	25.9 ± 7.6 (n = 498) T-value:9.44 P-value<0.01 DF:1010	23.1 ± 9.9 (n = 1746) T-value:20.27 P-value<0.01 DF:3643	20.8 ± 6.8 (n = 703) T-value:21.78 P-value<0.01 DF:2600	23.4 ± 7.0 (n = 625) T-value:17.65 P-value<0.01 DF:1540	18.6 ± 6.0 (n = 621) T-value:33.42 P-value<0.01 DF:1798
Cells size: 2.8 ± 0.5 (n = 50	3.8 ± 0.9 (n = 60) T-value:-7.35 P-value<0.01 DF:95	4.0 ± 0.9 (n = 60) T-value:-8.32 P-value<0.01 DF:96	4.6 ± 1.0 (n = 60) T-value:-12.53 P-value<0.01 DF:94	4.5 ± 1.3 (n = 60) T-value:-8.71 P-value<0.01 DF:78	4.2 ± 1.0 (n = 60) T-value:-9.11 P-value<0.01 DF:107

Table 6.1: Effect of the viscosity of the medium on the swimming speed and cells size of *S. marcescens*. We compared the cells velocity measured in LB medium to the cells velocity measured in LB medium that contains 3 % to 15 % of Ficoll 400. For each conditions the size of the cells were measured. The values presented are mean velocity values in (μm/s) (±) standard deviation values and cells size values in (μm) (±) standard deviation values. Statistical results were reported by T-value, P-value and Degree of Freedom (DF); n represents the numbers of data points.

6.2.3.2 Effect of viscosity on a population of swimming and swarming cells

In a second set of experiments, cells were grown for approximately 2 h in LB broth that contained different percentages of Ficoll 400 i.e. 3 % to 15 %. Ficoll 400 generated different populations of cells (short and elongated) that were tested to observe any different effects on velocity and cell size within the *Stripe* network filled with LB broth and 3 % to 15 % of Ficoll 400.

The swimming speed was for all conditions below the mean velocity measured in LB broth. Cells swam the fastest within 7 % and 9 % of Ficoll 400 (3.1 and 3.7 cP respectively) (Figure 6.14). Above 12 % of Ficoll 400 (6.6 cP), the viscosity reduced the cells velocities to 20 μm/s or below. The swimming velocity was proportional to the viscosity of the medium between 1.2 and 3.7 cP and was inversely proportional to the viscosity of the medium between 3.7 to 10.5 cP. The results indicate that *S.*

marcescens cells were more motile in concentrations of Ficoll 400 between 6 % and 9 %. The profile of cells size showed that the maximum cells length was reached for the same concentration of Ficoll 400 (from 7 % to 9 %) (Figure 6.15). The change in cells size was similar to the change in swimming velocity. The cells that were grown in LB broth containing a concentration of Ficoll 400 as small as 3 % were able to initiate elongated cells but the optimal viscosity for the mobility of swarming cells was between 3.1 and 3.7 cP.

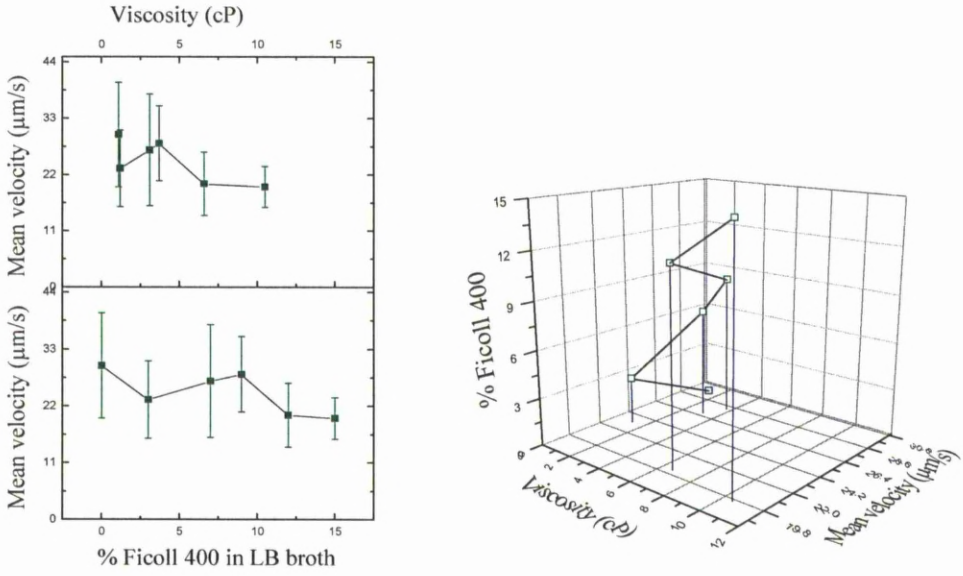

Figure 6.14: Shows the swimming speed profile of cells incubated in LB medium that contains 3 % to 15 % Ficoll 400 and loaded in the *Stripe* network filled with LB and 3 % to 15 % Ficoll 400. The mean velocity was represented against the percentage of Ficoll 400 in LB broth and against the viscosity of the medium. The curves were represented individually. The 3D curve represents velocity in µm/s versus viscosity in cP and viscosity in cP versus % Ficoll 400. Bars represent the standard deviation.

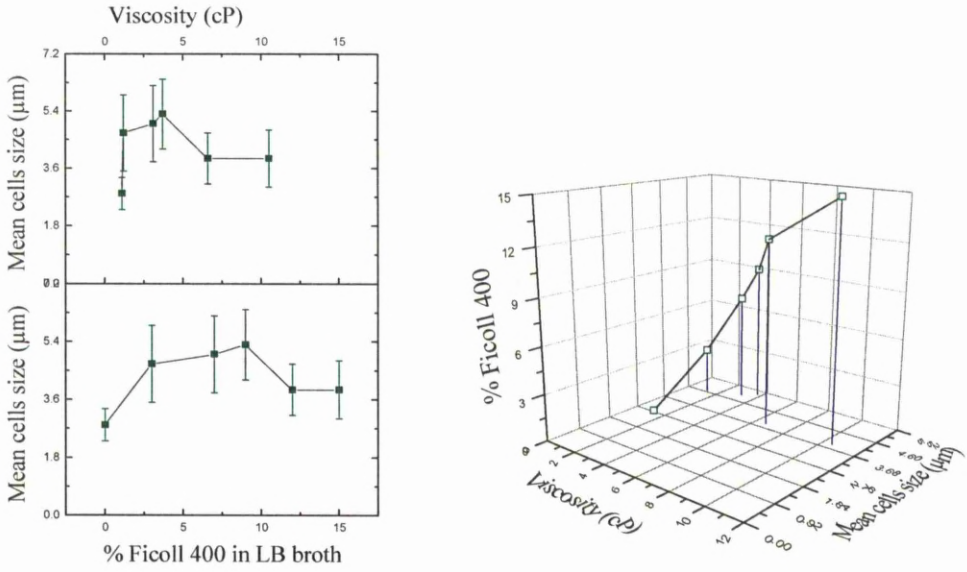

Figure 6.15: Mean cells size measured when cells where incubated in LB medium and containing Ficoll 400 and loaded in the *Stripe* network filled with LB broth and Ficoll 400 (3 % to 15 %). The mean cells size was represented against the percentage of Ficoll 400 in LB broth and against the viscosity of the medium. The curves were represented individually. The 3D curve represents cells size in µm versus viscosity in cP and viscosity in cP versus % Ficoll 400. Bars represent the standard deviation.

Two-tailed Student's *t*-tests were performed to check the impact of Ficoll 400 on the swimming speed and cells size of *S. marcescens* cells. The results are represented in Table 6.2. The velocity was significantly changed by the confinement (two-tailed unpooled Student's *t*-test). The cells size was also affected by the experimental conditions as shown by the Student's *t*-test (two-tailed unpooled Student's *t*-test).

Control-LB	3%	7%	9%	12%	15%
Velocity: 29.8 ± 10.2 (n = 1899)	23.2 ± 7.5 (n = 412) T-value:14.98 P-value<0.01 DF:775	26.8 ± 10.9 (n = 517) T-value:5.66 P-value<0.01 DF:777	28.1 ± 7.3 (n = 377) T-value:3.93 P-value<0.01 DF:698	20.2 ± 6.2 (n = 377) T-value:24.29 P-value<0.01 DF:840	19.6 ± 4.0 (n = 67) T-value:19.0 P-value<0.01 DF:100
Cells size: 2.8 ± 0.5 (n = 50)	4.7 ± 1.2 (n = 60) T-value:-11.01 P-value<0.01 DF:82	5.0 ± 1.2 (n = 60) T-value:-12.35 P-value<0.01 DF:82	5.3 ± 1.1 (n = 60) T-value:-15.24 P-value<0.01 DF:85	3.9 ± 0.8 (n = 60) T-value:-8.44 P-value<0.01 DF:103	3.9 ± 0.9 (n = 25) T-value:-5.57 P-value<0.01 DF:31

Table 6.2: Effect of the viscosity of the medium on the swimming speed of *S. marcescens* cells grown in LB and 3 % to 15 % of Ficoll 400 as well as the cells size. We compared the cells velocity measured in LB medium (control) to the cells velocity values measured in LB medium that contains 3 % to 15 % of Ficoll 400. The values presented are mean velocity values in (μm/s) (±) standard deviation values and cells size values in (μm) (±) standard deviation values. Statistical results were reported by T-value, P-value and Degree of Freedom (DF); n represents the numbers of data points.

6.2.3.3 Effect of LB liquid broth on a population of swimming and swarming cells

In a third set of experiments, cells were grown for approximately 2 h in LB broth that contained different percentages of Ficoll 400 i.e. 3 % to 15 % (1.2 to 10.5 cP) and were loaded within the *Stripe* network filled with LB medium only.

Figure 6.16 showed that as in the previous section the mean cells velocities were below the mean velocity observed when the cells were grown and swam in LB medium only. The velocity profile was quite similar across different concentrations of Ficoll 400 and close to 20 μm/s. The cell size profile was also quite similar for the different concentration of Ficoll 400; the cells maintained a constant size of ~3.7 μm (Figure 6.17). Media with a viscosity of ~ 1.1 cP were far from optimal for swarming cells which dedifferentiate into the swimming phenotype (Copeland, Weibel 2009). Swimming cells have a constant size and a constant velocity.

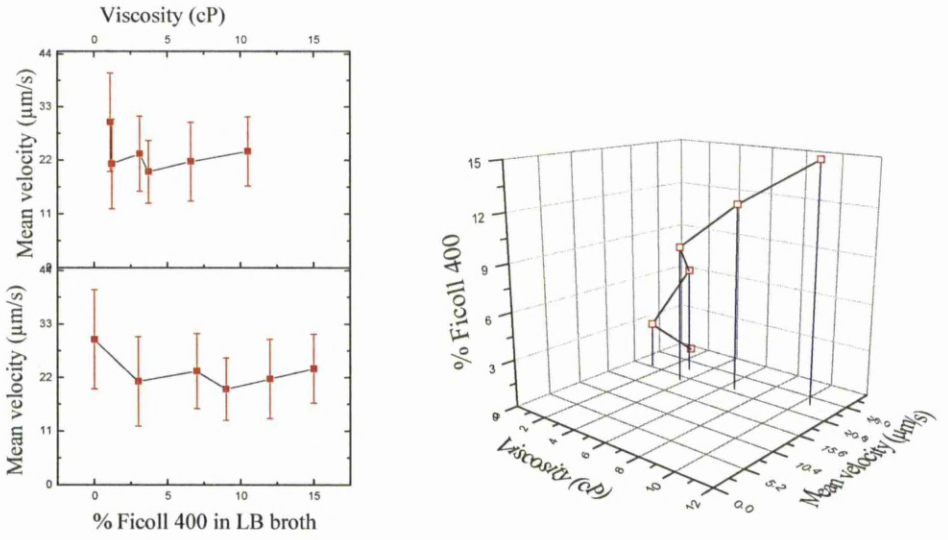

Figure 6.16: Swimming speed profile of cells incubated in LB medium that contains 3 % to 15 % Ficoll 400 and loaded in the *Stripe* network filled with LB medium only. The mean velocity was represented against the percentage of Ficoll 400 in LB broth and against the viscosity of the medium. The curves were represented individually. The 3D curve represents velocity in µm/s versus viscosity in cP and viscosity in cP versus % Ficoll 400. Bars represent the standard deviation.

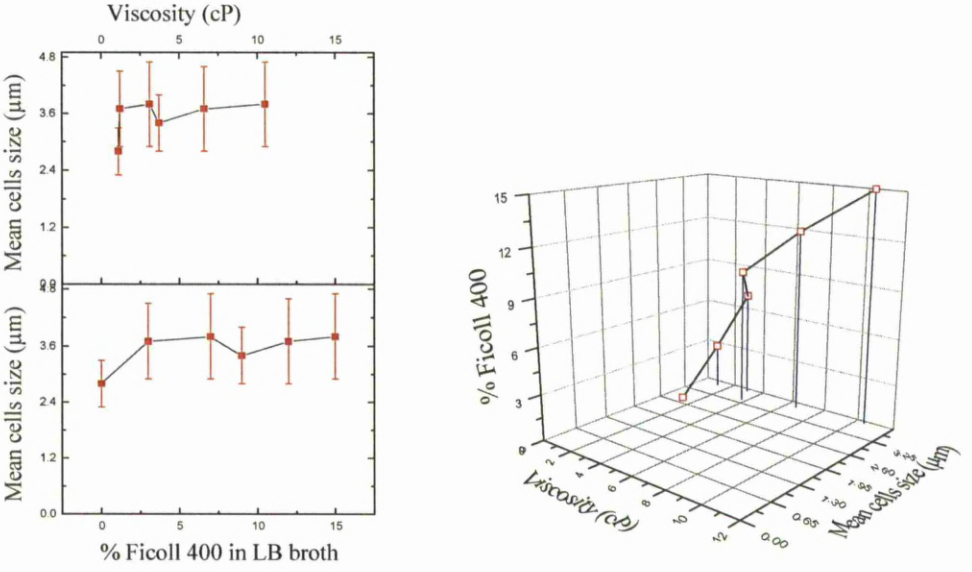

Figure 6.17: Mean cells size measured when cells where incubated in LB medium and different concentration of Ficoll 400 i.e. 3 % to 15 % and loaded in the *Stripe* network filled with LB only. The mean cells size was represented against the percentage of Ficoll 400 in LB broth and against the viscosity of the medium. The curves were represented individually. The 3D curve represents cells size in µm versus viscosity in cP and viscosity in cP versus % Ficoll 400. Bars represent the standard deviation.

Two-tailed Student's *t*-tests were performed to check the impact of Ficoll 400 on the swimming speed and cells size of *S. marcescens* cells. The results are represented in Table 6.3. The velocity was significantly changed by the confinement (two-tailed unpooled Student's *t*-test, except for 3 % Ficoll 400 where a pooled Student's *t*-test was used). The cells size was also affected by the experimental conditions as shown by the Student's *t*-test (two-tailed unpooled Student's *t*-test except for 9 % Ficoll 400 where a pooled Student's *t*-test was used. Data concerning 12 % and 15 % Ficoll 400 were log-transformed).

Control-LB	3%	7%	9%	12%	15%
Velocity: 29.8 ± 10.2 (n = 1899)	21.2 ± 9.2 (n = 525) T-value:18.45 P-value<0.01 DF:908	23.3 ± 7.7 (n = 547) T-value:15.99 P-value<0.01 DF:1145	19.6 ± 6.4 (n = 691) T-value:30.14 P-value<0.01 DF:1943	21.7 ± 8.1 (n = 628) T-value20.39 P-value<0.01 DF:1337	23.8 ± 7.1 (n = 481) T-value:14.97 P-value<0.01 DF:1034
Cells size: 2.8 ± 0.5 (n = 50)	3.7 ± 0.8 (n = 60) T-value:-6.94 P-value<0.01 DF:102	3.8 ± 0.9 (n = 60) T-value:-7.61 P-value<0.01 DF:97	3.4 ± 0.6 (n = 60) T-value:-4.98 P-value<0.01 DF:108	3.7 ± 0.9 (n = 60) T-value:-6.44 P-value<0.01 DF:107	3.8 ± 0.9 (n = 60) T-value:-7.09 P-value<0.01 DF:107

Table 6.3: Effect of LB medium on the swimming speed and cells size of *S. marcescens* swimming and swarming cells. We compared the cells velocity measured in LB medium (control) to the velocity of cells grown in LB medium that contains 3 % to 15 % of Ficoll 400 and swim in LB medium. The values presented are mean velocity values in (μm/s) (±) standard deviation values and cells size values in (μm) (±) standard deviation values. Statistical results were reported by T-value, P-value and Degree of Freedom (DF); n represents the numbers of data points.

In this section the velocity and sizes of *S. marcescens* cells loaded in viscous and non-viscous environments were observed. The results showed that swimming cells loaded into a viscous environment decreased their swimming speed with significant changes in the cells size. In section 6.2.2, results showed that swarming cells that measured more than 5 μm have an average speed of 23 μm/s. The velocity measured for swarming cells (percentage of Ficoll > 7 %) was similar to the velocity measured

for the cells swimming in LB broth only (~22 μm/s).When cells were grown and loaded into a viscous environment (section 6.2.3.2) a maximum cell velocity was seen for a viscosity between 3.1 cP and 3.7 cP. The same viscosity range made the cells elongate to more than 5 μm in length. Cells grown in a viscous environment and loaded into a non-viscous environment showed a similar swimming speed and a similar cells size.

6.4 Discussion

6.4.1 Introduction

S. marcescens has the ability to swim and swarm. On an agar plate a low concentration of agar is enough to initiate a swarming phenotype. Within liquid media the addition of polymer creates a favourable condition to initiate swarming cells. The motile behaviour and the morphology of *S. marcescens* varied by addition of different concentrations of Ficoll 400.

6.4.2 Initiation of *S. marcescens* swarming phenotype

The critical factor that determines whether cells swim, swarm or form colonies on an agar plate is the agar concentration. On media solidified with 0.4 to 0.8 % agar, *S. marcescens* swarms atop the agar surface (Eberl, Winson et al. 1996; Alberti, Harshey 1990). Observation of *S. marcescens* swarming plates showed the following characteristics (Eberl, Molin et al. 1999): the central part of a colony contains cells that are round-shape with few flagella. The middle of the colony contains cells that exhibited the swimming morphology. The edge of the colony contains highly motile, highly flagellated and elongated cells. Steager, Kim et al. (2008) used a tracking algorithm to study the velocity and the pattern formation of swarming cells on agar. They confirmed that the more motile cells were the ones at a region 500 μm – 1 mm away from the edge. The motion decreased at a region 2-4 mm away from the edge. Swarming bacteria are elongated hyper-flagellated and migrate cooperatively as a group across a surface. The development to a swarming phenotype on an agar plate

requires nutrients, the contact of individual cells to a surface and the contact between neighbouring bacteria as swarming is a highly coordinated migration of cells (Van Houdt, Givskov et al. 2007). The flagellar master operon (flhDC) and an N-acylhomoserine lactone (AHL)-dependent quorum sensing system are responsible for the regulation of flagellar motility and the cell population density (Givskov, Östling et al. 1998; Liu, Lai et al. 2000; Lindum, Anthoni et al. 1998; Horng, Deng et al. 2002). A single *Serratia marcescens* cell produces signalling molecules in the extra-cellular environment called autoinducers (AIs). When the cell density increases the concentration of the signalling molecules reaches a critical threshold that can be sensed by the swarming population which produce changes in gene expression and in surface motility (Van Houdt, Givskov et al. 2007). The concentric rings observed on an agar plate (Figure 5.2) are therefore the results of the relationship between swarming and quorum sensing (Daniels, Vanderleyden et al. 2004). Copeland, Flickinger et al. (2010) studied the flagella dynamics of *E. coli* swarming cells on agar plate by using the bi-arsenical dyes FIAsH and ReAsH and epifluorescence microscopy. They discovered that the bundles of flagella of individual bacteria are flexible and could bend during collisions with neighbour cells and that the flagella make transient contact with flagella from adjacent cells.

Ficoll is a highly branched polymer of sucrose and epichlorhydrin and was used in this study as a simple means of increasing the viscosity of the liquid media. According to Alberti, Harshey (1990) Ficoll 400 induced a swarming phenotype after 1 hour and increased thereafter. They found that the proportion of elongated cells was 30 % to 45 % with 5 % to 10 % Ficoll 400 after 2 hours. Ficoll 400 was used as the viscosity conferring polymer because they observed the best swarm cells in comparison to PVP (Polyvinylpirrolidone, a water-soluble polymer) or other Ficoll from different molecular-weight. Ficoll has the ability to constrain the movement of the bacterial flagella so the induction of swarming cells depends on physical properties of the medium. Alberti and Harshey showed that the addition of the polymer causes the cells to elongate and produce more flagella on the surface of cells. Within the Big maze network filled with LB broth and Ficoll 400 a population of elongated cells (body length > 5 μm) was observed but also cells that reached at

least 10 μm in length. This confirms the findings of Alberti, Harshey (1990) that Ficoll 400 is able to initiate swarming cells. Additionally the availability of the microfluidics networks makes it possible to also observe their dynamical behaviour in restricted geometries. Cells that were grown in viscous environment should already exhibit the swarming phenotype when added within the network. Cells that were loaded into a viscous environment should differentiate into the swarming phenotype within the network. Swarming cells were the ones measuring at least 5 μm in length. The most swarm cells were seen at concentrations between 6 % and 9 % Ficoll 400 when cells were grown first in Ficoll 400 as found by Alberti, Harshey (1990). Swarming is a cooperative behaviour where raft of cells progress across an agar plate in waves that appear as concentric rings (Steager, Kim et al. 2008). The experiments showed that within the two networks, individual motile swarming cells can be observed that swam in straight lines. Elongated cells with the tendency to swim in the middle of a channel rather than only along the channel wall were also observed.

For *S. marcescens*, flagellar expression is dependent on environmental factors. *Vibrio algynolyticus* exhibits a lateral and polar flagellum. Atsumi, Maekawa et al. (1996) examined the relationship between swimming speed and the viscosity of the medium made with PVP for each flagellar system. The mutant with only a lateral flagellum could swim in the high-viscosity environment (ca. 200 cP); the mutant with only a polar flagellum could not. As with *S. marcescens*, a viscous environment leads to the expression and synthesis of more flagella in *Vibrio algynolyticus*.

6.4.3 The effect of the microenvironment on the behaviour of *S. marcescens* cells

The study of swimming bacteria in viscous environments is relevant as bacteria are for example able to colonize the human tract which is a viscous environment (mucus gel at the stomach wall). Most of bacterial cells live in sticky conditions, e.g., surfaces of other organisms and biofilm (they live in various polymer solutions), rather than in Newtonian liquids, e.g., marine water (Magariyama, Kudo 2002).

Growth of *S. marcescens* in LB medium and LB medium containing 7 % Ficoll 400 demonstrated that viscosity did not have a significant negative effect. These results are in accordance with several studies that found that the viscosity of the growth medium did not affect the growth rates of any of the microorganisms studied (Ballesteros, Chirife et al. 1993; Lawrence, Korber et al. 1992). The lag phase and the exponential phase were slightly longer in solution of LB broth containing 7 % Ficoll 400. The viscosity of the medium could interfere with the transport processes between the cells and the aqueous environment which could slow down the microorganisms' growth (Gould, Christian 1988).

A few published works reported that some bacteria have the ability to swim well in viscous media (Shoesmith 1960; Schneider, Doetsch 1974; Kaiser, Doetsch 1975; Strength, Isani et al. 1976; Greenberg, Canale-Parola 1977a, 1977b). All types of flagellated bacteria exhibited an increase in swimming speed in more viscous solutions. For example Kaiser, Doetsch (1974) tested the swimming speed of *Leptospira interrogans* in methycellulose media. *L. interrogans* possesses internal flagella and moves by twisting back and forth. Schneider, Doetsch (1974) tested the swimming speed of *Pseudomonas aeruginosa* (single polar flagellation) in polyvinylpyrollidone (PVP) solutions as well as various peritrichously-flagellated bacteria like *E. coli*, *B. megaterium* and *S. marcescens*; *Spirillum serpens* (bipolar-flagellated bacterium); and *Thiospirillum jenense* (polar-flagellated bacterium). Various polymers have the ability to increase the swimming speed in bacteria. The solutions of viscous agents are highly structured and form loose quasi-rigid network easily penetrated by particles of microscopic size (Sundelof, Nyström, 1977; Winet 1976). The flagellar propulsion is probably enhanced by the gel-like structure of these solutions which exerts forces normal to a bacterial body (Berg, Turner 1979).
The maximum viscosities in which bacteria can swim depend on the structure of the organism. *Spirochaetes* have a helical body shape which allows them to better navigate through high viscosity than for example polar flagellated rod-shaped bacteria like *Pseudomonas*. For example, *Campylobacter jejuni* has a maximum velocity at 40 cP (Shigematsu, Umeda et al. 1998) compared with *P. aeruginosa* at 2 cP (Greenberg, Canale-Parola, 1977a). According to Magariyama, Kudo (2002), a

long, thin, helical shape is suitable for maintaining the swimming speed in viscous conditions containing polymer molecules because of the improved propulsion efficiency. The length of a slender body is much larger than the mesh size of a polymer network. The network forms a virtual tube around the slender body and the body moves easily in the tube but with difficulty outside the tube. The maximum viscosity that facilitates the movement of the bacteria is also species dependent. *P. aeruginosa* stopped swimming at 60 cP (Greenberg, Canale-Parola 1977a). Schneider, Doetsch (1973) observed the effect of viscosity on peritrichously flagellated bacteria among them *S. marcescens*. *S. marcescens* was tested in PVP 360 solutions and the maximum velocity occurred at 4.7 cP and reached ~40 μm/s. In one of the experiments *S. marcescens* cells were grown in LB broth first then tested in different concentration of Ficoll 400 (Figure 6.12). A maximum velocity of 25.9 μm/s was reached at 1.8 cP which is below the velocity measured with the control. The study of the cells size indicated that the shorter cells (~3.8 μm and 25.9 μm/s) swam faster than the most elongated cells (4.6 μm and 20.8 μm/s) (Figure 6.12 and 6.13) within viscous environment. Those results were in accordance with velocity measurements made within the *Big maze* network (Figure 6.8) that showed that the most elongated cells (between 5.5 μm and 8 μm) had a velocity approximately equal to the cells that swam in LB broth only (~22μm/s and ~23 μm/s respectively). With Ficoll 400, *S. marcescens* did not show the same increase in speed as with PVP 360. In their study on swarming phenotypes, Alberti, Harshey (1990) also tested PVP 360 along with other polymers. The best results in terms of swarm cells were found with Ficoll 400 but PVP 360 also showed good induction of swarm cells between 2 cP and 10 cP (0.5 to 2.5% PVP 360). For the cells grown beforehand in Ficoll 400 and then loaded in a viscous environment, the fastest cells were the most elongated ones (28.1 μm/s and 5.3 μm at 3.7 cP) (Figure 6.14 and 6.15). In that condition, the cells velocity was very close to the one measured with the control. The most elongated cells were initiated from a concentration of Ficoll 400 starting at 7 % which correspond to 3.1 cP. Cells that were grown first in LB broth containing different concentration of Ficoll 400 and then loaded into the *Stripe* structure filled with LB medium only showed shorter cells size and also slower or similar speed in comparison to the previous experiments where the growth medium and the network

were both filled with different concentration of Ficoll 400 (Figure 6.16 and 6.17). During their life cycle, swarming cells are able to dedifferentiate into the swimming phenotype when the surrounding medium is liquid. The latter experiments represent this situation and confirm that the cells phenotype change when the extra-cellular environment changes.

6.5 Conclusions

Microchannels systems offer the possibility of changing the extra-cellular environment of the cells, thus providing the opportunity to study the phenotypic behaviour of *S. marcescens*. From results obtained in this chapter, channels filled with different concentration of Ficoll 400 induced different cells phenotype which was quantified through the measurement of the size of the cells and the cells velocity. Light microscopy was used to confirm that the concentration of Ficoll 400 within 5 % to 10 % modified the phenotype of *S. marcescens* as described by Alberti, Harshey (1990). The maximum cells size of 8 μm to 10 μm in length was observed within the *Big maze* network that contained LB broth and 9 % of Ficoll 400. Those cells swam at ~22 μm/s through the channels and faster than the swimming cells (~18 μm/s). Results from a second set of experiments performed within the *Stripe* network revealed a maximum of 5.3 μm in length when the cells were first grown in LB broth containing 9 % of Ficoll 400 and then loaded in the *Stripe* network filled with both LB broth and 9 % Ficoll 400, while a maximum of 4.6 μm was observed when the cells were first grown in LB broth only and then loaded in LB broth that contains 9 % of Ficoll 400. The experiments revealed also that a decrease in velocity of the swimming cells was observed by the addition of Ficoll 400 in LB broth in comparison to the velocity measured in undiluted LB broth solution. Conversely, the fastest cells were also the most elongated one. Ficoll was effective in changing *S. marcescens* phenotype. *Serratia marcescens'* unique characteristics make it an excellent candidate to develop microdevices capable of measuring viscosity.

Chapter 7
Conclusions and future work

7.1 Overview of main research findings and contributions

What makes bacteria swimming possible is the use of their flagellar motor and its ability to rotate steadily and switch direction in response to environmental signals. Therefore, bacteria may by theory move in any direction. Unlike bacteria, filamentous fungi growth is extremely polar and extends at the tip, which is characterised by the initial establishment of one direction followed by its continuous maintenance. The fungal and bacterial species used in this thesis were naturally occurring wood pathogens (*Armillaria mellea*) and soil bacteria (*Serratia marcescens* and *Pseudomonas stutzeri*). Both environments are porous and heterogeneous. At the micrometer scale physical interactions include cells interactions with other cells, and with the surrounding fluid as well as with surfaces. The interactions of the cells with different networks were studied in this thesis to understand the behaviour of microorganisms in confined environments. Soft lithography associated with PDMS was used as a technique to create complex environments at the micrometer-scale. Microfluidic confinement enable the study of small populations of cells under identical conditions, faster and in conditions that better mimic an *in vivo* environment. Another important advantage of the PDMS-based microfluidic network is that it provided direct visual information on how a constraining environment may affect microorganisms' motility.

A. mellea was found to explore the mazes without any nutrient cues. The success rate was close or superior to 1. *A. mellea* was able to grow through every network exhibiting similar geometry-induced mechanisms. The branching pattern exhibited on plain agar was significantly different from the branching pattern in the confined environment where branching was initiated due to "tip-to-wall" collisions. This was unexpected as hyphal branching play a central role in the development of a fungal

mycelia colony. However, it revealed the importance of thigmotropism in fungal growth. The work revealed as well responses which were independent from the geometry. The data measured within the networks represented most likely the attributes *A. mellea* needs to colonize its natural environment and indicates that it might offer biological advantages to the species. *A. mellea* growth behaviour was changed by the confinement which indicates that (i) microfluidic networks were a very simple and efficient mean to observe fungal growth and (ii) filamentous fungi have developed adequate strategies to resolve geometrical problems. PDMS-based microfluidic environments are therefore an excellent means to investigate the sensing and orientation ability of *A. mellea* and have revealed, so far unreported space-searching strategies. The detail knowledge of fungal growth is beneficial for the control of fungal pathogen on medical devices and the design of microfluidics devices. The high density of features and obstacles has the ability to direct and/or stop fungal growth which is an ideal situation to apply antifungal drugs especially for *in vitro* device. Species-specific responses open the avenue for the design of surfaces that are species selective.

Serratia marcescens and *Pseudomonas stutzeri* were observed within PDMS made microfluidic networks. The species differ in their swimming pattern which was interesting to observe within the networks to evaluate their differences and similarities. The motility parameters measured in restricting geometries varied for both species and in comparison to those measured in non-confined environments. The microfluidic system provides direct visual information on the swimming behaviour of the bacteria. The data showed that bacteria were very efficient to swim through narrow channels. The work also showed that it was possible to control the spread of bacterial species in artificial maze-like structures. The understanding of the motility of single cells near surfaces is an important step towards the understanding of their population dynamics, which is relevant to the comprehension of the early stages of biofilm formation and bacterial infection. Boundary accumulation and wall switching as seen in this work could affect biofilm initiation in multiple ways: (i) in disrupting sensing and communication between cells, (ii) in discouraging space searching and (iii) adherence to surfaces. The ability to visualize bacteria within

porous media provide researcher a powerful tool for understanding the impact of bacteria transport on remediation strategies for environmental cleanup of polluted groundwater. A device like the *Stripe* network would be an easy and fast way to identify different species from sea samples through their motility behaviour as *P. stutzeri* and *S. marcescens* had a distinct swimming behaviour within straight channels. The *Stripe* network would also be ideal to develop antimicrobial susceptibility test through bacterial motility.

S. marcescens swim in liquid media but the species is also known to swarm when the viscosity of the media increases (Alberti, Harshey 1990). The authors showed that swarming is the result of physical constraint of the environments. The extra-cellular environment of the network was therefore modified by addition of Ficoll 400 to LB broth which results in the viscosity of the medium from 1.1 cP to 10.5 cP. The swimming and the swarming motility were observed in two networks of different channels width (15 μm and 10 μm). The effects of the viscosity of the media were quantified through the cells size and the cells velocity. Both parameters were changed in relation to the viscosity of the medium. The study of the temporal emergence of swarming from a single cell in response to its environment may provide insight about the mechanism use to translate through fluid.

The work presented in this thesis have provided (i) a new, flexible methodology for the study of the behavior of microorganisms in micro-confined spaces (ii) a better predictability of the behavior of bacterial and fungal species in natural micro-confined environments. The quantitative analysis of data obtained throughout this thesis confirmed that the micro-confinement in which the species grow is a non-negligible parameter for fungal and bacterial growth. Soft lithography provides a bridge between microbiologists and physical scientists or engineers. The applications by microbiologists can guide the development of new techniques and materials by physicists and engineers. The work presented demonstrates a novel way to use semi-conductor technology: to fabricate artificial structures in the micrometre range resembling the spatial properties of the habitat of filamentous fungi and bacteria.

7.2 Future work

The results obtained in the thesis chapters (4, 5 and 6) present future directions given in the following paragraphs.

Further investigation with fluorescence and confocal microscopy techniques will enable the understanding of fungal growth via the observation of intra-cellular events. Growth, branching and progress of growing apical tips will be monitored within the networks using the stain FM4-64 for example that stain the apical vesicle clusters within the Spitzenkörper or using growth-affected mutants (defective in polarity and/or branching). The networks have revealed, so far unreported space-searching strategies. Fungal hyphae showed the ability to efficiently find entries of the networks without physical contact with the walls. This observation was attributed to the formation of a self-generated ionic gradient which could guide the hyphae to find the exits. Inhibitors useful for identifying the importance of ionic sensing in directionality of apical growth will be used as well as inhibitors of calcium/proton and potassium/proton exchange channels. Hyphae navigated the networks thanks to contact with the walls which is a thigmotropic sensing. This response is thought to involve stretch activated calcium channels. Inhibitors of these channels will be used to study the role of thigmotropism.

Future work on bacterial motility will include the observation of the swimming behaviour in 3-D using optical coherence tomography (OCT) that enables observations inside the cells, in 3-D, with micrometer or sub-micrometer resolution. It is well known that bacterium flagella have different conformation and is important in bacterial pathogenicity. The staining of the flagellum will be useful to know its conformation close or away from a wall. Also new networks that specify the decision making processes for bacteria can be developed. These networks could have more 'cross-junction' combined with round-about that determines their directionality. Another direction could be the comparison of bacteria with different patterns of flagellation different from the one used in this thesis. Other species that have

internalised filaments can also be studied i.e. spirochetes. In general this work opens the avenue of the creation of a database of fungal and bacterial behaviour.

The initiation of elongated cells as well as their possible isolation will be useful for studying the attractions of elongated cells to surface in comparison to vegetative cells. Similarly, it will be useful for studying cell – fluid interactions. The initiation of different phenotype in a controllable manner would be helpful for examining the variation of gene and protein expression throughout the bacterial cell differentiation.

References

ADLER, J., 1969. Chemoreceptors in bacteria. *Science,* **166**(3913), pp. 1588-1597.

ADLER, J., 1965. Chemotaxis in *Escherichia coli, Cold Spring Harbor symposia on quantitative biology* 1965, Cold Spring Harbor Laboratory Press, pp. 289-292.

ADLER, J. and DAHL, M.M., 1967. A method for measuring the motility of bacteria and for comparing random and non-random motility. *Microbiology,* **46**(2), pp. 161-173.

ALBERTI, L. and HARSHEY, R.M., 1990. Differentiation of *Serratia marcescens* 274 into swimmer and swarmer cells. *Journal of Bacteriology,* **172**(8), pp. 4322-4328.

ALTSCHULER, S.J., ANGENENT, S.B., WANG, Y. and WU, L.F., 2008. On the spontaneous emergence of cell polarity. *Nature,* **454**(7206), pp. 886-889.

Apoga, D., Barnard, J., Craighead, H. G., Hoch, H. C., 2004. Quantification of substratum contact required for initiation of *Colletotrichum graminicola* appressoria. *Fungal Genetics and Biology,* **41**, pp. 1-12.

ARMITAGE, J., 2006. Bacterial behavior. *The Prokaryotes,* **2**, pp. 102-139.

ATSUMI, T., MAEKAWA, Y., YAMADA, T., KAWAGISHI, I., IMAE, Y. and HOMMA, M., 1996. Effect of viscosity on swimming by the lateral and polar flagella of *Vibrio alginolyticus. Journal of Bacteriology,* **178**(16), pp. 5024-5026.

BAHN, Y.S., XUE, C., IDNURM, A., RUTHERFORD, J.C., HEITMAN, J. and CARDENAS, M.E., 2007. Sensing the environment: lessons from fungi. *Nature Reviews Microbiology,* **5**(1), pp. 57-69.

BALLESTEROS, S.A., CHIRIFE, J. and BOZZINI, J.P., 1993. Specific solute effects on *Staphylococcus aureus* cells subjected to reduced water activity. *International journal of food microbiology,* **20**(2), pp. 51-66.

BARDY, S.L., NG, S.Y.M. and JARRELL, K.F., 2003. Prokaryotic motility structures. *Microbiology,* **149**(2), pp. 295-304.

BARTNICKI-GARCIA, S., 2002. Hyphal tip growth: outstanding questions. *MYCOLOGY SERIES,* **15**, pp. 29-58.

BARTNICKI-GARCIA, S., 1990. Role of vesicles in apical growth and a new mathematical model of hyphal morphogenesis. *Tip growth in plant and fungal cells*, pp. 211-232.

BARTNICKI-GARCIA, S., 1987. The cell wall: a crucial structure in fungal evolution. *Evolutionary biology of the fungi,* Cambridge University Press, Cambridge, pp. 389-403.

BARTNICKI-GARCIA, S., 1973. Fundamental aspects of hyphal morphogenesis, *Symp. Soc. Gen. Microbiol* 1973, pp. 245-267.

BARTNICKI-GARCIA, S., BARTNICKI, D.D., GIERZ, G., LÓPEZ-FRANCO, R. and BRACKER, C.E., 1995. Evidence that Spitzenkörper behavior determines the shape of a fungal hypha: a test of the hyphoid model. *Experimental mycology,* **19**(2), pp. 153-159.

BARTNICKI-GARCIA, S., HERGERT, F. and GIERZ, G., 1989. Computer simulation of fungal morphogenesis and the mathematical basis for hyphal (tip) growth. *Protoplasma,* **153**(1), pp. 46-57.

BEACHEY, E.H., 1981. Bacterial adherence: adhesin-receptor interactions mediating the attachment of bacteria to mucosal surfaces. *The Journal of infectious diseases,* **143**(3), pp. 325-345.

BERG, H.C., 2004. *E. coli* in Motion. Springer Verlag.

BERG, H.C., 2002. The rotary motor of bacterial flagella. *Annual Review of biochemistry*, **72**, pp. 19-54.

BERG, H.C., 2000. Constraints on models for the flagellar rotary motor. *Philosophical Transactions of the Royal Society of Londo. Series B: Biological Sciences,* **355**(1396), pp. 491-501.

BERG, H.C., 1975. Bacterial behaviour. *Nature,* **254**(5499), pp. 389-392.

BERG, H.C. and BROWN, D.A., 1972. Chemotaxis in *Escherichia coli* Analyzed by 3-Dimensional Tracking. *Nature,* **239**(5374), pp. 500-504.

BERG, H.C. and TURNER, L., 1990. Chemotaxis of bacteria in glass capillary arrays. *Escherichia coli*, motility, microchannel plate, and light scattering. *Biophysical journal,* **58**(4), pp. 919-930.

BERG, H.C. and TURNER, L., 1979. Movement of microorganisms in viscous environments. *Nature*, **278**, pp. 349-351.

BERG, J.M., TYMOCZKO, J.L., STRYER, L., 2002. Molecular Cell Biology. 5th ed., W.H. Freeman. ISBN 0-7167-4955-6.

BETTINGER, C.J., ZHANG, Z., GERECHT, S., BORENSTEIN, J.T. and LANGER, R., 2008. Enhancement of in vitro capillary tube formation by substrate nanotopography. *Advanced Materials,* **20**(1), pp. 99-103.

BIGGS, M.J.P., RICHARDS, R.G., GADEGAARD, N., WILKINSON, C.D.W. and DALBY, M.J., 2007. The effects of nanoscale pits on primary human osteoblast adhesion formation and cellular spreading. *Journal of Materials Science: Materials in Medicine,* **18**(2), pp. 399-404.

Bechinger, C., Giebel, K. F., Schnell, M., Leiderer, P., Deising, H. B., Bastmeyer, M, 1999. Optical measurements of invasive forces exerted by appressoria of a plant pathogenic fungus. *Science*, **285**, pp. 1896-1899.

BIONDI, S.A., QUINN, J.A. and GOLDFINE, H., 1998. Random motility of swimming bacteria in restricted geometries. *AICHE Journal,* **44**(8), pp. 1923-1929.

BOTTONE, E.J., NAGARSHETH, N. and CHIU, K., 1998. Evidence of self-inhibition by filamentous fungi accounts for unidirectional hyphal growth in colonies. *Canadian journal of microbiology,* **44**(4), pp. 390-393.

BOURETT, T. and HOWARD, R., 1991. Ultrastructural immunolocalization of actin in a fungus. *Protoplasma,* **163**(2), pp. 199-202.

BOWEN, A.D., DAVIDSON, F.A., KEATCH, R. and GADD, G.M., 2007. Effect of nutrient availability on hyphal maturation and topographical sensing in *Aspergillus niger*. *Mycoscience,* **48**(3), pp. 145-151.

BRADLEY, D.E., 1980. A function of *Pseudomonas aeruginosa* PAO polar pili: twitching motility. *Canadian journal of microbiology,* **26**(2), pp. 146-154.

BRAND, A. and GOW, N.A.R., 2009. Mechanisms of hypha orientation of fungi. *Current opinion in microbiology,* **12**(4), pp. 350-357.

BRUHN, J.N., 1998. Identification of *Armillaria* field isolates using isozymes and mycelial growth characteristics. *Mycopathologia,* **142**(2), pp. 89-96.

BRUNSWICK, H., 1924. Untersuchungen űber die geslechts und kernverhältnissen bei der Hymenomyceten gattung *Coprinus*. K. Goebel, Editor, *Botanische Abhandlungen*, Fisher, Jena, pp. 1-152.

BURRI, R. and STUTZER, A., 1895. Über Nitrat zerstörende Bakterien und den durch dieselben bedingten Stickstoffverlust. *Zentbl.Bakteriol.Parasitenkd.Abt.II,* **1**, pp. 257-265.

CHATTOPADHYAY, S., MOLDOVAN, R., YEUNG, C. and WU, X., 2006. Swimming efficiency of bacterium *Escherichia coli. Proceedings of the National Academy of Sciences,* **103**(37), pp. 13712-13717.

CHEN, C.S., MRKSICH, M., HUANG, S., WHITESIDES, G.M. and INGBER, D.E., 1998. Micropatterned surfaces for control of cell shape, position, and function. *Biotechnology progress,* **14**(3), pp. 356-363.

CHOI, C.H., HAGVALL, S.H., WU, B.M., DUNN, J.C.Y., BEYGUI, R.E. and KIM, C.J., 2007. Cell interaction with three-dimensional sharp-tip nanotopography. *Biomaterials,* **28**(9), pp. 1672-1679.

CHOU, L., FIRTH, J.D., UITTO, V.J. and BRUNETTE, D.M., 1995. Substratum surface topography alters cell shape and regulates fibronectin mRNA level, mRNA stability, secretion and assembly in human fibroblasts. *Journal of cell science,* **108**, pp. 1563-1573.

COPELAND, M.F. and WEIBEL, D.B., 2009. Bacterial swarming: a model system for studying dynamic self-assembly. *Soft Matter,* **5**(6), pp. 1174-1187.

COPELAND, M.F., FLICKINGER, S.T., TUSON, H.H. and WEIBEL, D.B., 2010. Studying the dynamics of flagella in multicellular communities of *Escherichia coli* by using biarsenical dyes. *Applied and Environmental Microbiology,* **76**(4), pp. 1241-1250.

CRAIG, R.F., 1978. Soil mechanics, 2nd Edition, Van Nostrand Reinhold.

CURTIS, A.S.G., CASEY, B., GALLAGHER, J.O., PASQUI, D., WOOD, M.A. and WILKINSON, C.D.W., 2001. Substratum nanotopography and the adhesion of biological cells. Are symmetry or regularity of nanotopography important? *Biophysical chemistry,* **94**(3), pp. 275-283.

DALBY, M.J., GADEGAARD, N. and WILKINSON, C.D.W., 2008. The response of fibroblasts to hexagonal nanotopography fabricated by electron beam lithography. *Journal of Biomedical Materials Research Part A,* **84**(4), pp. 973-979.

DALTON, B., WALBOOMERS, X.F., DZIEGIELEWSKI, M., EVANS, M.D.M., TAYLOR, S., JANSEN, J.A. and STEELE, J.G., 2001. Modulation of epithelial

tissue and cell migration by microgrooves. *Journal of Biomedical Materials Research,* **56**(2), pp. 195-207.

DANIELS, R., VANDERLEYDEN, J. and MICHIELS, J., 2004. Quorum sensing and swarming migration in bacteria. *FEMS microbiology reviews,* **28**(3), pp. 261-289.

DEPAMPHILIS, M. and ADLER, J., 1971. Fine structure and isolation of the hook-basal body complex of flagella from *Escherichia coli* and *Bacillus subtilis*. *Journal of Bacteriology,* **105**(1), pp. 384-395.

DIJKSTERHUIS, J., 2003. Confocal microscopy of Spitzenkörper dynamics during growth and differentiation of rust fungi. *Protoplasma,* **222**(1), pp. 53-59.

DILUZIO, W.R., TURNER, L., MAYER, M., GARSTECKI, P., WEIBEL, D.B., BERG, H.C. and WHITESIDES, G.M., 2005. *Escherichia coli* swim on the right-hand side. *Nature,* **435**(7046), pp. 1271-1274.

DISCHER, D.E., JANMEY, P. and WANG, Y., 2005. Tissue cells feel and respond to the stiffness of their substrate. *Science,* **310**(5751), pp. 1139-1143.

DONLAN, R.M. and COSTERTON, J.W., 2002. Biofilms: survival mechanisms of clinically relevant microorganisms. *Clinical microbiology reviews,* **15**(2), pp. 167-193.

DUFFY, D.C., MCDONALD, J.C., SCHUELLER, O.J.A. and WHITESIDES, G.M., 1998. Rapid prototyping of microfluidic systems in poly (dimethylsiloxane). *Analytical Chemistry,* **70**(23), pp. 4974-4984.

DUFFY, K.J. and FORD, R.M., 1997. Turn angle and run time distributions characterize swimming behavior for *Pseudomonas putida*. *Journal of Bacteriology,* **179**(4), pp. 1428-1430.

EBERL, L., MOLIN, S. and GIVSKOV, M., 1999. Surface motility of *Serratia liquefaciens* MG1. *Journal of Bacteriology,* **181**(6), pp. 1703-1712.

EBERL, L., WINSON, M.K., STERNBERG, C., STEWART, G.S.A.B., CHRISTIANSEN, G., CHHABRA, S.R., BYCROFT, B., WILLIAMS, P., MOLIN, S. and GIVSKOV, M., 1996. Involvement of N-acyl-l-homoserine lactone autoinducers in controlling the multicellular behaviour of *Serratia liquefaciens*. *Molecular microbiology,* **20**(1), pp. 127-136.

ELLISON, D., MUNDEN, A. and LEVCHENKO, A., 2009. Computational model and microfluidic platform for the investigation of paracrine and autocrine signaling in mouse embryonic stem cells. *Mol.BioSyst.,* **5**(9), pp. 1004-1012.

EVANS, C.S. and HEDGER, J.N., 2001. Degradation of plant cell wall polymers. *Fungi in bioremediation,* **23**, pp. 1-26.

FIDDY, C. and TRINCI, A.P.J., 1976. Mitosis, septation, branching and the duplication cycle in *Aspergillus nidulans*. *Microbiology,* **97**(2), pp. 169-184.

FILIPPONI, L., HANSON, K.L., LEE, A.P. and NICOLAU, D.V., 2005a. Negotiation of obstacles by fungi in micro-fabricated structures: to turn or not to turn? *Proceedings of IEEE*, pp. 391-392.

FILIPPONI, L., HANSON, K.L., LEE, A.P. and NICOLAU, D.V., 2005b. Polymer microstructures for cellular growth studies, *Proceedings of SPIE*, pp. 45-51.

FISCHER-PARTON, S., PARTON, R., HICKEY, P., DIJKSTERHUIS, J., ATKINSON, H. and READ, N., 2000. Confocal microscopy of FM4-64 as a tool for analysing endocytosis and vesicle trafficking in living fungal hyphae. *Journal of microscopy,* **198**(3), pp. 246-259.

FLEMMING, R., MURPHY, C., ABRAMS, G., GOODMAN, S. and NEALEY, P., 1999. Effects of synthetic micro-and nano-structured surfaces on cell behavior. *Biomaterials,* **20**(6), pp. 573-588.

FORD, R.M., PHILLIPS, B.R., QUINN, J.A. and LAUFFENBURGER, D.A., 1991. Measurement of bacterial random motility and chemotaxis coefficients: I. Stopped-flow diffusion chamber assay. *Biotechnology and bioengineering,* **37**(7), pp. 647-660.

FOX, R.T.V., 2000. *Armillaria* root rot: biology and control of honey fungus. Intercept.

FRASER, G.M. and HUGHES, C., 1999. Swarming motility. *Current opinion in microbiology,* **2**(6), pp. 630-635.

FRICKER, M., LEE, J., BEBBER, D., TLALKA, M., HYNES, J., DARRAH, P., WATKINSON, S. and BODDY, L., 2008. Imaging complex nutrient dynamics in mycelial networks. *Journal of microscopy,* **231**(2), pp. 317-331.

FRYMIER, P.D. and FORD, R.M., 1997. Analysis of bacterial swimming speed approaching a solid–liquid interface. *AICHE Journal,* **43**(5), pp. 1341-1347.

FRYMIER, P.D., FORD, R.M., BERG, H.C. and CUMMINGS, P.T., 1995. Three-dimensional tracking of motile bacteria near a solid planar surface. *Proceedings of the National Academy of Sciences,* **92**(13), pp. 6195-6199.

FUHR, M., SCHUBERT, M., SCHWARZE, F. and HERRMANN, H., 2011. Modelling the hyphal growth of the wood-decay fungus *Physisporinus vitreus*. *Fungal Biology*, **115**, pp.919-932.

GERECHT, S., BETTINGER, C.J., ZHANG, Z., BORENSTEIN, J.T., VUNJAK-NOVAKOVIC, G. and LANGER, R., 2007. The effect of actin disrupting agents on contact guidance of human embryonic stem cells. *Biomaterials,* **28**(28), pp. 4068-4077.

GIRBARDT, M., 1969. Die ultrastruktur der apikalregion von pilzhyphen. *Protoplasma,* **67**(4), pp. 413-441.

GIRBARDT, M., 1957. Der Spitzenkörper von *Polystictus versicolor* (L.). *Planta,* **50**(1), pp. 47-59.

GITAI, Z., 2005. The new bacterial cell biology: moving parts and subcellular architecture. *Cell,* **120**(5), pp. 577-586.

GIVSKOV, M., ÖSTLING, J., EBERL, L., LINDUM, P.W., CHRISTENSEN, A.B., CHRISTIANSEN, G., MOLIN, S. and KJELLEBERG, S., 1998. Two separate regulatory systems participate in control of swarming motility of *Serratia liquefaciens* MG1. *Journal of Bacteriology,* **180**(3), pp. 742-745.

GOMEZ, N. and SCHMIDT, C.E., 2004. Studies on Competitive Responses in Neurons to Extracellular Cues Using Microfabricated Systems. *Biomedical Engineering Society Annual Fall Meeting.*

GOUGOULI, M. and KOUTSOUMANIS, K.P., 2010. Modelling growth of *Penicillium expansum* and *Aspergillus niger* at constant and fluctuating temperature conditions. *International journal of food microbiology,* **140**(2), pp. 254-262.

GOULD, G. and CHRISTIAN, J., 1988. Characterization of the state of water in foods: biological aspects. In: SEOW, C.C., TENG, T.T., QUAH,C.H., editors; Food preservation by moisture control. London, United Kingdom: *Elsevier Applied Science*, pp. 43-56.

GREENBERG, E. and CANALE-PAROLA, E., 1977a. Motility of flagellated bacteria in viscous environments. *Journal of Bacteriology,* **132**(1), pp. 356-358.

GREENBERG, E. and CANALE-PAROLA, E., 1977b. Relationship between cell coiling and motility of spirochetes in viscous environments. *Journal of Bacteriology,* **131**(3), pp. 960-969.

GRIMONT, F. and GRIMONT, P.A.D., 1992. The genus *Serratia. The prokaryotes,* **3**, pp. 2822–2848.

GRINBERG, A. and HEATH, I.B., 1997. Direct Evidence for Ca^{2+} Regulation of Hyphal Branch Induction. *Fungal Genetics and Biology,* **22**(2), pp. 127-139.

GRISCOM, L., DEGENAAR, P., DENOUAL, M. and MORIN, F., 2002. Culturing of neurons in microfluidic arrays, *Microtechnologies in Medicine & Biology 2nd Annual International IEEE-EMB Special Topic Conference on* 2002, IEEE, pp. 160-163.

GROVE, S.N. and BRACKER, C.E., 1970. Protoplasmic organization of hyphal tips among fungi: vesicles and Spitzenkörper. *Journal of Bacteriology,* **104**(2), pp. 989-1009.

GUILLAUMIN, J.J., MOHAMMED, C., ANSELMI, N., COURTECUISSE, R., GREGORY, S., HOLDENRIEDER, O., INTINI, M., LUNG, B., MARXMÜLLER, H. and MORRISON, D., 1993. Geographical distribution and ecology of the *Armillaria* species in Western Europe. *European Journal of Forest Pathology,* **23**(6-7), pp. 321-341.

HANSON, K.L., NICOLAU JR, D.V., FILIPPONI, L., WANG, L., LEE, A.P. and NICOLAU, D.V., 2006. Fungi use efficient algorithms for the exploration of microfluidic networks. *Small,* **2**(10), pp. 1212-1220.

HANSON, K.L., FILIPPONI, L., LEE, A.P. and NICOLAU, D.V., 2005. Fungal growth in confined microfabricated networks, *Proceedings of SPIE* 2005, pp. 26-32.

HARRIS, S.D., 2008. Branching of fungal hyphae: regulation, mechanisms and comparison with other branching systems. *Mycologia,* **100**(6), pp. 823-832.

HARRIS, S.D., 1997. The Duplication Cycle in *Aspergillus nidulans. Fungal Genetics and Biology,* **22**(1), pp. 1-12.

HARRIS, S.D. and MOMANY, M., 2004. Polarity in filamentous fungi: moving beyond the yeast paradigm. *Fungal Genetics and Biology,* **41**(4), pp. 391-400.

HARRIS, S.D., READ, N.D., ROBERSON, R.W., SHAW, B., SEILER, S., PLAMANN, M. and MOMANY, M., 2005. Polarisome meets spitzenkörper: microscopy, genetics, and genomics converge. *Eukaryotic Cell,* **4**(2), pp. 225-229.

HARSHEY, R.M., 2003. Bacterial motility on a surface: many ways to a common goal. *Annual Reviews in Microbiology,* **57**(1), pp. 249-273.

HEATH, I.B., 1995. Integration and regulation of hyphal tip growth. *Canadian journal of botany,* **73**(S1), pp. 131-139.

HELD, M., BINZ, M., EDWARDS, C. and NICOLAU, D.V., 2009. Dynamic Behaviour of Fungi in Microfluidics–A comparative study, *Proc. of SPIE Vol* 2009, pp. 718213-718211.

HELD, M., EDWARDS, C. and NICOLAU, D.V., 2011. Probing the growth dynamics of *Neurospora crassa* with microfluidic structures. *Fungal Biology,* 115(6), pp. 493-505.

HELD, M., EDWARDS, C. and NICOLAU, D.V., 2009. Fungal intelligence; Or on the behaviour of microorganisms in confined micro-environments, *Journal of Physics: Conference Series* 2009, IOP Publishing, pp. 012005-1-012005-6.

HELD, M., KOMAROMY, A., FULGA, F., EDWARDS, C., BOYSEN, R.I., HEARN, M.T.W. and NICOLAU, D.V., 2009. Dynamic behaviour of microorganisms on microstructures. *Microelectronic Engineering,* **86**(4-6), pp. 1455-1458.

HELD, M., LEE, A.P., EDWARDS, C. and NICOLAU, D.V., 2010. Microfluidics structures for probing the dynamic behaviour of filamentous fungi. *Microelectronic Engineering,* **87**(5-8), pp. 786-789.

HENRICHSEN, J., 1972. Bacterial surface translocation: a survey and a classification. *Microbiology and Molecular Biology Reviews,* **36**(4), pp. 478-503.

HERRERA-ESTRELLA, A. and HORWITZ, B.A., 2007. Looking through the eyes of fungi: molecular genetics of photoreception. *Molecular microbiology,* **64**(1), pp. 5-15.

HOCH, H.C., STAPLES, R.C., WHITEHEAD, B., COMEAU, J. and WOLF, E.D., 1987. Signaling for growth orientation and cell differentiation by surface topography in *Uromyces. Science,* **235**(4796), pp. 1659-1662.

HOMMA, M., OOTA, H., KOJIMA, S., KAWAGISHI, I. and IMAE, Y., 1996. Chemotactic responses to an attractant and a repellent by the polar and lateral flagellar systems of *Vibrio alginolyticus*. *Microbiology,* **142**(10), pp. 2777-2783.

HORNG, Y.T., DENG, S.C., DAYKIN, M., SOO, P.C., WEI, J.R., LUH, K.T., HO, S.W., SWIFT, S., LAI, H.C. and WILLIAMS, P., 2002. The LuxR family protein SpnR functions as a negative regulator of N-acylhomoserine lactone-dependent quorum sensing in *Serratia marcescens*. *Molecular microbiology,* **45**(6), pp. 1655-1671.

HUANG, B., WU, H., KIM, S. and ZARE, R.N., 2005. Coating of poly (dimethylsiloxane) with n-dodecyl-β-d-maltoside to minimize nonspecific protein adsorption. *Lab on a Chip,* **5**(10), pp. 1005-1007.

HULME, S.E., DILUZIO, W.R., SHEVKOPLYAS, S.S., TURNER, L., MAYER, M., BERG, H.C. and WHITESIDES, G.M., 2008. Using ratchets and sorters to fractionate motile cells of *Escherichia coli* by length. *Lab Chip,* **8**(11), pp. 1888-1895.

HYDE, G.J. and ASHFORD, A.E., 1997. Vacuole motility and tubule-forming activity in *Pisolithus tinctorius* hyphae are modified by environmental conditions. *Protoplasma,* **198**(1), pp. 85-92.

HYDE, G.J. and HEATH, I.B., 1997. Ca^{2+} Gradients in Hyphae and Branches of *Saprolegnia ferax*. *Fungal Genetics and Biology,* **21**(2), pp. 238-247.

ISHIKAWA, T., SEKIYA, G., IMAI, Y., and YAMAGUCHI, T., 2007. Hydrodynamic interactions between two swimming bacteria. *Biophysical journal,* **93**(6), pp. 2217-2225.

KAISER, G. and DOETSCH, R., 1975. Enhanced translational motion of *Leptospira* in viscous environments. *Nature,* **255**, pp. 656-657.

KARURI, N.W., LILIENSIEK, S., TEIXEIRA, A.I., ABRAMS, G., CAMPBELL, S., NEALEY, P.F. and MURPHY, C.J., 2004. Biological length scale topography enhances cell-substratum adhesion of human corneal epithelial cells. *Journal of cell science,* **117**(Pt 15), pp. 3153-3164.

KASUGA, T. and GLASS, N.L., 2008. Dissecting colony development of *Neurospora crassa* using mRNA profiling and comparative genomics approaches. *Eukaryotic cell,* **7**(9), pp. 1549-1564.

KATSIKOGIANNI, M. and MISSIRLIS, Y., 2010. Interactions of bacteria with specific biomaterial surface chemistries under flow conditions. *Acta Biomaterialia,* **6**(3), pp. 1107-1118.

KATZ, D., GOLDSTEIN, D. and ROSENBERGER, R.F., 1972. Model for branch initiation in *Aspergillus nidulans* based on measurements of growth parameters. *Journal of Bacteriology,* **109**(3), pp. 1097-1100.

KLEINFELD, D., KAHLER, K. and HOCKBERGER, P., 1988. Controlled outgrowth of dissociated neurons on patterned substrates. *The Journal of neuroscience,* **8**(11), pp. 4098-4120.

KOGURE, K., IKEMOTO, E. and MORISAKI, H., 1998. Attachment of *Vibrio alginolyticus* to glass surfaces is dependent on swimming speed. *Journal of Bacteriology,* **180**(4), pp. 932-937.

KOJIMA, S. and BLAIR, D.F., 2001. Conformational change in the stator of the bacterial flagellar motor. *Biochemistry,* **40**(43), pp. 13041-13050.

KUDO, S., IMAI, N., NISHITOBA, M., SUGIYAMA, S. and MAGARIYAMA, Y., 2005. Asymmetric swimming pattern of *Vibrio alginolyticus* cells with single polar flagella. *FEMS microbiology letters,* **242**(2), pp. 221-225.

KUNCOVÁ-KALLIO, J. and KALLIO, P.J., 2006. PDMS and its suitability for analytical microfluidic devices, *Engineering in Medicine and Biology Society, 2006. EMBS'06. 28th Annual International Conference of the IEEE* 2006, IEEE, pp. 2486-2489.

LABBATE, M., QUECK, S.Y., KOH, K.S., RICE, S.A., GIVSKOV, M. and KJELLEBERG, S., 2004. Quorum sensing-controlled biofilm development in *Serratia liquefaciens* MG1. *Journal of Bacteriology,* **186**(3), pp. 692-698.

LAERMER, F. and URBAN, A., 2003. Challenges, developments and applications of silicon deep reactive ion etching. *Microelectronic Engineering,* **67**, pp. 349-355.

LAMOUR, A., TERMORSHUIZEN, A.J., VOLKER, D. and JEGER, M.J., 2007. Network formation by rhizomorphs of *Armillaria lutea* in natural soil: Their description and ecological significance. *FEMS microbiology ecology,* **62**(2), pp. 222-232.

LAUGA, E., DILUZIO, W.R., WHITESIDES, G.M. and STONE, H.A., 2006. Swimming in circles: motion of bacteria near solid boundaries. *Biophysical journal,* **90**(2), pp. 400-412.

LAWRENCE, J., KORBER, D. and CALDWELL, D., 1992. Behavioral analysis of *Vibrio parahaemolyticus* variants in high-and low-viscosity microenvironments by use of digital image processing. *Journal of Bacteriology,* **174**(17), pp. 5732-5739.

LEE, P.J., HUNG, P.J., SHAW, R., JAN, L. and LEE, L.P., 2005. Microfluidic application-specific integrated device for monitoring direct cell-cell communication via gap junctions between individual cell pairs. *Applied Physics Letters,* **86**, pp. 223902-1.

LEHRINGER, C., HILLEBRAND, K., RICHTER, K., ARNOLD, M., SCHWARZE, F.W.M.R. and MILITZ, H., 2010. Anatomy of bioincised Norway spruce wood. *International Biodeterioration & Biodegradation,* **64**(5), pp. 346-355.

LENHERT, S., MEIER, M.B., MEYER, U., CHI, L. and WIESMANN, H.P., 2005. Osteoblast alignment, elongation and migration on grooved polystyrene surfaces patterned by Langmuir-Blodgett lithography. *Biomaterials,* **26**(5), pp. 563-570.

LI, G., TAM, L.K. and TANG, J.X., 2008. Amplified effect of Brownian motion in bacterial near-surface swimming. *Proceedings of the National Academy of Sciences,* **105**(47), pp. 18355-18359.

LIANG, M.N., SMITH, S.P., METALLO, S.J., CHOI, I.S., PRENTISS, M. and WHITESIDES, G.M., 2000. Measuring the forces involved in polyvalent adhesion of uropathogenic *Escherichia coli* to mannose-presenting surfaces. *Proceedings of the National Academy of Sciences,* **97**(24), pp. 13092-13096.

LINDUM, P.W., ANTHONI, U., CHRISTOPHERSEN, C., EBERL, L., MOLIN, S. and GIVSKOV, M., 1998. N-Acyl-L-homoserine lactone autoinducers control production of an extracellular lipopeptide biosurfactant required for swarming motility of *Serratia liquefaciens* MG1. *Journal of Bacteriology,* **180**(23), pp. 6384-6388.

LIU, J.H., LAI, M.J., ANG, S., SHU, J.C., SOO, P.C., HORNG, Y.T., YI, W.C., LAI, H.C., LUH, K.T. and HO, S.W., 2000. Role offlhDC in the expression of the nuclease genenucA, cell division and flagellar synthesis in *Serratia marcescens*. *Journal of Biomedical Science,* 7(6), pp. 475-483.

LOCKERY, S.R., LAWTON, K.J., DOLL, J.C., FAUMONT, S., COULTHARD, S.M., THIELE, T.R., CHRONIS, N., MCCORMICK, K.E., GOODMAN, M.B. and PRUITT, B.L., 2008. Artificial dirt: microfluidic substrates for nematode neurobiology and behavior. *Journal of neurophysiology,* **99**(6), pp. 3136-3143.

LÖPEZ-FRANCO, R. and BRACKER, C.E., 1996. Diversity and dynamics of the Spitzenkörper in growing hyphal tips of higher fungi. *Protoplasma,* **195**(1), pp. 90-111.

MCCARTER, L.L., 2001. Polar flagellar motility of the *Vibrionaceae*. *Microbiology and molecular biology reviews,* **65**(3), pp. 445-462.

MACNAB, R.M. and AIZAWA, S.I., 1984. Bacterial motility and the bacterial flagellar motor. *Annual Review of Biophysics and Bioengineering,* **13**(1), pp. 51-83.

MADOU, M., 1997. Fundamentals of microfabrication. *CRC Press LLC.Capítulo,* **1**, pp. 1-50.

MAGARIYAMA, Y., ICHIBA, M., NAKATA, K., BABA, K., OHTANI, T., KUDO, S. and GOTO, T., 2005. Difference in bacterial motion between forward and backward swimming caused by the wall effect. *Biophysical journal,* **88**(5), pp. 3648-3658.

MAGARIYAMA, Y. and KUDO, S., 2002. A mathematical explanation of an increase in bacterial swimming speed with viscosity in linear-polymer solutions. *Biophysical journal,* **83**(2), pp. 733-739.

MAKAMBA, H., KIM, J.H., LIM, K., PARK, N. and HAHN, J.H., 2003. Surface modification of poly (dimethylsiloxane) microchannels. *Electrophoresis,* **24**(21), pp. 3607-3619.

MAO, H., CREMER, P.S. and MANSON, M.D., 2003. A sensitive, versatile microfluidic assay for bacterial chemotaxis. *Proceedings of the National Academy of Sciences,* **100**(9), pp. 5449-5454.

MATSUYAMA, T., BHASIN, A. and HARSHEY, R.M., 1995. Mutational analysis of flagellum-independent surface spreading of *Serratia marcescens* 274 on a low-agar medium. *Journal of Bacteriology,* **177**(4), pp. 987-991.

MATSUYAMA, T., TANIKAWA, T., NAkAGAWA, Y., 2011. Serrawettins and other surfactants produced by *Serratia*. Biosurfactants, Microbiology Monographs 20, DOI 10.1007/978-3-642-14490-5_4, Springer-Verlag Berlin Heidelberg 2011

MCBRIDE, M.J., 2001. Bacterial gliding motility: multiple mechanisms for cell movement over surfaces. *Annual Reviews in Microbiology,* **55**(1), pp. 49-75.

MCDANIEL, D.P. and ROBERSON, R.W., 2000. Microtubules are required for motility and positioning of vesicles and mitochondria in hyphal tip cells of *Allomyces macrogynus*. *Fungal Genetics and Biology,* **31**(3), pp. 233-244.

MCDONALD, J.C., DUFFY, D.C., ANDERSON, J.R., CHIU, D.T., WU, H., SCHUELLER, O.J.A. and WHITESIDES, G.M., 2000. Fabrication of microfluidic systems in poly (dimethylsiloxane). *Electrophoresis,* **21**(1), pp. 27-40.

METALLO, C.M., VODYANIK, M.A., DE PABLO, J.J., SLUKVIN, I.I. and PALECEK, S.P., 2008. The response of human embryonic stem cell-derived endothelial cells to shear stress. *Biotechnology and bioengineering,* **100**(4), pp. 830-837.

MENZ, W., MOHR, J. and PAUL, O., 2001. Microsystem Technology. WILEY-VCH Verlag GmbH, Weinheim, Germany.

MEYLE, J., GÜLTIG, K. and NISCH, W., 1995. Variation in contact guidance by human cells on a microstructured surface. *Journal of Biomedical Materials Research,* **29**(1), pp. 81-88.

MISIEK, M. and HOFFMEISTER, D., 2008. Processing sites involved in intron splicing of *Armillaria* natural product genes. *Mycological Research,* **112**(2), pp. 216-224.

MITCHELL, J.G., PEARSON, L., DILLON, S. and KANTALIS, K., 1995. Natural assemblages of marine bacteria exhibiting high-speed motility and large accelerations. *Applied and Environmental Microbiology,* **61**(12), pp. 4436-4440.

MOLIN, P., GERVAIS, P., LEMIERE, J.P. and DAVET, T., 1992. Direction of hyphal growth: a relevant parameter in the development of filamentous fungi. *Research in microbiology,* **143**(8), pp. 777-784.

MORRISON, D.J., 2004. Rhizomorph growth habit, saprophytic ability and virulence of 15 *Armillaria* species. *Forest Pathology,* **34**(1), pp. 15-26.

MWENJE, E. and RIDE, J.P., 1996. Morphological and biochemical characterization of *Armillaria* isolates from Zimbabwe. *Plant Pathology,* **45**(6), pp. 1036-1051.

NAKAGAKI, T., 2001. Smart behavior of true slime mold in a labyrinth. *Research in microbiology,* **152**(9), pp. 767-770.

NAKAGAKI, T., YAMADA, H. and TOTH, A., 2001. Path finding by tube morphogenesis in an amoeboid organism. *Biophysical chemistry,* **92**(1-2), pp. 47-52.

NAKAGAKI, T., YAMADA, H. and TÓTH, Á., 2000. Intelligence: Maze-solving by an *amoeboid* organism. *Nature,* **407**(6803), pp. 470-470.

NAKAI, T., KIKUDA, M., KURODA, Y. and GOTO, T., 2009. Speed, trajectory and increment in the number of cells of singly flagellated bacteria swimming close to boundaries. *Journal of Biomechanical Science and Engineering,* **4**(1), pp. 2-10.

NICOLAU, D.V., TAGUCHI, T., TANIGAWA, H. and YOSHIKAWA, S., 1996. Control of the neuronal cell attachment by functionality manipulation of diazo-naphthoquinone/novolak photoresist surface. *Biosensors and Bioelectronics,* **11**(12), pp. 1237-1252.

NICOLAU JR, D.V., BURRAGE, K., NICOLAU, D.V. and MAINI, P.K., 2008. 'Extremotaxis': Computing with a bacterial-inspired algorithm. *BioSystems,* **94**(1-2), pp. 47-54.

NOLL W., 1968. Chemistry and technology of silicones. Academic, New York.

PARK, S., HWANG, H., NAM, S.W., MARTINEZ, F., AUSTIN, R.H. and RYU, W.S., 2008. Enhanced *Caenorhabditis elegans* locomotion in a structured microfluidic environment. *PLoS One,* **3**(6), pp. 1-5.

PARK, S., WOLANIN, P.M., YUZBASHYAN, E.A., LIN, H., DARNTON, N.C., STOCK, J.B., SILBERZAN, P. and AUSTIN, R., 2003. Influence of topology on bacterial social interaction. *Proceedings of the National Academy of Sciences,* **100**(24), pp. 13910-13915.

PHILLIPS, B.R., QUINN, J.A. and GOLDFINE, H., 1994. Random motility of swimming bacteria: single cells compared to cell populations. *AIChE Journal,* **40**(2), pp. 334-348.

PLOMION, C., LEPROVOST, G. and STOKES, A., 2001. Wood formation in trees. *Plant Physiology,* **127**(4), pp. 1513-1523.

PORTER, J.R., 1976. Antony van Leeuwenhoek: tercentenary of his discovery of bacteria. *Microbiology and Molecular Biology Reviews,* **40**(2), pp. 260-269.

PRATS, C., LÓPEZ, D., GIRÓ, A., FERRER, J. and VALLS, J., 2006. Individual-based modelling of bacterial cultures to study the microscopic causes of the lag phase. *Journal of theoretical biology,* **241**(4), pp. 939-953.

PROSSER, J.I. and TRINCI, A.P.J., 1979. A model for hyphal growth and branching. *Microbiology,* **111**(1), pp. 153-164.

QIN, J. and WHEELER, A.R., 2006. Maze exploration and learning in *C. elegans*. *Lab Chip,* 7(2), pp. 186-192.

QUAKE, S.R. and SCHERER, A., 2000. From micro-to nanofabrication with soft materials. *Science,* **290**(5496), pp. 1536-1540.

RAJNICEK, A.M., FOUBISTER, L.E. and MCCAIG, C.D., 2007. Prioritising guidance cues: Directional migration induced by substratum contours and electrical gradients is controlled by a rho/cdc42 switch. *Developmental biology,* **312**(1), pp. 448-460.

RAMALHO-SANTOS, M. and WILLENBRING, H., 2007. On the origin of the term "stem cell". *Cell stem cell,* **1**(1), pp. 35-38.

RAMIA, M., TULLOCK, D.L. and PHAN-THIEN, N., 1993. The role of hydrodynamic interaction in the locomotion of microorganisms. *Biophysical journal,* **65**(2), pp. 755-778.

RANJARD, L. and RICHAUME, A., 2001. Quantitative and qualitative microscale distribution of bacteria in soil. *Research in microbiology,* **152**(8), pp. 707-716.

REYNAGA-PEÑA, C.G., GIERZ, G. and BARTNICKI-GARCIA, S., 1997. Analysis of the role of the Spitzenkörper in fungal morphogenesis by computer simulation of apical branching in *Aspergillus niger*. *Proceedings of the National Academy of Sciences of the United States of America,* **94**(17), pp. 9096-9101.

READ, N.D., KELLOCK, L.J., COLLINS, T.J. and GUNDLACH, A.M., 1997. Role of topography sensing for infection-structure differentiation in cereal rust fungi. *Planta,* **202**(2), pp. 163-170.

RICE, S., KOH, K., QUECK, S., LABBATE, M., LAM, K. and KJELLEBERG, S., 2005. Biofilm formation and sloughing in *Serratia marcescens* are controlled by quorum sensing and nutrient cues. *Journal of Bacteriology,* **187**(10), pp. 3477-3485.

RIQUELME, M. and BARTNICKI-GARCIA, S., 2004. Key differences between lateral and apical branching in hyphae of *Neurospora crassa*. *Fungal Genetics and Biology,* **41**(9), pp. 842-851.

RIQUELME, M., FISCHER, R. and BARTNICKI-GARCIA, S., 2003. Apical growth and mitosis are independent processes in *Aspergillus nidulans*. *Protoplasma,* **222**(3), pp. 211-215.

RIQUELME, M., REYNAGA-PEÑA, C.G., GIERZ, G. and BARTNICKI-GARCÍA, S., 1998. What Determines Growth Direction in Fungal Hyphae? *Fungal genetics and Biology,* **24**(1-2), pp. 101-109.

ROSSO, P. and HANSEN, E., 1998. Tree vigour and the susceptibility of Douglas fir to *Armillaria* root disease. *European Journal of Forest Pathology,* **28**(1), pp. 43-52.

SCHMID, J. and HAROLD, F.M., 1988. Dual roles for calcium ions in apical growth of *Neurospora crassa*. *Microbiology,* **134**(9), pp. 2623-2631.

SCHWARZE, F.W.M.R. and LANDMESSER, H., 2000. Preferential degradation of pit membranes within tracheids by the basidiomycete *Physisporinus vitreus*. *Holzforschung,* **54**(5), pp. 461-462.

SCHWARZE, F.W.M.R., LANDMESSER, H., ZGRAGGEN, B. and HEEB, M., 2006. Permeability changes in heartwood of *Picea abies* and *Abies alba* induced by incubation with *Physisporinus vitreus*. *Holzforschung,* **60**(4), pp. 450-454.

SCHWARZE, F.W.M.R., SPYCHER, M. and FINK, S., 2008. Superior wood for violins–wood decay fungi as a substitute for cold climate. *New Phytologist,* **179**(4), pp. 1095-1104.

SEGALL, J.E., MANSON, M.D. and BERG, H.C., 1982. Signal processing times in bacterial chemotaxis. *Nature,* **296**(5860), pp. 855-857.

SEMIGHINI, C.P. and HARRIS, S.D., 2008. Regulation of apical dominance in *Aspergillus nidulans* hyphae by reactive oxygen species. *Genetics,* **179**(4), pp. 1919-1932.

SHEMAROVA, I. and NESTEROV, V., 2005. Evolution of mechanisms of Ca^{2+} -signaling: role of calcium ions in signal transduction in prokaryotes. *Journal of Evolutionary Biochemistry and Physiology,* **41**(1), pp. 12-19.

SHEPHERD, V., ORLOVICH, D. and ASHFORD, A., 1993. Cell-to-cell transport via motile tubules in growing hyphae of a fungus. *Journal of cell science,* **105**(4), pp. 1173-1178.

SHIGEMATSU, M., UMEDA, A., FUJIMOTO, S. and AMAKO, K., 1998. Spirochaete-like swimming mode of *Campylobacter jejuni* in a viscous environment. *Journal of medical microbiology,* **47**(6), pp. 521-526.

SHIMKETS, L.J., 1999. Intercellular signalling during fruiting-body development of *Myxococcus xanthus*. *Annual Reviews in Microbiology,* **53**(1), pp. 525-549.

SHIMKETS, L.J. and BRUN, Y.V., 2000. Prokaryotic development: strategies to enhance survival. *Prokaryotic Development*, pp. 1–7.

SCHNEIDER, W.R. and DOETSCH, R., 1974. Effect of viscosity on bacterial motility. *Journal of Bacteriology,* **117**(2), pp. 696-701.

SHOESMITH, J., 1960. The measurement of bacterial motility. *Journal of general microbiology,* **22**(2), pp. 528-535.

SINGHVI, R., KUMAR, A., LOPEZ, G.P., STEPHANOPOULOS, G.N., WANG, D., WHITESIDES, G.M. and INGBER, D.E., 1994. Engineering cell shape and function. *Science,* **264**(5159), pp. 696-698.

SOLLA, A., TOMLINSON, F. and WOODWARD, S., 2002. Penetration of *Picea sitchensis* root bark by *Armillaria mellea*, *Armillaria ostoyae* and *Heterobasidion annosum*. *Forest Pathology,* **32**(1), pp. 55-70.

SRINIVASAN, S., VARGAS, M.M. and ROBERSON, R.W., 1996. Functional, organizational, and biochemical analysis of actin in hyphal tip cells of *Allomyces macrogynus*. *Mycologia,* , pp. 57-70.

STEAGER, E., KIM, C.B., PATEL, J., BITH, S., NAIK, C., REBER, L. and KIM, M.J., 2007. Control of microfabricated structures powered by flagellated bacteria using phototaxis. *Applied Physics Letters,* **90**(26), pp. 263901-1-263901-3.

STEWART, P.S., 2003. Diffusion in Biofilms. *Journal of Bacteriology*, 185(5), pp. 1485-1491.

STRENGTH, W., ISANI, B., LINN, D., WILLIAMS, F., VANDERMOLEN, G.E., LAUGHON, B.E. and KRIEG, N., 1976. Isolation and characterization of *Aquaspirillum fasciculus* sp. nov., a rod-shaped, nitrogen-fixing bacterium having unusual flagella. *International Journal of Systematic Bacteriology,* **26**(2), pp. 253-268.

STROOCK, A.D. and WHITESIDES, G.M., 2002. Components for integrated poly (dimethylsiloxane) microfluidic systems. *Electrophoresis,* **23**, pp. 3461-3473.

SUNDELÖF, L.O. and NYSTRÖM, B., 1977. Sedimentation behavior and particle shape in concentrated macromolecular solutions. *Journal of Polymer Science: Polymer Letters Edition,* **15**(6), pp. 377-384.

TEIXEIRA, A.I., ABRAMS, G.A., BERTICS, P.J., MURPHY, C.J. and NEALEY, P.F., 2003. Epithelial contact guidance on well-defined micro-and nanostructured substrates. *Journal of cell science,* **116**(Pt 10), pp. 1881-1892.

TEIXEIRA, A.I., MCKIE, G.A., FOLEY, J.D., BERTICS, P.J., NEALEY, P.F. and MURPHY, C.J., 2006. The effect of environmental factors on the response of human corneal epithelial cells to nanoscale substrate topography. *Biomaterials,* **27**(21), pp. 3945-3954.

THANBICHLER, M., WANG, S.C. and SHAPIRO, L., 2005. The bacterial nucleoid: a highly organized and dynamic structure. *Journal of cellular biochemistry,* **96**(3), pp. 506-521.

THOMAS, H.E., 1934. Studies on *Armillaria mellea* (Vahl) Quel., infection, parasitism, and host resistance. *J.agric.Res,* **48**(3), pp. 187-218.

TRINCI, A.P.J., 1978. The duplication cycle and vegetative development in moulds. *The filamentous fungi,* **3**, pp. 132–163.

TRINCI, A.P.J., 1974. A study of the kinetics of hyphal extension and branch initiation of fungal mycelia. *Microbiology,* **81**(1), pp. 225-236.

VAN DER HEIJDEN, M.G.A., BARDGETT, R.D. and VAN STRAALEN, N.M., 2008. The unseen majority: soil microbes as drivers of plant diversity and productivity in terrestrial ecosystems. *Ecology Letters,* **11**(3), pp. 296-310.

VAN HOUDT, R., GIVSKOV, M. and MICHIELS, C.W., 2007. Quorum sensing in *Serratia. FEMS microbiology reviews,* **31**(4), pp. 407-424.

VAN NIEL, C.B. and ALLEN, M.B., 1952. A note on *Pseudomonas stutzeri. Journal of Bacteriology,* **64**(3), pp. 413-422.

VIGEANT, M.A.S., FORD, R.M., WAGNER, M. and TAMM, L.K., 2002. Reversible and irreversible adhesion of motile *Escherichia coli* cells analyzed by total internal reflection aqueous fluorescence microscopy. *Applied and Environmental Microbiology,* **68**(6), pp. 2794-2801.

VIGEANT, M. and FORD, R.M., 1997. Interactions between motile *Escherichia coli* and glass in media with various ionic strengths, as observed with a three-

dimensional-tracking microscope. *Applied and Environmental Microbiology,* **63**(9), pp. 3474-3479.

VIRAG, A. and GRIFFITHS, A.J.F., 2004. A mutation in the *Neurospora crassa* actin gene results in multiple defects in tip growth and branching. *Fungal Genetics and Biology,* **41**(2), pp. 213-225.

WADHAMS, G.H. and ARMITAGE, J.P., 2004. Making sense of it all: bacterial chemotaxis. *Nature Reviews Molecular Cell Biology,* **5**(12), pp. 1024-1037.

WÄHLSTROM, K.T. and JOHANSSON, M., 1992. Structural responses in bark to mechanical wounding and *Armillaria ostoyae* infection in seedlings of *Pinus sylvestris*. *European Journal of Forest Pathology,* **22**(2), pp. 65-76.

WANG, X., OHLIN, C.A., LU, Q. and HU, J., 2008. Cell directional migration and oriented division on three-dimensional laser-induced periodic surface structures on polystyrene. *Biomaterials,* **29**(13), pp. 2049-2059.

WATTERS, M.K. and GRIFFITHS, A.J.F., 2001. Tests of a cellular model for constant branch distribution in the filamentous fungus *Neurospora crassa*. *Applied and Environmental Microbiology,* **67**(4), pp. 1788-1792.

WATTERS, M.K., HUMPHRIES, C., DE VRIES, I. and GRIFFITHS, A.J.F., 2000. A homeostatic set point for branching in *Neurospora crassa*. *Mycological Research,* **104**(5), pp. 557-563.

WATTERS, M.K., VIRAG, A., HAYNES, J. and GRIFFITHS, A.J.F., 2000. Branch initiation in *Neurospora* is influenced by events at the previous branch. *Mycological Research,* **104**(7), pp. 805-809.

WATTS, H.J., 1998. Thigmotropism and stretch-activated channels in the pathogenic fungus *Candida albicans*. *Microbiology,* **144**(3), pp. 689-695.

WEDLICH-SOLDNER, R., ALTSCHULER, S., WU, L. and LI, R., 2003. Spontaneous cell polarization through actomyosin-based delivery of the Cdc42 GTPase. *Science,* **299**(5610), pp. 1231-1235.

WEIBEL, D.B., DILUZIO, W.R. and WHITESIDES, G.M., 2007. Microfabrication meets microbiology. *Nature Reviews Microbiology,* **5**(3), pp. 209-218.

WEST, M., BURDASH, N.M. and FREIMUTH, F., 1977. Simplified silver-plating stain for flagella. *Journal of clinical microbiology,* **6**(4), pp. 414-419.

WINET, H., 1976. Ciliary propulsion of objects in tubes: wall drag on swimming Tetrahymena (Ciliata) in the presence of mucin and other long-chain polymers. *Journal of Experimental Biology,* **64**(2), pp. 283-302.

WHITESIDES, G.M., OSTUNI, E., TAKAYAMA, S., JIANG, X. and INGBER, D.E., 2001. Soft Lithography in Biology and Biochemistry. *Annual Review of Biomedical Engineering,* **3**(1), pp. 335-373.

XIA, Y. and WHITESIDES, G.M., 1998. Soft lithography. *Annual Review of Materials Science,* **28**(1), pp. 153-184.

YAO, X., JERICHO, M., PINK, D. and BEVERIDGE, T., 1999. Thickness and elasticity of gram-negative *Murein sacculi* measured by atomic force microscopy. *Journal of Bacteriology,* **181**(22), pp. 6865-6875.

YIM, E.K.F., REANO, R.M., PANG, S.W., YEE, A.F., CHEN, C.S. and LEONG, K.W., 2005. Nanopattern-induced changes in morphology and motility of smooth muscle cells. *Biomaterials,* **26**(26), pp. 5405-5413.

ZEN, A., NEHER, D., SILMY, K., HOLLÄNDER, A., ASAWAPIROM, U. and SCHERF, U., 2005. Improving the performance of organic field effect transistor by optimizing the gate insulator surface. *Japanese journal of applied physics.Pt.1, Regular papers & short notes,* **44**(6), pp. 3721-3727.

ZHOU, X.L., STUMPF, M.A., HOCH, H.C. and KUNG, C., 1991. A mechanosensitive channel in whole cells and in membrane patches of the fungus *Uromyces. Science,* **253**(5026), pp. 1415-1417.

Appendix: Frequency distribution of *S. marcescens* and *P. stutzeri* within the *Stripe* network

Serratia marcescens

2 µm channel

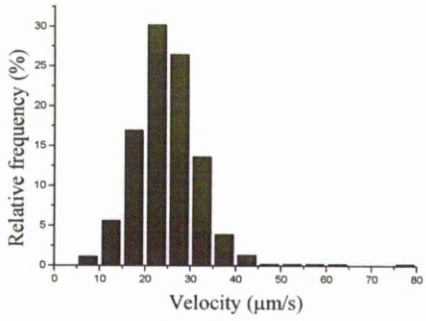

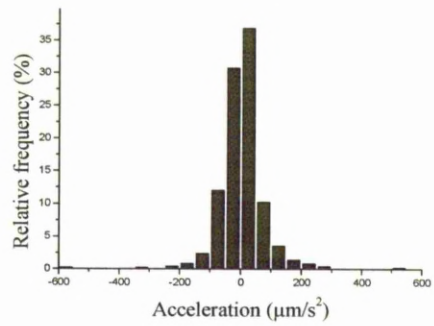

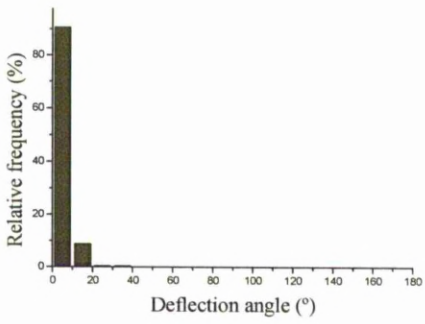

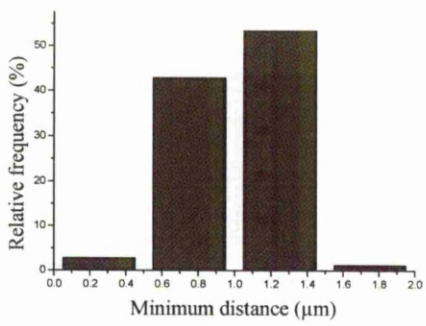

3 µm channel

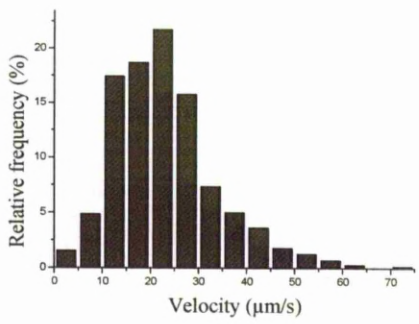

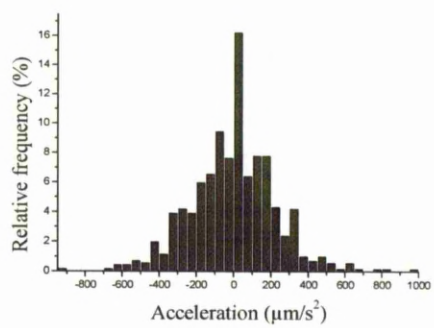

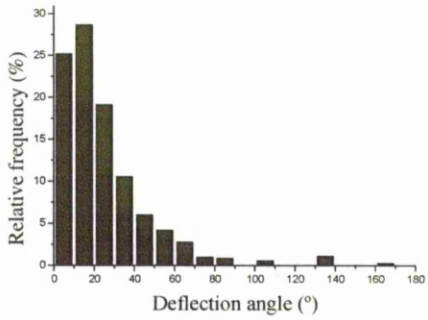
Relative frequency (%)
Deflection angle (°)

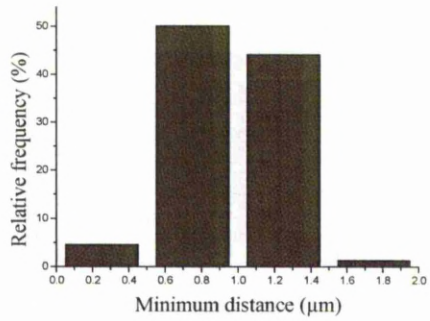
Relative frequency (%)
Minimum distance (μm)

4 μm channel

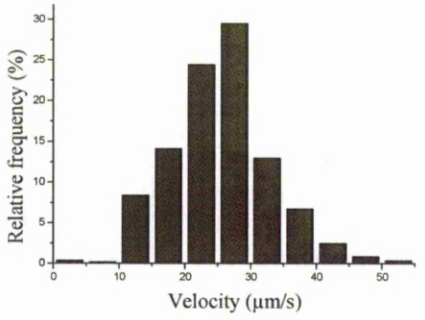
Relative frequency (%)
Velocity (μm/s)

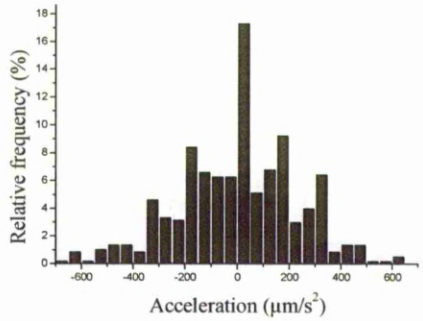
Relative frequency (%)
Acceleration (μm/s²)

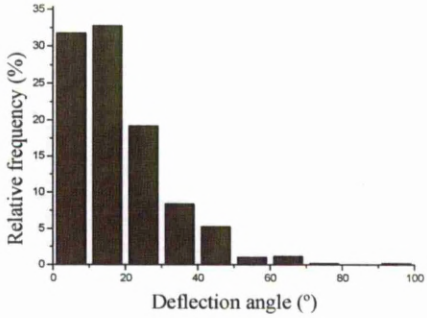
Relative frequency (%)
Deflection angle (°)

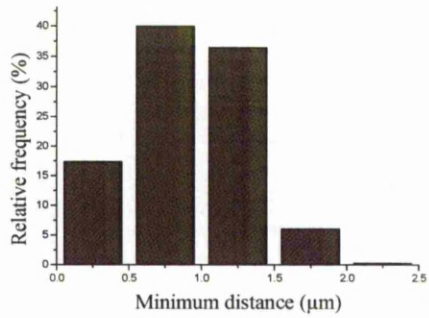
Relative frequency (%)
Minimum distance (μm)

5 µm channel

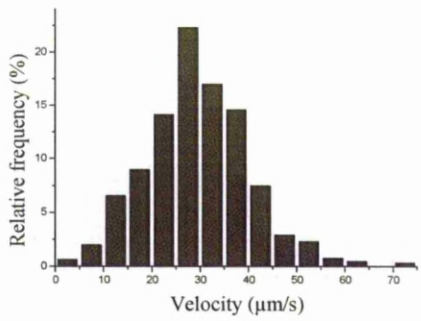

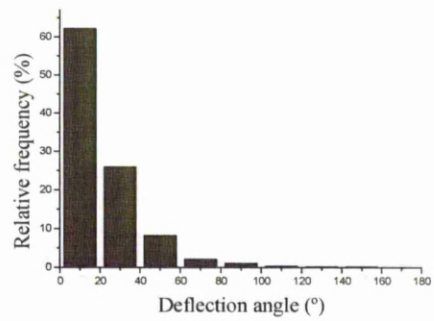

6 µm channel

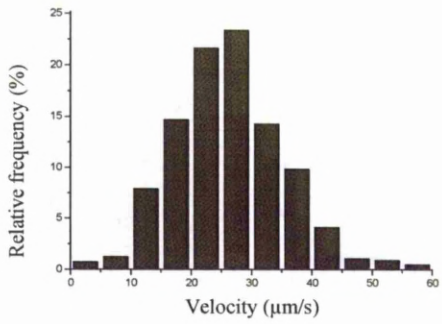

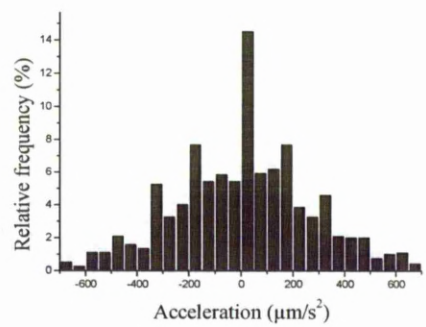

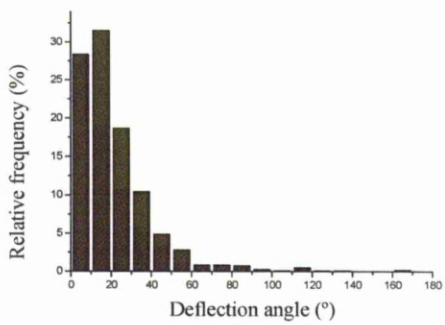

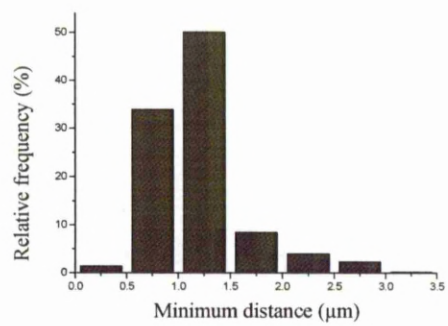

7 μm channel

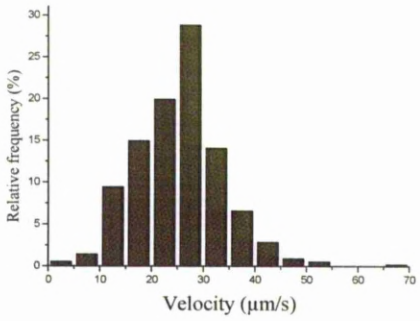

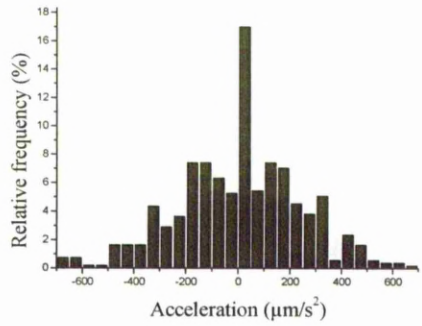

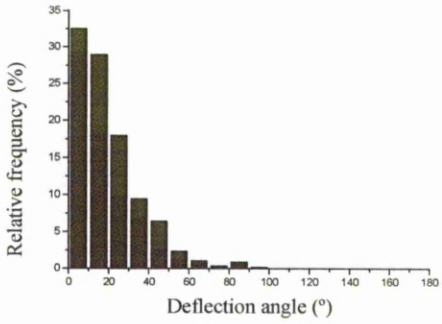

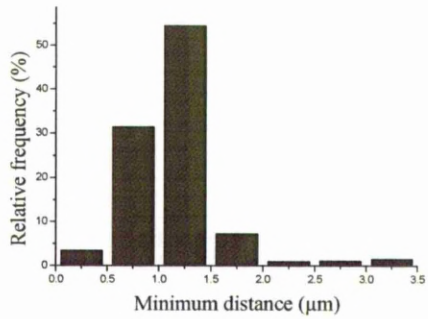

8 μm channel

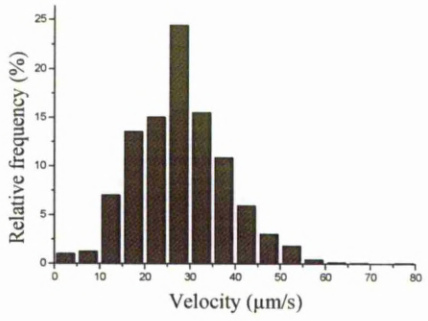

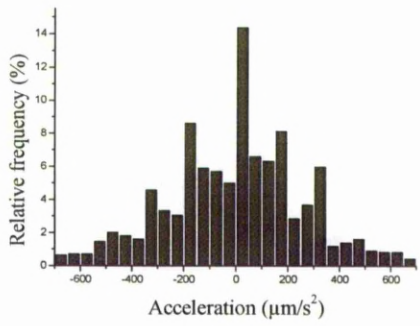

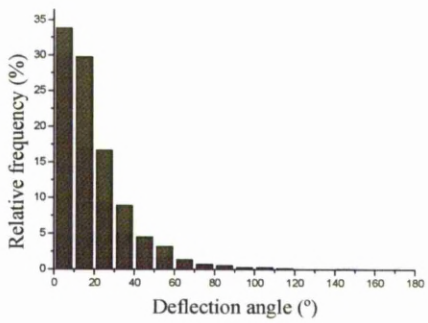

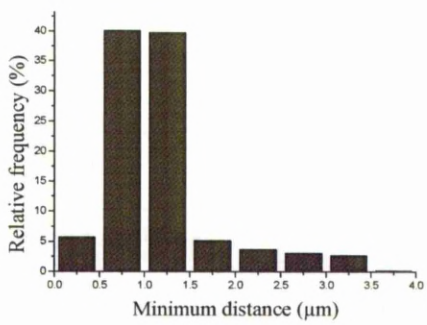

9 µm channel

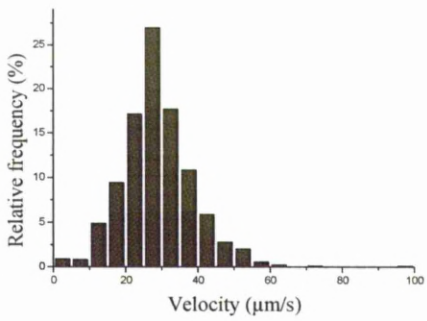

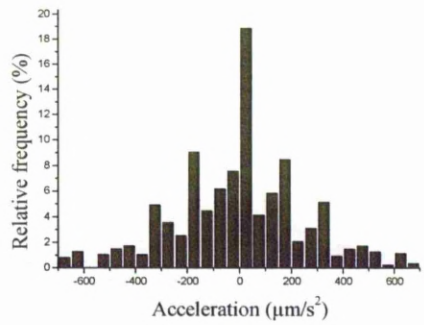

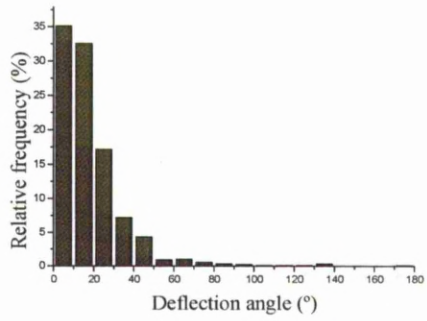

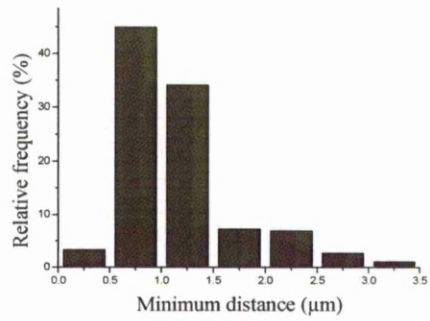

10 µm channel

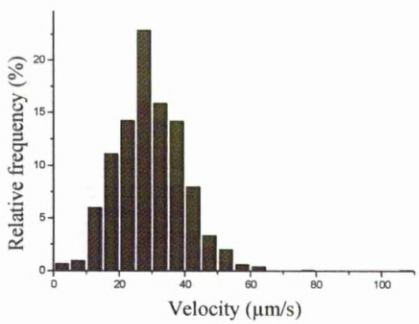

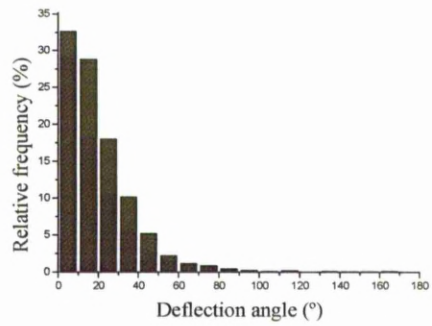

Pseudomonas stutzeri

2 µm channel

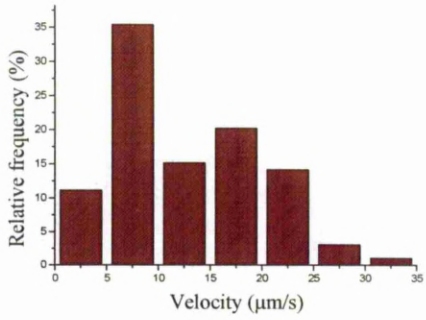

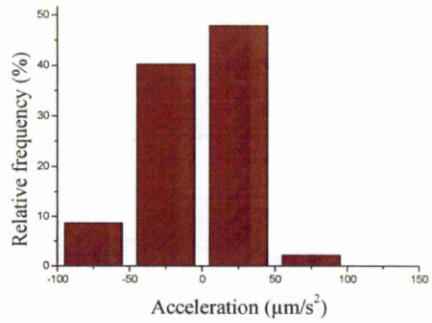

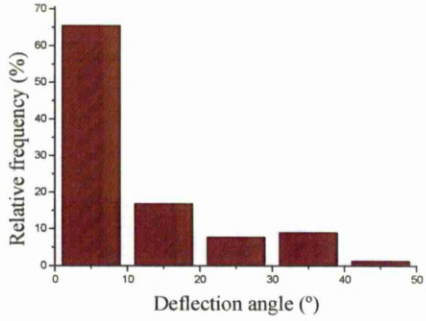

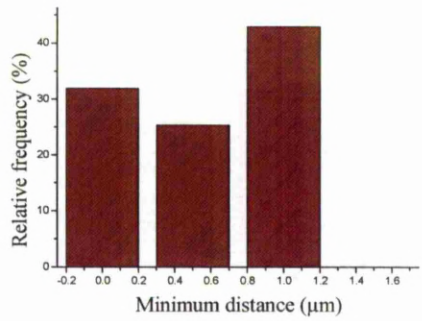

3 µm channel

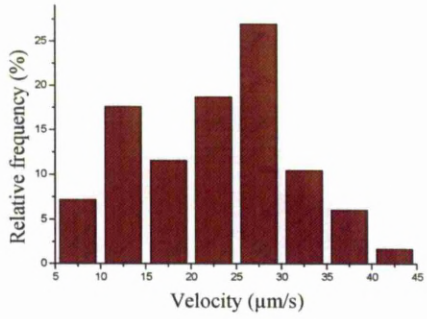

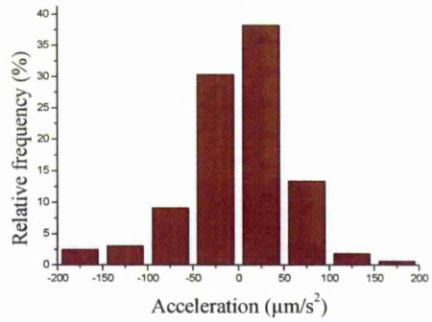

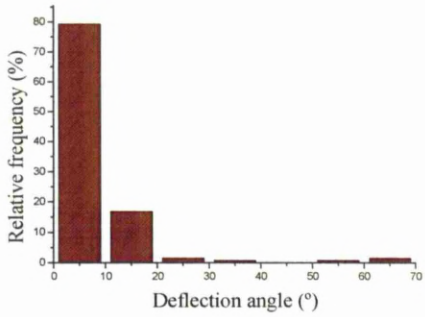
Relative frequency (%)
Deflection angle (°)

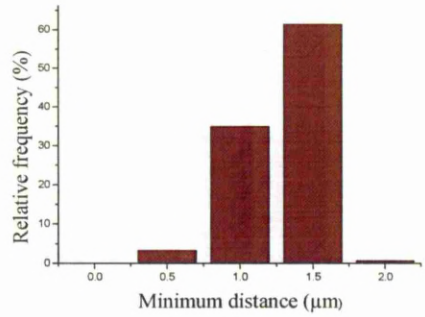
Relative frequency (%)
Minimum distance (μm)

4 μm channel

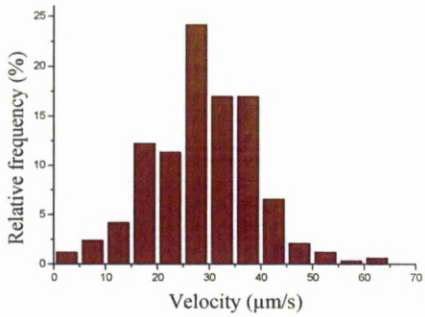
Relative frequency (%)
Velocity (μm/s)

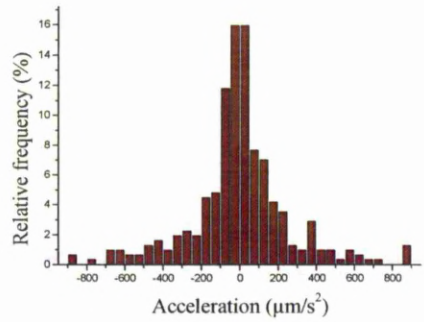
Relative frequency (%)
Acceleration (μm/s²)

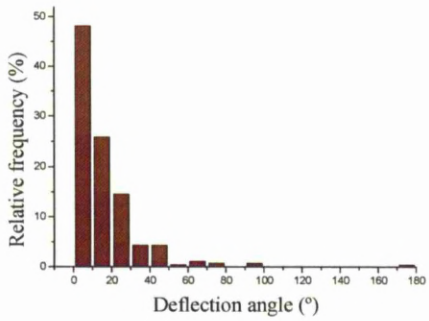
Relative frequency (%)
Deflection angle (°)

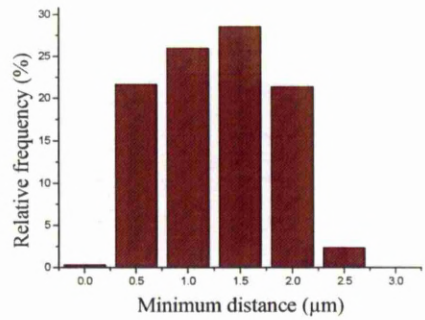
Relative frequency (%)
Minimum distance (μm)

5 μm channel

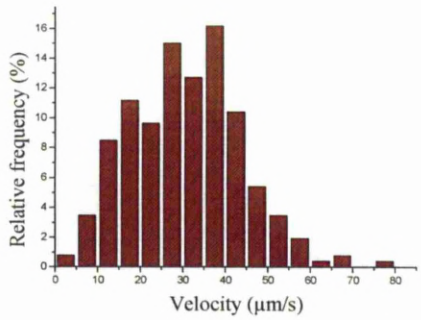

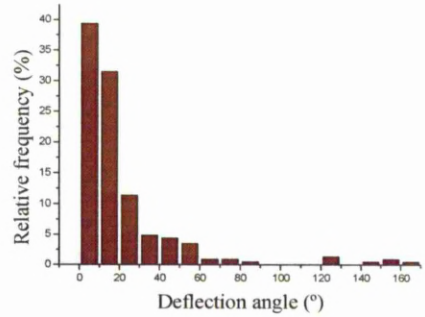

6 μm channel

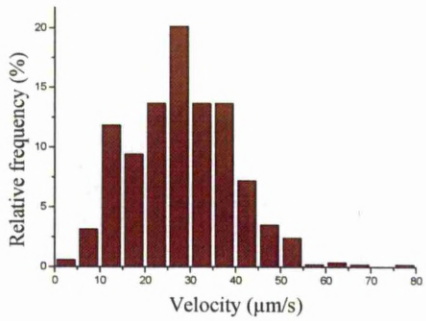

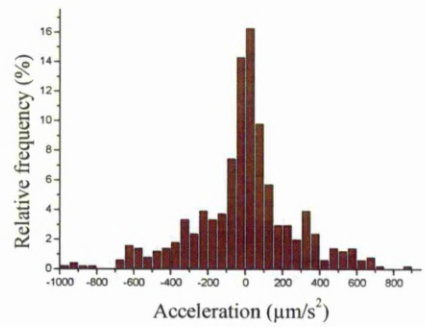

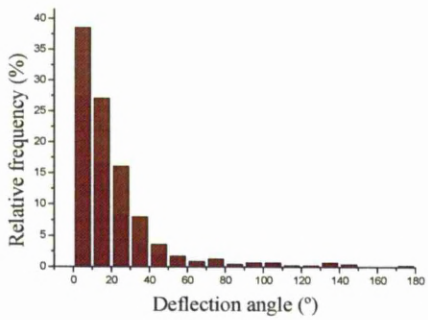

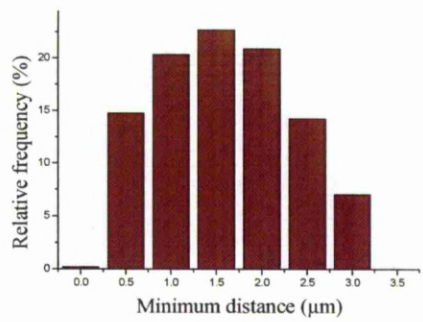

7 µm channel

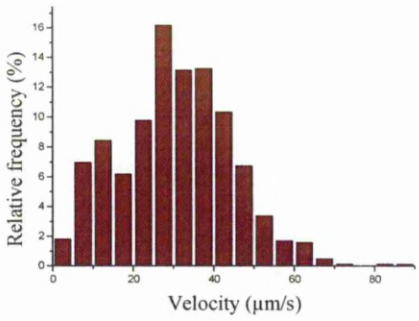

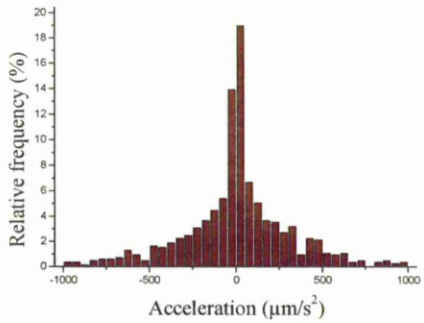

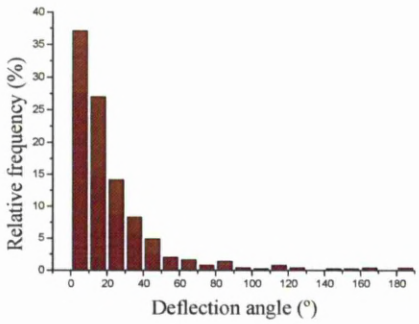

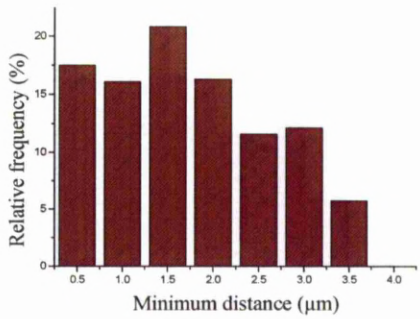

8 µm channel

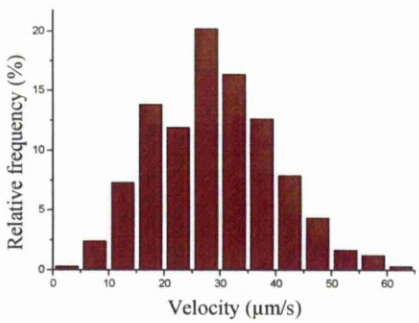

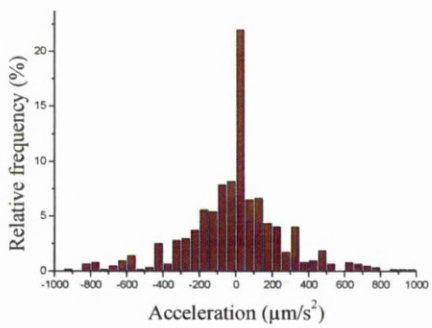

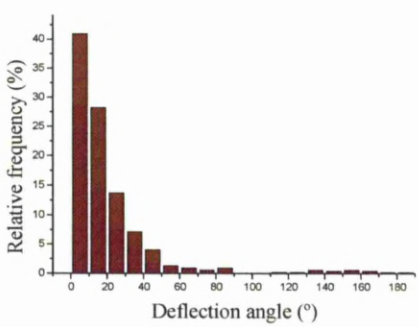

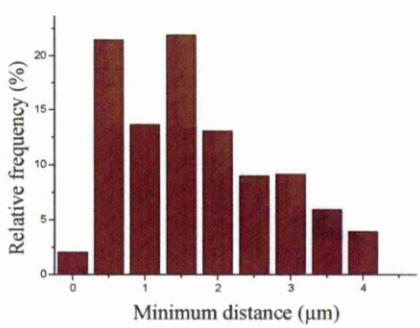

9 µm channel

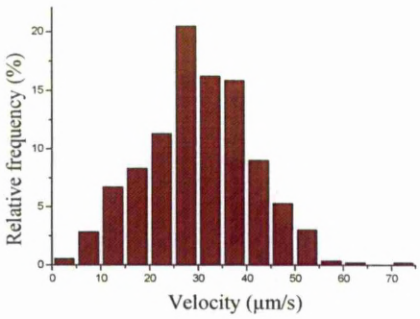

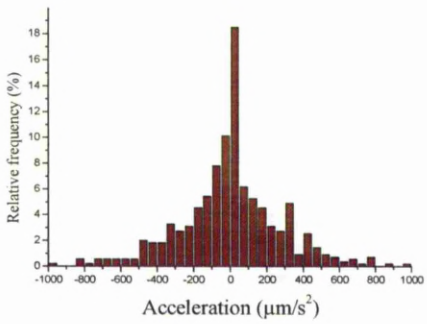

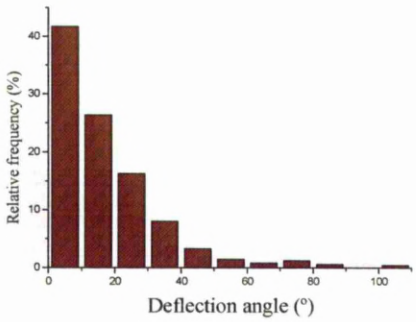

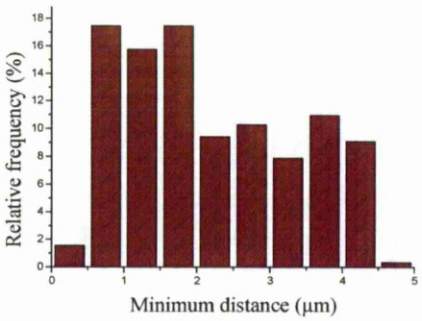

10 µm channel